Shamsudin, Mohd Hafizi (2015) Thermo-mechanical behaviour of woven cloth laminates. PhD thesis.

http://theses.gla.ac.uk/6479/

Copyright and moral rights for this thesis are retained by the author

A copy can be downloaded for personal non-commercial research or study, without prior permission or charge

This thesis cannot be reproduced or quoted extensively from without first obtaining permission in writing from the Author

The content must not be changed in any way or sold commercially in any format or medium without the formal permission of the Author

When referring to this work, full bibliographic details including the author, title, awarding institution and date of the thesis must be given

Glasgow Theses Service
http://theses.gla.ac.uk/
theses@gla.ac.uk

Thermo-mechanical Behaviour of Woven Cloth Laminates

A Thesis submitted in fulfilment of the requirement

for the Degree of Doctor of Philosophy

Aerospace Sciences

School of Engineering

University of Glasgow

By:

Mohd Hafizi Shamsudin

April 2015

©Mohd Hafizi Shamsudin, 2015

Abstract

Balanced and symmetric laminates are pervasive in design practice for the simple reason that thermal warping distortions are associated with non-symmetric laminate designs. Design practice, particularly in the Aerospace sector, has become entrenched and risk averse, hence the reluctance to move away from this simple design rule. However to unlock the full potential of composite laminates, the coupling interactions between in-plane and out-of-plane, must now be considered. Thermally stable laminates can now be achieved through sophisticated tailoring design strategies, leading to mechanically coupled materials properties with immunity to thermal warping distortion. This unique quality is known as the hygro-thermally curvature-stable (HTCS). The Extension-Twisting (and Shearing-Bending) coupled laminate is one particular class of coupled laminate with HTCS properties, which is an enabling technology for tilt-rotor aircraft. This class of laminate may be derived using standard ply angle orientations i.e. +45, –45, 0 and 90°, which in comparison to free form angle ply orientations, developed through an optimisation technique, will facilitate the requirement for ply terminations, whilst preserving the Extension-Twisting coupling behaviour within the entire laminate tapered design. Free form angle laminates make thickness tapering virtually impossible, particularly if maintaining consistent coupling behaviour within the entire laminate is a design constraint. Extension-Twisting coupled laminates derived from standard angle orientations with HTCS properties are shown to exist only for 8-, 12-, 16- and 20-ply number groupings, and an assessment of the configurations for each twist magnitude and buckling load strength is presented for each case. The limited number of groupings these coupled laminate solutions is shown to be the result of employing unidirectional material.

The above restrictions for UD material may be relaxed for laminates with balanced Plain weave material, which are shown to be inherently thermally curvature stable. Balanced

Plain weave material results in a broader design space for mechanically coupled laminates; irrespective of the ply angle orientations and ply number grouping. This benefit provides more flexibility for laminate tailoring and thickness tapering; where the mechanical coupling behaviour and immunity to thermal warping distortions is maintained throughout, it also opens up the possibility of changing the coupling behaviour through a novel ply termination strategy. Where standard ply angle orientations are a design constraint, seven unique classes of mechanically coupled laminates exist with interactions between Extension, Shearing, Bending, and Twisting.

Alternative woven cloth architecture are also considered. For instance, 5-Harness Satin (5HS) weave material, possesses straighter load-carrying fibres and low crimp angle, gives rise to improve mechanical performance in comparison to Plain weave material, in which maximum fibre kinking potentially exists. However, due to the unsymmetric nature of the 5HS weave architecture, a single layer of this material is shown to be thermally unstable, therefore a method is presented to predict the thermal warping curvature and eliminate their effect by applying suitable lamination strategies.

Table of Contents

List of Tables

List of Figures

Acknowledgement

The completion of this doctoral thesis could not have been possible without the help and kind assistance of the nice people around me, to only some of whom I can possibly express their particulars here.

First and foremost, I would like to express my utmost gratitude to my supervisor Dr. Christopher York, for his unconditional guidance and support throughout my PhD. I could not have imagined finishing this Phd, if it wasn't for his unreserved help and for his invaluable time spent helping me from the beginning of my Phd and towards the final completion of this thesis. At times where I felt lost, he inspires and motivates, which I could not wish for a better or friendlier supervisor.

I would also like to express my gratitude to Dr. Jérôme Rosseau for his technical assistance in the fabrication of the test specimens. His dedicated time and effort, in guiding me throughout the fabrication and experimental procedures, is truly appreciated.

My thanks also go to the staffs of the Aerospace science department, especially to Elaine McNamara and Amanda Smith, who have helped me a lot in various administration matters.

My deepest gratitude also goes to my beloved wife Shahriratul Azniza Mohamed. Admirably her great patience, constant support and understanding, especially in tough times during my PhD, from which my deepest thanks and gratitude likewise does not suffice.

Finally a special love to my parents and my two sons Ammar Danial and Asyraf Danial.

Author's Declaration

I declare that except where explicit reference is made to the work of others, this dissertation is the result of my own work. This work has not been submitted for any other degree at the University of Glasgow or any other institution.

Mohd Hafizi Shamsudin

Definitions / Abbreviations

$\mathbf{A}$, A_{ij}	=	extensional stiffness matrix and its elements (i,j = 1, 2, 6).
$\mathbf{B}$, B_{ij}	=	coupling stiffness matrix and its elements (i,j = 1, 2, 6).
$\mathbf{D}$, D_{ij}	=	bending stiffness matrix and its elements (i,j = 1, 2, 6).
$\mathbf{A}_{ij+}$, $\mathbf{A}_{ij-}$	=	Contribution of angle-ply to the extensional stiffness matrix
$\mathbf{A}_{ij\bigcirc}$, $\mathbf{A}_{ij\bullet}$	=	Contribution of cross-ply to the extensional stiffness matrix
$\mathbf{B}_{ij+}$, $\mathbf{B}_{ij-}$	=	Contribution of angle-ply to the coupling stiffness matrix
$\mathbf{B}_{ij\bigcirc}$, $\mathbf{B}_{ij\bullet}$	=	Contribution of cross-ply to the coupling stiffness matrix
$\mathbf{D}_{ij+}$, $\mathbf{D}_{ij-}$	=	Contribution of angle-ply to the bending stiffness matrix
$\mathbf{D}_{ij\bigcirc}$, $\mathbf{D}_{ij\bullet}$	=	Contribution of cross-ply to the bending stiffness matrix
$\sum A_{+}$, $\sum A_{-}$	=	Sum of angle-ply non-dimensional parameters for extensional (**A**)
$\sum A_{\bigcirc}$, $\sum A_{\bullet}$	=	Sum of cross-ply non-dimensional parameters for extensional (**A**)
$\sum B_{+}$, $\sum B_{-}$	=	Sum of angle-ply non-dimensional parameters for coupling (**B**)
$\sum B_{\bigcirc}$, $\sum B_{\bullet}$	=	Sum of cross-ply non-dimensional parameters for coupling (**B**)
$\sum D_{+}$, $\sum D_{-}$	=	Sum of angle-ply non-dimensional parameters for bending (**D**)
$\sum D_{\bigcirc}$, $\sum D_{\bullet}$	=	Sum of cross-ply non-dimensional parameters for bending (**D**)
$E_{1,2}$, G_{12}	=	in-plane Young's moduli and shear modulus.
H	=	laminate thickness (= number of plies, $n \times$ ply thickness, t).
$M_{x, y, xy}$	=	moment resultants.
$N_{x, y, xy}$	=	force resultants.
$\mathbf{M}^{Thermal}$	=	thermal moment resultant vector (=$\{M_x^{Thermal}, M_y^{Thermal}, M_{xy}^{Thermal}\}^T$).
$\mathbf{N}^{Thermal}$	=	thermal force resultant vector (=$\{N_x^{Thermal}, N_y^{Thermal}, N_{xy}^{Thermal}\}^T$).
Q_{ij}	=	reduced stiffness (i,j = 1, 2, 6).
U_i	=	laminate invariant (i = 1,2,3,4,5).
z_k	=	layer k interface distance from laminate mid-plane.
$\alpha_{1,2}$, α_{Iso}	=	principal and isotropic coefficients of thermal expansion.
$\boldsymbol{\varepsilon}$	=	vector of in-plane strains (=$\{\varepsilon_x, \varepsilon_y, \varepsilon_{xy}\}^T$).
$\boldsymbol{\kappa}$	=	vector of curvatures (=$\{\kappa_x, \kappa_y, \kappa_{xy}\}^T$).
ν_{ij}	=	Poisson ratio (i, j = 1, 2).
θ_k	=	ply orientation for layer k.
β	=	Off-axis angle orientation applied from the principal material axis
$\xi_{1\text{-}4}$	=	lamination parameters for extensional stiffness.
$\xi_{5\text{-}8}$	=	lamination parameters for coupling stiffness.
$\xi_{9\text{-}12}$	=	lamination parameters for bending stiffness.

$+, -, \pm$	=	angle plies, used in stacking sequence definition.
$\bigcirc, \bullet$	=	cross-plies, used in stacking sequence definition.
n_+, n_-	=	Extensional stiffness parameter for angle-ply subsequences.
$n_\bigcirc, n_\bullet$	=	Extensional stiffness parameters for cross-ply subsequences.
χ_+, χ_-	=	Coupling stiffness parameters for angle-ply subsequences.
$\chi_\bigcirc, \chi_\bullet$	=	Coupling stiffness parameters for cross-ply subsequences.
ζ_+, ζ_-	=	Bending stiffness parameters for angle-ply subsequences.
$\zeta_\bigcirc, \zeta_\bullet$	=	Bending stiffness parameters for cross-ply subsequences.
κ_G	=	Gaussian curvature.
δ	=	Deviation from flatness.

CHAPTER 1:

Introduction

Composite materials are becoming ever more popular primarily in applications demanding tremendous weight savings, particularly in the aerospace and spacecraft industries. The trend in the use of advanced composite materials in transport aircraft structures has gradually increased since the 1970s (Ilcewicz *et al*., 2000). Again, this was driven by a requirement for greater weight saving, allowing for greater range and/or payload capacity for the airline operator, hence contributing to cost efficiency. Figure 1.1 illustrates the weight percentage of advanced composite materials used on aircraft structures. By contrast, use in military applications was said to be ahead by about 10 years (Ilcewicz *et al*., 2000). The use of advanced composite materials in military rotorcraft was also evident in the early 1980s, with the composite weight as a percentage of total structural weight (see Fig. 1.2) constituting more than 40% (Dobyns *et al*., 2000).

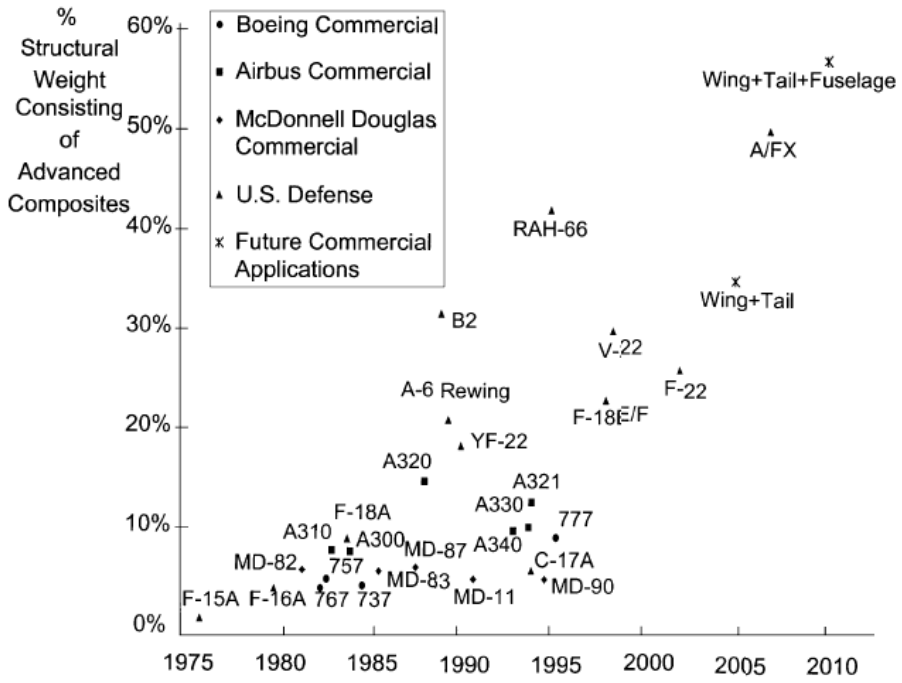

Figure 1.1 – Percentage use of advanced composite materials in aircraft structural application, (after Ilcewicz *et al*., 2000).

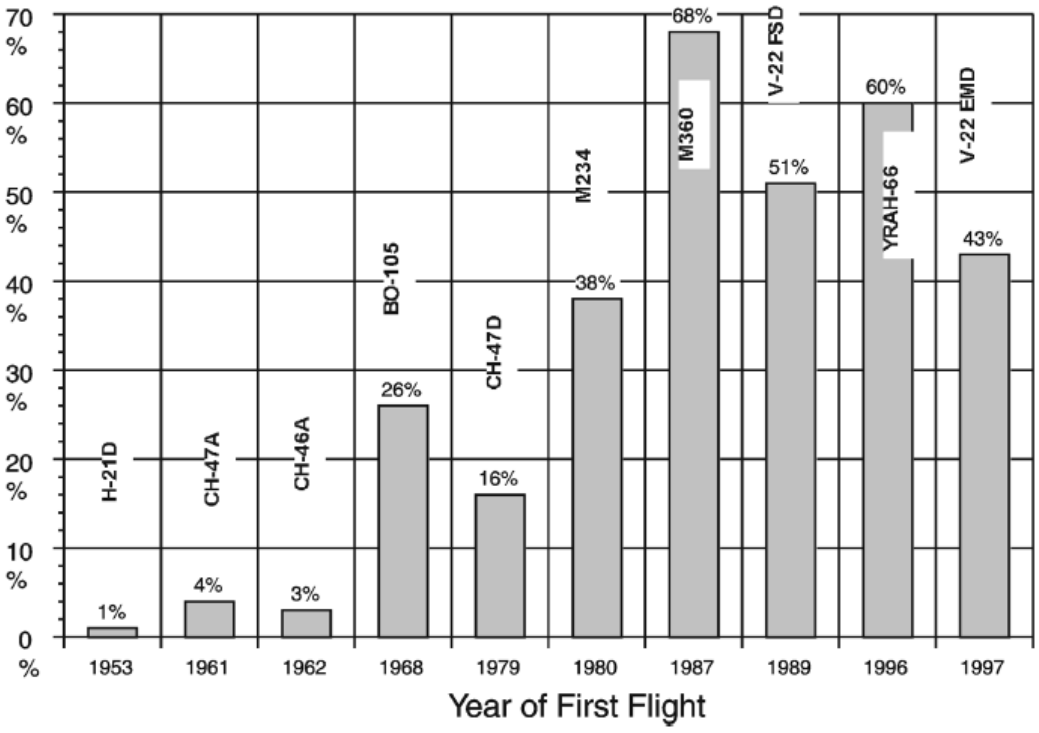

Figure 1.2 – Percentage use of advanced composite materials in rotorcraft structures, (after Dobyns *et al*., 2000).

On a more recent development, the newly launched commercial B787 Dreamliner from the manufacturer Boeing, which had its maiden commercial service in the year 2011 is made from 50% advanced carbon fibre composite materials by weight, 20% Aluminium, 15% Titanium, 10% Steel and 5% other materials. This distribution of material across different parts of the aircraft structure is shown illustratively in Fig. 1.3.

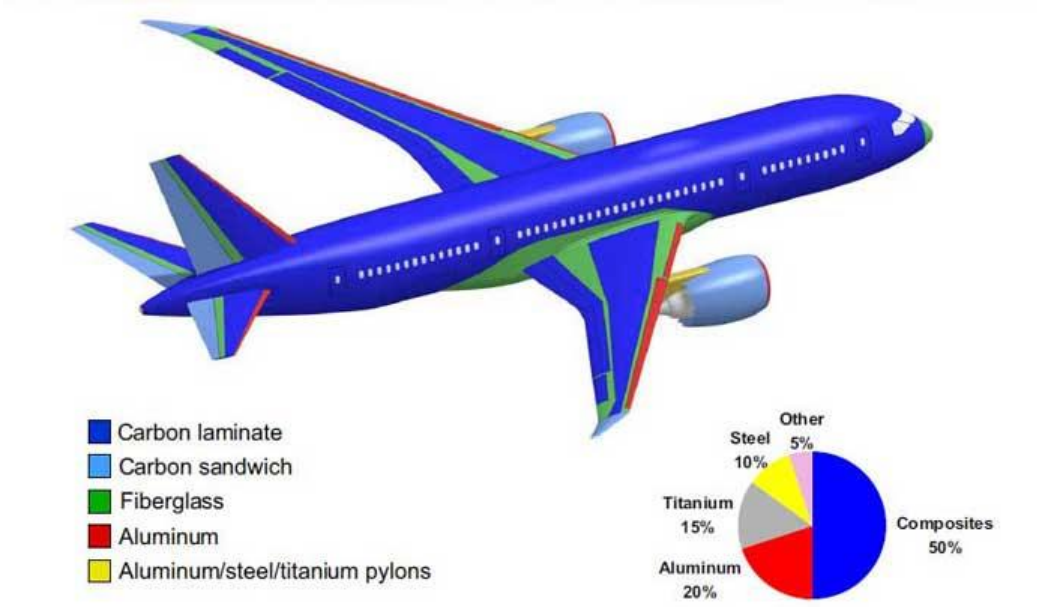

Figure 1.3 – Distribution of materials by weight used for the Boeing 787 Dreamliner structures, (after Freissinet, 2011).

Despite the growing use of the composite materials in the aerospace industry, they are often used only in their simplest form, to mimic the metallic materials that they are replacing, which serves only to fulfil the weight saving requirement through the use of lower density material. The term simplest form here refers to the laminate tailoring strategy employed, which generally involves laminates with balanced and symmetric construction. A balanced laminate is one in which every angle-ply layer in the laminate with specific thickness material properties and fibre orientation, have an identical layer but with opposite sign (Hyer, 2009). A symmetric laminate is defined as one in which the stacking sequence in one half of the laminate is mirrored about the laminate mid-plane. An example of a balance and symmetric laminate configuration is illustrated in Fig. 1.4.

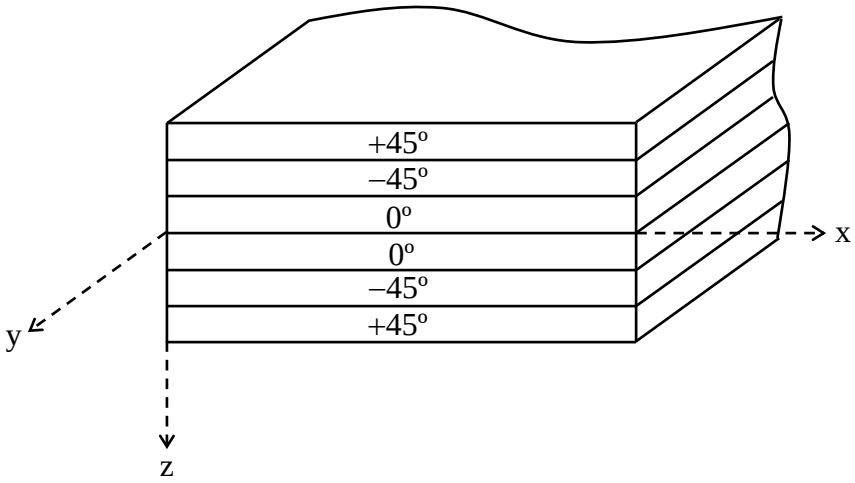

Figure 1.4 – Balanced and symmetric laminate configuration. A balanced laminate is one in which every angle-ply layer in the laminate with specific thickness material properties and fibre orientation, have an identical layer but with opposite sign (Hyer, 2009). A symmetric laminate is defined as one in which the stacking sequence in one half of the laminate is mirrored about the laminate mid-plane.

Balanced and symmetric laminate designs remain the preferred lamination strategy to date, due to their uncomplicated design technique. More importantly, the significance of the symmetric design rule is well-known to guarantee a warp-free or distortion free condition following the high temperature curing process, generally employed in the manufacture of high strength composite materials. The fibres and epoxy both have different thermal properties, which implies that they behaved differently under high temperature conditions. It is therefore crucial to understand the interaction of the different thermal contractions in layers constructed at different angle orientations within the laminate, following the high temperature manufacturing process.

Laminate thermal warping is illustrated in Fig. 1.5, and occurs as a result of the manifestation of residual thermal stresses within each layer of a laminate, following a high temperature curing process. Adopting the symmetric design rule was mathematically proven to give $\mathbf{B} = 0$ and hence cancel out the effect of the thermal stresses by pairing layers of identical orientation symmetrically about the laminate mid-plane.

Figure 1.5 – Example of a thermal warping behaviour from a non-symmetric 6-ply laminate with a stacking sequence of [45/0/–45/–45/90/45]$_T$; with Extension-Bending and Bending-Twisting mechanical coupling behaviour.

Unfortunately, non-symmetrical laminate are often associated with thermal warping distortion, as illustrated in Fig. 1.5, which was derived from a 6-ply laminate with a stacking sequence of [45/0/–45/–45/90/45]$_T$. The layers contributing to the non-symmetric condition for this 6-ply laminate are the 0 and 90º (the cross-symmetric cross-ply layers) underlined. This example also serves to demonstrate another important aspect of the laminate stacking sequence design: a manufacturing error relating to the lamination angle of a single layer within the laminate design can have a tremendous effect on the overall physical behaviour of the laminate.

The widespread belief that non-symmetric laminates result in thermal warping distortion, explains the continuing reluctance of many laminate designers to move away from the symmetric design rule. By contrast, a previous study from York (2009) has shown that symmetric design rule was not the necessary condition to achieve warp-free or flat laminate during manufacturing. The design space for achieving warp-free laminates were in fact shown to be populated with predominantly non-symmetric laminates design. An example is given in Fig. 1.6 for the 7-ply anti-symmetric laminate plate manufactured with the stacking sequence of [+45/–45/–45/0]$_{AS}$, confirming the warp-free condition.

Figure 1.6 – Warp-free laminate condition observed for a 7-ply anti-symmetric laminate with the stacking sequence of [+45/−45/−45/0/+45/+45/−45]; with fully uncoupled mechanical behaviour.

Another form of anti-symmetric laminate, which has been shown to possess immunity to this thermal warping distortion is the 8-ply laminate design first discovered by Winckler (1985), shown in Eq. (1.1).

$$[\theta/(\theta+90)_2/\theta/-\theta/(-\theta+90)_2/-\theta]_T \tag{1.1}$$

The laminate can viewed as being constructed from two sub-sequence i.e. $[\theta/(\theta+90)_2/\theta]$ and $[-\theta/(-\theta+90)_2/-\theta]$, both of which are symmetric, yet anti-symmetrically disposed about the laminate mid-plane. It was observed by Winckler (1985) that the two sub-sequence would retain their warp-free condition after combining in this way.

An equally important observation made on this laminate design, is the unique mechanical coupling interaction that exists between extension and twisting; such behaviour does not exist in conventional materials such as aluminium. This coupling behaviour is illustrated in Fig. 1.7 (a) and (b), where the two sub-sequence laminates having equal Extension-Shearing coupling but reacting at opposite direction are bonded together to form an anti-symmetric laminate configuration resulting in an Extension-Twisting coupling effect.

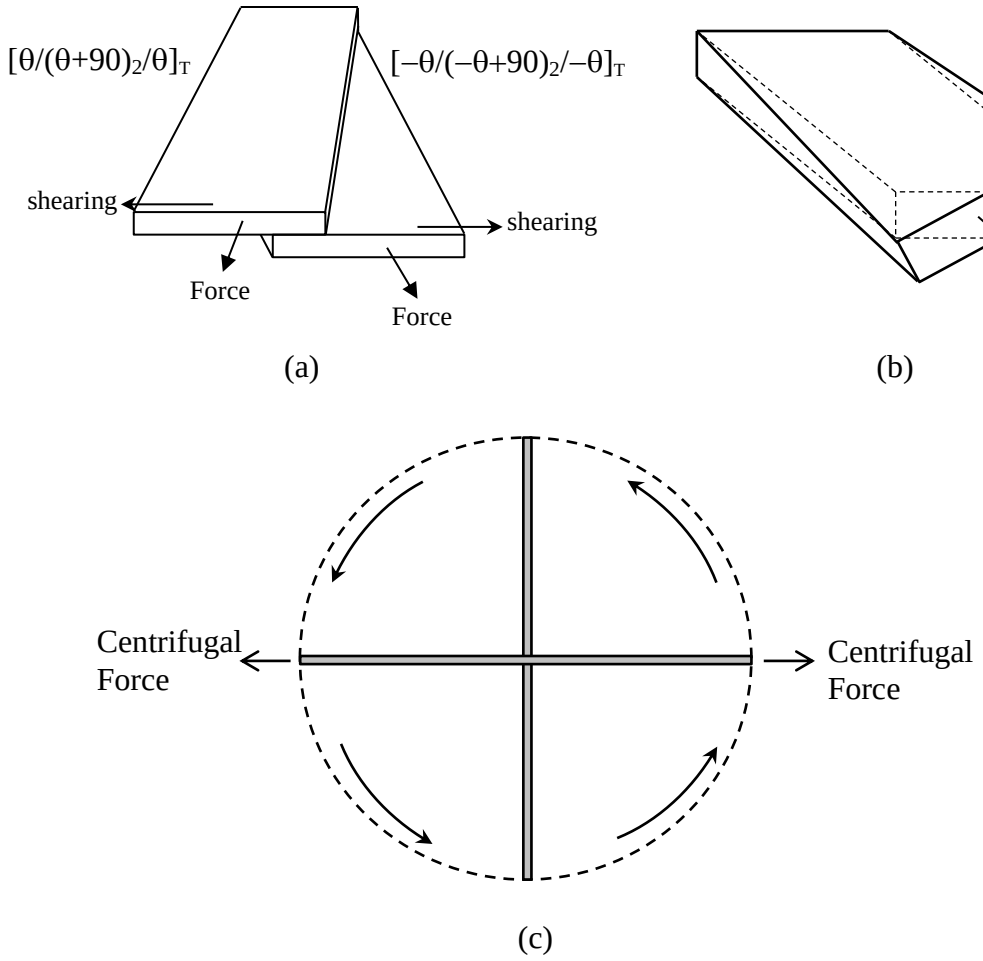

Figure 1.7 – (a) Two unbonded sub-sequence laminates exhibiting Extension-Shearing coupling at different direction; (b) Extension-Twisting coupling effect result from bonding the two Extension-Shearing sub-laminates; (c) Centrifugal force in spinning rotor blades, which acts as the extensional load on the blades and in turn induces the twisting behaviour, as a consequent of the Extension-Twisting coupling within the rotor blades.

This unique Extension-Twisting coupling from composite material is seen as an enabling technology for aeroelastic compliant rotor blades for tilt rotor aircraft (Nixon, 1987), as shown in Fig. 1.8. Here, Extension-Twisting coupling, at the structural or blade level, is used to develop an optimised twist distribution along the blade for both hover and forward flight: a change in rotor speed, and the resulting centrifugal forces, provides the required twist differential between the two flight regimes, see Fig. 1.7(c). This behaviour is achieved from laminate level Extension-Shearing coupling, but through off-axis alignment of a balanced and symmetric laminate. However, such laminate designs possess significant Bending-Twisting coupling at the box level, leading to detrimental effects on the compression buckling strength of the blade, which is an important static design constraint.

Figure 1.8 – V-22 Osprey demonstrating the transition phase of the tilt rotor blade from the helicopter mode to the airplane mode.

Another example of aeroelastic tailoring, which has been successfully exploited from composite material in the past, is the interaction between bending and twisting employed in the X-29 forward swept wing aircraft, as illustrated in Fig. 1.9.

Figure 1.9 – State-of-the-art composite employed in the X-29 forward swept wing aircraft.

Here the Bending-Twisting coupling helps to alleviate excessive high angle of attack of the wing, which occurs as a result of aerodynamic lift: where the lift force exerted on the wing will cause the wing bending upward and consequently, forcing a higher angle of attack. By incorporating the Bending-Twisting coupling, will allow for the wing to twist, but in the

opposite direction i.e. downward under similar aerodynamic loading. This reduces the high angle of attack of the wing, hence avoiding any structural failure of the wing in flight.

The potential use of these mechanically coupled laminates demonstrated by the above examples, have spurred many research works in the literatures. Among which have gained considerable interest is the study on optimised thermally stable Extension-Twisting coupled laminates (Haynes and Armanios, 2010, Cross *et al*., 2008, Chen, 2003), which is generally achieved using free form angles (i.e. arbitrary angles) laminate. Although optimum twisting was achieved (Haynes and Armanios, 2010), however, laminates derived from free form angles are difficult to manufacture due to its intricate angle and often susceptible to angle misalignment during manufacturing. In addition, laminate design using free form angles impose a disadvantage whenever laminate thickness tapering is required, where it is impossible to maintain the optimum Extension-Twisting coupling throughout the laminate, whilst simultaneously preserving the thermally stable properties.

By contrast Extension-Twisting coupled laminates derived from standard ply angles orientation, +45, –45, 0, 90º present a better alternative; where they are easy to manufacture and provide a better platform for performing laminate thickness tapering. This has been the motivation for the research work reported in this thesis, addressing on mechanically coupled laminates with immunity to thermal warping distortions derived using standard ply angles orientation, particularly focusing on Extension-Twisting coupled laminates.

Extension-Twisting coupled laminates with immunity to thermal warping distortions, derived from standard angle ply orientations, exist for 8-, 12-, 16- and 20-ply number groupings (York, 2011). An assessment of the configurations for each twist magnitude and buckling load strength for each case, which have not been properly addressed in the literature, is reported in this thesis.

The limited number of groupings these coupled laminate solutions is shown to be the result of employing unidirectional material. This restriction for unidirectional material may be relaxed for laminates with balanced Plain weave material, which are shown to be inherently thermally curvature stable. Balanced Plain weave material results in a broader design space for mechanically coupled laminates; irrespective of the ply angle orientations and ply number grouping. This benefit provides more flexibility for laminate tailoring and thickness tapering where the mechanical coupling behaviour and immunity to thermal warping distortions is maintained throughout. Where standard ply angle orientations are a design constraint, definitive listings on the classifications of mechanically coupled laminates with balanced Plain weave, which has not been addressed in the literature, is reported in this thesis.

Finally, the attention of work in this thesis is turned towards an alternative woven cloth architecture, i.e, 5-Harness Satin (5-HS) weave material; which possesses straighter load-carrying fibres and low crimp angle, gives rise to improved mechanical performance in comparison to balanced Plain weave material, in which maximum fibre kinking potentially exists. However, because of the non-symmetric architecture of the 5-HS weave, a single layer of this material is shown to be thermally unstable. Therefore a method is reported in this thesis to predict the thermal warping curvature and eliminate their effect by applying suitable lamination strategies.

1.1 Problem statement

In order for mechanically coupled laminates possessing immunity to thermal warping distortions to be exploited for potential enabling technology, the laminate design to this special class of laminates should be practical and flexible to adapt to different design requirement, including laminate thickness tapering.

The current interest given towards these mechanically coupled laminates, have focused on optimizing the coupling quality of the laminate, which generally result in free form or arbitrary angle laminates. This form of laminate is difficult to manufacture and making thickness tapering virtually impossible.

Thermally stable coupled laminates derived from standard angle ply orientations, is easier to manufacture, and practical for different laminate design requirement, including thickness tapering. Thermally stable coupled laminates from different material systems, i.e., unidirectional and woven cloth, derived using standard angle orientations will provide better for option to cater for different laminate design requirement, compared with coupled laminates with free form angles.

1.2 Research aim

This research work is aimed at investigating the potential of unique thermally stable coupled laminates for aerospace applications using 3 different material systems, i.e., unidirectional, balanced plain weave and 5-Harness Satin weave, derived from standard angle ply orientations in which the thickness can be tapered through ply terminations, whilst maintaining the same mechanical coupling behaviour at the point where the plies are terminated.

1.3 Research objectives

In order for the research aim to be achieved, several objectives must be met. The objectives for this research are described below:

1. Assess the twist magnitude and buckling performance of thermally stable Extension-Twisting (and Shearing-Bending) coupled laminates, from unidirectional material.

2. Determine the classifications of mechanically coupled laminate classes achievable from balanced Plain weave material, and the number of solutions, which they exist when derived using standard angle ply orientations.

3. Predict the thermal warping behaviour of 5-Harness Satin weave laminates using experimental and numerical procedures.

1.4 Research publications

Results from the research works discussed in this thesis, has been published as part of journal papers and conference proceedings, which are listed below:

1. Shamsudin, M. H., Rousseau, J., Verchery, G. & York, C. B. (2011) Experimental validation of the mechanical coupling response for hygro-thermally curvature-stable laminated composite materials. In *6th International Conference on Supply on the Wings*, Frankfurt, Germany.

2. Shamsudin, M. H., Chen, J. & York, C. B. (2013) Bounds on the compression buckling strength of hygro-thermally curvature-stable laminate with Extension-Twisting coupling. *International Journal of Structural Integrity* **4(4)**:477-486.

3. Shamsudin, M. H. & York, C. B. (2011) Mechanically coupled laminates with balanced plain weave. *Composite Structures* **107**: 416-428.

4. Shamsudin, M. H., Rousseau, J. & York, C. B. (2013) Warping curvature predictions for non-symmetric woven cloth laminates. In *12th Designing Against Deformation & Fracture of Composite Materials: Engineering For Integrity Large Composite Structures (DFC-12/SI-6)*, Cambridge, England.

1.5 Thesis overview

This section presents the overview of the chapters contributing to the entire thesis.

Chapter 2 – Laminate characterisation

This chapter discusses the characterisation of coupled laminates, performed through the laminate stiffness matrix or popularly known as the ABD matrix, which is based upon the fundamental of the classical lamination theory (CLT). A notation system that describes the physical form of the respective ABD stiffness matrix used by the Engineering Sciences Data Unit (ESDU) for classifying the different classes of coupled laminates is presented, and will be employed throughout the current research work. In addition, the concept of using non-dimensional parameters as a mean of calculating the elements of the ABD stiffness matrix is discussed.

Chapter 3 - Classification of uncoupled and coupled laminates

This chapter presents a literature review of research work on laminates possessing uncoupled and coupled behaviour.

Chapter 4 - Coupled laminates with hygro-thermally curvature-stable (HTCS) properties

This chapter discusses the method used to combat thermal warping distortion for mechanically coupled laminates, resulting from the high temperature curing process. In general specially curved tooling is required to counteract warping distortion of the laminate during manufacturing. However, this is often at great expense. The preferred approach is to design laminates possessing a warp-free attribute whilst the unique mechanical coupling interactions within the laminate are preserved. This immunity to thermal warping distortion is known as the hygro-thermally curvature-stable (HTCS) condition. The rules for achieving mechanically coupled laminates with HTCS properties are discussed.

Chapter 5 - HTCS coupled laminate solutions with Extension-Twisting coupling

This chapter focusses on a particular class of HTCS coupled laminate possessing Extension-Twisting coupling. The laminate designs discussed in this chapter will be confined to those derived from standard angle orientations i.e. +45, −45, 0 and 90º. The laminate coupling performance will be assessed via FEM simulation and experimental testing. In addition, an assessment of the critical buckling loads for laminates with Extension-Twisting coupling behaviour will be discussed.

Chapter 6 - Mechanically coupled laminates with balanced plain weave

This chapter presents the classification of mechanically coupled laminate classes available for woven cloth material with balanced plain weave. The laminate designs reported in this chapter are also confined to standard angle orientations, and consist of uncoupled and

coupled laminates. Tapering design strategy available under the coupled laminate solutions is also discussed.

Chapter 7 - Thermal warping prediction for 5-harness satin weave

This chapter presents an investigation of the thermal warping of 5-Harness Satin weave laminates. The work is based upon an experimental observation of warping within individual layers, which are verified via FEM simulations. Strategy for eliminating thermal distortions in laminate designs with 5-Harness Satin weave material is developed.

Chapter 8 - Conclusion and Future work

This final chapter presents conclusions on the work presented in this thesis, and recommendation for future research in the area of mechanically coupled laminates.

CHAPTER 2:

Laminate characterisation

Laminated composite materials are typically characterised in terms of their response to mechanical and/or thermal loading, which can be described from the classical lamination theory through the well-known ABD stiffness matrix given in Eq. (2.1).

$$\begin{Bmatrix} N_x \\ N_y \\ N_{xy} \end{Bmatrix} = \begin{bmatrix} A_{11} & A_{12} & A_{16} \\ & A_{22} & A_{26} \\ \text{Sym.} & & A_{66} \end{bmatrix} \begin{Bmatrix} \varepsilon_x \\ \varepsilon_y \\ \gamma_{xy} \end{Bmatrix} + \begin{bmatrix} B_{11} & B_{12} & B_{16} \\ & B_{22} & B_{26} \\ \text{Sym.} & & B_{66} \end{bmatrix} \begin{Bmatrix} \kappa_x \\ \kappa_y \\ \kappa_{xy} \end{Bmatrix}$$
$$\begin{Bmatrix} M_x \\ M_y \\ M_{xy} \end{Bmatrix} = \begin{bmatrix} B_{11} & B_{12} & B_{16} \\ & B_{22} & B_{26} \\ \text{Sym.} & & B_{66} \end{bmatrix} \begin{Bmatrix} \varepsilon_x \\ \varepsilon_y \\ \gamma_{xy} \end{Bmatrix} + \begin{bmatrix} D_{11} & D_{12} & D_{16} \\ & D_{22} & D_{26} \\ \text{Sym.} & & D_{66} \end{bmatrix} \begin{Bmatrix} \kappa_x \\ \kappa_y \\ \kappa_{xy} \end{Bmatrix} \tag{2.1}$$

The ABD stiffness matrix in Eq. (2.1) arises from the plane-stress assumption and the Kirchhoff hypothesis for thin plates, both of which are discussed in Appendix A. The characteristic behaviour of a laminate can be understood from Eq. (2.1). It provides a description of the coupling behaviour, not present in conventional materials, i.e. coupling between in-plane (i.e. extension or membrane) and out-of-plane (i.e. bending or flexure)

responses when $\mathbf{B}_{ij} \neq 0$ in Eq. (2.1), coupling between in-plane shear and extension when $\mathbf{A}_{16}$, $\mathbf{A}_{26} \neq 0$, and coupling between bending and twisting when $\mathbf{D}_{16}$, $\mathbf{D}_{26} \neq 0$. The force and moment vector components in Eq. (2.1) account for the combined effects of mechanical, thermal and hygral loading.

The unique coupling behaviour of laminates, which was briefly mentioned in Chapter 1 is dependent on the form of the elements in each of the extensional (**A**), coupling (**B**) and bending (**D**) stiffness matrices of Eq. (2.1). The Engineering Sciences Data Unit or ESDU (1994) adopted an extended subscript notation system defining the nature on the form of the respective matrix. For instance a fully populated extensional stiffness matrix is denoted as $\mathbf{A}_{F,}$ and implies that the laminate has coupling between extension and shearing and; a fully populated bending stiffness matrix, is denoted as $\mathbf{D}_F$ and implies that the laminate has Bending-Twisting coupling. These coupling responses arise from the non-zero elements, $\mathbf{A}_{16}$, $\mathbf{A}_{26}$ and $\mathbf{D}_{16}$, $\mathbf{D}_{26}$ as illustrated in Table 2.1 (a) and (b) respectively. Note that the second column of Table 2.1 gives the response-based labelling system after York (2010), describing the coupling behaviour through the *cause* and *effect* relationships, which correspond to the form of the stiffness matrices. Consider an unbalanced symmetric laminate with the stacking sequence $[\alpha/-\alpha/\alpha]_{T,}$ which was shown to have the following form of ABD stiffness matrix:

$$\begin{bmatrix} A_{11} & A_{12} & A_{16} & 0 & 0 & 0 \\ A_{12} & A_{22} & A_{26} & 0 & 0 & 0 \\ A_{16} & A_{26} & A_{66} & 0 & 0 & 0 \\ 0 & 0 & 0 & D_{11} & D_{12} & D_{16} \\ 0 & 0 & 0 & D_{12} & D_{22} & D_{26} \\ 0 & 0 & 0 & D_{16} & D_{26} & D_{66} \end{bmatrix} \tag{2.2}$$

This would be represented as $\mathbf{A_F B_0 D_F}$ using the ESDU subscript notation, the non-zero elements $\mathbf{A}_{16}$, $\mathbf{A}_{26}$ and $\mathbf{D}_{16}$, $\mathbf{D}_{26}$ signify that the laminate has Extension-Shearing coupling, $\mathbf{A}_F$, and Bending-Twisting coupling, $\mathbf{D}_F$.

Table 2.1 – Subscript notation, response based labelling and associated form of the: (a) extensional stiffness matrix, (A) and; (b) bending stiffness matrix, (D).

(a)

Subscript notation (ESDU, 1994)	Response-based labelling (York, 2010)	Matrix form
$\mathbf{A}_S$	Simple laminate	$\begin{bmatrix} A_{11} & A_{12} & 0 \\ A_{12} & A_{22} & 0 \\ 0 & 0 & A_{66} \end{bmatrix}$
$\mathbf{A}_F$	Extension-Shear; *E-S*	$\begin{bmatrix} A_{11} & A_{12} & A_{16} \\ A_{12} & A_{22} & A_{26} \\ A_{16} & A_{26} & A_{66} \end{bmatrix}$

(b)

Subscript notation (ESDU, 1994)	Response-based labelling (York, 2010)	Matrix form
$\mathbf{D}_S$	Simple laminate	$\begin{bmatrix} D_{11} & D_{12} & 0 \\ D_{12} & D_{22} & 0 \\ 0 & 0 & D_{66} \end{bmatrix}$
$\mathbf{D}_F$	Bending-Twisting; *B-T*	$\begin{bmatrix} D_{11} & D_{12} & D_{16} \\ D_{12} & D_{22} & D_{26} \\ D_{16} & D_{26} & D_{66} \end{bmatrix}$

The coupling (**B**) is denoted by $\mathbf{B}_0$, signifying a null **B** matrix or in other words there is no in-plane to out-of-plane coupling taking place, which is expected from a symmetric laminate configuration. Based on the *cause* and *effect* relationship, this $\mathbf{A_F B_0 D_F}$ laminate would have the associated response-based labelling *E-S;B-T*, denoting that extension will cause a shearing effect (*E-S*), and bending will cause a twisting effect (*B-T*). Each cause and effect pair is underlined and is reversible. A semicolon is introduced to distinguish between couplings relating to the extensional (**A**), coupling (**B**) and bending (**D**) stiffness matrices, respectively.

For the balanced and symmetric laminate, with stacking sequence: $[\alpha/-\alpha/-\alpha/\alpha]_T$ (Decolon, 2002), gives rise to the matrix relationship given in Eq. (2.3). Here the laminate can be represented by $\mathbf{A_S B_0 D_F}$ using the subscript notation, indicating the existence of bending-twisting coupling for a balanced and symmetric laminate.

$$\begin{bmatrix} A_{11} & A_{12} & 0 & 0 & 0 & 0 \\ A_{12} & A_{22} & 0 & 0 & 0 & 0 \\ 0 & 0 & A_{66} & 0 & 0 & 0 \\ 0 & 0 & 0 & D_{11} & D_{12} & D_{16} \\ 0 & 0 & 0 & D_{12} & D_{22} & D_{26} \\ 0 & 0 & 0 & D_{16} & D_{26} & D_{66} \end{bmatrix} \tag{2.3}$$

By contrast the coupling matrix (**B**) can exists in a number of different forms, with each form having a major influence on the relationship between in-plane and out-of-plane response of a given laminate. Adopting similar but extended subscript notation, to that presented in ESDU (1994) and the response-based labelling after York (2010), the different forms of coupling $\mathbf{B}\neq 0$ will be discussed Chapter 3, in which the various classes of mechanically coupled laminate behaviour will be introduced.

2.1 Non-dimensional parameters

York (2011) uses non-dimensional parameters in the calculation for the laminate stiffness properties. The method is particularly convenient since it is independent of the material properties and fibre orientations. To demonstrate the use of this method, consider a laminate example with the stacking sequence: $[+/-/\bigcirc/\bullet/\bullet/\bigcirc/+/-]_T$, where the symbols +, –, ○ and ● are used to replace the standard angles 45, –45, 0 and 90º respectively.

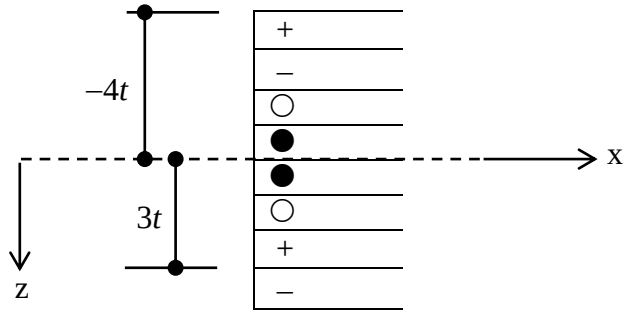

Figure 2.1 – Illustration of ply interface distance (z) with respect to the laminate mid-plane and constant ply thickness, *t* , for laminate stacking sequence $[+/-/\bigcirc/\bullet/\bullet/\bigcirc/+/-]_T$.

The calculation of the non-dimensional bending (**D**) stiffness parameters will be shown; the non-dimensional extensional (**A**) and coupling (**B**) stiffness parameters can be derived in a similar manner. In this example the elements of the bending (**D**) stiffness matrix are calculated from Eq. (2.4).

$$D_{ij} = \int_{-H/2}^{H/2} \bar{Q}_{ij} z^2 dz = \frac{1}{3}\sum_{k=1}^{N} \bar{Q}_{ij_k} (z_k^3 - z_{k-1}^3) \tag{2.4}$$

where z represents the distance from the laminate mid-plane, see Fig. 2.1, and is expressed in terms of ply thickness, *t*, which result to the following:

$$\begin{aligned} \mathrm{D_{ij}} = \{&\bar{\mathrm{Q}}_{\mathrm{ij+}}((-3t)^3 - (-4t)^3) + \bar{\mathrm{Q}}_{\mathrm{ij-}}((-2t)^3 - (-3t)^3) + \bar{\mathrm{Q}}_{\mathrm{ijo}}((-t)^3 - (-2t)^3) + \\ &\bar{\mathrm{Q}}_{\mathrm{ij\bullet}}((0)^3 - (-t)^3) + \bar{\mathrm{Q}}_{\mathrm{ij\bullet}}((t)^3 - (0)^3) + \bar{\mathrm{Q}}_{\mathrm{ijo}}((2t)^3 - (t)^3) + \\ &\bar{\mathrm{Q}}_{\mathrm{ij+}}((3t)^3 - (2t)^3) + \bar{\mathrm{Q}}_{\mathrm{ij-}}((4t)^3 - (3t)^3)\}/3 \end{aligned} \tag{2.5}$$

$$\mathrm{D_{ij}} = (37t^3\bar{\mathrm{Q}}_{\mathrm{ij+}} + 19t^3\bar{\mathrm{Q}}_{\mathrm{ij-}} + 7t^3\bar{\mathrm{Q}}_{\mathrm{ijo}} + t^3\bar{\mathrm{Q}}_{\mathrm{ij\bullet}} + t^3\bar{\mathrm{Q}}_{\mathrm{ij\bullet}} + 7t^3\bar{\mathrm{Q}}_{\mathrm{ijo}} + 19t^3\bar{\mathrm{Q}}_{\mathrm{ij+}} + 37t^3\bar{\mathrm{Q}}_{\mathrm{ij-}})/3$$

The subscripts i, j =1, 2, 6. Simplifying Eq. (2.5) and collecting terms gives:

$$\begin{aligned} D_{ij+} &= (56t^3/3)\bar{Q}_{ij+} \text{ and} \\ D_{ij-} &= (56t^3/3)\bar{Q}_{ij-} \end{aligned} \tag{2.6}$$

for angle plies and the cross ply terms are given by:

$$\begin{aligned} D_{ijo} &= (14t^3/3)\bar{Q}_{ijo} \text{ and} \\ D_{ij\bullet} &= (2t^3/3)\bar{Q}_{ij\bullet} \end{aligned} \tag{2.7}$$

The bending stiffness terms in Eqs. (2.6) and (2.7) can also be written in alternative form:

$$\begin{aligned} D_{ij+} &= (\zeta_+ t^3/12)\bar{Q}_{ij+} & D_{ijo} &= (\zeta_o t^3/12)\bar{Q}_{ijo} \\ D_{ij-} &= (\zeta_- t^3/12)\bar{Q}_{ij-} & D_{ij\bullet} &= (\zeta_\bullet t^3/12)\bar{Q}_{ij\bullet} \end{aligned} \tag{2.8}$$

where ζ_+, ζ_-, $\zeta_\circ$ and $\zeta_\bullet$ are the non-dimensional parameters. Comparing the form of Eq. (2.6) and (2.7) with Eq. (2.8) gives $\zeta_+ = 224$, $\zeta_- = 224$, $\zeta_\circ = 56$ and $\zeta_\bullet = 8$. These non-dimensional parameters can also be derived in tabular form, see Table 2.2, where n_+, n_-, $n_\circ$, $n_\bullet$ and χ_+, χ_-, $\chi_\circ$, $\chi_\bullet$ are the non-dimensional parameters related to the extensional (**A**) and coupling (**B**) stiffness respectively. The contribution of the angle-plies and cross-plies for the extensional (**A**) and coupling (**B**) are given by:

$$\begin{aligned} A_{ij+} &= (n_+ t)\bar{Q}_{ij+} & B_{ij+} &= (\chi_+ t^2/4)\bar{Q}_{ij+} \\ A_{ij-} &= (n_- t)\bar{Q}_{ij-} & B_{ij-} &= (\chi_- t^2/4)\bar{Q}_{ij-} \\ A_{ijo} &= (n_o t)\bar{Q}_{ijo} & B_{ijo} &= (\chi_o t^2/4)\bar{Q}_{ijo} \\ A_{ij\bullet} &= (n_\bullet t)\bar{Q}_{ij\bullet} & B_{ij\bullet} &= (\chi_\bullet t^2/4)\bar{Q}_{ij\bullet} \end{aligned} \tag{2.9}$$

where for the example stacking sequence under consideration; $n_+ = (\sum A_+) = 2$, $n_- = (\sum A_-) = 2$, $n_\circ = (\sum A_\circ) = 2$ and $n_\bullet = (\sum A_\bullet) = 2$; $\chi_+ = (2\times\sum B_+) = -4$, $\chi_- = (2\times\sum B_-) = 4$, $\chi_\circ =$

$(2\times\sum B_{\circ}) = 0$ and $\chi_{\bullet} = (2\times\sum B_{\bullet}) = 0$. Using these non-dimensional parameters along with the transformed reduced stiffnesses, $\bar{Q}_{ij}$, highlight the contributions of the respective angle-ply and cross-ply in the calculation for the elements of the stiffness matrix, using the following relationship:

$$
\begin{aligned}
A_{ij} &= \{n_{+}\bar{Q}_{ij+} + n_{-}\bar{Q}_{ij-} + n_{o}\bar{Q}_{ijo} + n_{\bullet}\bar{Q}_{ij\bullet}\}t \\
B_{ij} &= \{\chi_{+}\bar{Q}_{ij+} + \chi_{-}\bar{Q}_{ij-} + \chi_{o}\bar{Q}_{ijo} + \chi_{\bullet}\bar{Q}_{ij\bullet}\}t^{2}/4 \\
D_{ij} &= \{\zeta_{+}\bar{Q}_{ij+} + \zeta_{-}\bar{Q}_{ij-} + \zeta_{o}\bar{Q}_{ijo} + \chi_{\bullet}\bar{Q}_{ij\bullet}\}t^{3}/12
\end{aligned}
\qquad (2.10)
$$

Table 2.2 – Summary of the non-dimensional parameter calculation for extensional (A), coupling (B) and bending (D) stiffness for the stacking sequence: $[+/-/○/●/●/○/+/-]_T$.

			A					**B**					**D**			
Ply	(°)	(z_k-z_{k-1})	$A\Sigma_+$	$A\Sigma_-$	$A\Sigma_○$	$A\Sigma_●$	$(z^2_k-z^2_{k-1})$	$2□B\Sigma_+$	$2□B\Sigma_-$	$2□B\Sigma_○$	$2□B\Sigma_●$	$(z^3_k-z^3_{k-1})$	$4□D\Sigma_+$	$4□D\Sigma_-$	$4□D\Sigma_○$	$4□D\Sigma_●$
			2	**2**	**2**	**2**		**–4**	**4**	**0**	**0**		**224**	**224**	**56**	**8**
1	+	1	1				–7	–7				37	37			
2	–	1		1			–5		–5			19		19		
3	○	1			1		–3			–3		7			7	
4	●	1				1	–1				–1	1				1
5	●	1				1	1				1	1				1
6	○	1			1		3			3		7			7	
7	+	1	1				5	5				19	19			
8	–	1		1			7		7			37		37		

2.1.1 Lamination parameters

Lamination parameters were originally introduced by Tsai and Hahn (1980), featuring ply angle dependent parameters, which is convenient when performing laminate stiffness tailoring. The use of lamination parameters combined with the previously discussed non-dimensional parameters, is useful and relevant to work presented in this thesis, which focuses on laminate solutions derived for standard angle orientations, +, –, ○, ●.

Tsai and Hahn (1980) used double angle expressions to replace the usual higher order trigonometric functions for the transformation equations relating to the reduced stiffness in Eq. (2.11).

$$\begin{aligned}
\bar{Q}_{11} &= Q_{11}\cos^4\theta + 2(Q_{12}+2Q_{66})\sin^2\theta\cos^2\theta + Q_{22}\sin^4\theta \\
\bar{Q}_{12} &= (Q_{11}+Q_{22}-4Q_{66})\sin^2\theta\cos^2\theta + Q_{12}(\sin^4\theta+\cos^4\theta) \\
\bar{Q}_{16} &= (Q_{11}-Q_{12}-2Q_{66})\sin\theta\cos^3\theta + (Q_{12}-Q_{22}+2Q_{66})\sin^3\theta\cos\theta \\
\bar{Q}_{22} &= Q_{11}\sin^4\theta + 2(Q_{12}+2Q_{66})\sin^2\theta\cos^2\theta + Q_{22}\cos^4\theta \\
\bar{Q}_{26} &= (Q_{11}-Q_{12}-2Q_{66})\sin^3\theta\cos\theta + (Q_{12}-Q_{22}+2Q_{66})\sin\theta\cos^3\theta \\
\bar{Q}_{66} &= (Q_{11}+Q_{22}-2Q_{12}-2Q_{66})\sin^2\theta\cos^2\theta + Q_{66}(\sin^4\theta+\cos^4\theta)
\end{aligned} \tag{2.11}$$

where cosθ and sinθ are replaced with *m* and *n* respectively, giving:

$$\begin{aligned}
\bar{Q}_{11} &= Q_{11}m^4 + 2(Q_{12}+2Q_{66})n^2m^2 + Q_{22}n^4 \\
\bar{Q}_{12} &= (Q_{11}+Q_{22}-4Q_{66})n^2m^2 + Q_{12}(n^4+m^4) \\
\bar{Q}_{16} &= (Q_{11}-Q_{12}-2Q_{66})nm^3 + (Q_{12}-Q_{22}+2Q_{66})n^3m \\
\bar{Q}_{22} &= Q_{11}n^4 + 2(Q_{12}+2Q_{66})n^2m^2 + Q_{22}m^4 \\
\bar{Q}_{26} &= (Q_{11}-Q_{12}-2Q_{66})n^3m + (Q_{12}-Q_{22}+2Q_{66})nm^3 \\
\bar{Q}_{66} &= (Q_{11}+Q_{22}-2Q_{12}-2Q_{66})n^2m^2 + Q_{66}(n^4+m^4)
\end{aligned} \tag{2.12}$$

The double angle expressions replacing the higher order trigonometric functions of *m* and *n* in the above equations are shown in Eq. (2.13).

$$
\begin{aligned}
m^4 &= \frac{1}{8}(3+4\cos 2\theta+\cos 4\theta)\\
m^3 n &= \frac{1}{8}(2\sin 2\theta+\sin 4\theta)\\
m^2 n^2 &= \frac{1}{8}(1-\cos 4\theta)\\
mn^3 &= \frac{1}{8}(2\sin 2\theta-\sin 4\theta)\\
n^4 &= \frac{1}{8}(3-4\cos 2\theta+\cos 4\theta)
\end{aligned}
\tag{2.13}
$$

The transformed reduced stiffness can now be presented as:

$$
\begin{aligned}
\bar{Q}_{11} &= U_1 + U_2\cos 2\theta + U_3\cos 4\theta\\
\bar{Q}_{12} &= U_4 - U_3\cos 4\theta\\
\bar{Q}_{16} &= \frac{1}{2}U_2\sin 2\theta + U_3\sin 4\theta\\
\bar{Q}_{22} &= U_1 - U_2\cos 2\theta + U_3\cos 4\theta\\
\bar{Q}_{26} &= \frac{1}{2}U_2\sin 2\theta - U_3\sin 4\theta\\
\bar{Q}_{66} &= U_5 - U_3\cos 4\theta
\end{aligned}
\tag{2.14}
$$

where U_i are defined as

$$
\begin{aligned}
U_1 &= \frac{(3Q_{11}+3Q_{22}+2Q_{12}+4Q_{66})}{8} \quad U_2 = \frac{(Q_{11}-Q_{22})}{2} \quad U_3 = \frac{(Q_{11}+Q_{22}-2Q_{12}-4Q_{66})}{8}\\
U_4 &= \frac{(Q_{11}+Q_{22}+6Q_{12}-4Q_{66})}{8} \qquad\qquad U_5 = \frac{(Q_{11}+Q_{22}-2Q_{12}+4Q_{66})}{8}
\end{aligned}
\tag{2.15}
$$

The U_i are also known as the laminate invariants (Tsai and Hahn, 1980). Equation (2.14) is particularly useful, in understanding the polar or Mohr's circle transformations, exploited by Verchery (1979). The ply angle dependent parameters that modify the laminate invariants U_2 and U_3 are described (Tsai and Hahn, 1980) as lamination parameters.

These lamination parameters can be defined in condensed form as:

$$\begin{aligned}
\xi_1, \xi_2, \xi_3, \xi_4 &= \frac{1}{n}\sum_{k=1}^{n}(z_k - z_{k-1})(\cos 2\theta_k, \cos 4\theta_k, \sin 2\theta_k, \sin 4\theta_k) \\
\xi_5, \xi_6, \xi_7, \xi_8 &= \frac{2}{n^2}\sum_{k=1}^{n}(z_k^2 - z_{k-1}^2)(\cos 2\theta_k, \cos 4\theta_k, \sin 2\theta_k, \sin 4\theta_k) \\
\xi_9, \xi_{10}, \xi_{11}, \xi_{12} &= \frac{4}{n^3}\sum_{k=1}^{n}(z_k^3 - z_{k-1}^3)(\cos 2\theta_k, \cos 4\theta_k, \sin 2\theta_k, \sin 4\theta_k)
\end{aligned} \tag{2.16}$$

The *ABD* stiffness matrix is derived from the laminate invariants and lamination parameters:

$$\begin{aligned}
A_{11} &= (U_1 + \xi_1 U_2 + \xi_2 U_3)H & A_{12} = A_{21} &= (-\xi_2 U_3 + U_4)H \\
A_{16} = A_{61} &= (\xi_3 U_2/2 + \xi_4 U_3)H & A_{22} &= (U_1 - \xi_1 U_2 + \xi_2 U_3)H \\
A_{26} = A_{62} &= (\xi_3 U_2/2 - \xi_4 U_3)H & A_{66} &= (-\xi_2 U_3 + U_5)H \\
\\
B_{11} &= (\xi_5 U_2 + \xi_6 U_3)H^2/4 & B_{12} = B_{21} &= (-\xi_6 U_3)H^2/4 \\
B_{16} = B_{61} &= (\xi_7 U_2/2 + \xi_8 U_3)H^2/4 & B_{22} &= (-\xi_5 U_2 + \xi_6 U_3)H^2/4 \\
B_{26} = B_{62} &= (\xi_7 U_2/2 - \xi_8 U_3)H^2/4 & B_{66} &= (-\xi_6 U_3)H^2/4 \\
\\
D_{11} &= (U_1 + \xi_9 U_2 + \xi_{10} U_3)H^3/12 & D_{12} = D_{21} &= (U_4 - \xi_{10} U_3)H^3/12 \\
D_{16} = D_{61} &= (\xi_{11} U_2/2 + \xi_{12} U_3)H^3/12 & D_{22} &= (U_1 - \xi_9 U_2 + \xi_{10} U_3)H^3/12 \\
D_{26} = D_{62} &= (\xi_{11} U_2/2 - \xi_{12} U_3)H^3/12 & D_{66} &= (-\xi_{10} U_3 + U_5)H^3/12
\end{aligned} \tag{2.17}$$

Since the laminate invariants, U_i are material dependent properties, laminate tailoring can be easily performed through the use of lamination parameters, including opportunities of laminate stiffness properties using these are linear design variables (Fukunaga and Vanderplaats, 1991, Fukunaga and Sekine, 1994, Diaconu and Sekine, 2003, Chen, 2003, Thuwis *et al.*, 2009).

The lamination parameters of Eq. (2.16) can also be expressed in terms of the non-dimensional parameters (York, 2011):

$$\begin{aligned}
\xi_1 &= (n_+\cos(2\theta_+) + n_-\cos(2\theta_-) + n_\bigcirc\cos(2\theta_\bigcirc) + n_\bullet\cos(2\theta_\bullet))/n \\
\xi_2 &= (n_+\cos(4\theta_+) + n_-\cos(4\theta_-) + n_\bigcirc\cos(4\theta_\bigcirc) + n_\bullet\cos(4\theta_\bullet))/n \\
\xi_3 &= (n_+\sin(2\theta_+) + n_-\sin(2\theta_-) + n_\bigcirc\sin(2\theta_\bigcirc) + n_\bullet\sin(2\theta_\bullet))/n \\
\xi_4 &= (n_+\sin(4\theta_+) + n_-\sin(4\theta_-) + n_\frown\sin(4\theta_\frown) + n_\blacktriangle\sin(4\theta_\blacktriangle))/n
\end{aligned} \tag{2.18}$$

$$\begin{aligned}
\xi_5 &= (\chi_+\cos(2\theta_+) + \chi_-\cos(2\theta_-) + \chi_\bigcirc\cos(2\theta_\bigcirc) + \chi_\bullet\cos(2\theta_\bullet))/n^2 \\
\xi_6 &= (\chi_+\cos(4\theta_+) + \chi_-\cos(4\theta_-) + \chi_\bigcirc\cos(4\theta_\bigcirc) + \chi_\bullet\cos(4\theta_\bullet))/n^2 \\
\xi_7 &= (\chi_+\sin(2\theta_+) + \chi_-\sin(2\theta_-) + \chi_\bigcirc\sin(2\theta_\bigcirc) + \chi_\bullet\sin(2\theta_\bullet))/n^2 \\
\xi_8 &= (\chi_+\sin(4\theta_+) + \chi_-\sin(4\theta_-) + \chi_\frown\sin(4\theta_\frown) + \chi_\blacktriangle\sin(4\theta_\blacktriangle))/n^2
\end{aligned} \tag{2.19}$$

$$\begin{aligned}
\xi_9 &= (\zeta_+\cos(2\theta_+) + \zeta_-\cos(2\theta_-) + \zeta_\bigcirc\cos(2\theta_\bigcirc) + \zeta_\bullet\cos(2\theta_\bullet))/n^3 \\
\xi_{10} &= (\zeta_+\cos(4\theta_+) + \zeta_-\cos(4\theta_-) + \zeta_\bigcirc\cos(4\theta_\bigcirc) + \zeta_\bullet\cos(4\theta_\bullet))/n^3 \\
\xi_{11} &= (\zeta_+\sin(2\theta_+) + \zeta_-\sin(2\theta_-) + \zeta_\bigcirc\sin(2\theta_\bigcirc) + \zeta_\bullet\sin(2\theta_\bullet))/n^3 \\
\xi_{12} &= (\zeta_+\sin(4\theta_+) + \zeta_-\sin(4\theta_-) + \zeta_\frown\sin(4\theta_\frown) + \zeta_\blacktriangle\sin(4\theta_\blacktriangle))/n^3
\end{aligned} \tag{2.20}$$

The form of the lamination parameters presented above is relevant to the work presented in this thesis, where the use of non-dimensional parameters facilitate quick and easy calculation to the lamination parameters, which is then used to perform an exhaustive search of laminates with unique coupling behaviour derived from standard angle orientations.

CHAPTER 3:

Classifications of thermo-mechanically coupled laminate

This chapter presents a literature review of laminates that possess thermal and/or mechanical coupled behaviour, but with specific reference to uncoupled behaviour, where the term uncoupled here implies that no in-plane and out-of-plane coupling exists.

The discussion presented in this chapter is organised into two sections, beginning with laminate classes where the coupling matrix $\mathbf{B} = 0$, which is denoted as $\mathbf{B}_0$ using the subscript symbol notation, as given in the examples of Eqs. (2.2) and (2.3) in chapter 2. By contrast, the second section addresses laminates where the coupling matrix $\mathbf{B} \neq 0$, the various forms of which have a major influence on the relationship between in-plane and out-of-plane response. The condition for the extensional (**A**) and bending (**D**) matrices for the two respective cases can either be coupled or uncoupled, see Table 2.1. The various classes of these thermo-mechanically coupled laminate will be discussed in detailed.

3.1 Laminates with B = 0.

The Engineering Sciences Data Unit (ESDU, 1994) presented three different laminate classes possessing **B** = 0. Indeed two of these classes have been briefly introduced in Chapter 2, namely $\mathbf{A_S B_0 D_F}$ and $\mathbf{A_F B_0 D_F}$. The final class is the $\mathbf{A_S B_0 D_S}$, which is uncoupled in both extension (**A**) and bending (**D**).

The $\mathbf{A_S B_0 D_F}$ class represents the form of the ABD matrix given in Eq. (2.3) and is commonly encountered in laminates with balanced and symmetric configurations. This designation indicates that the laminate has an uncoupled extensional (**A**) stiffness matrix, but with Bending-Twisting coupling due to the fully populated bending (**D**) stiffness matrix. Symmetric laminate configurations are well-known for suppressing coupling between the in-plane to out-of-plane behaviour, **B** = 0. Balanced laminates on the other hand guarantee that the laminate is uncoupled in extension (Jones, 1975) and denoted $\mathbf{A_S}$ in accordance with the ESDU notation. Werren and Norris (1953) are credited with being the first to report on the development of this laminate class, although the work aimed to achieve quasi-isotropy also referred to as extensional isotropy (Jones, 1975). Isotropy is usually associated with conventional materials, implying the same properties in all directions, but, in this case it was observed only for the in-plane properties. The laminate configuration from Werren and Norris (1953) was based on the balanced and symmetric configuration of an $\pi/3$ laminate with 24 plies, built from four repeating groups of $[(0^o/60^o/\text{-}60^o)_4]_S$. However balanced and symmetric construction is not a necessary requirement for achieving this $\mathbf{A_S B_0 D_F}$ laminate (York and Weaver, 2010). In fact this commonly used design rule has been shown to populate only a small fraction of the entire design space of the $\mathbf{A_S B_0 D_F}$ laminate class; the remaining solutions were found to be generally non-symmetric laminates. In addition, Bending-Twisting coupling that exists within this laminate class was shown to have a detrimental effect on the compression

buckling strength of the laminate, which is often ignored by many designers, who continue to adopt the balanced and symmetric design rule.

Finally the $\mathbf{A}_F\mathbf{B}_0\mathbf{D}_F$ laminate class signifies the existence of both Bending-Twisting and Extension-Shearing coupling, resulting from full populated extensional (**A**) and bending (**D**) stiffness matrices, see Eq. (2.2). This laminate class was shown in the previous chapter to be the result of unbalanced and symmetric laminate construction (Decolon, 2002). Hearmon (1943) presented his observation on this laminate class, from which the Extension-Shearing and Bending-Twisting were achieved from off-axis alignment of the material principal axis. Indeed, applying off-axis alignment to a balanced and symmetric laminate configuration gives rise to an $\mathbf{A}_F\mathbf{B}_0\mathbf{D}_F$ laminate, except for those possessing extensionally isotropic behaviour. Greenhalgh *et al*. (1993a) developed a manufacturing method *quasi-unbalanced* that resulted in a similar coupled laminate class, for use as part of a wing-box beam exhibiting Bending-Twisting coupling. The technique is achieved by filament winding two sections with opposite helical directions, after which these sections are combined to create a two-cell box-beam having a *quasi-unbalanced* symmetric stacking sequence. The wing-box beam design was used as part of an investigation for self-correcting behaviour in aircraft wing and rotor blades; the undesirable bending and twisting excursions exposed to aircraft wings and rotor blades due to unsteady aerodynamic loadings is corrected by the opposite twisting of the wing-box to restore the wing or rotor blades to its normal position (Greenhalgh *et al*., 1993b). Fukunaga and Sekine (1994) presented work on laminate design for acquiring the desired stiffness properties in symmetric laminates with Extension-Shearing and/or Bending-Twisting coupling. The fundamental approach to the work was based on the use of lamination parameters, discussed previously in chapter 2, which were used to acquire an ideal physical laminate design i.e. tailored thickness and angle configuration of each layer within a laminate leading towards optimised coupling responses.

The fully uncoupled laminate class given by ESDU has the designation $\mathbf{A}_S\mathbf{B}_0\mathbf{D}_S$ and is referred to as a specially orthotropic laminate; both descriptions are also synonymous with fully orthotropic laminate (York, 2009). Caprino and Visconti (1982) presented a design rule for achieving an orthotropic laminate, for which the Bending-Twisting is eliminated using an anti-symmetric stacking sequence, used by many (Jones, 1999, Niu, 1999) to derive laminates with $B \neq 0$. The rule proposed the use of two symmetric angle ply sub-laminates leading to the following anti-symmetric configuration:

$$[+--+-++-]_T \equiv [\pm/\mp]_A \tag{3.1}$$

Hence for this fully uncoupled laminate, a minimum of 8 plies is required. In fact the laminate configuration given in Eq. (3.1) was discovered in the original work by Bartholomew (1977), in which a series of laminates were derived, consisting of symmetric and anti-symmetric stacking sequences with fully uncoupled orthotropic properties. These laminate stacking sequence listings with up to 21 plies later published in ESDU (1982), from which the minimum number of plies observed for this laminate class can be achieved with the anti-symmetric configuration of Eq. (3.1) for the even ply numbers, and Eq. (3.2) for odd number of plies.

$$[+\theta/-\theta/-\theta/*/+\theta/+\theta/-\theta] \tag{3.2}$$

Note that the use of the asterisk (*) in the 7-ply stacking sequence of Eq. (3.2) denotes either a 0 or 90º layer.

Lagace *et al*. (1986) addressed the buckling response of various non-symmetric laminates. A 12-ply fully orthotropic laminate, $[0_3/90_3]_S$, served as a benchmark laminate to the other

coupled laminates investigated in the study. However no information was given concerning the derivation of these stacking sequences.

Bartholomew (1977) observed that the design space for fully orthotropic laminates is dominated by the anti-symmetric laminate configurations. Indeed this had also been the observation of more recent work from York (2009), addressing subgroups within this fully orthotropic laminate class that includes extensionally isotropic laminates (EILs) designated as $\mathbf{A}_I\mathbf{B}_0\mathbf{D}_S$, fully isotropic laminates (FILs) designated as $\mathbf{A}_I\mathbf{B}_0\mathbf{D}_I$, and quasi-homogeneous orthotropic laminates (QHOLs). Note that the subscript 'I' was adopted in the notation presented, which implies isotropic stiffness properties. The EILs that possess isotropic behaviour, in the extensional stiffness (**A**) only, satisfy the following conditions:

$$A_{11} = A_{22}$$

and

$$A_{66} = (A_{11} - A_{12}) / 2 \tag{3.3}$$

Meanwhile in the case of FILs, elements of the bending stiffness (**D**) are concomitant with the extensional stiffness (**A**), through

$$D_{ij} = A_{ij}H^2 / 12 \tag{3.4}$$

where H is the total thickness of the laminate.

Fukunaga (1990) presented work on developing approximations to FILs based on the design configuration of Eq. (3.1), where this was achieved using free form angles and ply thickness variations and then applying an optimisation routine to minimise the lamination parameters i.e. $\xi_i = 0$ (i = 1, 12). By contrast, Wu and Avery (1992) adopted the strategy of *shuffling* the layers for the top half of a symmetric EILs (Werren and Norris, 1953) to

satisfy the condition presented in Eq. (3.3) and (3.4). This resulted in the identification of stacking sequences for $\pi/3$ FILs with a minimum of 36 plies. However relaxing this symmetry constraint led to the identification of 18-ply FILs (Vannucci and Verchery, 2002).

Fully isotropic laminates offer and ideal comparator with conventional materials and can also be particularly useful as benchmark configurations for which other laminate classes (uncoupled and coupled) can be assessed. However given the limited availability of FIL configurations, which are possible only for certain ply number groupings, equivalent fully isotropic laminates have been introduced (York, 2010). The equivalent extensionally isotropic stiffness properties were created by Tsai and Hahn (1980):

$$\mathbf{A}_{iso} = \mathbf{A}_{11} = \mathbf{A}_{22} = E_{iso}H / (1 - \nu_{iso}^2) = U_1 H \tag{3.5}$$

$$\mathbf{A}_{12} = \nu_{iso}\mathbf{A}_{11} \tag{3.6}$$

$$\mathbf{A}_{66} = U_5 H \tag{3.7}$$

from which the elements for the coupling ($\mathbf{B}_{iso}$) and bending ($\mathbf{D}_{iso}$) follow:

$$B_{Iso} = E_{Iso}H^2/(1 - \nu_{Iso}^2)/4 = U_1 H^2/4 \tag{3.8}$$

$$D_{Iso} = E_{Iso}H^3/(1 - \nu_{Iso}^2)/12 = U_1 H^3/12 \tag{3.9}$$

The QHOLs, first introduced by Kandil and Verchery (1988), is synonymous to quasi homogenous anisotropic laminate later introduced by Wu and Avery (1992). QHOLs are unique due to the concomitant relationship of the extensional (**A**) to bending (**D**) stiffness

properties, i.e. the laminate satisfies the condition $D_{ij} = A_{ij} H^2/12$ of Eq. (3.4) but not Eq. (3.3) i.e., $A_{66} \neq (A_{11} - A_{12})/2$. The QHOLs present some benefits to laminate designers when optimising the extensional (**A**) properties of the laminate is of major interest, since the bending (**D**) properties are calculated directly from the extensional (**A**) stiffnesses calculated using Eq. (3.4).

A novel class of uncoupled laminate has been the subject of recent research by York (2015), which complements the list of uncoupled laminate classes given earlier in ESDU (1994). This new class of uncoupled laminate is classified as $\mathbf{A}_F\mathbf{B}_0\mathbf{D}_S$, indicating Extension-Shearing coupling in the laminate but uncoupled in bending. Definitive listings of laminate solutions with up to 21 plies are derived from standard angle orientations i.e. $+\theta$, $-\theta$, 0, and 90º. Here the symmetry design rule was again relaxed, revealing that the entire design space was populated with non-symmetric laminates. In addition, through a like with like comparison study, the $\mathbf{A}_F\mathbf{B}_0\mathbf{D}_S$ laminate performed better than the $\mathbf{A}_F\mathbf{B}_0\mathbf{D}_F$ in terms of the buckling strength performance, due to the absence of the Bending-Twisting coupling.

Figure 3.1 shows the free thermal response of the four classes of B = 0 laminate (York, 2010). The figures are presented in the form of the ABD with subscript symbol notation, with the first three figures give the classification of the uncoupled classes presented earlier from ESDU (1994), while the last shows the novel classification from York (2008). Note that the stacking sequences presented, represent the minimum number of plies possible for each class, where symbols + and − are used to represent standard angle plies, +45 and −45°, while ○ and ● are used to represent cross plies, 0 and 90°. The stacking sequence of Fig. 3.1(a), for the fully orthotropic laminate class, is the stacking sequence from Bartholomew (1977) mentioned earlier in Eq. (3.2). Meanwhile the second figure showing the case for the $\mathbf{A}_S\mathbf{B}_0\mathbf{D}_F$ class is given by a 4-ply balanced and symmetric stacking

sequence. Figure 3.1(c) presents a 2-ply unbalanced symmetric stacking sequence for $\mathbf{A_F B_0 D_F}$ class.

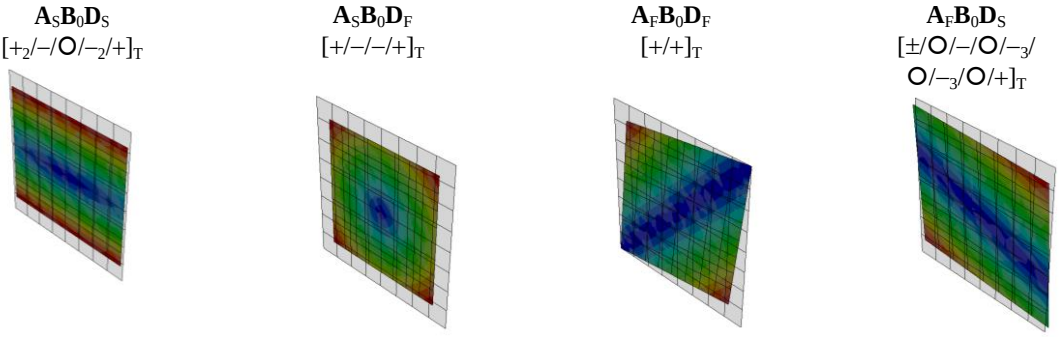

Figure 3.1 – Laminate classes with B = 0, using the ABD subscript notation of the laminate classification presented by ESDU (1994). Figure (d) presents the novel uncoupled laminate class from York (2008). Note that the stacking sequences shown represent solution from the minimum ply number grouping of the respective class.

Note that applying off-axis alignment of any of the stacking sequences for the uncoupled classes shown in Fig. 3.1 will generally result in stiffness properties of the $\mathbf{A_F B_0 D_F}$ class; exceptions include EILs and FILs.

3.2 Laminates with B ≠ 0.

In addition to the Extension-Shearing and Bending-Twisting coupling discussed in the previous section, a laminate is generally said to be coupled when the coupling matrix **B** ≠ 0. The form of the coupling (**B**) matrix has a major influence on the outcome of the interactions between in-plane and out-of-plane coupling. Indeed ESDU (1994) presented an **ABD** subscript notation to differentiate between the five distinct forms of the coupling (**B**) matrix. This is summarised in Table 3.1, following the same format presented earlier for the case of extensional (**A**) and bending (**D**) stiffnesses in Table 2.1. Combining these forms of the coupling (**B**) with those of the extensional (**A**) and bending (**D**) in Table 2.1, leads to the seven coupled laminate classes from ESDU (1994), summarized in Table 3.2.

Table 3.1 – The subscript notation, response based labelling and associated form of the coupling stiffness (B).

Subscript notation (ESDU, 1994)	Response-based labelling (York, 2010)	Matrix form
$\mathbf{B}_l$	Extension-Bending; *E-B*	$\begin{bmatrix} B_{11} & 0 & 0 \\ 0 & B_{22} & 0 \\ 0 & 0 & 0 \end{bmatrix}$
$\mathbf{B}_t$	Extension-Twisting and Shearing-Bending; *E-T-S-B*	$\begin{bmatrix} 0 & 0 & B_{16} \\ 0 & 0 & B_{26} \\ B_{16} & B_{26} & 0 \end{bmatrix}$
$\mathbf{B}_{lt}$	Extension-Bending, Extension-Twisting and Shearing-Bending; *E-B-E-T-S-B*	$\begin{bmatrix} B_{11} & 0 & B_{16} \\ 0 & B_{22} & B_{26} \\ B_{16} & B_{26} & 0 \end{bmatrix}$
$\mathbf{B}_S$	Extension-Bending and Shearing-Twisting; *E-B-S-T*	$\begin{bmatrix} B_{11} & B_{12} & 0 \\ B_{12} & B_{22} & 0 \\ 0 & 0 & B_{66} \end{bmatrix}$
$\mathbf{B}_F$	Extension-Bending, Shearing-Bending, Extension-Twisting, and Shearing-Twisting; *E-B-S-B-E-T-S-T*	$\begin{bmatrix} B_{11} & B_{12} & B_{16} \\ B_{12} & B_{22} & B_{26} \\ B_{16} & B_{26} & B_{66} \end{bmatrix}$

Table 3.2 – Laminate configurations and the response based labelling for the seven classes of coupled laminates presented by ESDU (1994).

Subscript Notation	Laminate Configurations (ESDU, 1994)	Response based labelling (York, 2010)
$\mathbf{A}_S\mathbf{B}_l\mathbf{D}_S$	[0/90] [0/0/90/0] [90/0/90/0]	Extension-Bending; *E-B*
$\mathbf{A}_S\mathbf{B}_t\mathbf{D}_S$	[45/–45] [30/–30/30/–30] [30/30/–30/–30]	Extension-Twisting and Shearing-Bending; *E-T*-*S-B*
$\mathbf{A}_S\mathbf{B}_{lt}\mathbf{D}_S$	[0/45/–45/90]	Extension-Bending, Extension-Twisting and Shearing-Bending; *E-B*-*E-T*-*S-B*
$\mathbf{A}_S\mathbf{B}_S\mathbf{D}_S$	[0/30/–30/–30/0/30/30/–30]	Extension-Bending and Shearing-Twisting; *E-B*-*S-T*
$\mathbf{A}_S\mathbf{B}_F\mathbf{D}_F$	[0/45/–45]	Extension-Bending, Shearing-Bending, Extension-Twisting, Shearing-Twisting and Bending-Twisting; *E-B*-*S-B*-*E-T*-*S-T*:*B-T*
$\mathbf{A}_F\mathbf{B}_t\mathbf{D}_F$	[30/–30/–30]	Extension-Shearing, Extension-Twisting, Shearing-Bending and Bending-Twisting; *E-S*:*E-T*-*S-B*:*B-T*
$\mathbf{A}_F\mathbf{B}_F\mathbf{D}_F$	[30/–30/0/–30]	Extension-Shearing, Extension-Bending, Shearing-Bending, Extension-Twisting, Shearing-Twisting and Bending-Twisting; *E-S*:*E-B*-*S-B*-*E-T*-*S-T*:*B-T*

Recent work (York, 2010) on coupled laminates has expanded the search, leading to the discovery of thirteen additional coupled laminate classes. The thermal responses of the twenty-four laminate classes, including the seven previously defined by ESDU, are shown in Figs. 3.2 to 3.5. Figures 3.2 and 3.3 contain combinations that are extensionally uncoupled, i.e. all designations begin with $\mathbf{A}_S$, whilst Figs. 3.4 and 3.5 contain combinations with Shearing-Extension coupling, i.e., all designations begin with $\mathbf{A}_F$. Laminates in Figs 3.2 and 3.5 are uncoupled in bending ($\mathbf{D}_S$), whereas Figs 3.3 and 3.4

contain combinations with Bending-Twisting coupling ($\mathbf{D}_F$). The complex forms of the coupling (**B**) stiffness matrix appear in the same (row) location in each figure, beginning and ending with the Extension-Bending ($\mathbf{B}_l$) and fully coupled form ($\mathbf{B}_F$), respectively. The example stacking sequences adjacent to each illustration are representative of the minimum ply number grouping for each laminate class; for angle ply laminates with or without cross plies, where symbols +, –, ○, ● represent standard angle ply orientations +45, –45, 0 and 90°, respectively. Note that the contours in these figures represent the stress field distribution, due to the free thermal contraction response.

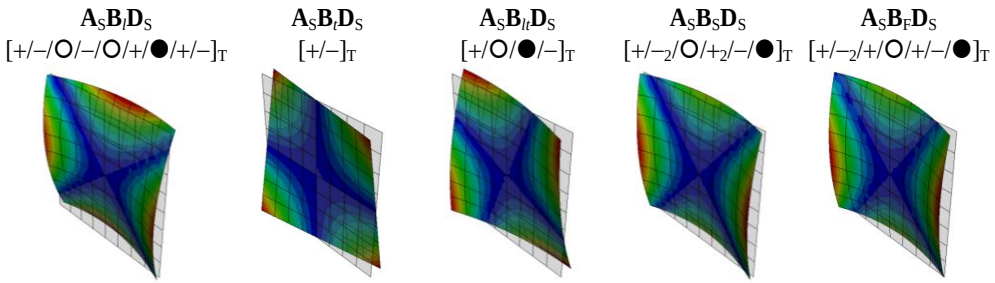

Figure 3.2 – Isolated coupling responses, due to free thermal contraction, for: ($A_SB_lD_S$) *B-E* laminate with Bending-Extension coupling; ($A_SB_tD_S$) *B-S*-*T-E* laminate with Bending-Shearing and Twisting-Extension coupling; ($A_SB_{lt}D_S$) *B-E*-*B-S*-*T-E* laminate with Bending-Extension, Bending-Shearing and Twisting-Extension coupling; ($A_SB_SD_S$) *B-E*-*T-S* laminate with Bending-Extension and Twisting-Shearing coupling and; ($A_SB_FD_S$) *B-E*-*B-S*-*T-E*-*T-S* or fully coupled laminate, (after York, 2010).

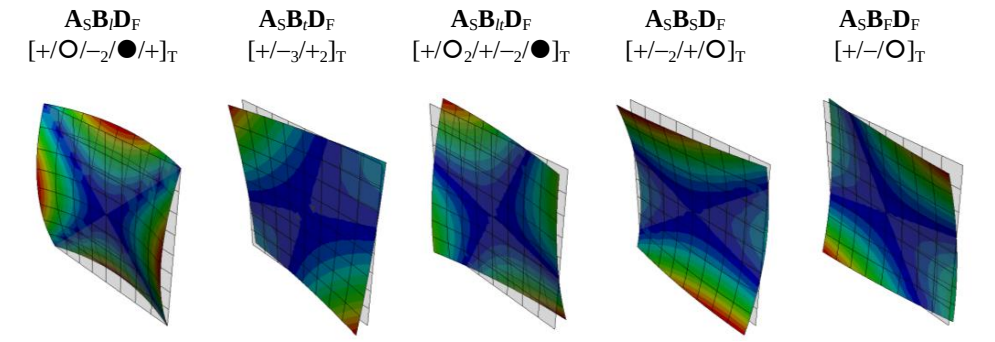

Figure 3.3 – Coupling responses, due to free thermal contraction, for laminates with Bending-Twisting coupling *B-T* combined with: ($A_SB_lD_F$) *B-E* or Bending-Extension coupling; ($A_SB_tD_F$) *B-S*-*T-E* or Bending-Shearing and Twisting-Extension coupling; ($A_SB_{lt}D_F$) *B-E*-*B-S*-*T-E* or Bending-Extension, Bending-Shearing and Twisting-Extension coupling; ($A_SB_SD_F$) *B-E*-*T-S* or Bending-Extension and Twisting-Shearing coupling and; ($A_SB_FD_F$) *B-E*-*B-S*-*T-E*-*T-S* or fully coupled laminate, (after York, 2010).

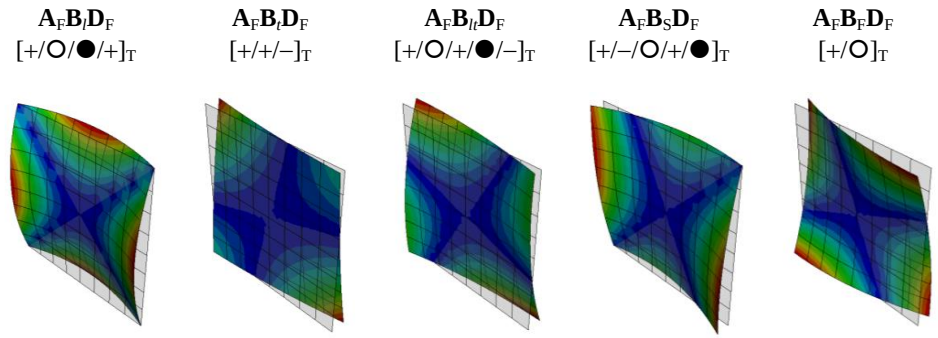

Figure 3.4 – Coupling responses, due to free thermal contraction, for laminates with Extension-Shearing and Bending-Twisting coupling *E-S*;*B-T* combined with: ($A_FB_lD_F$) *B-E* or Bending-Extension coupling; ($A_FB_tD_F$) *B-S*-*T-E* or Bending-Shearing and Twisting-Extension coupling; ($A_FB_{lt}D_F$) *B-E*-*B-S*-*T-E* or Bending-Extension, Bending-Shearing and Twisting-Extension coupling; ($A_FB_SD_F$) *B-E*-*T-S* or Bending-Extension and Twisting-Shearing coupling and; ($A_FB_FD_F$) *B-E*-*B-S*-*T-E*-*T-S* or fully coupled laminate, (after York, 2010).

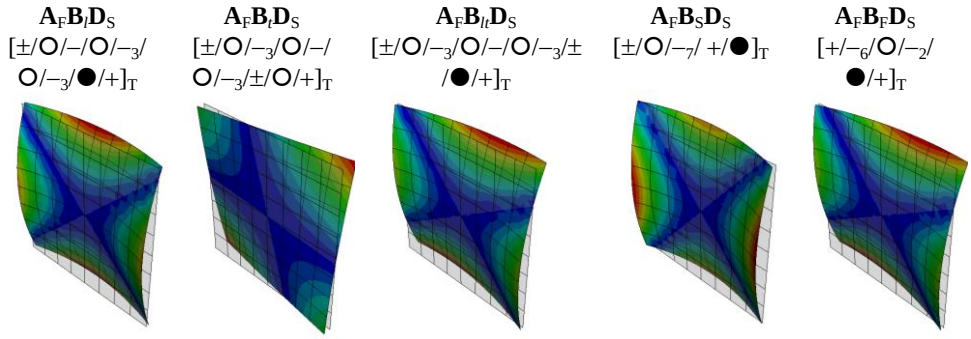

Figure 3.5 – Coupling responses, due to free thermal contraction, for laminates with Extension-Shearing coupling *E-S* combined with: ($A_FB_lD_S$) *B-E* or Bending-Extension coupling; ($A_FB_tD_S$) *B-S*-*T-E* or Bending-Shearing and Twisting-Extension coupling; ($A_FB_{lt}D_S$) *B-E*-*B-S*-*T-E* or Bending-Extension, Bending-Shearing and Twisting-Extension coupling; ($A_FB_SD_S$) *B-E*-*T-S* or Bending-Extension and Twisting-Shearing coupling and; ($A_FB_FD_S$) *B-E*-*B-S*-*T-E*-*T-S* or fully coupled laminate, (after York, 2010).

It is important to note that the thermal responses of the coupled laminates shown in Figs 3.2 to 3.5 are performed on a small element of a laminate, representing a larger size laminate. Hence the response observed on the deformed shapes illustrated in Figs. 3.2 to 3.5 are saddle shaped, as predicted by classical laminate theory (CLT). The prediction of the final cured shape of non-symmetric laminates has been the subject of investigation by Hyer (1981a, 1981b, 1982).

Hyer (1981b) observed the cured shapes of a non-symmetric cross-ply laminates i.e. laminates consisting of 0 and 90° ply orientations tend to be largely cylindrical in nature

rather than the saddle shape predicted by CLT. These observations were explained in term of the relationship between the laminate side length and the laminate curvatures respectively, as illustrated in Fig. 3.6. Although Fig. 3.6 is describe a particular cross-ply non-symmetric laminate with the stacking sequence $[0°/0°/90°/90°]_T$, such behaviour were observed across a broad range of other non-symmetric laminates (Dano and Hyer, 2002, Jun and Hong, 1992, Jun and Hong, 1990). For this particular example, saddle shape as predicted from the classical laminate theory, was observed in specimen with side lengths of upto 35mm. Above this side length, trifurcation occurs, although line **BD,** representing the continuation of the saddle shaped solution was recognised to be unstable.

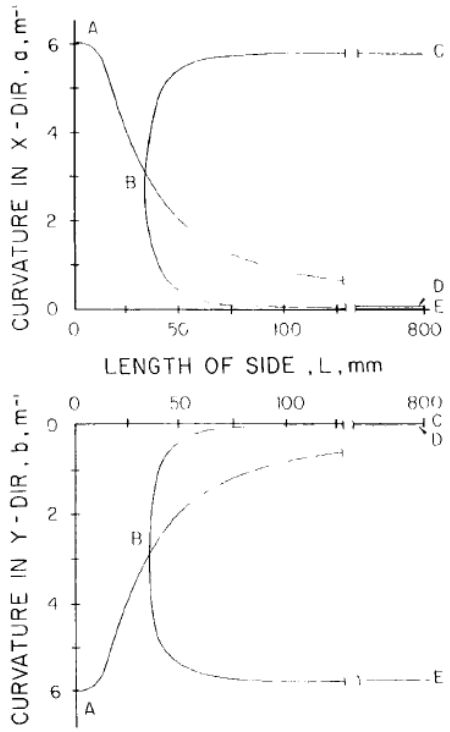

Figure 3.6 – The cured shape solutions for a non-symmetric laminate, $[0°/0°/90°/90°]_T$, (after Hyer, 1982).

The branches formed by the line **BC** and **BE** represent a stable configuration, resulting in a cylindrical cured shape, with the line **BC** indicating a larger curvature in the x-direction and a smaller curvature in the y-direction, from which the values asymptotically approach a constant value, with maximum curvature in the x-direction and zero curvature in the y-

direction for increasing side length, this relationship is reversed in branch **BE**. The cured shapes prescribed in Fig. 3.6 can also be explained through the illustration given in Fig. 3.7 (a), where: shape (a) governs the condition at uncured state; shape (b) depicts the saddle shape as predicted from CLT, which has been shown to be true for non-symmetric laminates with side-length less than the identified critical length (denoted by point **B** from Fig. 3.6); shapes (c) and (d) show the two possible cylindrical shapes obtained for laminate side lengths exceeding the critical length.

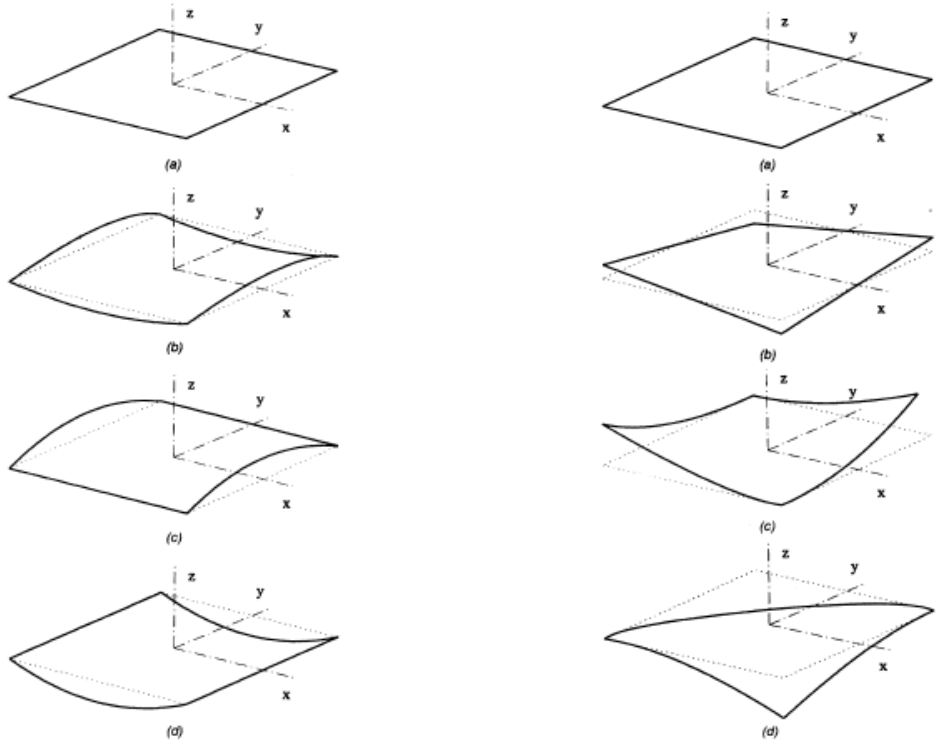

(a) (b)

Figure 3.7 – Room temperature shapes of: (a) cross-ply laminates; (b) angle-ply laminates, (after Hyer, 1981).

Meanwhile Fig. 3.7 (b) follows the same logic, but now shown for non-symmetric angle-ply laminates. It should be noted (Dano and Hyer, 2002, Hyer, 1981b) that it is possible to obtain one cylindrical shape from the other through *snap-through* action. The factors influencing the occurrence of one cylindrical shape in favour of the other during manufacturing have been highlighted by Betts *et al*. (2010).

Rousseau *et al*. (2011) performed an experimental observation on the cured shape of coupled laminates defined in Figs. 3.2 to 3.5, where majority of the results were observed to yield cylindrical shapes similar to those illustrated in Fig. 3.7 (a) or (b). The final cured shape of the coupled laminates from Rousseau *et al*. (2011) are illustrated in Figs. 3.8 to 3.11, which are presented in an identical manner to the CLT predictions presented in Figs. 3.2 to 3.5 respectively. Analytical (Betts *et al*., 2010) and numerical (Schlecht and Schulte, 1999, Schlecht *et al*., 1995), predictions of these deformations have been shown to produce good agreement with experimental results.

$\mathbf{A_S B_l D_S}$ $\mathbf{A_S B_t D_S}$ $\mathbf{A_S B_{lt} D_S}$ $\mathbf{A_S B_S D_S}$ $\mathbf{A_S B_F D_S}$

Figure 3.8 – Cured shape responses of square plate, for: ($A_S B_l D_S$) *B-E* laminate with Bending-Extension coupling; ($A_S B_t D_S$) *B-S*-*T-E* laminate with Bending-Shearing and Twisting-Extension coupling; ($A_S B_{lt} D_S$) *B-E*-*B-S*-*T-E* laminate with Bending-Extension, Bending-Shearing and Twisting-Extension coupling; ($A_S B_S D_S$) *B-E*-*T-S* laminate with Bending-Extension and Twisting-Shearing coupling and; ($A_S B_F D_S$) *B-E*-*B-S*-*T-E*-*T-S* or fully coupled laminate.

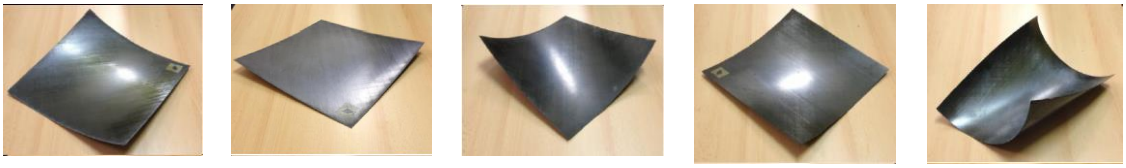

$\mathbf{A_S B_l D_F}$ $\mathbf{A_S B_t D_F}$ $\mathbf{A_S B_{lt} D_F}$ $\mathbf{A_S B_S D_F}$ $\mathbf{A_S B_F D_F}$

Figure 3.9 – Cured shape responses of square plate for laminates having Bending-Twisting coupling (D_F) *B-T* combined with: ($A_S B_l D_F$) *B-E* or Bending-Extension coupling; ($A_S B_t D_F$) *B-S*-*T-E* or Bending-Shearing and Twisting-Extension coupling; ($A_S B_{lt} D_F$) *B-E*-*B-S*-*T-E* or Bending-Extension, Bending-Shearing and Twisting-Extension coupling; ($A_S B_S D_F$) *B-E*-*T-S* or Bending-Extension and Twisting-Shearing coupling and; ($A_S B_F D_F$) *B-E*-*B-S*-*T-E*-*T-S* or fully coupled laminate.

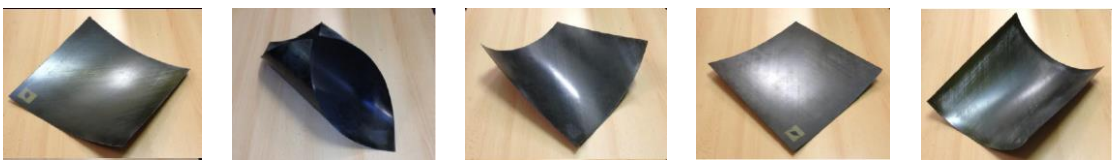

$\mathbf{A_F B_l D_F}$ $\mathbf{A_F B_t D_F}$ $\mathbf{A_F B_{lt} D_F}$ $\mathbf{A_F B_S D_F}$ $\mathbf{A_F B_F D_F}$

Figure 3.10 – Cured shape responses of square plate for laminates having Extension-Shearing (A_F) *E-S* and Bending-Twisting (D_F) *B-T* coupling combined with: ($A_F B_l D_F$) *B-E* or Bending-Extension coupling; ($A_F B_t D_F$) *B-S*-*T-E* or Bending-Shearing and Twisting-Extension coupling; ($A_F B_{lt} D_F$) *B-E*-*B-S*-*T-E* or Bending-Extension, Bending-Shearing and Twisting-Extension coupling; ($A_F B_S D_F$) *B-E*-*T-S* or Bending-Extension and Twisting-Shearing coupling and; ($A_F B_F D_F$) *B-E*-*B-S*-*T-E*-*T-S* or fully coupled laminate.

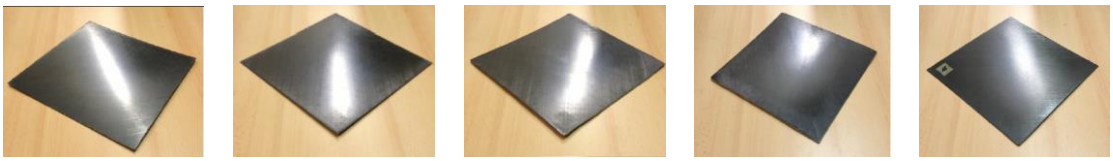

$\mathbf{A_F B_l D_S}$ $\mathbf{A_F B_t D_S}$ $\mathbf{A_F B_{lt} D_S}$ $\mathbf{A_F B_S D_S}$ $\mathbf{A_F B_F D_S}$

Figure 3.11 – Cured shape responses of square plate for laminates having Extension-Shearing (A_F) *E-S* coupling combined with: ($A_F B_l D_S$) *B-E* or Bending-Extension coupling; ($A_F B_t D_S$) *B-S*-*T-E* or Bending-Shearing and Twisting-Extension coupling; ($A_F B_{lt} D_S$) *B-E*-*B-S*-*T-E* or Bending-Extension, Bending-Shearing and Twisting-Extension coupling; ($A_F B_S D_S$) *B-E*-*T-S* or Bending-Extension and Twisting-Shearing coupling and; ($A_F B_F D_S$) *B-E*-*B-S*-*T-E*-*T-S* or fully coupled laminate.

Whitney and Leissa (1969) formulated a closed form solution to observe the influence of the Extension-Bending coupling for this $\mathbf{A_S B_l D_S}$ laminate class under transverse loading. The findings revealed a significant increase in the static deflection in comparison to an orthotropic plates, i.e., when the coupling is neglected (Whitney, 1969). A similar closed form solution was developed by the author but for laminates exhibiting Extension-Twisting and shearing-bending coupling i.e. $\mathbf{A_S B_t D_S}$ coupled laminates, from which a similar conclusion was drawn. In addition, a decrease in the fundamental vibration frequencies and buckling loads was also observed (Whitney and Leissa, 1969) as a consequence of the coupling attribute from these coupled laminate classes i.e. $\mathbf{A_S B_l D_S}$ and $\mathbf{A_S B_t D_S}$. However the effort of quantifying the buckling strength of the whole spectrum of the Extension-Twisting and shearing-bending ($\mathbf{A_S B_t D_S}$) coupled laminates possessing HTCS properties has only recently been presented (Shamsudin *et al*., 2013a), which will be discussed in the next chapter.

Extension-Twisting (and Shearing-Bending) coupled laminates ($\mathbf{A_S B_t D_S}$) with HTCS properties have had an important implication on the perspective of coupled laminates following their initial discovery by (Winckler, 1985), and studies into possible practical application (Nixon, 1987). Others have investigated various means of improving the performance of the Extension-Twisting coupling, eg. to achieve optimum twisting effect from the $\mathbf{A_S B_t D_S}$ coupled laminates (Haynes and Armanios, 2010, Chen, 2003). Haynes

and Armanios (2011) also considered the optimisation of Extension-Twisting, together with Bending-Twisting coupling i.e. $\mathbf{A}_S\mathbf{B}_t\mathbf{D}_F$, searching for stacking sequence solutions that give optimum condition for both Extension-Twisting and Bending-Twisting coupling. However, the authors (Haynes and Armanios, 2011) found that such optimal conditions cannot be fulfilled simultaneously.

The unique cured shape profiles of the coupled laminates in Figs. 3.8 to 3.11, may provide an enabling technology in various applications, but require further research. Alternatively mechanically coupled laminates possessing HTCS properties are immediately applicable. HTCS coupled laminates are immune to thermal warping distortions that result from high temperature curing during manufacturing, while at the same time preserve the mechanical coupling attributes within the laminates. Coupled laminates possessing these attractive characteristics are a key part of the current research work presented in this thesis and the requirements for achieving coupled HTCS laminates will be addressed in the following chapter.

CHAPTER 4:

Mechanically coupled laminates with Hygro-Thermally Curvature-Stable (HTCS) conditions.

This chapter begins by addressing some of the theories that have been presented in the literature for achieving coupled laminates with hygro-thermally curvature-stable (HTCS) conditions. Attention is then turned towards the strategy adopted in the current work to identify the so-called *parent classes* of coupled laminate possessing HTCS properties; derived from standard ply angle orientations.

The work found in the literature addressing coupled laminates with HTCS conditions has been motivated from an early discovery made by Winckler (1985), who proposed the concept of bonding two sub-laminates possessing Extension-Shearing coupling of equal and opposite magnitude, resulting in a laminate with Extension-Twisting and Shearing-Bending coupling or $\mathbf{A}_S\mathbf{B}_t\mathbf{D}_S$ laminates. This concept has been explained illustratively in Figs. 1.7(a) and (b). A more crucial observation by Winckler was the fact that thermal stability exists within the sub-laminates, enabling this Extension-Twisting and Shearing-Bending coupled laminate to possess immunity to the thermal warping distortion that

would otherwise result from the high temperature curing process, i.e. the laminate remains flat.

The lamination parameters given in Eq. (2.16), developed originally by Tsai and Hahn (1980) have had a major influence on subsequent developments in HTCS laminate design by Chen (2003) and Cross *et al.* (2008), assuming uniform temperature and/or moisture change. Chen (2003) presented three theories in relation to HTCS laminates where:

a) a laminate is considered HTCS, if the lamination parameters satisfy the following conditions:

$$\xi_1 = \xi_3 = \xi_5 = \xi_7 = 0 \tag{4.1}$$

b) if a laminate possesses HTCS, either the condition given in Eq. (4.1) is fulfilled or the laminate possesses equal thermal expansion coefficients in the two orthogonal direction:

$$\alpha_{11} = \alpha_{22} \tag{4.2}$$

c) a laminate composed of HTCS sub-laminates will remain HTCS at the laminate level. Weaver (2005) extended the work of Chen (2003) and presented similar HTCS conditions, however, the rules are stated in the form of the thermal force and moment vectors:

$$\begin{gathered} N_x^{Thermal} = N_y^{Thermal} \\ N_{xy}^{Thermal} = M_x^{Thermal} = M_y^{Thermal} = M_{xy}^{Thermal} = 0 \end{gathered} \tag{4.3}$$

The thermal forces and moment vectors can be calculated from the laminate invariants in Eq. (2.15) and lamination parameters in Eq. (2.16), as:

$$\begin{Bmatrix} N_x^{Thermal} \\ N_y^{Thermal} \\ N_{xy}^{Thermal} \end{Bmatrix} = \frac{H}{2} \begin{Bmatrix} (U_1+U_4)(\alpha_1+\alpha_2)+U_2(\alpha_1-\alpha_2)+\xi_1[U_2(\alpha_1+\alpha_2)+(U_1+2U_3-U_4)(\alpha_1-\alpha_2)] \\ (U_1+U_4)(\alpha_1+\alpha_2)+U_2(\alpha_1-\alpha_2)-\xi_1[U_2(\alpha_1+\alpha_2)+(U_1+2U_3-U_4)(\alpha_1-\alpha_2)] \\ \xi_3[U_2(\alpha_1+\alpha_2)+(U_1+2U_3-U_4)(\alpha_1-\alpha_2)] \end{Bmatrix} \Delta T$$

$$\begin{Bmatrix} M_x^{Thermal} \\ M_y^{Thermal} \\ M_{xy}^{Thermal} \end{Bmatrix} = \frac{H^2}{8} \begin{Bmatrix} \xi_5[U_2(\alpha_1+\alpha_2)+(U_1+2U_3-U_4)(\alpha_1-\alpha_2)] \\ -\xi_5[U_2(\alpha_1+\alpha_2)+(U_1+2U_3-U_4)(\alpha_1-\alpha_2)] \\ \xi_7[U_2(\alpha_1+\alpha_2)+(U_1+2U_3-U_4)(\alpha_1-\alpha_2)] \end{Bmatrix} \Delta T \quad (4.4)$$

where H is the total thickness of the laminate and ΔT is the temperature difference.

Diaconu and Sekine (2003) extended these lamination parameter relationships to account for linear through thickness variation of temperature and/or moisture. However, the correct equations are to be found in an erratum (Diaconu and Sekine, 2004), which inspired Weaver (2005) to derive the uniform temperature case; independently confirming the findings of others (Tsai and Hahn, 1980, Chen, 2003).

It should be noted that moisture equilibrium is achieved over an extended time period and with uncertainties regarding uniformity of distribution, whereas in thin laminate construction, a uniform temperature state is achieved almost instantaneously. Indeed, the case of uniform temperature change has been revisited more recently by York (2011), demonstrating the entire range of mechanical coupling mechanisms that can be achieved with immunity to warping distortion. York (2011) also presented the necessary conditions for HTCS, from which the laminate stiffness properties are observed to be square symmetric in the extensional (**A**) and coupling (**B**) matrices, along with fulfilling the conditions of Eq. (4.3). The term square symmetric implies equal stiffness on principal axes (Tsai and Hahn, 1980), or in other words the elements of the extensional stiffness matrix $\mathbf{A}_{11} = \mathbf{A}_{22}$ and coupling stiffness matrix $\mathbf{B}_{11} = \mathbf{B}_{22}$. It is worth noting, that the bending (**D**) stiffness does not influence the HTCS condition.

4.1 HTCS laminate design

To demonstrate the rules of HTCS mathematically, consider an example for carbon-fibre/epoxy material, calculated for a set of 12-ply laminates with the following stacking sequences:

$$\begin{aligned} &\text{S1} && [-/+/+/\bigcirc/-/-/+/\bullet/\bullet/\bullet/\bigcirc/\bigcirc]_T \\ &\text{S2} && [-/+/+/-/+/-/-/+/\bullet/\bigcirc/\bigcirc/\bullet]_T \end{aligned} \tag{4.5}$$

For convenience the first laminate stacking sequence is labelled by S1, and S2 for the second. The assessment begins by calculating the non-dimensional parameters for both laminates, where the procedures for performing this were discussed in Chapter 2. A summary of the calculation of the non-dimensional parameters for laminate S1 is given in Table 4.1, from which the following values arise: for extensional stiffness (**A**) $n_+ = 3$, $n_- = 3$, $n_\bigcirc = 3$ and $n_\bullet = 3$; for coupling stiffness (**B**) χ_+ (= $2\times\sum B_+$) = -30, χ_- (= $2\times\sum B_-$) = -30, $\chi_\bigcirc$ (= $2\times\sum B_\bigcirc$) = 30 and $\chi_\bullet$ (= $2\times\sum B_\bullet$) = 30 and; for bending (**D**) ζ_+ (= $4\times\sum D_+$) = 396, ζ_- (= $4\times\sum D_-$) = 396, $\zeta_\bigcirc$ (= $4\times\sum D_\bigcirc$) = 684 and $\zeta_\bullet$ (= $4\times\sum D_\bullet$) = 252.

Similarly for laminate S2, using the values calculated from Table 4.2 result in the following values for the non-dimensional parameters: for extensional stiffness (**A**) $n_+ = 4$, $n_- = 4$, $n_\bigcirc = 2$ and $n_\bullet = 2$; for coupling stiffness (**B**) χ_+ (= $2\times\sum B_+$) = -32, χ_- (= $2\times\sum B_-$) = -32, $\chi_\bigcirc$ (= $2\times\sum B_\bigcirc$) = 32 and $\chi_\bullet$ (= $2\times\sum B_\bullet$) = 32 and; for bending stiffness (**D**) ζ_+ (= $4\times\sum D_+$) = 448, ζ_- (= $4\times\sum D_-$) = 448, $\zeta_\bigcirc$ (= $4\times\sum D_\bigcirc$) = 392 and $\zeta_\bullet$ (= $4\times\sum D_\bullet$) = 440.

Applying these non-dimensional parameters in Eqs. (2.18) to (2.20), gives the values for the lamination parameters for both laminate S1 and S2, where the non-zero lamination parameters are given, respectively as:

Table 4.1 – Summary of the non-dimensional parameters for the extensional (A), coupling (B), and bending (D) stiffness, calculated for laminate S1 [–/+/+/○/–/–/+/●/●/●/○/○]$_T$.

			A					B					D			
Ply	(°)	(z_k-z_{k-1})	$A\Sigma_+$	$A\Sigma_-$	$A\Sigma_\circ$	$A\Sigma_\bullet$	$(z^2_k-z^2_{k-1})$	$B\Sigma_+$	$B\Sigma_-$	$B\Sigma_\circ$	$B\Sigma_\bullet$	$(z^3_k-z^3_{k-1})$	$D\Sigma_+$	$D\Sigma_-$	$D\Sigma_\circ$	$D\Sigma_\bullet$
			3	**3**	**3**	**3**		**-15**	**-15**	**15**	**15**		**99**	**99**	**171**	**63**
1	–	1		1			-11		-11			91		91		
2	+	1	1				-9	-9				61	61			
3	+	1	1				-7	-7				37	37			
4	○	1			1		-5			-5		19			19	
5	–	1		1			-3		-3			7		7		
6	–	1		1			-1		-1			1		1		
7	+	1	1				1	1				1	1			
8	●	1				1	3				3	7				7
9	●	1				1	5				5	19				19
10	●	1				1	7				7	37				37
11	○	1			1		9			9		61			61	
12	○	1			1		11			11		91			91	

Table 4.2 – Summary of the non-dimensional parameters for the extensional (A), coupling (B), and bending (D) stiffness, calculated for laminate S2 $[-/+/+/-/+/-/-/+/\bullet/\circ/\circ/\bullet]_T$.

			A					B					D			
Ply	(°)	(z_k-z_{k-1})	$A\Sigma_+$	$A\Sigma_-$	$A\Sigma_\circ$	$A\Sigma_\bullet$	$(z^2_k-z^2_{k-1})$	$B\Sigma_+$	$B\Sigma_-$	$B\Sigma_\circ$	$B\Sigma_\bullet$	$(z^3_k-z^3_{k-1})$	$D\Sigma_+$	$D\Sigma_-$	$D\Sigma_\circ$	$D\Sigma_\bullet$
			4	**4**	**2**	**2**		**-16**	**-16**	**16**	**16**		**112**	**112**	**98**	**110**
1	–	1		1			-11		-11			91		91		
2	+	1	1				-9	-9				61	61			
3	+	1	1				-7	-7				37	37			
4	–	1		1			-5		-5			19		19		
5	+	1	1				-3	-3				7	7			
6	–	1		1			-1		-1			1		1		
7	–	1		1			1		1			1		1		
8	+	1	1				3	3				7	7			
9	●	1				1	5				5	19				19
10	○	1			1		7			7		37			37	
11	○	1			1		9			9		61			61	
12	●	1				1	11				11	91				91

$$\xi_6 = 0.833,\ \xi_9 = 0.250 \text{ and } \xi_{10} = 0.083 \tag{4.6}$$

$$\xi_2 = -0.333,\ \xi_6 = 0.889,\ \xi_9 = -0.028 \text{ and } \xi_{10} = -0.037 \tag{4.7}$$

It is evident from the lamination parameters in Eq. (4.6) and (4.7), that both laminates satisfy the HTCS condition of the first theorem given by Chen (2003) i.e. $\xi_1 = \xi_3 = \xi_5 = \xi_7 = 0$.

However, in order to demonstrate a complete example of the use of the non-dimensional parameters for the calculation of the laminate stiffness properties, consider the carbon-fibre/epoxy material of AS4/3501-6 with the material properties given in the second column of Table 4.3.

Table 4.3 – Property comparisons for unidirectional and balanced plain weave (Hexcel™) intermediate modulus carbon/epoxy materials. Values in parentheses indicate compressive moduli.

	Unidirectional	Plain Weave
E_{11} (GPa)	170 (150)	90 (80)
$E_{22} = E_{33}$ (GPa)	9 (11)	90 (80*)
G_{12} (GPa)	4.4	5
ν_{12}	0.27	0.05
t (mm)	0.183	0.366
σ_1^T (MPa)	2,400	900
σ_1^C (MPa)	-1,600	-800
σ_2^T (MPa)	80	850
σ_2^C (MPa)	-250	-750
τ_{12}^F (MPa)	95	80
α_{11} (10^{-6}/°C)	–1	–1
α_{22} (10^{-6}/°C)	26	–1

* Compressive moduli E2 = E1 assumed instead of published value, E2 = 75 GPa.

Hence, the reduced stiffnesses can be readily calculated from Eq. (9.19), leading to the following values:

$$Q_{11} = 170{,}659,\ Q_{12} = 2{,}439,\ Q_{22} = 9{,}035 \text{ and } Q_{66} = 4{,}400 \text{ (N/mm}^2\text{)} \tag{4.8}$$

Subsequently the laminate invariants are calculated from the above reduced stiffness values using Eq. (2.15), which yield

$$\begin{gathered} U_1 = 70{,}195,\ U_2 = 80{,}812,\ U_3 = 19{,}652,\ U_4 = 22{,}091 \text{ and} \\ U_5 = 24{,}052 \text{ (N/mm}^2\text{)} \end{gathered} \tag{4.9}$$

Using the values of the lamination parameters in Eqs. (4.6) and (4.7) along with the calculated laminate invariants, U_i in Eq. (4.9) the elements of the stiffness matrix for both laminates can be obtained from Eq. (2.17), and are summarised in Table 4.4.

Table 4.4 – The stiffness matrices for the 12-ply laminate S1, $[-/+/+/○/-/-/+/●/●/●/○/○]_T$, and laminate S2, $[-/+/+/-/+/-/-/+/●/○/○/●]_T$.

	S1	S2
Extensional (**A**) stiffness (N/mm)	$\begin{bmatrix} 154{,}148 & 48{,}512 & 0 \\ 48{,}512 & 154{,}148 & 0 \\ 0 & 0 & 52{,}818 \end{bmatrix}$	$\begin{bmatrix} 139{,}763 & 62{,}898 & 0 \\ 62{,}898 & 139{,}763 & 0 \\ 0 & 0 & 67{,}203 \end{bmatrix}$
Coupling (**B**) stiffness (N)	$\begin{bmatrix} 19{,}744 & -19{,}744 & 0 \\ -19{,}744 & 19{,}744 & 0 \\ 0 & 0 & -19{,}744 \end{bmatrix}$	$\begin{bmatrix} 21{,}060 & -21{,}060 & 0 \\ -21{,}060 & 21{,}060 & 0 \\ 0 & 0 & -21{,}060 \end{bmatrix}$
Bending (**D**) stiffness (N.mm)	$\begin{bmatrix} 81{,}222 & 18{,}050 & 0 \\ 18{,}050 & 45{,}563 & 0 \\ 0 & 0 & 19{,}781 \end{bmatrix}$	$\begin{bmatrix} 59{,}324 & 20{,}138 & 0 \\ 20{,}138 & 59{,}324 & 0 \\ 0 & 0 & 21{,}868 \end{bmatrix}$

By inspection of the stiffness matrices in Table 4.4, square symmetry, defined as equal stiffness on principal axes (Tsai and Hahn, 1980), exist where $\mathbf{A}_{11} = \mathbf{A}_{22}$. Through calculation reveals that $\mathbf{A}_{66} = (\mathbf{A}_{11} - \mathbf{A}_{12})/2 = 43{,}884$ for laminate S1, implying the laminate possess in-plane isotropy properties, however, not for laminate S2. Note that square symmetry also exists under additional Extension-Shearing coupling, where $\mathbf{A}_{11} = \mathbf{A}_{22}$ and $\mathbf{A}_{26} = -\mathbf{A}_{16}$, which arises for off-axis material alignment. In addition square symmetry is also observed in the coupling (**B**) matrix, but depending on the off-axis material alignment, the relationship of the elements, $\mathbf{B}_{ij}$, can exist in one of three forms: $\mathbf{B}_{11} = \mathbf{B}_{22} = -\mathbf{B}_{12} = -\mathbf{B}_{66}$ or; $\mathbf{B}_{26} = -\mathbf{B}_{16}$ or; $\mathbf{B}_{11} = \mathbf{B}_{22} = -\mathbf{B}_{12} = -\mathbf{B}_{66}$ and $\mathbf{B}_{26} = -\mathbf{B}_{16}$.

Meanwhile the thermal force and moment vectors are calculated using Eq. (4.4), following a temperature change $\Delta T = -180^{o}C$, typical of the cooling phase in a high temperature curing process. By inspection of Eq. (4.4), the lamination parameters ξ_1 , ξ_3, ξ_5 and ξ_7 all equates to zero, which simplifies the equations:

$$\begin{Bmatrix} N_x^{Thermal} \\ N_y^{Thermal} \\ N_{xy}^{Thermal} \end{Bmatrix} = \frac{H}{2} \begin{Bmatrix} (U_1+U_4)(\alpha_1+\alpha_2)+U_2(\alpha_1-\alpha_2) \\ (U_1+U_4)(\alpha_1+\alpha_2)+U_2(\alpha_1-\alpha_2) \\ 0 \end{Bmatrix} \Delta T$$
$$\begin{Bmatrix} M_x^{Thermal} \\ M_y^{Thermal} \\ M_{xy}^{Thermal} \end{Bmatrix} = \frac{H^2}{8} \begin{Bmatrix} 0 \\ 0 \\ 0 \end{Bmatrix} \Delta T \qquad (4.10)$$

The thermal force vectors in Eq. (4.10) can be calculated using the laminate invariants in Eq. (4.9), which yield the following results for both laminate S1 and S2:

$$\begin{Bmatrix} N_x^{Thermal} \\ N_y^{Thermal} \\ N_{xy}^{Thermal} \end{Bmatrix} = \begin{Bmatrix} -24.8 \\ -24.8 \\ 0 \end{Bmatrix} \text{N/mm} \quad \text{and} \quad \begin{Bmatrix} M_x^{Thermal} \\ M_y^{Thermal} \\ M_{xy}^{Thermal} \end{Bmatrix} = \begin{Bmatrix} 0 \\ 0 \\ 0 \end{Bmatrix} \text{N.mm/mm} \qquad (4.11)$$

The resulting in-plane strains, $\boldsymbol{\varepsilon} = \mathbf{aN}$, and curvatures, $\boldsymbol{\kappa} = \mathbf{b}^{\mathbf{T}}\mathbf{N}$, can be calculated from the inverse of the ABD relations given in Table 4.4 for laminate S1 and S2, as shown in Eqs. (4.12) and (4.13) respectively. Note that the value of (**a**) and (**b**) compliance matrix is obtained from the inverse of the whole 6 x 6 ABD stiffness matrix of Table 4.4. Square symmetry also exists in the compliance (**a)** matrix but not in the coupling compliance matrix ($\mathbf{b}^{\mathrm{T}}$). However, a special relationship was observed within $\mathbf{b}^{\mathrm{T}}$ (York, 2011) where: $\mathbf{b}_{21} = -\mathbf{b}_{11}$, $\mathbf{b}_{12} = -\mathbf{b}_{22}$ and, when present $\mathbf{b}_{16} = -\mathbf{b}_{26}$.

$$\begin{Bmatrix} \varepsilon_x \\ \varepsilon_y \\ \gamma_{xy} \end{Bmatrix} = \begin{bmatrix} a_{11} & a_{12} & a_{16} \\ a_{12} & a_{11} & -a_{16} \\ a_{16} & -a_{16} & a_{66} \end{bmatrix} \begin{Bmatrix} N_x^{Thermal} \\ N_y^{Thermal} \\ N_{xy}^{Thermal} \end{Bmatrix} = 10^{-9} \begin{bmatrix} 9,819 & -4,885 & 0 \\ -4,885 & 9,819 & 0 \\ 0 & 0 & 30,201 \end{bmatrix} \begin{Bmatrix} -24.8 \\ -24.8 \\ 0 \end{Bmatrix} = \begin{Bmatrix} -122\mu \\ -122\mu \\ 0 \end{Bmatrix}$$

$$\begin{Bmatrix} \kappa_x \\ \kappa_y \\ \kappa_{xy} \end{Bmatrix} = \begin{bmatrix} b_{11} & -b_{11} & b_{61} \\ -b_{22} & b_{22} & b_{62} \\ b_{16} & -b_{16} & b_{66} \end{bmatrix} \begin{Bmatrix} N_x^{Thermal} \\ N_y^{Thermal} \\ N_{xy}^{Thermal} \end{Bmatrix} = 10^{-9} \begin{bmatrix} -5,472 & 5,472 & 0 \\ 8,539 & -8,539 & 0 \\ 0 & 0 & 30,145 \end{bmatrix} \begin{Bmatrix} -24.8 \\ -24.8 \\ 0 \end{Bmatrix} = \begin{Bmatrix} 0 \\ 0 \\ 0 \end{Bmatrix} \quad (4.12)$$

$$\begin{Bmatrix} \varepsilon_x \\ \varepsilon_y \\ \gamma_{xy} \end{Bmatrix} = \begin{bmatrix} a_{11} & a_{12} & a_{16} \\ a_{12} & a_{11} & -a_{16} \\ a_{16} & -a_{16} & a_{66} \end{bmatrix} \begin{Bmatrix} N_x^{Thermal} \\ N_y^{Thermal} \\ N_{xy}^{Thermal} \end{Bmatrix} = 10^{-9} \begin{bmatrix} 17,295 & -12,361 & 0 \\ -12,361 & 17,295 & 0 \\ 0 & 0 & 21,312 \end{bmatrix} \begin{Bmatrix} -24.8 \\ -24.8 \\ 0 \end{Bmatrix} = \begin{Bmatrix} -122\mu \\ -122\mu \\ 0 \end{Bmatrix}$$

$$\begin{Bmatrix} \kappa_x \\ \kappa_y \\ \kappa_{xy} \end{Bmatrix} = \begin{bmatrix} b_{11} & -b_{11} & b_{61} \\ -b_{22} & b_{22} & b_{62} \\ b_{16} & -b_{16} & b_{66} \end{bmatrix} \begin{Bmatrix} N_x^{Thermal} \\ N_y^{Thermal} \\ N_{xy}^{Thermal} \end{Bmatrix} = 10^{-9} \begin{bmatrix} -15,558 & 15,558 & 0 \\ 14,819 & -14,819 & 0 \\ 0 & 0 & 20,524 \end{bmatrix} \begin{Bmatrix} -24.8 \\ -24.8 \\ 0 \end{Bmatrix} = \begin{Bmatrix} 0 \\ 0 \\ 0 \end{Bmatrix} \quad (4.13)$$

It is clear from Eqs. (4.12) and (4.13) that both laminates exhibits equal thermal strains in the principal axis directions and no thermal shearing strains exist, but more importantly no curvatures are registered as a result of the temperature change. Therefore this work example validates the rules for HTCS laminate design given by others (Cross *et al*., 2008, York, 2011) i.e, the conditions of square symmetry in the extensional (**A**) and coupling (**B**)

stiffnesses, together with thermal isotropy in the thermal force vector, while the moment vector equates to zero, Eq. (4.11).

The HTCS or warp free condition for laminates S1 and S2 have been verified experimentally, see Fig. 4.1. Figures. 4.2 and 4.3 give the off-axis alignment relationship of the lamination parameters for laminates S1 and S2 respectively. It is clear that laminate S1 possesses extensionally isotropic behaviour, where the extensional (**A**) properties are invariant with off-axis angle orientation, β.

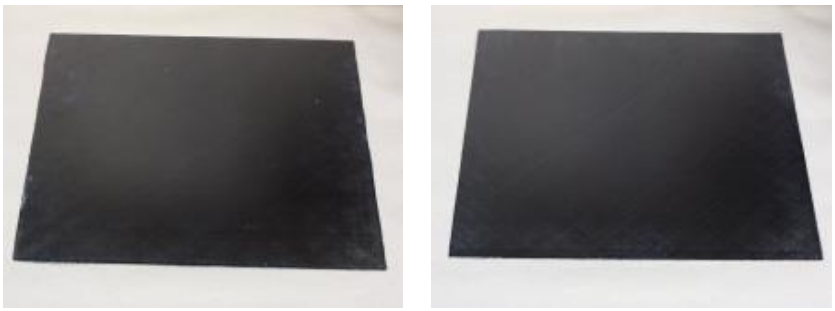

(a) (b)

Figure 4.1 – Confirmation on the hygro-thermally curvature-stable attribute for the 12-ply laminate: (a) laminate S1, with stacking sequence $[-/+/+/○/-/-/+/●/●/●/○/○]_T$; (b) laminate S2, with stacking sequence $[-/+/+/-/+/-/-/+/●/○/○/●]_T$.

However, this is not the case for laminate S2, where uncoupled extensional stiffness (**A**) occur at off-axis orientations $\beta = m\pi/4$ intervals (with $m = 0, 1, 2, 3\ldots$); all other off-axis alignments result in Extension-Shearing coupled laminates. The coupling stiffness (**B**) for the two laminates are shown to be of similar form with respect to their off-axis alignment conditions, where: a) at off-axis alignment $\beta = m\pi/4$, the laminates possess Extension-Bending and Shearing-Twisting (*E-B*;*S-T*) coupling; b) at $\beta = m\pi/4 + \pi/8$, the laminates possess Extension-Twisting and Shearing-Bending (*E-T*;*S-B*) coupling; c) and at all other off-axis alignments, a full populated coupling stiffness (**B**) matrix exists, possessing Extension-Bending, Shearing-Twisting, Extension-Twisting, and Shearing-Bending (*E-B*;*S-T*;*E-T*;*S-B*).

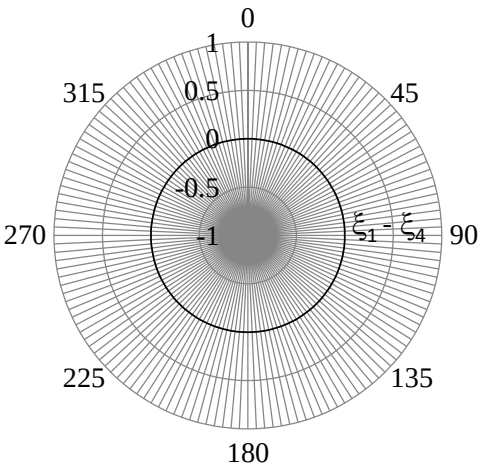

(a) Extensional (**A**)

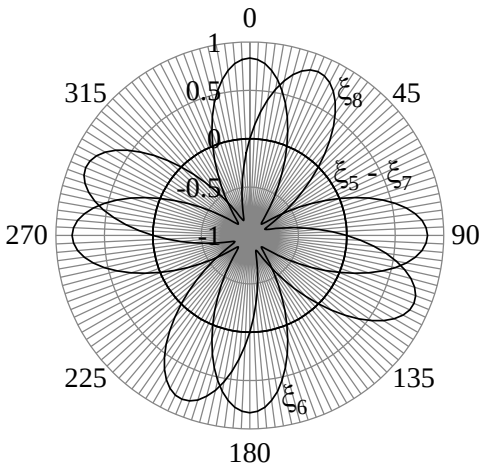

(b) Coupling (**B**)

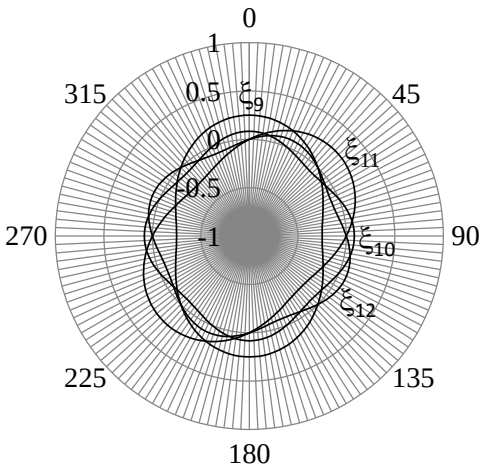

(c) Bending (**D**)

Figure 4.2 – Polar plots of the lamination parameters for laminate S1 corresponding to off-axis material alignment, $0° \leq \beta \leq 360°$, with stacking sequence $[-/+/+/○/-/-/+/●/●/●/○/○]_T$; (a) ξ_1 - ξ_4 for Extensional stiffness (A): (b) ξ_5 - ξ_8 for Coupling stiffness (B): and ξ_9 - ξ_{12} for Bending stiffness (D).

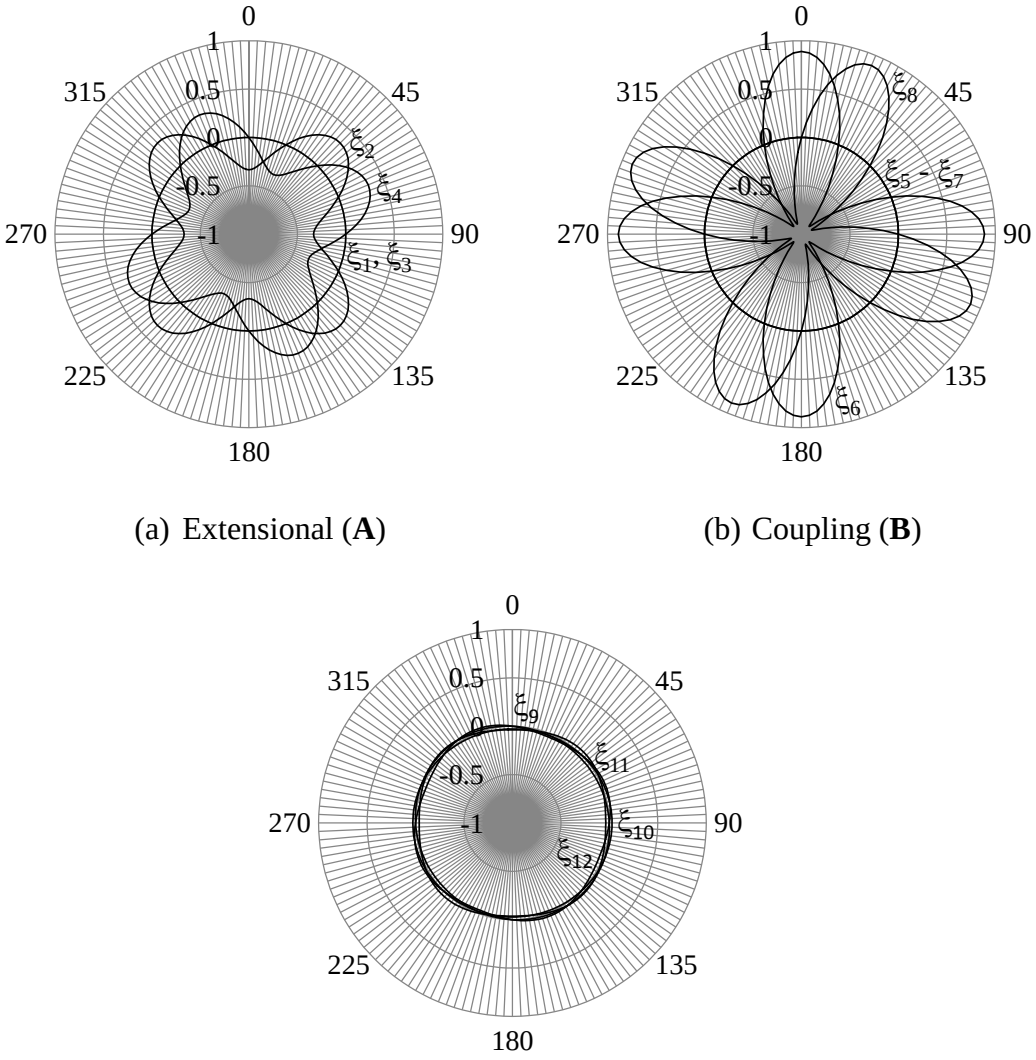

(a) Extensional (**A**) (b) Coupling (**B**)

(c) Bending (**D**)

Figure 4.3 – Polar plots of the lamination parameters for laminate S2 corresponding to off-axis material alignment, $0° \leq \beta \leq 360°$, with stacking sequence $[-/+/+/-/+/-/-/+/●/○/○/●]_T$; (a) ξ_1 - ξ_4 for Extensional stiffness (A): (b) ξ_5 - ξ_8 for Coupling stiffness (B): and ξ_9 - ξ_{12} for Bending stiffness (D).

Figures 4.2(c) and 4.3(c), signify that Bending-Twisting coupling exists for the two laminates at all alignments apart from when the material is axis aligned. Nevertheless the bending stiffness (**D**) properties for laminate S2, shown in Fig. 4.3 (c) have an interesting characteristic; the lamination parameters indicate that the behaviour closely approximates isotropic behaviour, a condition that can contribute to improving the compression buckling strength performance of the laminate, since the $\mathbf{D}_{16}$ and $\mathbf{D}_{26}$ terms are known to have a detrimental effect, if compared against laminates with equal bending (**D**) but $\mathbf{D}_{16} = \mathbf{D}_{26} = 0$.

Note that the *cause-effect* relationships in the response based labelling presented in Table 2.1 and Table 3.1, corresponding to the form of the stiffness matrix are reversible and have complete duplicity with respect to the compliance matrix for the coupled laminates, but only if the extensional stiffness [**A**] and the bending stiffness [**D**] matrices are uncoupled or simple, see Table 4.5.

Table 4.5 – Comparisons of HTCS laminate stiffness and compliance matrices for different cause-effect relationships.

	$\mathbf{A_S B_S D_S}$ laminate, (*E-B-S-T*)
Stiffness Matrix	$\begin{Bmatrix} N_x \\ N_y \\ N_{xy} \\ M_x \\ M_y \\ M_{xy} \end{Bmatrix} = \left[\begin{array}{ccc:ccc} A_{11} & A_{12} & 0 & B_{11} & -B_{11} & 0 \\ A_{12} & A_{11} & 0 & -B_{11} & B_{11} & 0 \\ 0 & 0 & A_{66} & 0 & 0 & B_{66} \\ \hdashline B_{11} & -B_{11} & 0 & D_{11} & D_{12} & 0 \\ -B_{11} & B_{11} & 0 & D_{12} & D_{22} & 0 \\ 0 & 0 & -B_{11} & 0 & 0 & D_{66} \end{array}\right] \begin{Bmatrix} \varepsilon_x \\ \varepsilon_y \\ \gamma_{xy} \\ \kappa_x \\ \kappa_y \\ \kappa_{xy} \end{Bmatrix}$
Compliance Matrix	$\begin{Bmatrix} \varepsilon_x \\ \varepsilon_y \\ \gamma_{xy} \\ \kappa_x \\ \kappa_y \\ \kappa_{xy} \end{Bmatrix} = \left[\begin{array}{ccc:ccc} a_{11} & a_{12} & 0 & b_{11} & -b_{22} & 0 \\ a_{12} & a_{11} & 0 & -b_{11} & b_{22} & 0 \\ 0 & 0 & a_{66} & 0 & 0 & b_{66} \\ \hdashline b_{11} & -b_{11} & 0 & d_{11} & d_{12} & 0 \\ -b_{22} & b_{22} & 0 & d_{12} & d_{22} & 0 \\ 0 & 0 & b_{66} & 0 & 0 & d_{66} \end{array}\right] \begin{Bmatrix} N_x \\ N_y \\ N_{xy} \\ M_x \\ M_y \\ M_{xy} \end{Bmatrix}$
	$\mathbf{A_S B_t D_F}$ laminate, (*E-T-S-B;B-T*)
Stiffness Matrix	$\begin{Bmatrix} N_x \\ N_y \\ N_{xy} \\ M_x \\ M_y \\ M_{xy} \end{Bmatrix} = \left[\begin{array}{ccc:ccc} A_{11} & A_{12} & 0 & 0 & 0 & B_{16} \\ A_{12} & A_{11} & 0 & 0 & 0 & -B_{16} \\ 0 & 0 & A_{66} & B_{16} & -B_{16} & 0 \\ \hdashline 0 & 0 & B_{16} & D_{11} & D_{12} & D_{16} \\ 0 & 0 & -B_{16} & D_{12} & D_{22} & D_{26} \\ B_{16} & -B_{16} & 0 & D_{16} & D_{26} & D_{66} \end{array}\right] \begin{Bmatrix} \varepsilon_x \\ \varepsilon_y \\ \gamma_{xy} \\ \kappa_x \\ \kappa_y \\ \kappa_{xy} \end{Bmatrix}$
Compliance Matrix	$\begin{Bmatrix} \varepsilon_x \\ \varepsilon_y \\ \gamma_{xy} \\ \kappa_x \\ \kappa_y \\ \kappa_{xy} \end{Bmatrix} = \left[\begin{array}{ccc:ccc} a_{11} & a_{12} & a_{16} & b_{11} & -b_{22} & b_{16} \\ a_{12} & a_{11} & -a_{16} & -b_{11} & b_{22} & -b_{16} \\ a_{16} & -a_{16} & a_{66} & b_{61} & b_{62} & b_{66} \\ \hdashline b_{11} & -b_{11} & b_{61} & d_{11} & d_{12} & d_{16} \\ -b_{22} & b_{22} & b_{62} & d_{12} & d_{22} & d_{26} \\ b_{16} & -b_{16} & b_{66} & d_{16} & d_{26} & d_{66} \end{array}\right] \begin{Bmatrix} N_x \\ N_y \\ N_{xy} \\ M_x \\ M_y \\ M_{xy} \end{Bmatrix}$

Extension-Shearing and/or Bending-Twisting coupling give rise to secondary couplings, which generally result in a full populated compliance matrix. For example applying the off-axis alignment of $\beta = m\pi/4 + \pi/8$ for laminate S1 give rise to $\mathbf{A_S B_t D_F}$ coupled laminate, see Fig. 4.2, where a comparison of the *cause-effect* for the *E-T*-*S-B*;*B-T* coupled laminate with respect to the form of the compliance matrix in Table 4.5 reveals that an applied mechanical force resultant N_x, gives rise to twisting curvatures as well as extensional strains as a result of the Extension-Twisting (*E-T*) coupling behaviour, but also to secondary bending curvatures, which arise from the twisting curvatures as a result of Bending-Twisting (*B-T*) coupling behaviour, i.e., $\mathbf{b}_{11} \neq 0$. Finally, the secondary bending curvatures lead to tertiary shearing strains through Shearing-Bending (*S-B*) coupling behaviour, i.e., $a_{16} \neq 0$. In this example the relatives magnitudes of the secondary couplings of the $\mathbf{A_S B_t D_F}$ coupled laminates are revealed through calculation of the compliance matrix, Eq. (4.14).

$$\begin{Bmatrix} \varepsilon_x \\ \varepsilon_y \\ \gamma_{xy} \\ \kappa_x \\ \kappa_y \\ \kappa_{xy} \end{Bmatrix} = 10^{-9} \left[\begin{array}{ccc:ccc} 9,918 & -4,984 & -198 & 1,350 & 819 & -14,542 \\ -4,984 & 9,918 & 198 & -1,350 & -819 & 14,542 \\ -198 & 198 & 29,805 & -12,373 & 16,711 & 1,061 \\ \hdashline 1,350 & -1,350 & -12,373 & 20,686 & -12,414 & -7,221 \\ 819 & -819 & 16,711 & -12,414 & 32,291 & -4,383 \\ -14,542 & 14,542 & 1,061 & -7,221 & -4,383 & 77,805 \end{array}\right] \begin{Bmatrix} N_x \\ N_y \\ N_{xy} \\ M_x \\ M_y \\ M_{xy} \end{Bmatrix} \quad (4.14)$$

However, this scenario serves to demonstrates the validity of the *cause-effect* relationships from the response based labelling system, based on the form of the stiffness matrix, rather than compliance matrix, not only as general descriptor of the laminate coupling behaviour, but also for assessing the presence of any secondary couplings without the requirement for matrix inversion.

4.2 HTCS coupled laminates solutions

The axis aligned condition of laminate S1 and S2 will be generally considered as the HTCS *parent classes* laminate since more complex combinations of coupled laminate classes are derivable through off-axis alignment. The parent class for laminate S1 and S2 are denoted by $\mathbf{A}_I\mathbf{B}_S\mathbf{D}_S$ and $\mathbf{A}_S\mathbf{B}_S\mathbf{D}_S$ respectively, with the subscript 'I' following the extensional stiffness (**A**) for laminate S1 signifying the existence of extensionally isotropic condition. Identification of other HTCS parent class laminates with different ply number groupings are performed algorithmically via a FORTRAN computer code, from which non-dimensional parameters of the entire laminate design space for each ply number groupings are used as an input data to calculate the laminate's lamination parameters and stiffness properties. Laminates fulfilling the requirement of HTCS are filtered and written in a separate file. The procedures are performed for a series of laminate ply number groupings ranging from 4-ply to 21-ply i.e. within the thin ply laminates, where the total number of laminate solutions derived from standard angle orientations i.e. +45, –45, 0 and 90º under each respective ply number groupings are summarized in Table 4.6.

Table 4.6 – Number of standard angle orientation stacking sequence solutions for 4-21-ply number groupings.

n-ply	Standard angles stacking sequence solutions	*n*-ply	Standard angles stacking sequence solutions
4	256	13	67,108,864
5	1,024	14	268,435,456
6	4,096	15	1,073,741,824
7	16,384	16	4,294,967,296
8	65,536	17	17,179,869,184
9	262,144	18	67,819,476,736
10	1,048,576	19	274,877,906,944
11	4,194,304	20	1,099,511,627,776
12	16,777,216	21	4,398,046,511,104

A recent study (York, 2011) has revealed that for the case of standard angle-ply orientations, HTCS coupled laminates are restricted to 8-, 12-, 16- and 20-ply number groupings. The number of solutions within each parent class is listed in Table 4.7 for ply

number groupings. Here the extensional stiffness (**A**) matrix for all the parent classes are shown to be uncoupled, or simple, with the first two categories designated with the subscript 'I', signifying extensionally isotropic behaviour, as in the case of laminate S1 mentioned above. By contrast, the bending stiffness (**D**) are shown to be either uncoupled, or simple, or with Bending-Twisting coupling. The family of mechanically coupled laminates with $\mathbf{B} \neq 0$, which occur as a consequence of applied off-axis alignment of the parent class laminate has been shown (York, 2011) to exist in 9 out of the 24 classes of coupled laminates, which are illustrated in Fig. 4.44.

Table 4.7 – Summary on the number of solutions for the coupled parent laminate classes possessing HTCS properties with 8-, 12-, 16- and 20-plies.

	8-Ply	12-Ply	16-Ply	20-Ply
$\mathbf{A_IB_SD_S}$	-	8	264	17118
$\mathbf{A_IB_SD_F}$	6	280	23652	2429067
$\mathbf{A_SB_SD_S}$	-	6	524	35610
$\mathbf{A_SB_SD_F}$	-	410	40808	4638933

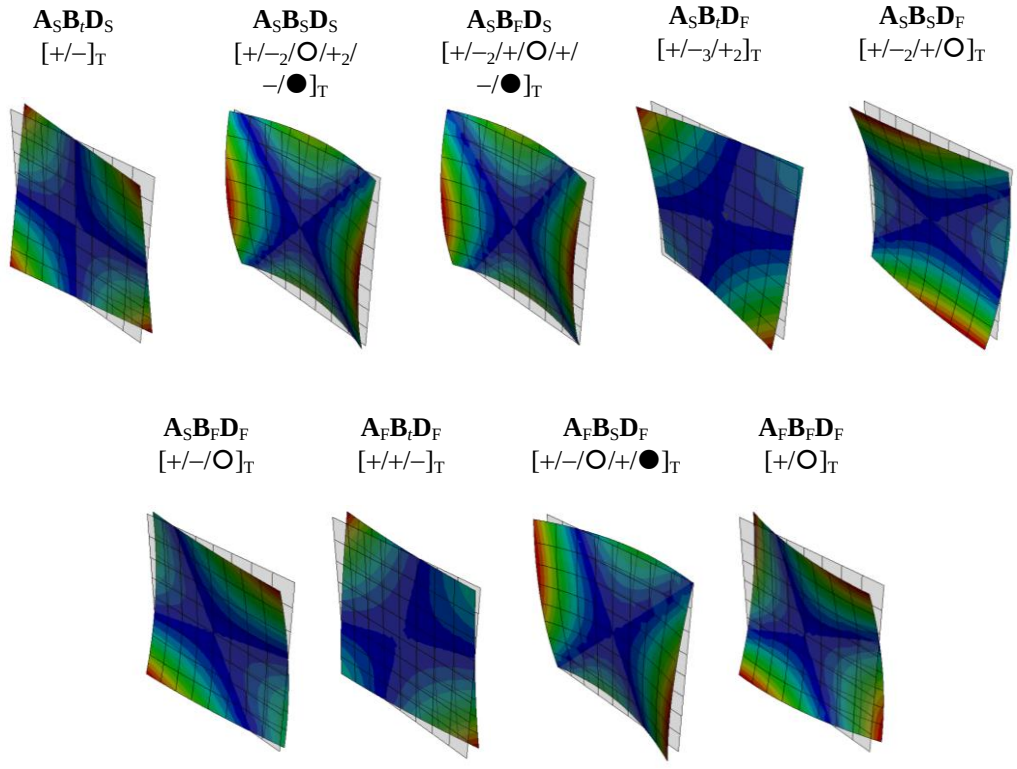

Figure 4.4 – The coupling responses from Figs. 3.2 - 3.5 that had been identified with the hygro-thermally curvature-stable condition, (after York, 2011).

4.3 Conclusion

Rules governing warp free conditions for coupled laminates have been discussed. Confirmations to these rules have been demonstrated in this chapter, through mathematical verification of two laminates S1 and S2. Both laminates were shown to have lamination parameters $\xi_1 = \xi_3 = \xi_5 = \xi_7 = 0$, which satisfy the requirement for HTCS. Further calculation also reveals that they possesses square symmetry relationship for the extensional (**A**) and coupling (**B**), i.e., $\mathbf{A}_{11} = \mathbf{A}_{22}$ and $\mathbf{B}_{11} = \mathbf{B}_{22}$, together with the relationship of $N_x^{Thermal} = N_y^{Thermal}$ and $M_x^{Thermal} = M_y^{Thermal} = M_{xy}^{Thermal} = 0$ being satisfied. Identification of HTCS coupled laminates with up to 21 plies and with standard ply angles were performed using a non-dimensional parameter formulation. The HTCS laminates identified under axis-aligned conditions are referred to as the parent laminate classes, possessing Extension-Bending and Shearing-Twisting coupling ($\mathbf{B}_S$), from which more complex coupling behaviour can be achieved through the application of off-axis alignment. Nevertheless, the existence of such HTCS coupled laminate classes are limited to only 9 out of the 24 laminate classes previously described. Further restriction concerning HTCS coupled laminates derived from standard angle orientations, relate to the limited number of ply number groupings in which they exist i.e. laminates with 8-, 12-, 16- and 20-plies.

One particular coupled laminate class, which has gained increasing interest over the past years, is the one possessing Extension-Twisting and Shearing-Bending coupling ($\mathbf{A}_S\mathbf{B}_t\mathbf{D}_S$). This coupling behaviour can be obtained through applying off-axis alignment of $\beta = m\pi/4 + \pi/8$ (with m = 0, 1, 2, 3..) to the HTCS parent laminate class. Additional Extension-Shearing and/or Bending-Twisting coupling i.e. $\mathbf{A}_F\mathbf{B}_t\mathbf{D}_F$ and $\mathbf{A}_S\mathbf{B}_t\mathbf{D}_F$ laminate classes exist with immunity to thermal warping distortion. These laminate classes will be the subject of discussion in the next chapter.

CHAPTER 5:

HTCS coupled laminate solutions with Extension-Twisting Coupling

This chapter addresses a particular class of the HTCS coupled laminate, which has gained increasing interest over recent years, possessing Extension-Twisting and Shearing-Bending coupling ($\mathbf{A}_S\mathbf{B}_t\mathbf{D}_S$). This class of coupled laminate has been researched extensively in the application of aero-elastic compliant rotor blades(Nixon, 1987), an enabling technology for tilt rotor aircraft. Assessment of the twist magnitude and buckling performance for the $\mathbf{A}_S\mathbf{B}_t\mathbf{D}_S$ laminate solutions, derived from standard angle-ply orientations, is investigated in this chapter; the assessment of the twist magnitude is performed using a modified Finite Element (FE) model; while the buckling performance is assessed using a close form buckling solution available for this class of coupled laminate.

The interesting feature of a tilt-rotor aircraft is their dual flight mode, i.e. hover mode (helicopter) and cruise mode (airplane). The mixing of the two flight modes has presented a challenge in terms of the blade design requirements. For example, the rotor speeds for the experimental XV−15 tilt-rotor aircraft of Fig. 5.1 operates at 20% less speed during cruise

mode compared to hover mode, which suggests that different blade twist distributions are required for the rotor blades between the two modes to obtain different operating conditions. Figure 5.2 shows the power required in both the hover and cruise modes as a function of linear blade twist (Nixon, 1988). It is evident from the figure, that the optimum blade twist is between 20 and 45 degrees for both hover and cruise mode respectively. The cross over point shown in Fig. 5.2 correspond to a 36 degree blade linear twist over a total blade length of 150 in., which contributes to a 6% improvement in the power requirement in both hover and cruise modes.

Figure 5.1 – XV-15 Tilt rotor aircraft, (after Martin *et al*., 2000).

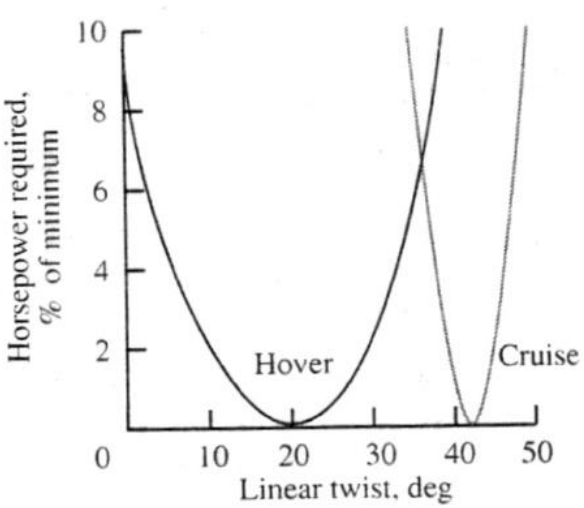

Figure 5.2 – Blade twist against power requirement for XV-15 tilt rotor aircraft, where the linear twist recorded over a total blade length of 150 in., (after Nixon, 1988).

Nixon (1987) presented a passive blade control concept, which was to vary the blade twist between the two flight regimes using an Extension-Twisting coupled rotor blade. Here, Extension-Twisting at the structural or blade level is used to develop an optimised twist distribution along the blade for both hover and forward flight: a change in rotor speed and the resulting centrifugal forces provides the required twist differential between the two flight regimes. This passive blade twist control concept was tested experimentally using Extension-Twisting coupled circular tubes, representative of tilt-rotor blade spars, manufactured from several Hygro-thermally stable (HTCS) layups; where the investigation revealed that a 6-ply $[20/\text{-}70_2]_S$ laminate provided the optimum design, generating a twist rate of 0.384 to 0.487 deg/in., and satisfying the twist rate design requirement of between 0.216 and 0.333 deg/in for the XV−15 baseline design.

A series of investigations subsequently followed (Lake *et al*., 1992, Lake *et al*., 1994, Nixon, 1988), further expanding the work, including an experimental study for the actual Extension-Twisting coupled rotor blades design, shown in Fig. 5.3. Here, a set of composite rotor blades with symmetrical NACA (NACA 0012) airfoil design were manufactured using a prepreg plain weave material, where an off-axis alignment of 20° was applied to the principal material axis with respect to the principal structural axis. Two configurations were presented in the investigation: (a) a ballasted configuration, with additional masses introduce within the blade, see Fig. 5.3 and, (b) an unballasted configuration, with no additional masses introduce in the blade structure. Configuration (a) recorded a twist magnitude of 5.24° over the span length of 42.5 in. compared with configuration (b); both recorded at 100% rotor speed.

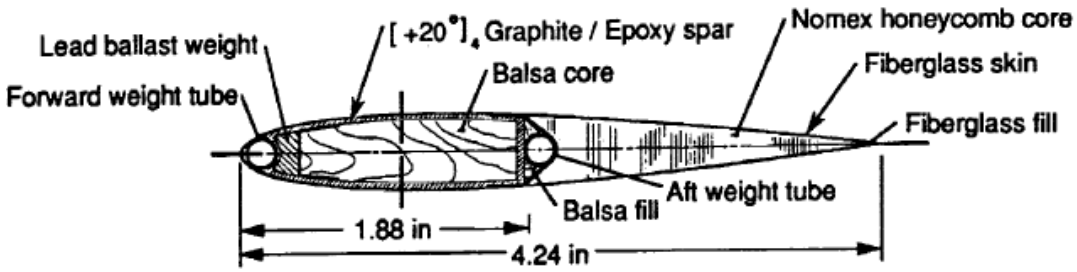

Figure 5.3 – Cross-section of the Extension-Twisting model for the tilt-rotor blade design, with a blade span of 42.5 in. (after Lake *et al.*, 1992).

Although the practicality of the passive blade control concept has been proven from the abovementioned studies, a typical tilt-rotor blade aircraft would generally require much higher twist rate. Arguably this would be difficult to achieve from closed cell geometry such as the rotor blade cross section in Fig. 5.3, due to the high torsional stiffness. Dancila *et al.* (1998) therefore proposed a star-shaped cross-section, illustrated in Fig. 5.4 in an effort to preserve a high level of Extension-Twisting coupling. In addition a star-shape cross-section with closed circular core was also proposed, providing the combined performance of an open and closed cell; resulting in a compromise between high torsional stiffness from the closed cell and substantial Extension-Twisting coupling from the open cell.

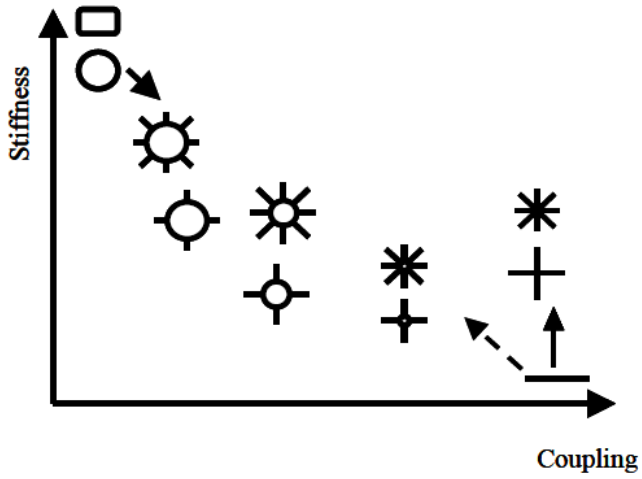

Figure 5.4 – Stiffness against Coupling relationship of various star-shaped cross-sections, (after Dancila *et al.*, 1998).

This has led others to investigate laminates with optimised Extension-Twisting coupling, with the aim of achieving maximum twist rate performance in rotor blade designs. Chen (2003) had an optimisation procedure based on lamination parameters to maximise the Extension-Twisting of a laminate, which resulted in a free-form stacking sequence configuration of the following form:

$$[14.62/16.21/-69.56/21.63/-66.34/-59.38/-55.98/-49.52/49.13/56.01/61.46/64.36/-21.3/69.04/-7.01/-4.88]_T \quad (5.1)$$

Cross *et al*. (2008) extended the work from Chen, but focusing on the minimum possible ply number groupings. This resulted in a 5-ply anti-symmetric configuration:

$$[76.3/-33.6/0/33.6/-76.3]_T \quad (5.2)$$

Haynes & Armanios (2010) adopted a similar optimisation routine to extend the search for optimised Extension-Twisting coupling ranging from 5- to 10-ply laminates. It is noteworthy that the 5-ply laminate solution is in fact identical to the solution from Cross *et al*. (2008), in Eq. (5.2), after rotation through $\pi/4$.

$$\begin{array}{cc} \text{5-ply} & [-58.7/11.4/45/78.6/-31.3]_T \\ \text{6-ply} & [21.2/-63.8/-48.7/48.7/63.8/-21.2]_T \\ \text{7-ply} & [14.1/-76.9/-73.9/-45/-16.1/-13.2/75.7]_T \\ \text{8-ply} & [-21.5/72.1/57.9/-29.6/29.6/-57.9/-72.1/21.5]_T \\ \text{9-ply} & [25.5/-79/32.5/-62.9/49.9/27.4/57/-10.6/64.9]_T \\ \text{10-ply} & [16.2/-69/-65.3/31.8/42.1/-42.1/-31.8/65.3/69/-16.2]_T \end{array} \quad (5.3)$$

It is evident from the above works, that employing an optimisation routine will generally result in a laminate stacking sequence with free form angles. Such stacking sequences are difficult to manufacture and are often susceptible to ply angle misalignment, which results in erroneous stiffness properties and warping distortions.

By contrast HTCS laminate with Extension-Twisting (and Shearing-Bending) coupling, were derived (York, 2011) from standard angle orientations of 45, –45, 0 and 90°, have been shown to suffer less from warping distortions. The assessment of the coupling and buckling strength performance for this laminate class have been addressed (Shamsudin *et al*., 2013a); the twisting magnitude are shown to be equally attractive to the competing laminates derived from free form angles and outperform in terms of the buckling strength.

5.1 HTCS Extension-Twisting coupled laminates with standard ply angles.

York (2011) demonstrated that 6, 20, 260 and 3,076 laminate solutions exist with 8, 12, 16 and 20 plies respectively, all of which possess extensional isotropy, i.e. the extensional stiffness (**A**) properties are invariant with off-axis orientation, as given in Table 5.1.

Table 5.1 – Number of solutions for the Extension-Twisting and shearing-bending ($\mathbf{A_S B_t D_S}$) coupled laminates, available from two parent class laminates of; $\mathbf{A_I B_S D_I}$: and with additional Bending-Twisting $\mathbf{A_I B_S D_F}$, (after York, 2011).

n	$\mathbf{A_S B_t D_S}$ <u>*E-T-S-B*</u>	
	Parent Laminate: $\mathbf{A_I B_S D_I}$ $\beta = \pi/8 + m\pi/4$ $m = 0, 1, 2, 3\ldots$	Parent Laminate: $\mathbf{A_I B_S D_F}$ $\beta = \pi/8 + m\pi/2$; ($\beta = -\pi/8 + m\pi/2$) $m = 0, 1, 2, 3$; ($m = 0, 1, 2, 3$)
8	-	3 (3)
12	-	10 (10)
16	8	126 (126)
20	-	1,538 (1,538)

In addition, a number of 16 ply laminates were found to possess concomitant stiffness properties, i.e. $\mathbf{D}_{ij} = \mathbf{A}_{ij}H^2/12$. The subscript 'I' is therefore used for both the extensional stiffness ($\mathbf{A}_I$) and bending stiffness ($\mathbf{D}_I$) in Table 5.1, to signify the isotropic stiffness condition. The laminate stacking sequences for these 16 ply laminates are given in Table 5.2.

Table 5.2 – 8 solutions of the 16-ply laminate possessing concomitant stiffness properties, $\mathbf{D_{ij}} = \mathbf{A_{ij}}H^2/12$, (after York, 2011).

16 ply laminate stacking sequences
$[-++-+--+\bullet\circ\circ\bullet\circ\bullet\bullet\circ]_T$
$[-++-\bullet\circ\circ\bullet+--+\circ\bullet\bullet\circ]_T$
$[-+\bullet\circ+-\circ\bullet+-\circ\bullet-+\bullet\circ]_T$
$[-\bullet+\circ+\circ-\bullet+\circ-\bullet-\bullet+\circ]_T$
$[-++-+--+\circ\bullet\bullet\circ\bullet\circ\circ\bullet]_T$
$[-++-\circ\bullet\bullet\circ+--+\bullet\circ\circ\bullet]_T$
$[-+\circ\bullet+-\bullet\circ+-\bullet\circ-+\circ\bullet]_T$
$[-\circ+\bullet+\bullet-\circ+\bullet-\circ-\circ+\bullet]_T$

The $\mathbf{A_S B_t D_S}$ laminate solutions were derived from a parent class having the additional Bending-Twisting coupling i.e. $\mathbf{A_I B_S D_F}$. Under the $\mathbf{A_I B_S D_F}$ parent class laminate two sets of equal solutions are shown in Table 5.1 i.e. under the off axis alignment of $\beta = \pi/8 + m\pi/2$ and $\beta = -\pi/8 + m\pi/2$, where $m = 0, 1, 2, 3$. The number of solutions related to the latter off-axis rotation is given in parentheses in Table 5.1.

Complete listings of laminate stacking sequences for the 8- and 12-ply number groupings are given in Table 5.3 in order of increasing lamination parameter, ξ_8, i.e. the variable influencing the magnitude of the Extension-Twisting coupling, see Eq. (2.17).

Table 5.3 – Stacking sequences listings for $\mathbf{A_S B_t D_S}$ laminates, derived through off-axis alignment from the parent class laminate of $\mathbf{A_I B_S D_F}$ for the 8- and 12-ply number groupings.

n	Stacking sequences $\beta = \pi/8 + m\pi/2$ $m = 0, 1, 2, 3$	 $\beta = -\pi/8 + m\pi/2$ $m = 0, 1, 2, 3$	ξ_8
8	L1 : $[-++-\circ\bullet\bullet\circ]_T$	L4 : $[-++-\bullet\circ\circ\bullet]_T$	$\pm$ 1.00
	L2 : $[-+\circ\bullet+-\bullet\circ]_T$	L5 : $[-+\bullet\circ+-\circ\bullet]_T$	$\pm$ 0.50
	L3 : $[-\circ+\bullet+\bullet-\circ]_T$	L6 : $[-\bullet+\circ+\circ-\bullet]_T$	$\pm$ 0.25
12	$[-+-++\circ-\bullet\bullet\circ\bullet\circ]_T$	$[-+-++\bullet-\circ\circ\bullet\circ\bullet]_T$	$\pm$ 0.94
	$[-+-+\circ+\bullet-\bullet\circ\bullet\circ]_T$	$[-+-+\bullet+\circ-\circ\bullet\circ\bullet]_T$	$\pm$ 0.83
	$[-+-\circ++\bullet\bullet-\circ\bullet\circ]_T$	$[-+-\bullet++\circ\circ-\bullet\circ\bullet]_T$	$\pm$ 0.72
	$[-\circ-+++\bullet\bullet\bullet\circ-\circ]_T$	$[-\bullet-+++\circ\circ\circ\bullet-\bullet]_T$	$\pm$ 0.50
	$[-+\bullet+\circ\circ--\bullet+\bullet\circ]_T$	$[-+\circ+\bullet\bullet--\circ+\circ\bullet]_T$	$\pm$ 0.39
	$[-+\bullet\circ+\circ-\bullet-+\bullet\circ]_T$	$[-+\circ\bullet+\bullet-\circ-+\circ\bullet]_T$	$\pm$ 0.28
	$[-+\bullet\circ\circ+\bullet--+\bullet\circ]_T$	$[-+\circ\bullet\bullet+\circ--+\circ\bullet]_T$	$\pm$ 0.17
	$[-\circ\bullet\circ++\bullet\bullet-+-\circ]_T$	$[-\bullet\circ\bullet++\circ\circ-+-\bullet]_T$	$\mp$ 0.17
	$[-\circ\bullet++\circ-\bullet\bullet+-\circ]_T$	$[-\bullet\circ++\bullet-\circ\circ+-\bullet]_T$	$\pm$ 0.06
	$[-\circ\bullet+\circ+\bullet-\bullet+-\circ]_T$	$[-\bullet\circ+\bullet+\circ-\circ+-\bullet]_T$	$\mp$ 0.06

Note that the laminates in any given row of Table 5.3, have equal ξ_8 magnitudes, but opposite signs; the $\pm$ sign in front of the ξ_8 value signifies that the laminate with the off-axis rotation of $\beta = \pi/8 + m\pi/2$ produces a positive ξ_8 value, while the laminate with off-axis rotation of $\beta = -\pi/8 + m\pi/2$ has a negative ξ_8 value; and vice versa for the $\mathbb{R}$ sign. The associated changes of laminate stiffness properties due to off-axis alignment are best

visualised with a polar plot of lamination parameters as shown in Figs. 5.5 and 5.6, which gives the result for the two laminates in the first row of Table 5.3, ie., with stacking sequences of $[-/+/+/-/○/●/●/○]_T$ and $[-/+/+/-/●/○/○/●]_T$, respectively.

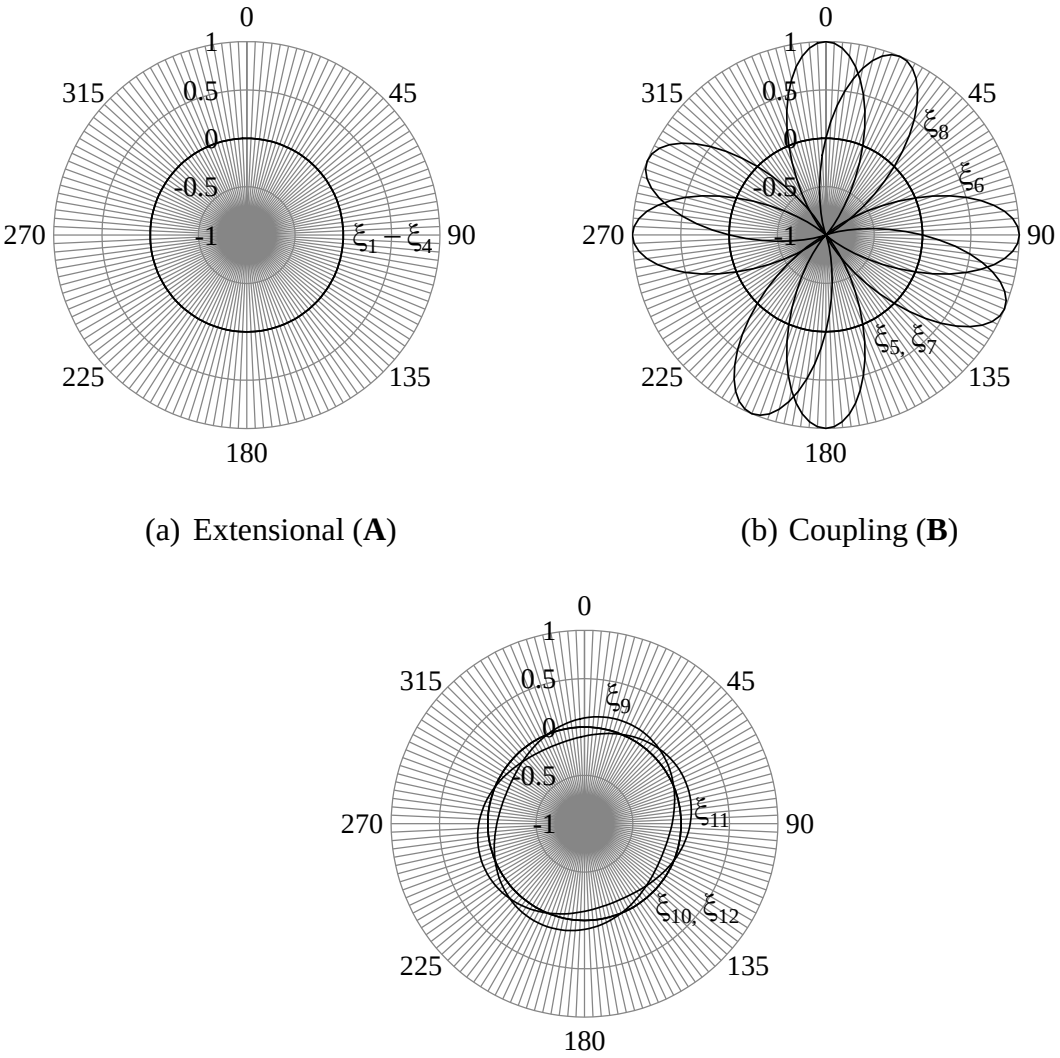

(a) Extensional (**A**)

(b) Coupling (**B**)

(c) Bending (**D**)

Figure 5.5 – Polar plots of the lamination parameters for the 8-ply laminate, $[-/+/+/-/○/●/●/○]_T$; (a) ξ_1 - ξ_4 representing extensional stiffness (A): (b) ξ_5 - ξ_8 for Coupling stiffness (B): and ξ_9 - ξ_{12} for Bending stiffness (D).

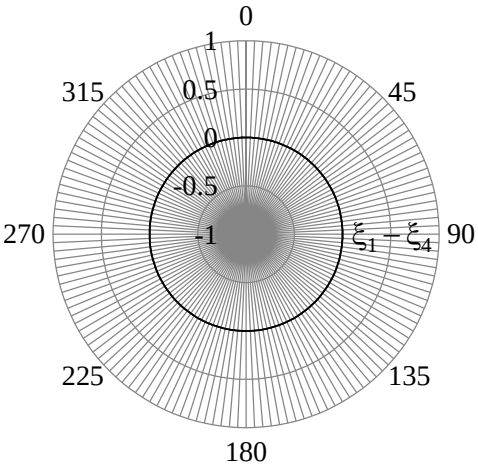

(a) Extensional (**A**)

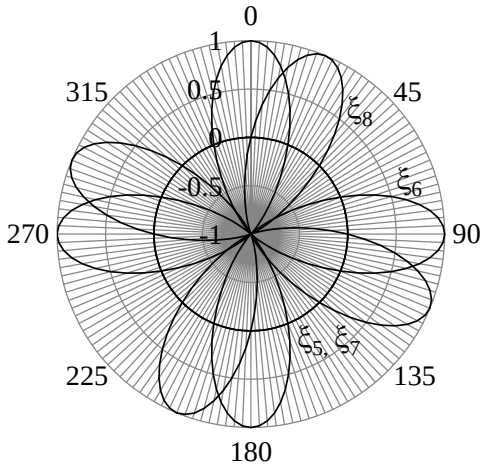

(b) Coupling (**B**)

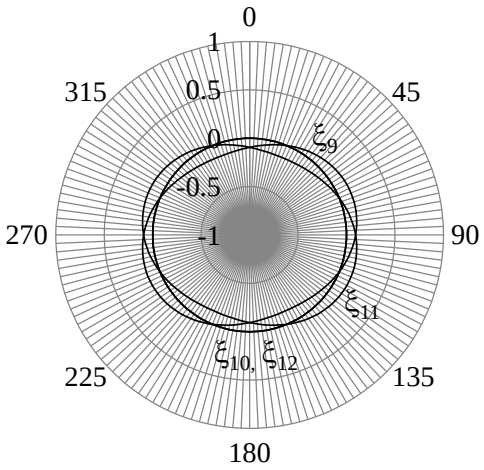

(c) Bending (**D**)

Figure 5.6 – Polar plots of the lamination parameters for the 8-ply laminate, $[-/+/+/-/\bullet/\circ/\circ/\bullet]_T$; (a) ξ_1 - ξ_4 for extensional stiffness (A): (b) ξ_5 - ξ_8 for Coupling stiffness (B): and ξ_9 - ξ_{12} for Bending stiffness (D).

It is clear from both figures that the extensional (**A**) properties are invariant of the off-axis alignment. While the pattern of the coupling (**B**) are identical in both figures, the bending (**D**) differs only in the lamination parameters ξ_9 and ξ_{11}, where there is a 45° rotational shift observed. For an off-axis rotation of $\beta = \pi/8 + m\pi/2$ the contribution of the lamination parameters, $\xi_{11} = 0$ for the laminate shown in Fig 5.5, which renders $\mathbf{D}_{16} = \mathbf{D}_{26} = 0$ from Eq. (2.17). However the same off-axis rotation for the laminate given in Fig. 5.6 leads to Bending-Twisting coupling within the laminate, since $\xi_{11} \neq 0$, hence D_{16}, $D_{26} \neq 0$. The

opposite effect is seen under the off-axis rotation of $\beta = -\pi/8 + m\pi/2$ (–22.5°) for the two laminates in Figs. 5.5 and 5.6. Abridged listings for the 16- and 20-ply laminate stacking sequence solutions are given in Table B1and Table B2 of Appendix B, respectively.

5.2 Extension-Twisting coupling investigation

The twisting rotation for an Extension-Twisting coupled laminate, $\mathbf{A_S B_t D_S}$, has been assessed using several methods in the literature. For instance a complex analytical model was adopted by Armanios *et al*. (1996), resulting in a closed form solution relating the applied extension force to the twisting magnitude. Others have explored numerical methods (Hodges *et al*., 1987, Haynes and Armanios, 2010), including the finite element technique to simulate experiment tests (Nixon, 1987, Haynes and Armanios, 2010, Shamsudin *et al*., 2011). Nevertheless a preliminary assessment of the magnitude of the Extension-Twisting response can be obtained from the compliance $\mathbf{b}_{16}$, see Table 4.5. The compliance term $\mathbf{b}_{16}$, from which the twisting curvature, κ_{xy} can be assessed, can be expressed as:

$$b_{16} = \frac{B_{16}(B_{16}^2 P_1 + A_{66}P_2 - A_{16}P_5)}{B_{16}^2 P_7 + A_{66}P_6 + 2A_{16}^2(D_{66}P_2 + P_4) - 4A_{16}B_{16}^2 P_5}$$

with:

$$\begin{aligned} P_1 &= D_{11} + 2D_{12} + D_{22} & P_5 &= D_{12}D_{16} + D_{16}D_{22} - D_{11}D_{26} - D_{12}D_{26} \\ P_2 &= D_{12}^2 - D_{11}D_{22} & P_6 &= 2B_{16}^2 P_2 - (A_{11} - A_{12})(D_{66}P_2 + P_4) \\ P_3 &= (D_{16} + D_{26})^2 & P_7 &= 2B_{16}^2 P_1 - (A_{11} - A_{12})(D_{66}P_1 - P_3) \\ P_4 &= D_{16}^2 D_{22} - 2D_{12}D_{16}D_{26} + D_{11}D_{26}^2 \end{aligned} \tag{5.4}$$

The above expression of the compliance $\mathbf{b}_{16}$ is obtained through mathematical manipulation using Mathematica software. The compliance $\mathbf{b}_{16}$ is dependent on the form of the ABD stiffness matrix; in particular when coupling in the extensional stiffness (**A**) and/or bending stiffness (**D**) exist. However, in the absence of these couplings, i.e. for $\mathbf{A_S B_t D_S}$ laminates, Eq. (5.4) degenerates into a simpler form:

$$b_{16} = \frac{B_{16}}{2B_{16}^2 + (A_{12} - A_{11})D_{66}} \tag{5.5}$$

Haynes and Armanios (2010) have performed finite element modelling in ABAQUS, predicting the twisting rotation for $\mathbf{A_S B_t D_S}$ laminates with optimum $\mathbf{b}_{16}$ value, from which the results were found to be in good agreement with the experimental results. This shows the feasibility of using commercial finite element package to predict accurately the twisting rotation for the $\mathbf{A_S B_t D_S}$ laminate class. The finite element (ABAQUS) simulation from Haynes and Armanios (2010) was performed using a nonlinear (geometry) analysis. The specimen, with a dimensions of 178 mm length and 25.4 mm width, was modelled with thin shell (S8R5) elements; 5 elements across the width and 38 elements along the length of the specimen; the boundary conditions, one end of the specimen is clamped with the other an edge load is applied; the specimen is loaded up to a maximum tensile load of 2,225N, using load increments of 445N.

This finite element model is replicated here to assess the twisting magnitude of similar classes of coupled laminate, in particular those given in Table 5.3. However, several modelling parameters have been altered for the purpose of this study. The laminate twisting magnitude is assessed up to an axial load corresponding to the predicted failure load, calculated from the commonly adopted Tsai-Wu failure criterion (Hyer, 2009):

$$F_1\sigma_1 + F_2\sigma_2 + F_{11}\sigma_1^2 + F_{22}\sigma_2^2 + F_{66}\tau_{12}^2 - \sqrt{F_{11}F_{22}}\sigma_1\sigma_2 = 1$$

where,

$$F_1 = \frac{1}{\sigma_1^T} + \frac{1}{\sigma_1^C} \qquad F_2 = \frac{1}{\sigma_2^T} + \frac{1}{\sigma_2^C} \qquad F_{11} = -\frac{1}{\sigma_1^T \sigma_1^C} \qquad F_{22} = -\frac{1}{\sigma_2^T \sigma_2^C} \qquad F_{66} = \left(\frac{1}{\tau_{12}^F}\right)^2 \tag{5.6}$$

The Tsai-Wu failure parameters are given in Table 5.4, which represent a standard carbon/epoxy material with the properties given in Table 4.3. The boundary conditions, matching the experiment, were applied via rigid body elements to a reference node at which the load was applied and axial extension and rotation measured. A mesh density double that used by Haynes and Armanios (2010) was found necessary to achieve good

convergence. This revised finite element model, illustrated in Fig. 5.7 is used to assess the twisting response of the laminate stacking sequence presented in Table 5.3 and the results are presented in Fig. 5.8.

Table 5.4 – Tsai-Wu failure parameters for Graphite/Epoxy material.

σ_1^T = 2400 MPa	F_1 = -0.21 (1/GPa)
σ_1^C = –1600 MPa	F_2 = 8.50 (1/GPa)
σ_2^T = 80 MPa	F_{11} = 0.26 (1/GPa)^2
σ_2^C = -250 MPa	F_{22} = 50 (1/GPa)^2
τ_{12}^F = 95 MPa	F_{66} = 111 (1/GPa)^2

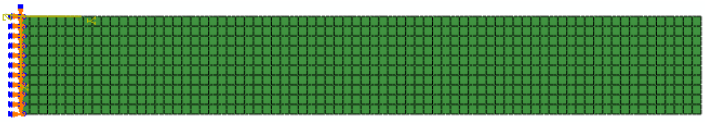

(a)

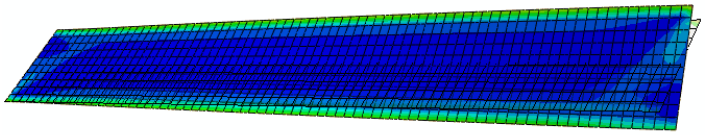

(b)

Figure 5.7 – Revised finite element model illustrating: (a) the number of elements along the length and across the width and; (b) Extension-Twisting deformation, with the contour represents the stress distribution after deformation.

Laminates L1 to L3 corresponds to the 8-ply laminates given in the order of increasing ξ_8 in the second column of Table 5.3, while laminates L4 to L6 are given in the third column of Table 5.3 having equal value of ξ_8 to laminates L1 to L3 respectively, however with opposite sign. Note that the predicted Tsai-Wu failure load decreases with increasing $\mathbf{B}_{16}$ value, as shown in Fig. 5.8.

Figure 5.8 gives the result for the six 8-ply HTCS $\mathbf{A}_S\mathbf{B}_t\mathbf{D}_S$ laminates with which the highest coupling magnitude, i.e. L1 and L4 are capable of generating a twist rate as high as 181 Deg./m and 185 Deg./m respectively, while L3 and L6 laminates, with weaker coupling, result in a twist rate of 46 Deg./m and 44 Deg./m respectively.

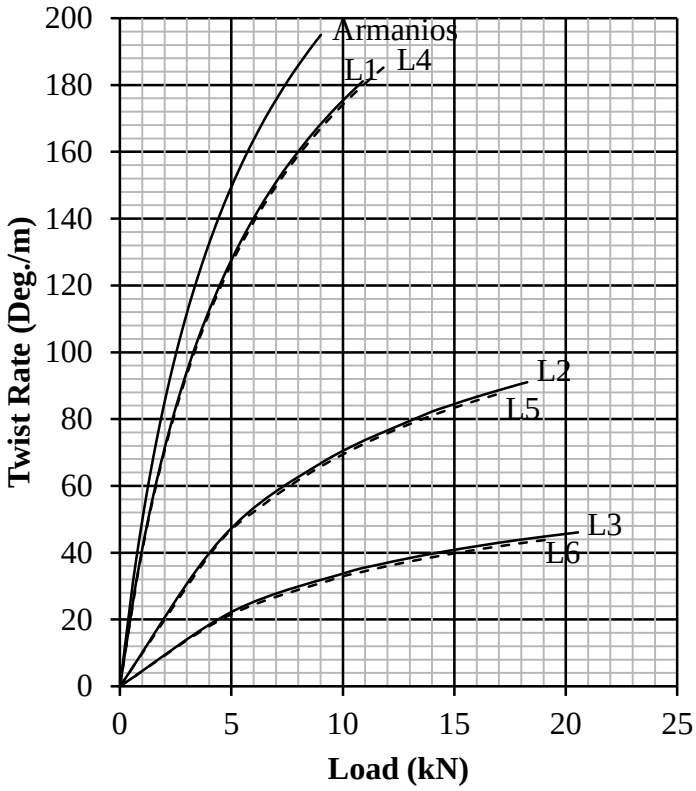

Figure 5.8 – Twist rate vs Load for the six 8-ply HTCS Extension-Twisting solutions.

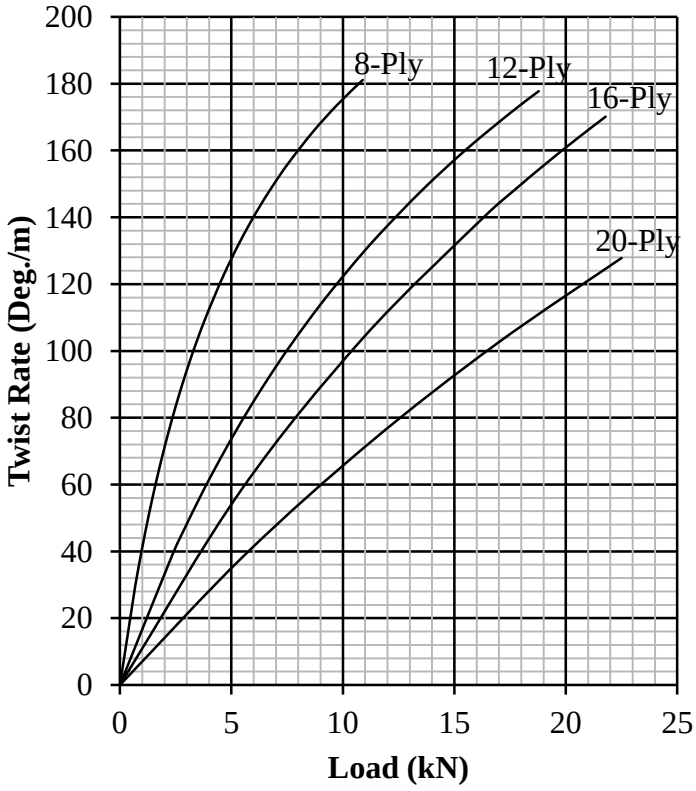

Figure 5.9 – Twist rate vs Load for the maximum Extension-Twisting solution for each ply number grouping.

Figure 5.9 provides a comparison between the maximum twist rates achievable for 8-, 12-, 16-, and 20-ply solutions, simulated using similar modelling parameters; corresponding to stacking sequences: $[(-22.5/67.5)_S/(22.5/-67.5)_S]_T$, $[(-22.5/\ 67.5)_2/67.5/\pm22.5/-67.5_2\ /22.5/-67.5/22.5]_T$, $[(-22.5/67.5)_{S2}\ /(22.5/-67.5)_{S2}]_T$, and $[-22.5_2\ /67.5_2\ /\ -22.5/67.5_3\ /(-22.5/22.5)_2\ /-67.5_3/(22.5/-67.5)_S/22.5]_T$, respectively.

The results in Fig. 5.8 and 5.9 are obtained with the specimen geometry modelled with a constant width, *a* and length, *L*. In other words, it is simulated under constant aspect ratio (*L*/*a*), which in this case where the specimen length, *L* = 178 and width, *a* = 25.4 gives an aspect ratio of 7. Note that the specimen for the results shown in Fig. 5.8 has a constant width to thickness ratio (*a*/*b*); where the specimen thickness, *b* is calculated by multiplying the number of plies, *n* with the lamina thickness, *t* = 0.183 mm, see Table 4.3, which gives *b* = 1.464 mm for the 8-ply laminate and a width to thickness ratio (*a*/*b*) of approximately 17. Figure 5.10 gives the results on the 8-ply laminate L1 tested under different aspect ratio conditions and with different width to thickness ratio value.

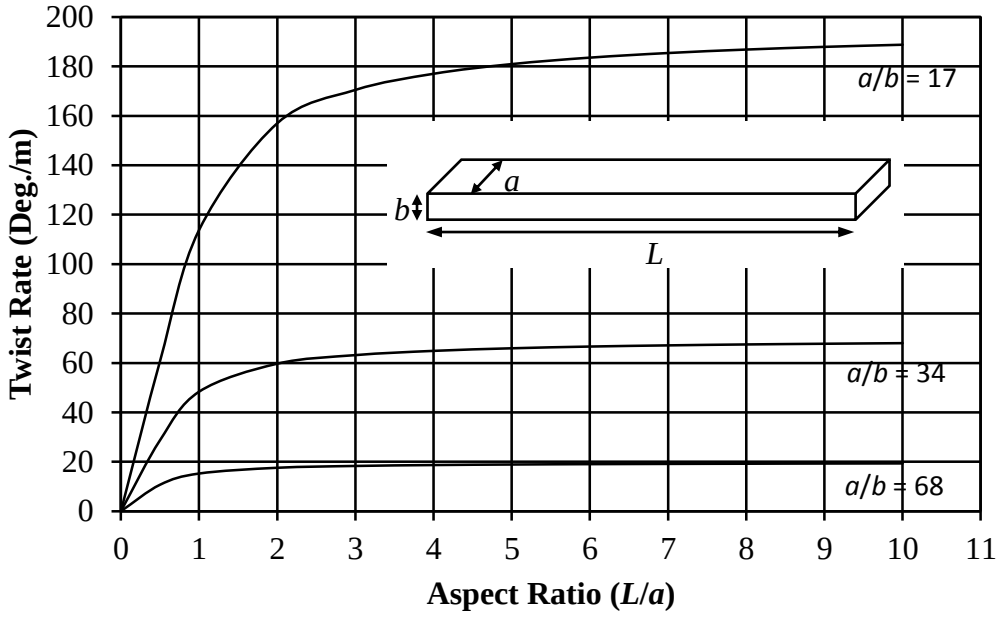

Figure 5.10 – The twist rate for the 8-ply laminate L1: $[-++-\bigcirc\bullet\bullet\bigcirc]_T$, modelled using different aspect ratio (*L*/*a*) value and at different width to thickness ratio (*a*/*b*) value.

Figure 5.10 shows a non-linear relationship for the twist rate with increasing aspect ratio value. The twist rate is shown to have a greater increase in low aspect ratio value but not in high aspect ratio value; the twist rate appears to be constant at a high aspect ratio if looking at specimen with higher value of width to thickness ratio. A smaller curve is shown in Fig. 5.10 for specimen having higher width to thickness ratio (*a*/*b*) value. Here the specimen thickness, *b* is constant, hence doubling the specimen width, *a* will double the value of the width to thickness ratio. The effect from which decreases the overall twist rate in the laminate by an average of 62%, which is shown by the line with *a*/*b* = 17 and 34. The trend for the twist rate with increasing aspect ratio and different width to thickness ratio is the same for all other 8-ply laminates, i.e. L2 – L6.

By contrast the results in Fig. 5.9 have different width to thickness (*a*/*b*) ratio due to the different ply number grouping, which result in different thicknesses. Figure 5.11 gives the comparison for the 8-, 12-, 16- and 20-ply number groupings, for different aspect ratio value but with constant width to thickness ratio (*a*/*b*) of 17. Note that the stacking sequences for the ply group in Fig. 5.11 is similar to the ones in Fig. 5.9.

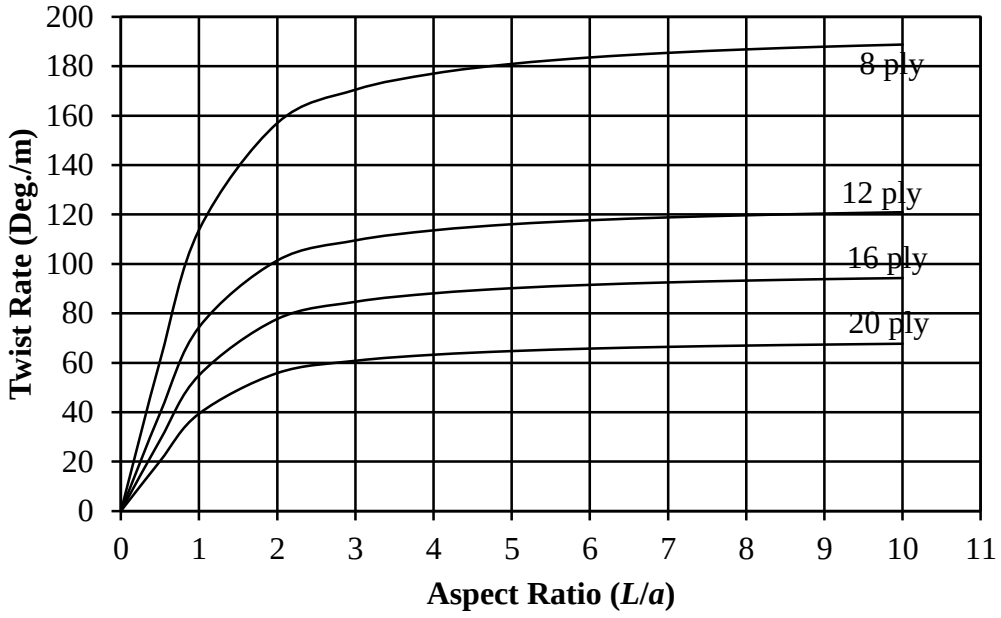

Figure 5.11 - Twist rate vs Aspect ratio for the maximum Extension-Twisting solution for each ply number grouping, with equal width to thickness ratio of *a*/*b* = 17.

Experimental tests were performed for specimens with Extension-Twisting coupling, aimed at validating the FE model. The laminates chosen for the test are laminate S1 and S2, previously discussed in Chapter 4; because these laminates possesses additional Extension-Shearing and/or Bending-Twisting coupling, the effect of these additional couplings on the overall twist magnitude can be assessed. The specimens of dimensions 24mm x 240mm cut at off-axis orientation $\beta = 22.5°$ from 380mm square plate specimen for laminates S1 and S2. The plate specimens were manufactured by Airbus, see Fig. 4.1, using a proprietary unidirectional carbon-fibre/epoxy material and high temperature/pressure cure cycle, for which the resulting properties are found to be slightly different to the ones presented in Table 4.3, i.e, with Young's modulus, $E_{11} = 170$ GPa and $E_{22} = 8$ GPa, Poisson's ratio, $\nu_{12} = 0.3$, shear modulus, $G_{12} = 4.5$ GPa and ply thickness, t = 0.183 mm. An Instron E10000 tension-torsion test rig, see Fig. 5.12, was employed to assess the magnitude of the Extension-Twisting coupling for each specimen. The tests were performed under load control, maintaining zero torque, up to a maximum tensile load of 2,225N, using load increments of 445N, and thus allowing the linearity of twist angle variation to be assessed.

Figure 5.12 – Experimental test performed for laminate S1 and S2 using the Instron E10000 tension-torsion machine.

Figure 5.13 (a) and (b) illustrates the Extension-Twisting coupling behaviour of the two laminate classes i.e. $\mathbf{A}_I\mathbf{B}_t\mathbf{D}_F$ and $\mathbf{A}_F\mathbf{B}_t\mathbf{D}_F$ respectively. The results of the experimental tests are presented together with the finite element simulation results for direct comparison. The figures demonstrate that the finite element simulations are in good agreement with the experimental results. At maximum load (2225N) these results equate to a twist angle of 5.8º and 7.2º over a gauge length of 180mm for laminate SP25 and SP27 respectively. It is evident that the additional effect of Extension-Shearing and/or Bending-Twisting coupling is seen to increase the twist magnitude of the specimen. Laminate S2 ($\mathbf{A}_F\mathbf{B}_t\mathbf{D}_F$) has a 24% increase in the twisting magnitude above laminate S1 ($\mathbf{A}_I\mathbf{B}_t\mathbf{D}_F$).

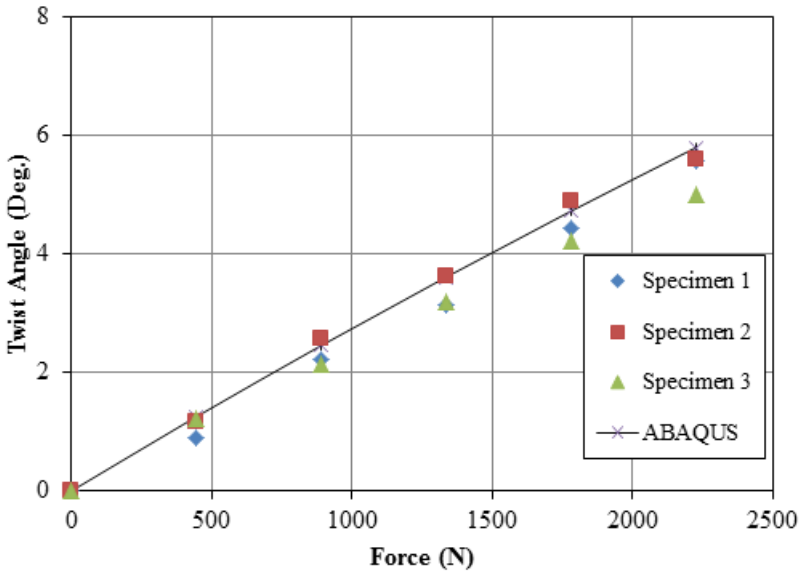

(a)

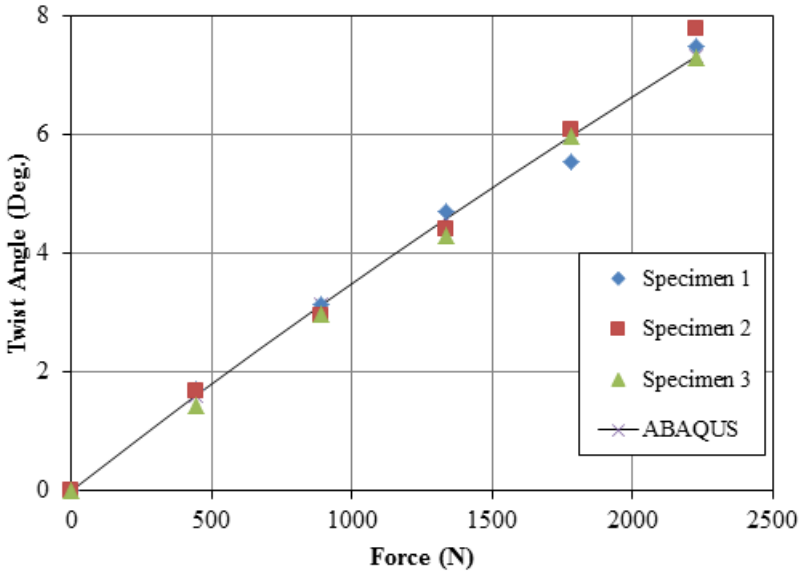

(b)

Figure 5.13 – Comparison of the twist angle vs. force, between experimental and ABAQUS results for: (a) Laminate S1 and; (b) LaminateS2.

Figure 5.14 shows the twist rate magnitudes for laminate S1 and S2, which are simulated up to their maximum predicted failure load. Laminate S2 was observed up to a maximum force of approximately 12kN, producing a maximum twist rate of 139 Deg./m. The same loading for laminate S1 produced a twist rate of approximately 115 Deg./m; but possesses a higher failure load. Also shown in Fig. 5.14 is a 12-ply $\mathbf{A}_S\mathbf{B}_t\mathbf{D}_S$ coupled laminate with the stacking sequence: $[-/+/-/+/\bigcirc/+/\bullet/-/\bullet/\bigcirc/\bullet/\bigcirc]_T$, where the laminate possesses identical stiffness properties to laminate S1, except that the Bending-Twisting terms ($\mathbf{D}_{16}$ and $\mathbf{D}_{26}$) are zero.

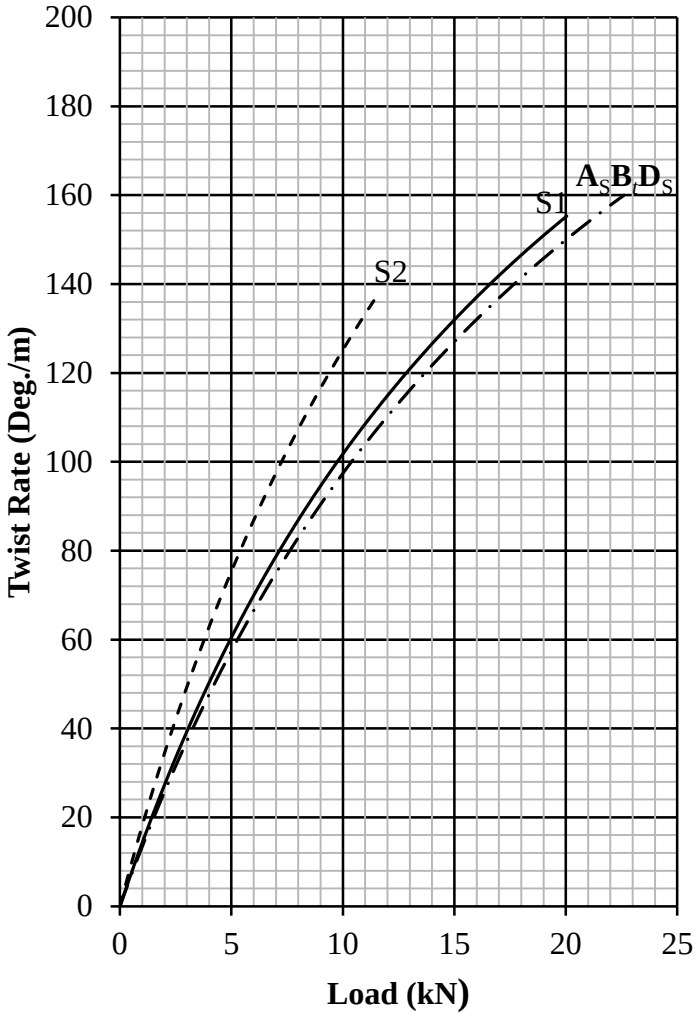

Figure 5.14 – Twist rate vs load for S1 and S2 simulated under maximum Tsai-wu failure load. Also shown is an $A_S B_t D_S$ laminate that has matching stiffness properties with laminate S1.

5.3 Buckling assessment

Closed form solutions for compression buckling and natural frequency prediction of simply supported rectangular panels are well known and well documented in the literature for both isotropic materials and orthotropic laminated composite materials. Less well known are closed form solutions for coupled laminates, derived previously for cross-ply laminates (Jones, 1975), possessing Extension-Bending coupling, and for angle-ply laminates (Whitney and Leissa, 1969), with Extension-Twisting (and Shearing-Bending) coupling. This is perhaps due to the widespread misunderstanding of coupled laminate buckling behaviour to which these closed form buckling equations correspond. For instance, many results have been presented for the buckling problem with simply supported boundary conditions, on the false assumption that bifurcation buckling occurs: simply supported rectangular plates consisting of cross-ply laminates with Extension-Bending coupling will in fact bend, and not buckle, under in-plane compressive load.

Early work investigating the effect of coupling on the buckling strength for simply supported rectangular anti-symmetric angle-ply laminated plates (Whitney and Leissa, 1970) concluded that a decrease in the plate buckling strength, with respect to the fully uncoupled laminate solution, occurs at all plate aspect ratios. This work however precluded the possibility that Extension-Twisting coupling can be achieved by other forms of laminate stacking sequence (York, 2012).

Bounds on the critical buckling load for the 8-, 12-, 16- and 20-ply HTCS Extension-Twisting (and Shearing-Bending), coupled $\mathbf{A}_S\mathbf{B}_t\mathbf{D}_S$ laminates are therefore investigated, using the closed-form buckling solution of Eq. (5.8), derived elsewhere (Whitney and Leissa, 1969, Jones, 1999). Here the values m and n are the number of buckle half wavelengths in the x and y directions, respectively.

The bounds for the critical buckling load are presented in non-dimensional form,

$$k_x = (N_x b^2)/(\pi^2 D_{iso}) \tag{5.7}$$

across a range of plate aspect ratios, where:

$$N_x = (a/m\pi)^2 \left\{ T_{33} + (2T_{12}T_{23}T_{13} - T_{22}T_{13}^2 - T_{11}T_{23}^2) / (T_{11}T_{22} - T_{12}^2) \right\}$$

with

$$\begin{aligned}
T_{11} &= A_{11}(m\pi/a)^2 + A_{66}(n\pi/b)^2 \\
T_{12} &= (A_{12} + A_{66})(m\pi/a)(n\pi/b) \\
T_{13} &= -(3B_{16}(m\pi/a)^2 + B_{26}(n\pi/b)^2)(n\pi/b) \\
T_{22} &= A_{22}(n\pi/b)^2 + A_{66}(m\pi/a)^2 \\
T_{23} &= -(B_{16}(m\pi/a)^2 + 3B_{26}(n\pi/b)^2)(m\pi/a) \\
T_{33} &= D_{11}(m\pi/a)^4 + 2(D_{12} + 2D_{66})(m\pi/a)^2(n\pi/b)^2 + D_{22}(n\pi/b)^4
\end{aligned} \tag{5.8}$$

and D_{Iso} is given in Eq. (3.9). Note that if the terms $\mathbf{B}_{16} = \mathbf{B}_{26} = 0$, Eq. (5.8) degenerates to a simpler form given by:

$$N_x = \pi^2 \left[D_{11}\left[\frac{m}{a}\right]^2 + 2(D_{12} + 2D_{66})\left[\frac{n}{b}\right]^2 + D_{22}\left[\frac{n}{b}\right]^4 \left[\frac{a}{m}\right]^2 \right] \tag{5.9}$$

Through inspection of Eq. (5.9) the minimum critical buckling load, N_x occurs when n = 1. Therefore the critical buckling load, N_x is dependent on m, i.e. the buckle half-waves in the x-direction, and also the plate aspect ratio, *a*/*b*. Figure 5.15 illustrate the buckling curve for different aspect ratio and different m value for the case of equivalent fully isotropic laminate (FIL).

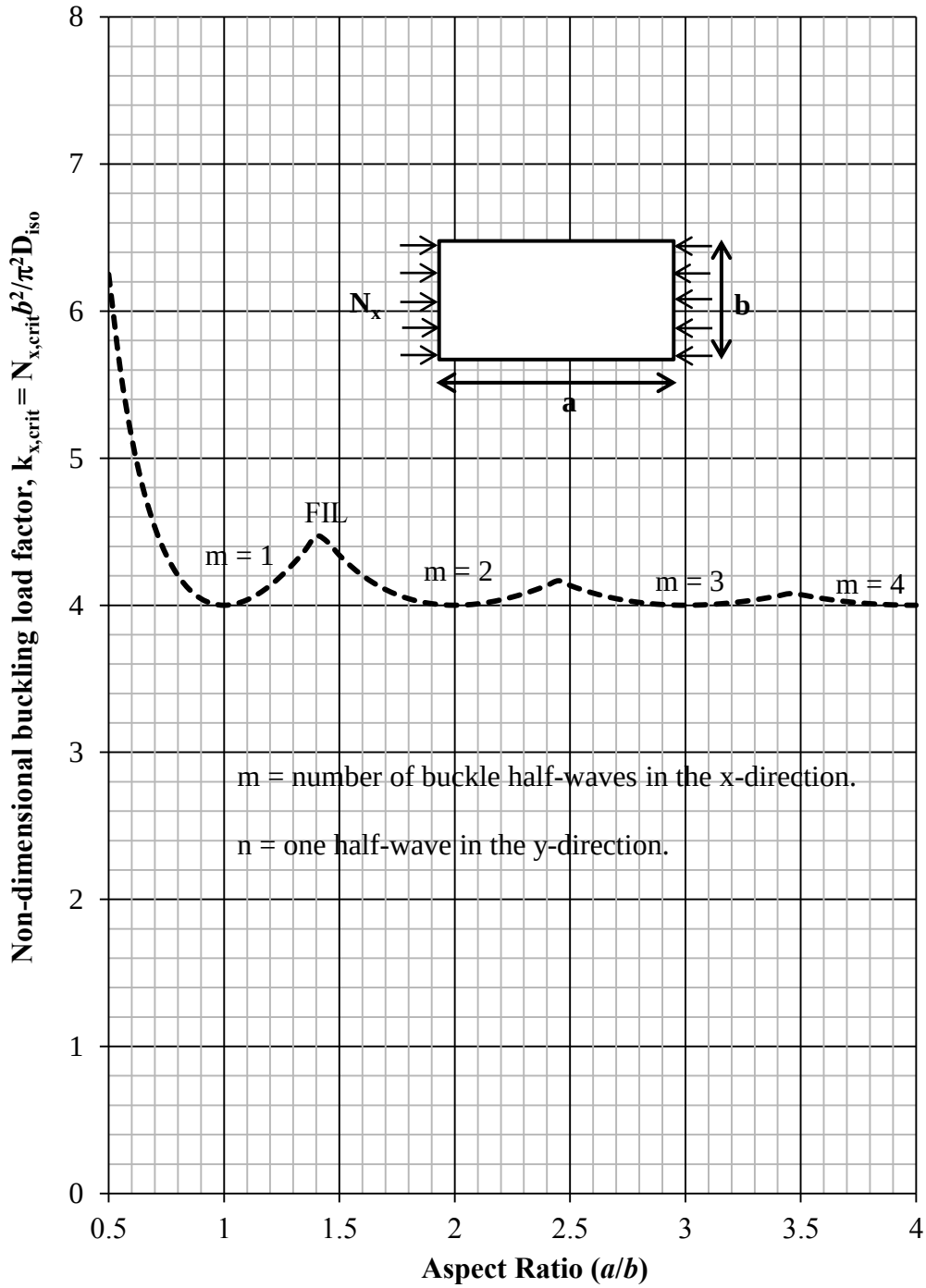

Figure 5.15 – Buckling curve for equivalent fully isotropic laminate (FIL), where the lowest k_x value corresponds to a value of 4.

Figures 5.16 to 5.19 illustrate the curves of the critical buckling load for the 8-, 12-, and 16- and 20-ply HTCS laminate solutions with Extension-Twisting (and Shearing-Bending) coupling behaviour. The buckling curve for an equivalent fully isotropic laminate (FILs) is also plotted on each figure for comparison.

The bounds in Figs. 5.16 to 5.19 reveal that HTCS Extension-Twisting coupled laminate configurations all fall on or below the buckling strength of the equivalent fully isotropic laminates (FIL). The 8-ply laminate example given earlier i.e. laminate L1 and L4, has the highest Extension-Twisting coupling magnitude in its ply number grouping, but this results in up to a 16% reduction in buckling strength compared to the equivalent fully isotropic laminate; it represents the lower bound curve shown in Fig. 5.16.

Also presented in Fig. 5.16 are two competing laminate designs from the literature. The buckling envelope corresponding to Haynes and Armanios (2010) represents a configuration that has been optimised for maximum Extension-Twisting coupling, resulting in a configuration with free-form angle orientations: $[-21.5/72.1/57.9/-29.6/29.6/-57.9/-72.1/21.5]_T$. However, the effect of increased Extension-Twisting coupling can be seen to have a negative influence on the laminate buckling strength, and the buckling envelope falls below the lower bound for laminates with standard ply orientations in Fig. 5.16. The buckling envelope corresponding to $[20/-70/20/-70/-70/20/-70/20]_T$ Nixon (1987), represents an Extension-Shear coupled laminate, which has been used in tilt-rotor blade designs to produce Extension-Twisting coupling behaviour at the structural level. Here, an 8-ply balanced and symmetric stacking sequence, $[(0/90)_2]_S$, with off-axis material alignment of 20°, gives rise to the Extension-Shearing coupling behaviour at the laminate level. However, the off-axis alignment also introduces Bending-Twisting coupling, which has a significant impact on the compression buckling strength (York and Weaver, 2010). Given that no exact closed form solution exists for laminates with

Extension-Shearing and Bending-Twisting coupling, this buckling envelope was developed using a commercial finite element code. The buckling strength for this class of coupled laminate is shown to be up to 11% lower than the equivalent fully isotropic laminate.

Similarly the buckling curves for S1 and S2 laminates are obtained using the finite element method, with the results presented in Fig. 5.20. Figure 5.20 presents the $\mathbf{A}_S\mathbf{B}_t\mathbf{D}_S$ coupled laminate, which has matching stiffness properties with laminate S1. The results shown in the figure confirm the predictions from others (Fukunaga and Sekine, 1994, York and Weaver, 2010) that a reduction in buckling strength occurs as a consequence of the Bending-Twisting coupling in the laminate. Meanwhile, the critical buckling load of laminate S2 is shown to be similar to laminate S1.

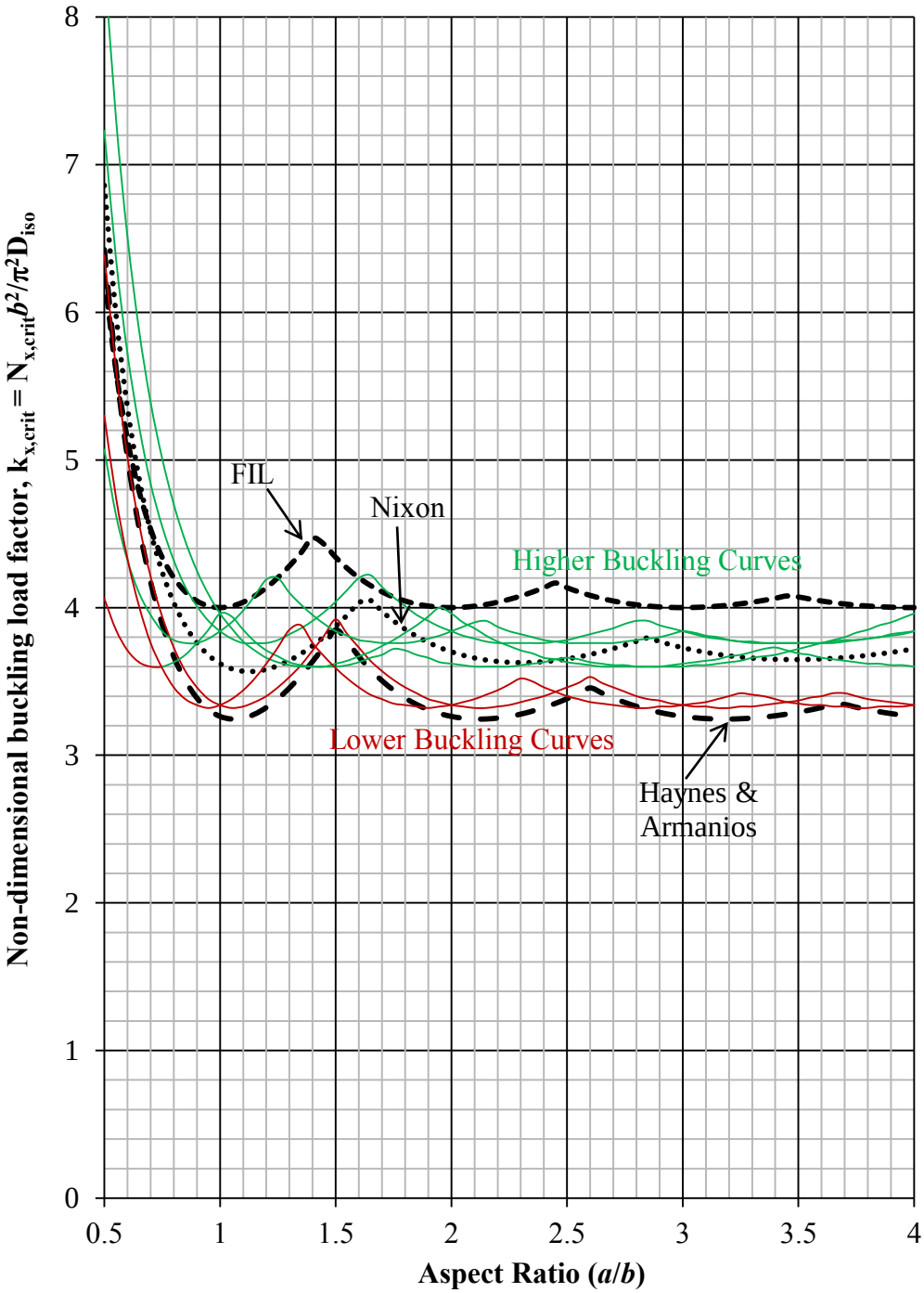

Figure 5.16 – The compression buckling curves of the 8-ply Extension-Twisting (and shearing-bending) coupled HTCS laminates.

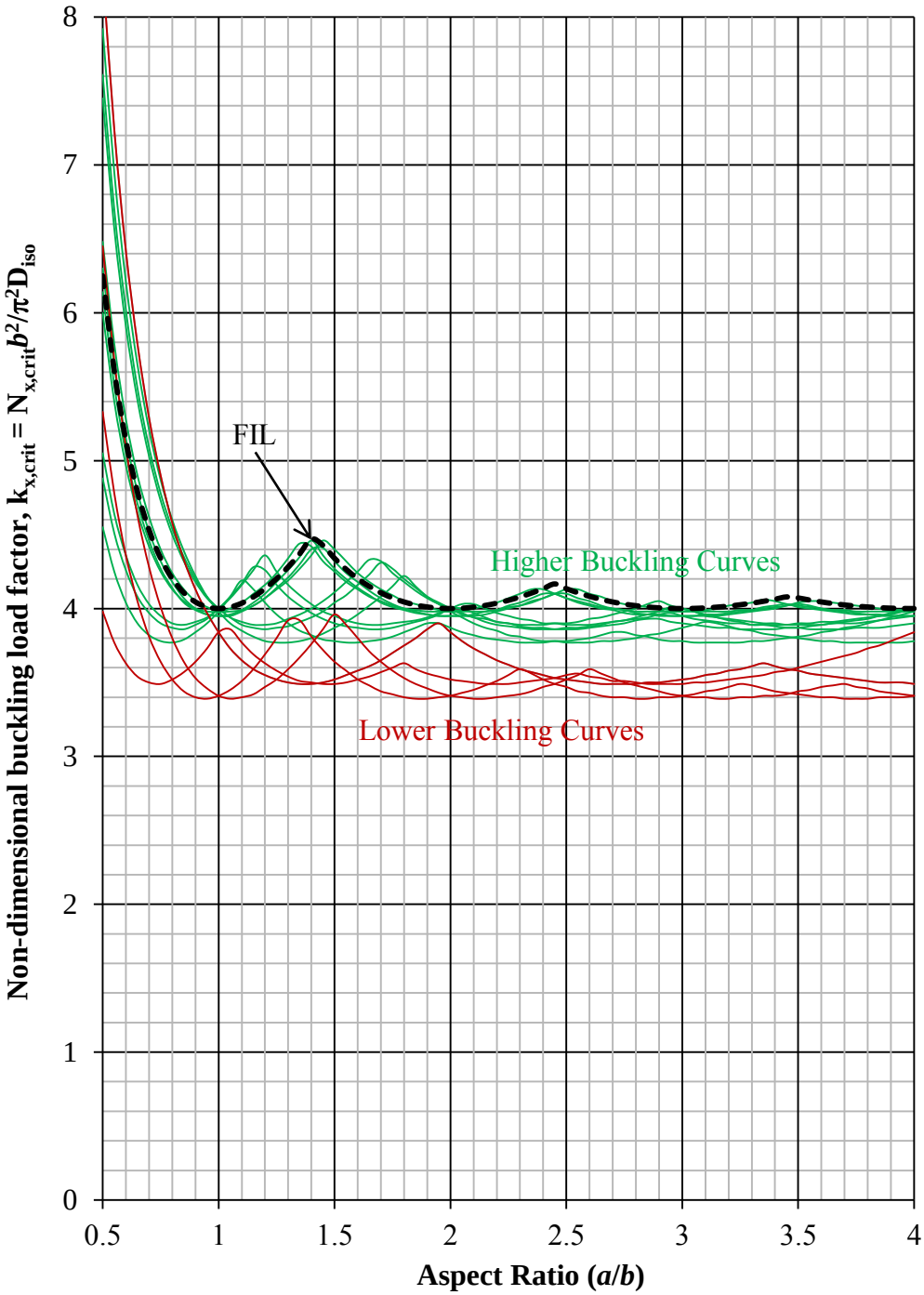

Figure 5.17 – The compression buckling curves of the 12-ply Extension-Twisting (and shearing-bending) coupled HTCS laminates.

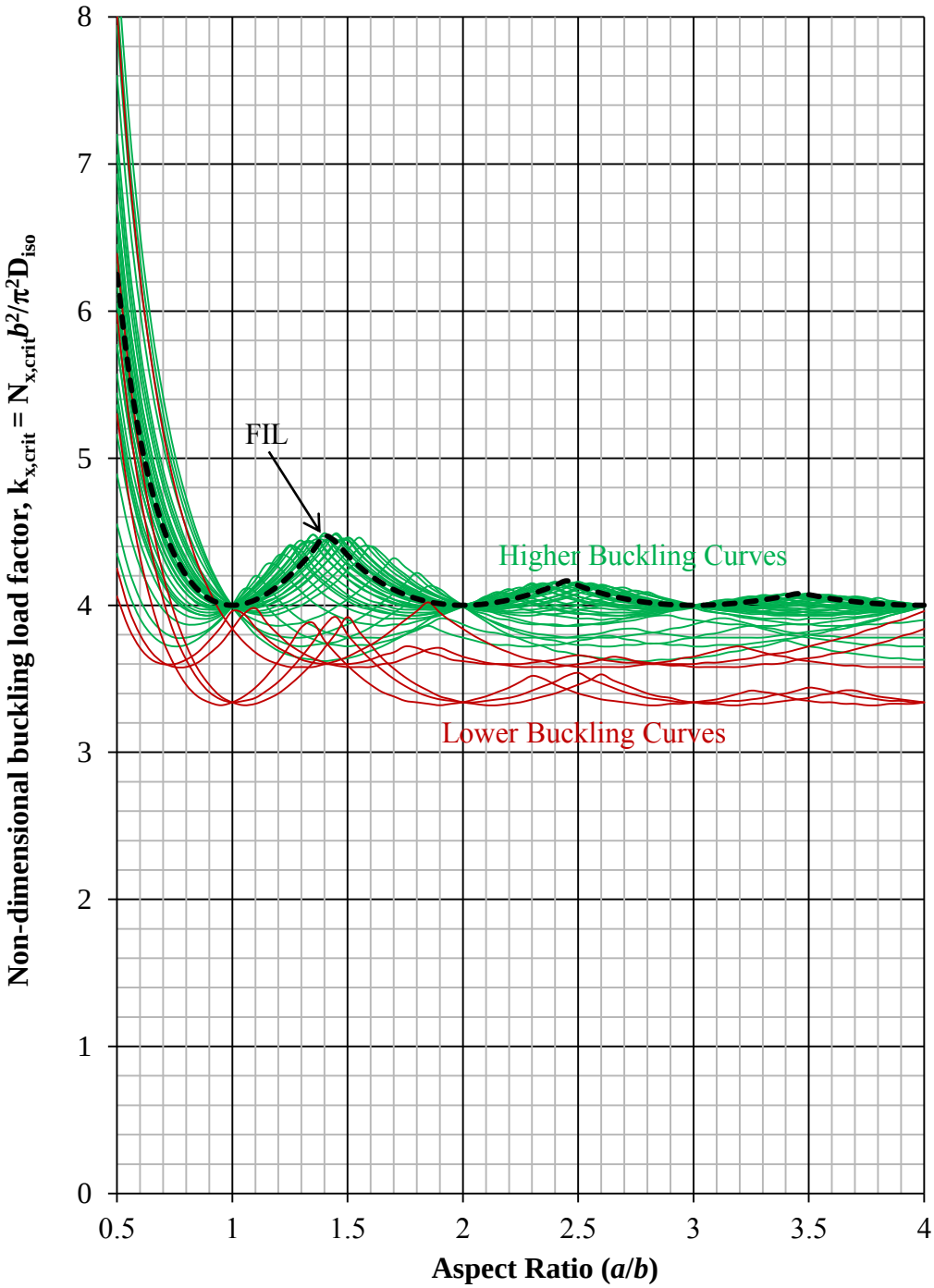

Figure 5.18 – The compression buckling curves of the 16-ply Extension-Twisting (and shearing-bending) coupled HTCS laminates.

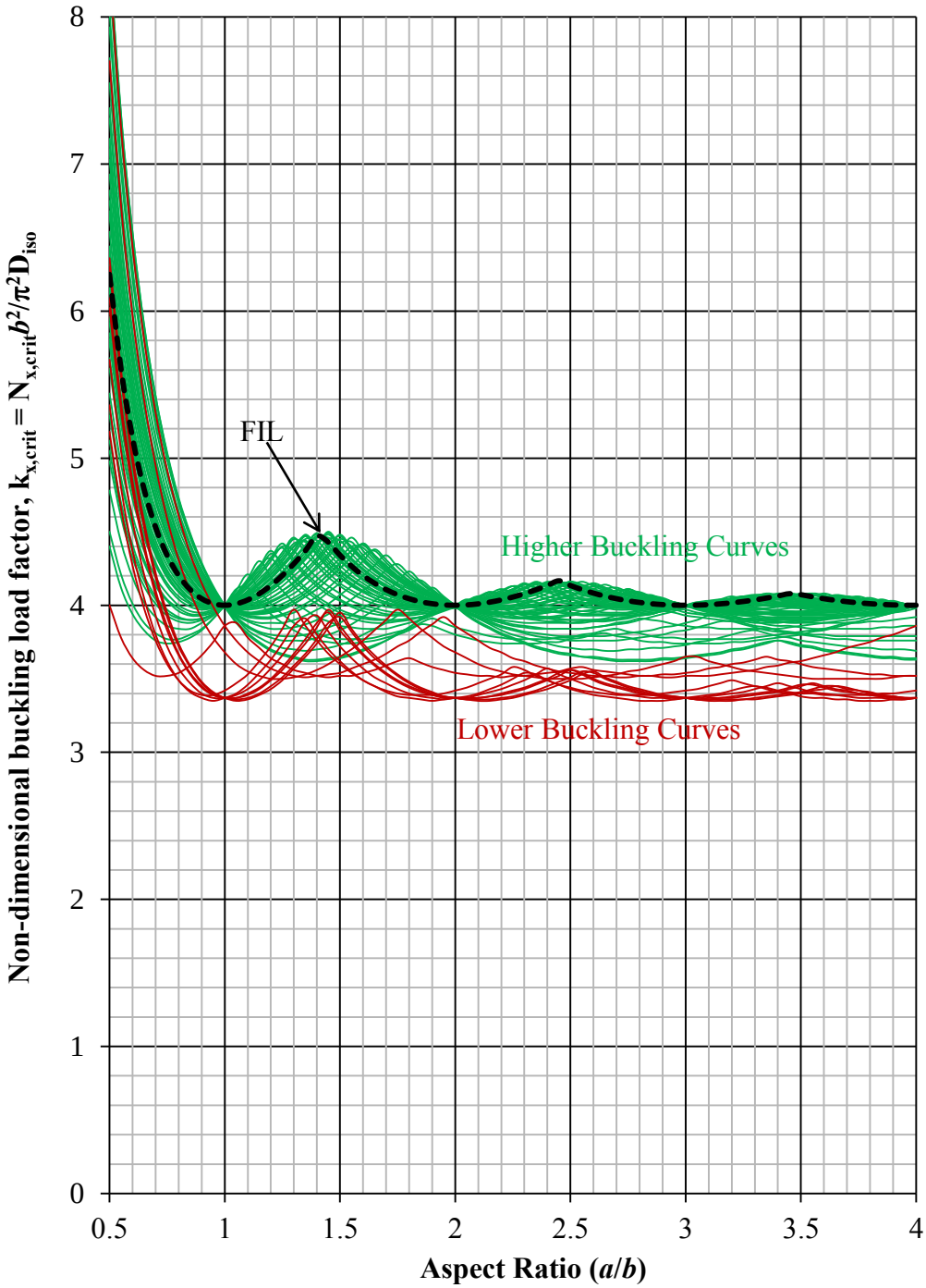

Figure 5.19 – The compression buckling curves of the 20-ply Extension-Twisting (and shearing-bending) coupled HTCS laminates.

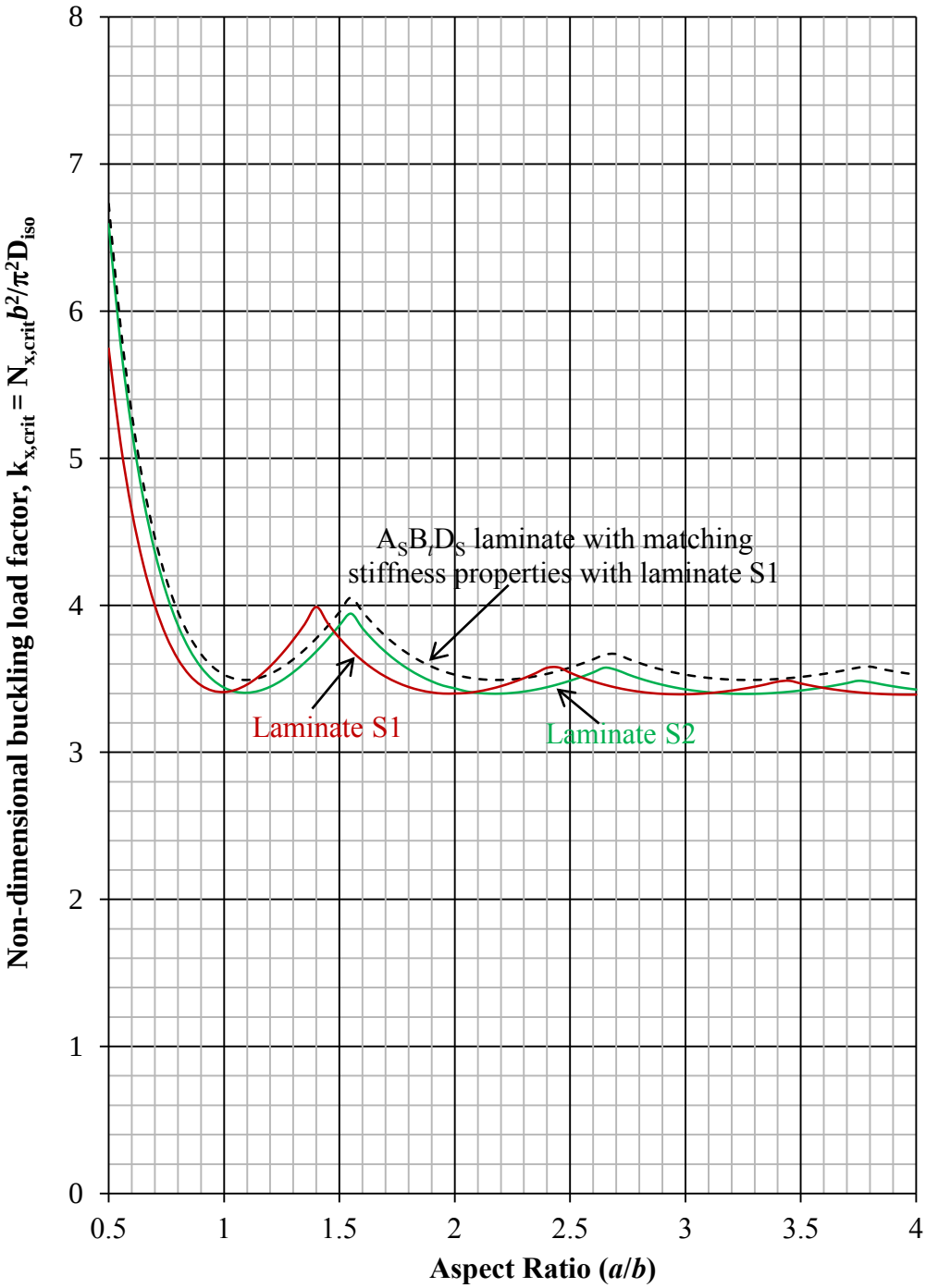

Figure 5.20 – The compression buckling curves for laminate S1 ($A_IB_tD_F$) and laminate S2 ($A_FB_tD_F$). Also shown is an $A_SB_tD_S$ laminate $[-/+/-/+/○/+/●/-/●/○/●/○]_T$ which has matching stiffness properties with laminate S1.

5.4 Conclusion

An assessment of the structure response of HTCS laminates with Extension-Twisting (and shearing-bending) mechanical coupling behaviour has been reported. Results from finite element predictions for Extension-Twisting of HTCS laminates, accounting for non-linear (geometry), have been shown to demonstrate excellent agreement with experimental results. The additional of Extension-Shearing and/or Bending-Twisting coupling at the laminate level has been found to have an increasing effect on the total magnitude of the Extension-Twisting coupling behaviour.

The buckling curves have been presented for HTCS laminates with Extension-Twisting (and shearing-bending) coupling for 8-, 12-, 16- and 20-ply laminate solutions. All laminates are based on standard ply orientations to which an off-axis orientation is then applied. The upper-bound buckling envelopes are all shown to fall on or below the buckling curve representing the equivalent fully isotropic laminate, used here as a datum configuration against which all comparisons have been made.

Laminates derived from free form angle orientations, which have been optimised for maximum Extension-Twisting coupling, have been shown to fall below the lower-bound buckling envelope of laminates with standard ply orientations. Extension-Shearing coupled laminates, which can also be configured to produce Extension-Twisting at the wing box level were found to have a similar buckling strength to the new designs presented.

CHAPTER 6

Mechanically Coupled Laminates with Balanced Plain Weave

Composite laminates made from woven cloth materials are now commonplace in secondary structure applications, e.g. flight control surfaces, and are noteworthy for their improved damage tolerance compared with their unidirectional material counterparts. They are however most often used in their simplest form, i.e. balanced and symmetric laminates, to mimic the metallic materials that they are replacing, which serves only as weight reducing strategy. Laminate tailoring using woven cloth materials offers the possibility of adding additional functionality to the material, alongside weight reduction, by introducing unique mechanical interactions between in-plane and out-of-plane deformations.

A single layer of plain weave material is known to possess thermal stability, i.e., immunity to thermal warping distortions. This can be understood from physical reasoning alone, where equal numbers of identical warp and weft fibres exist within a single layer, thus representing an architecture described as square symmetric (Tsai and Hahn, 1980), i.e., with equal stiffness on principal axes. Woven cloth architectures with square symmetric

properties are generally classified as symmetric, as in plain weave and 2 x 2 twill weave, illustrated in Fig. 6.1 (a) and (b) respectively. Non-symmetric woven cloth architectures, e.g. 5-harness satin weave as illustrated by Fig. 6.1 (c), have warp-dominated fibres on one side of the geometric mid-plane and weft-dominated fibres on the other. A single layer of non-symmetric woven cloth possesses coupling between in-plane and out-of-plane deformation, hence thermal warping distortions arise in such architectures (Shamsudin *et al*., 2013b).

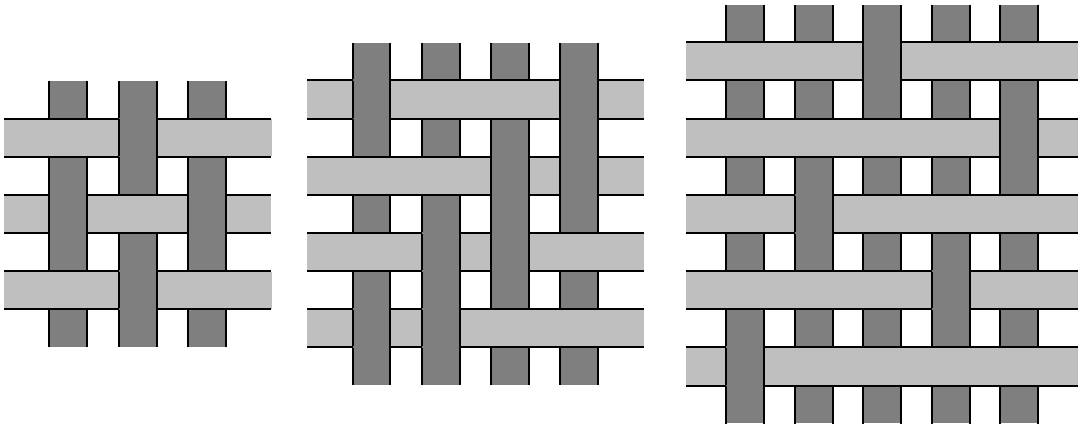

Figure 6.1 – General types of woven fabric preforms: (a) Plain weave; (b) 2x2 Twill weave and; (c) 5-Harness Satin weave.

Balanced plain weave architecture, illustrated in Fig. 6.2, can be characterised as high crimp fabric, where the crimp angle is typically of the order of 45°. Micro-mechanical modelling (Ishikawa and Chou, 1982, Naik and Shembekar, 1992a, Raju and Wang, 1994) has helped in understanding the mechanisms leading to observed reductions in elastic properties and mechanical performance in such high crimp fabrics, compared to non-crimp fabric or unidirectional laminated material (see Table 4.3). Ishikawa (1982) proposed three analytical models, which have formed the basis of many subsequent analytical models (Naik and Shembekar, 1992a, Raju and Wang, 1994). These three models are the Mosaic model, fibre undulation model and the bridging model.

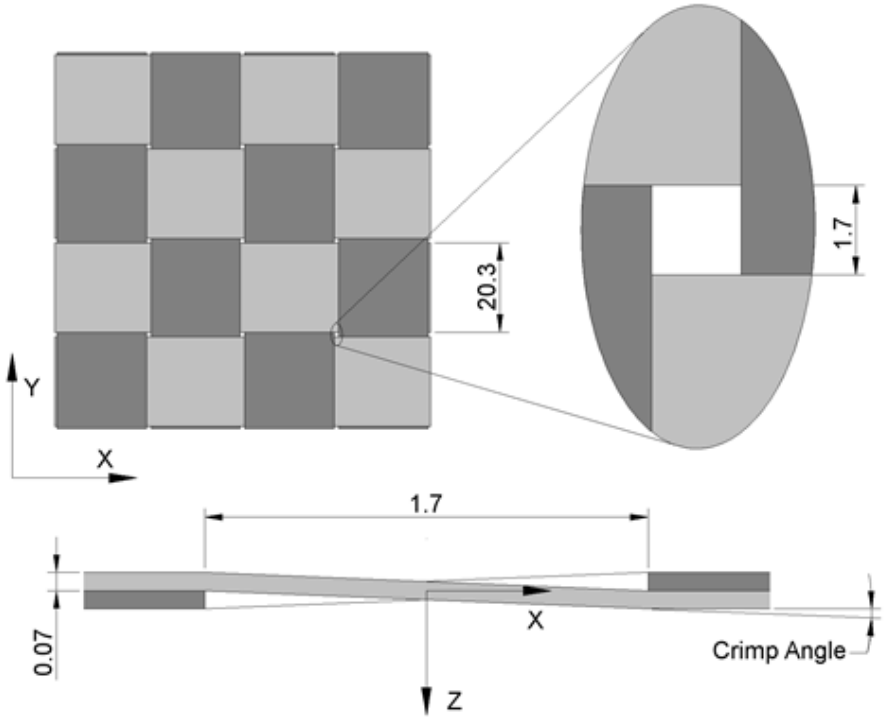

Figure 6.2 – Balanced plain weave architecture, illustrating a plain weave view of a representative volume element with exploded details. Dimensions provided are representative of (TeXtreme®) spread tow fabric with 70μm tape thickness and 2.5° crimp angle.

The Mosaic model is an ideal assemblage of asymmetrical cross-ply laminates where the crimp, or undulations, of the fibres have been omitted in the model as illustrated in Fig. 6.3. Hence this model is the simplest model of the three. Indeed Soykasap (2011) evaluated this Mosaic model against two other simple analytical models, which are the rule of mixtures and the composite beam and concluded that while the in-plane properties prediction agrees relatively well, the flexural properties do not. A refined Mosaic model was proposed by Ishikawa and Chou (1982), in which the fibre undulation and geometrical shape functions were incorporated into the model, see Fig. 6.4. This fibre undulation model was later renamed as the crimp model (Ishikawa *et al*., 1985).

Nevertheless, the shape of the fibres was only considered along the fill direction, hence this model was given known to many as the one-dimensional model. However it revealed a decrease in the elastic properties in plain weave material due to the fibre undulation (Ishikawa and Chou, 1982).

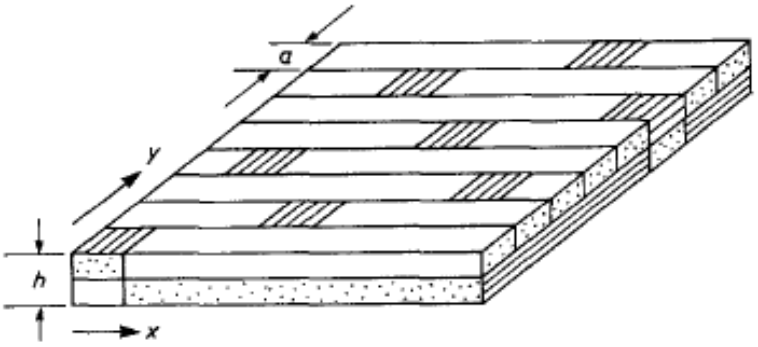

Figure 6.3 – The Mosaic model, (after Ishikawa and Chou, 1982).

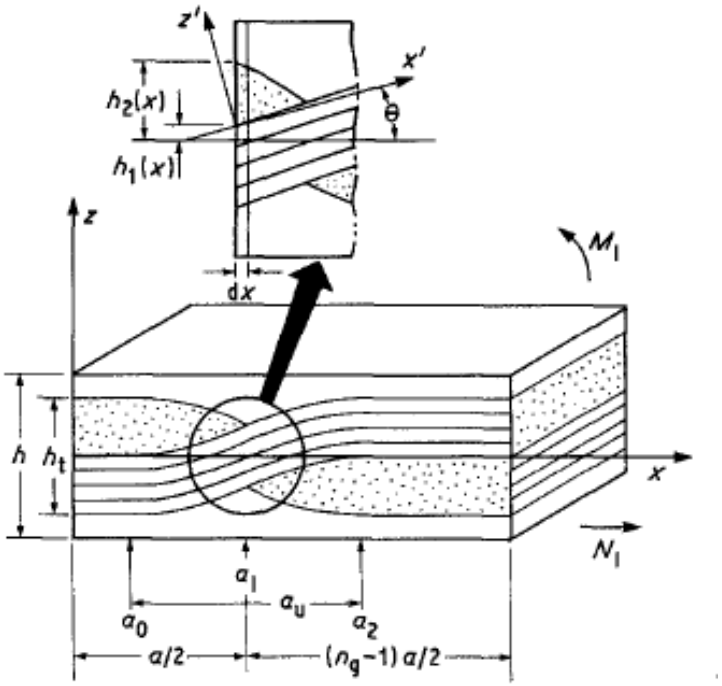

Figure 6.4 – Fibre Undulation model, which takes into account the effects of the crimp in the fibres, (after Ishikawa and Chou, 1982).

Further refinements of the crimp model were later performed by Naik and Shembekar (1992a), where continuity of the warp fibres were taken into account in the geometrical description, illustrated in Fig. 6.5, which categorise it as a two-dimensional approach. Another refinement of the crimp model was to account for the influence of possible gaps between the yarns. Indeed this two-dimensional approach yielded better prediction of the

elastic stiffness properties, i.e. closer to experimental predictions in comparison to the one-dimensional model. By contrast the bridging model is a combination of the Mosaic and fibre undulation model, see Fig. 6.6, which is relevant in the context of Satin weave material since the interlaced region (region C) is surrounded with straighter fibres (region A, B, E, D). Here the straighter fibres act as load-carrying bridges between adjacent interlaced region, hence the implied name bridging model.

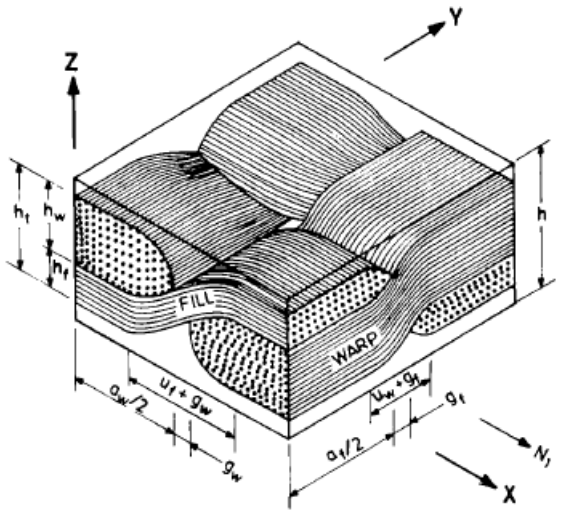

Figure 6.5 – A two dimensional geometrical model, which is a refinement from the fibre undulation model or crimp model by incorporating the shape of the warp fibre into the model, (after Naik and Shembekar, 1992a).

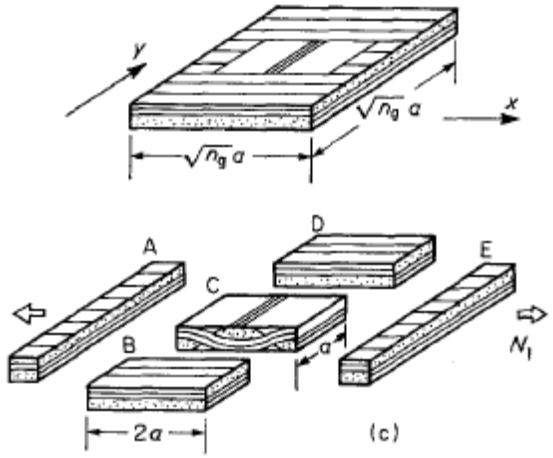

Figure 6.6 – The bridging model, which is a combination of the mosaic model and the fibre undulation model, (after Ishikawa and Chou, 1982).

Micro-mechanical modelling is generally based on a single layer, or lamina, and on the basis of representative volume element (RVE). However, multi-layer models are more realistic within the context of the current research, and have for instance demonstrated the importance of incorporating random phase shift (Shembekar and Naik, 1992, Naik and Shembekar, 1992b) in the relative weave position between layers, but such modelling strategies quickly approach current computational limits. Indeed, present lamina level micro-mechanical modelling strategies have been shown (Ishikawa *et al*., 1985) to incorrectly predict the laminate level elastic properties; the significant differences in elastic properties between single layer and 8-layer balanced plain weave laminate have been demonstrated experimentally (Jekabsons and Bystrom, 2002). Indeed it has been observed that the elastic modulus increases, with increasing number of layers, up to an asymptotic value corresponding to the 8-layer balanced plain weave laminate (Ishikawa *et al*., 1985, Naik and Shembekar, 1992b). The use of analytical models generally requires assumptions to be made with respect to the stress or strain fields in the composite, which are often found to be satisfactory in the case of elastic stiffness prediction.

Whitcomb (1989) carried out a three-dimensional finite element analysis of plain weave composites, which allows more detailed interrogation of the stress field across the thickness of the composite. The analysis was performed on several stacked repeating unit cells, investigating the influence of the fibre arrangements within the laminate. Similarly Foye (1993) developed a finite element scheme based upon the unit cell, where the geometrical model was meshed using inhomogeneous elements; called replacement elements. Meanwhile Whitcomb and Woo (1994) developed a macro-element to enhance the computational efficiency for elasticity analysis of heterogeneous materials. The macro-element accounts for the details of the microstructure within an element; containing several sub-domains within an element that can be assigned different material properties. Macro-elements were used to study the effect of fibre tow misalignment on a two-layered stacked

plain weave laminate (Woo and Whitcomb, 1997) where the results corresponded to the analytical predictions from Naik and Shembekar (Naik and Shembekar, 1992b, Shembekar and Naik, 1992). Woo (2005) later included the influence of different fibre orientations on two-ply stacked plain weave laminates, in the attempt to study the effect of both fibre phase shift and angle orientations on the engineering properties of plain weave laminates.

Meanwhile Marrey and Sankar (1997) developed a finite element technique called the Direct Micro-Mechanical (DMM) modelling method, which allows for computing the plate stiffness coefficients i.e. **ABD** matrices of the textile composite. This technique is similar to the continuum method for modelling textile composites as homogeneous materials (Marrey and Sankar, 1993), which was used for predicting the elastic properties of the textile composite, but only differs in terms of the adopted periodic boundary conditions for the plate since the approach treated the textile composite as a homogeneous plate instead. Karkkainen and Sankar (2006) later employed the DMM technique to investigate the stress gradient effect in textile composites, assuming that the stress state is not uniform across the studied Repetitive Volume Element (RVE). To account for the non-uniformity, or gradient, improvement in the current DMM model was made to include the effect of the moment [M] vector, see Eq. (2.1), which in general has been neglected in conventional models by assuming a uniform stress state with only the force [N] vector. However accounting for the moment vector [M] was found to be small.

Spread tow, or thin ply reinforcement offers an enabling technology for enhanced mechanical performance in plain weave architecture. TeXtreme®, see Fig. 6.2, balanced plain weave architecture can now be produced with crimp angles as small as 2.5º by weaving flat tapes, rather than yarns, where tape widths of 20mm and tape thickness of 70μm result in properties approaching those of non-crimp fabric. The substantial reduction in crimp angle opens the possibility of adopting a simple analytical model rather for

analysing laminate characteristic. Classical Lamination Theory (CLT), which assumes homogeneity with the composite material provide a good initial estimate of the composite plate stiffness properties without requiring a sophisticated micro-mechanics modelling calculation, particularly if the influence of the fibre crimp is less dominant, as in the case of the Textreme® woven cloth material. Therefore, the work on classification of mechanically coupled laminate classes from balanced plain weave may be achieved from the assumptions of equal modulus, $E_1 = E_2$, with the added restrictions that each layer in the laminate has identical material properties and thickness, and that layers differ only by their orientation.

6.1 Characterisation of balanced plain weave laminate

Due to the balanced nature of a single layer of plain weave, i.e., equal fibre volume fractions in the 0 and 90º directions, see Fig. 6.2, the warp and weft directions are indistinguishable, thus justifying the equal modulus ($E_1 = E_2$) condition assumed. Hence, standard ply angle orientations, 0, 90 and ±45º, simplify to 0 and 45º; since the orthogonal counterparts, 90 and -45°, possess exactly the same properties, respectively. In addition, the laminate invariant $U_2 = 0$, since $Q_{11} = Q_{22}$ follows directly from the equal modulus assumption. The thermal coefficients $\alpha_1 = \alpha_2 = \alpha_{Iso}$ follow from the same physical reasoning, and are also readily demonstrated from α_{Iso} for the equivalent isotropic laminate and the reduced form for balanced plain weave, i.e.:

$$\alpha_{iso} = \frac{\alpha_1 + \alpha_2}{2} + \frac{(\alpha_1 - \alpha_2)U_2}{2(U_1 + 2U_4)}$$
$$\alpha_{iso} = \frac{\alpha_1 + \alpha_2}{2} \tag{6.1}$$

Note that mechanical isotropy also leads to thermal isotropy but the reverse is not necessarily true, i.e., thermal isotropy does not guarantee mechanical isotropy. As a result of the simplifications, the elements of the ABD matrix in Eq. (2.17) simplify compared to those for laminates containing layers of unidirectional material, giving:

$$\begin{aligned} A_{11} &= \{U_1 + \xi_2 U_3\}H & A_{12} = A_{21} &= \{-\xi_2 U_3 + U_4\}H & A_{16} = A_{61} &= \{\xi_4 U_3\}H \\ A_{22} &= \{U_1 + \xi_2 U_3\}H & A_{26} = A_{62} &= \{-\xi_4 U_3\}H & A_{66} &= \{-\xi_2 U_3 + U_5\}H \end{aligned} \tag{6.2}$$

$$\begin{aligned} B_{11} &= \{\xi_6 U_3\}H^2/4 & B_{12} = B_{21} &= \{-\xi_6 U_3\}H^2/4 & B_{16} = B_{61} &= \{\xi_8 U_3\}H^2/4 \\ B_{22} &= \{\xi_6 U_3\}H^2/4 & B_{26} = B_{62} &= \{-\xi_8 U_3\}H^2/4 & B_{66} &= \{-\xi_6 U_3\}H^2/4 \end{aligned} \tag{6.3}$$

$$\begin{aligned} &D_{11}=\{U_1+\xi_{10}U_3\}H^3/12 \quad D_{12}=D_{21}=\{U_4-\xi_{10}U_3\}H^3/12 \quad D_{16}=D_{61}=\{\xi_{12}U_3\}H^3/12 \\ &D_{22}=\{U_1+\xi_{10}U_3\}H^3/12 \quad D_{26}=D_{62}=\{-\xi_{12}U_3\}H^3/12 \quad D_{66}=\{-\xi_{10}U_3+U_5\}H^3/12 \end{aligned} \tag{6.4}$$

And for the force and moment vectors:

$$\begin{Bmatrix} N_x^{Thermal} \\ N_y^{Thermal} \\ N_{xy}^{Thermal} \end{Bmatrix} = H\begin{Bmatrix} (U_1+U_4)\alpha_{iso} \\ (U_1+U_4)\alpha_{iso} \\ 0 \end{Bmatrix}\Delta T \qquad \begin{Bmatrix} M_x^{Thermal} \\ M_y^{Thermal} \\ M_{xy}^{Thermal} \end{Bmatrix} = \begin{Bmatrix} 0 \\ 0 \\ 0 \end{Bmatrix} \tag{6.5}$$

Involving a reduced set of laminate invariants, U_i:

$$\begin{aligned} U_1&=\frac{(6Q_{11}+2Q_{12}+4Q_{66})}{8} \qquad U_3=\frac{(2Q_{11}-2Q_{12}-4Q_{66})}{8} \\ U_4&=\frac{(2Q_{11}+6Q_{12}-4Q_{66})}{8} \qquad U_5=\frac{(2Q_{11}-2Q_{12}+4Q_{66})}{8} \end{aligned} \tag{6.6}$$

and consequently a reduced set of lamination parameter constraints:

$$\begin{aligned} \xi_2, \xi_4&= \frac{1}{n}\sum_{k=1}^{n}(z_k - z_{k-1})(\cos 4\theta_k, \sin 4\theta_k) \\ \xi_6, \xi_8&= \frac{2}{n^2}\sum_{k=1}^{n}(z_k^2 - z_{k-1}^2)(\cos 4\theta_k, \sin 4\theta_k) \\ \xi_{10}, \xi_{12}&= \frac{4}{n^3}\sum_{k=1}^{n}(z_k^3 - z_{k-1}^3)(\cos 4\theta_k, \sin 4\theta_k) \end{aligned} \tag{6.7}$$

Additionally, for axis-aligned laminates, i.e. where the principal material axis is coincident with the system or structural axis, the lamination parameters ξ_4, ξ_8, and ξ_{12} are zero for standard ply angle orientations (0 and 45°), and correspond to $A_{16} = A_{26} = 0$, $B_{16} = B_{26} = 0$ and $D_{16} = D_{26} = 0$, respectively. Different forms of the ABD matrix arise from off-axis alignment β, of the principal material axis with respect to the system or structural axis for

unidirectional and plain weave materials. The square symmetric forms giving rise to HTCS laminates are summarised in Tables 6.1 and 6.2. The square symmetric form of each of these matrices, which is common to all balanced plain weave laminates, implies that the general form remains unchanged, but because the magnitude of the terms vary sinusoidally, specific off-axis rotations, β, render certain coupling terms zero. This unique feature can therefore be exploited to tailor the mechanical coupling properties, without affecting the immunity to thermal warping distortions.

Table 6.1 – Square symmetric forms of the extensional [A] and bending [D] stiffness matrices for uncoupled (Simple) with $\beta = m\pi/4$ and coupled behaviour with $\beta \neq m\pi/4$.

Extensional [**A**]		Bending [**D**]	
Simple	<u>*E-S*</u>	Simple	<u>*B-T*</u>
$[\mathbf{A}_S]$ $\begin{bmatrix} A_{11} & A_{12} & 0 \\ A_{12} & A_{11} & 0 \\ 0 & 0 & A_{66} \end{bmatrix}$ $\xi_4 = 0$	$[\mathbf{A}_F]$ $\begin{bmatrix} A_{11} & A_{12} & A_{16} \\ A_{12} & A_{11} & -A_{16} \\ A_{16} & -A_{16} & A_{66} \end{bmatrix}$	$[\mathbf{D}_S]$ $\begin{bmatrix} D_{11} & D_{12} & 0 \\ D_{12} & D_{11} & 0 \\ 0 & 0 & D_{66} \end{bmatrix}$ $\xi_{12} = 0$	$[\mathbf{D}_F]$ $\begin{bmatrix} D_{11} & D_{12} & D_{16} \\ D_{12} & D_{11} & -D_{16} \\ D_{16} & -D_{16} & D_{66} \end{bmatrix}$

Table 6.2 – Coupling [B] stiffness matrices with square symmetry, and associated cause-effect relationship, subscript notation and lamination parameter constraints, for coupled behaviour with respect to material axis alignment, β.

$\beta = m\pi/4$	$\beta = \pi/8 + m\pi/4$	$\beta \neq m\pi/2,\ \pi/8 + m\pi/4$
	(m = 0, 1, 2, 3, ...)	
<u>*E-B*</u>-<u>*S-T*</u>	<u>*E-T*</u>-<u>*S-B*</u>	<u>*E-B*</u>-<u>*S-B*</u>-<u>*E-T*</u>-<u>*S-T*</u>
$[\mathbf{B}_S]$ $\begin{bmatrix} B_{11} & -B_{11} & 0 \\ -B_{11} & B_{11} & 0 \\ 0 & 0 & -B_{11} \end{bmatrix}$ $\xi_8 = 0$	$[\mathbf{B}_t]$ $\begin{bmatrix} 0 & 0 & B_{16} \\ 0 & 0 & -B_{16} \\ B_{16} & -B_{16} & 0 \end{bmatrix}$ $\xi_6 = 0$	$[\mathbf{B}_F]$ $\begin{bmatrix} B_{11} & -B_{11} & B_{16} \\ -B_{11} & B_{11} & -B_{16} \\ B_{16} & -B_{16} & -B_{11} \end{bmatrix}$

Table 6.1 demonstrates these relationships for the extensional [**A**] and bending [**D**] stiffness properties, which are uncoupled when the principal material axes are orthogonal to the system or structural axes, but are coupled in Extension-Shearing (<u>*E-S*</u>) and Bending-

Twisting (*B-T*), respectively, for all other axis alignments. Table 6.2 demonstrates the more complicated relationships for the coupling [**B**] matrix.

For instance Extension-Twisting and shearing-bending (*E-T-S-B*) coupling, presented in the middle column of Table 6.2, is of particular practical interest for rotor blade design; Extension-Twisting coupling is also the response most easily validated experimentally (Shamsudin *et al*., 2011). Tables 6.1 and 6.2 also provide a comparison between response based labelling and the ESDU (ESDU, 1994) subscript notation, as well as the associated lamination parameter constraints described below Eq. (6.7)

Isotropy in the thermal force vector of Eq. (6.5), a zero thermal moment vector, and square symmetry in the extensional [**A**] and coupling [**B**] stiffness matrices are the necessary conditions for HTCS laminates (York, 2011, Verchery, 2011). The equal principal strains that result from the isotropic thermal force vector imply that the Mohr's circle for strain transformations degenerates to a point (in the same way that Mohr's circle for stress degenerates to a point under a hydrostatic stress state), hence thermal strains are identical in all directions and therefore plies of any orientation may be laminated together without warping following post-cure cool-down. It is worth noting that the bending [**D**] stiffness matrix is square symmetric for all balanced plain weave laminates, but this is not a necessary condition for HTCS laminates, as demonstrate elsewhere (York, 2011) for laminates consisting of unidirectional material.

In fact only two parent classes exist for laminates with balanced plain weave and standard ply angle orientations: the Simple ($\mathbf{A}_S\mathbf{B}_0\mathbf{D}_S$) laminate and; the Extension-Bending and Shearing-Twisting (*E-B-S-T*) coupled ($\mathbf{A}_S\mathbf{B}_S\mathbf{D}_S$) laminate. All other mechanical coupling responses arise from off-axis orientation, β, of the principal material axes of these parent laminates, with respect to the system or structural axes.

6.2 Uncoupled laminates with balanced plain weave

The most commonly adopted method for achieving fully uncoupled laminates is through the use of balanced and symmetric construction. However, non-symmetric laminate configurations are now known to dominate the design space of Simple (uncoupled) laminates. The Simple ($\mathbf{A}_S\mathbf{B}_0\mathbf{D}_S$) laminate is identified from solutions with lamination parameters:

$$\xi_6 = \xi_8 = 0 \tag{6.8}$$

where $\xi_8 = 0$ due to the standard ply angle orientations adopted**.**

A sub-group of fully isotropic ($\mathbf{A}_I\mathbf{B}_0\mathbf{D}_I$) laminates also exist from within the Simple ($\mathbf{A}_S\mathbf{B}_0\mathbf{D}_S$) laminate class, and can be identified through the additional lamination parameter constraints:

$$\xi_2 = \xi_4 = \xi_{10} = \xi_{12} = 0 \tag{6.9}$$

from which Eqs. (6.2) and (6.4) reveal that the extensional [**A**] and bending [**D**] stiffness matrices respectively depend solely on the laminate invariants, U_i, i.e. the material properties. Here, the extensional stiffnesses:

$$A_{11} = A_{22} \text{ and } A_{66} = (A_{11} - A_{12})/2 \tag{6.10}$$

are concomitant with the bending stiffnesses, i.e.:

$$D_{ij} = A_{ij}H^2/12 \tag{6.11}$$

which together correspond to the fully isotropic condition.

The polar plots of Fig. 6.7 demonstrate the lamination parameter and extensional stiffness variations for a single layer of balanced plain weave fabric with off-axis orientation $0° \leq \beta \leq 360°$. The more common form, demonstrating effective moduli, is also presented. Note that Eq. (6.11) applies in the single layer case, hence $\xi_{10} = \xi_2$ and $\xi_{12} = \xi_4$.

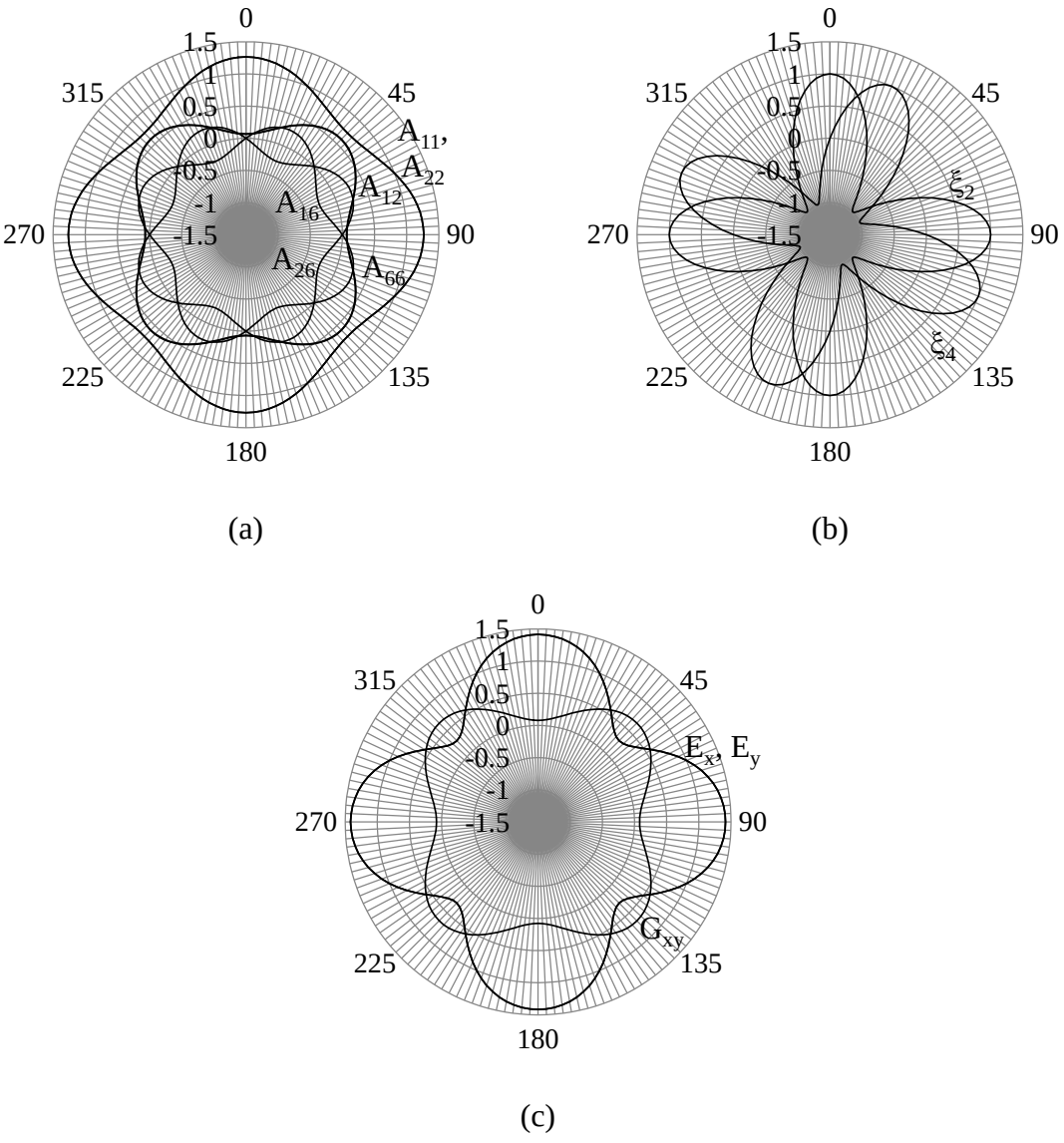

Figure 6.7 – Polar plots for off-axis material alignment, $0° \leq \beta \leq 360°$, of: (a) extensional stiffness, A_{ij}; (b) lamination parameters, ξ_2, ξ_4 and; (c) effective moduli for a single layer of balanced plain weave, $E_x = E_y = (A_{11}A_{22} - A_{12}^2)/A_{22}t$ and $G_{xy} = A_{66}/t$.

Vincenti *et al*. (2001) adopted the polar method, developed by Verchery (1979), to investigate specific properties of uncoupled balanced plain weave laminates. Some interesting solutions were given demonstrating that the square symmetric concomitant

properties in extension and bending can also be tailored, through the use of non-standard ply angle orientations, so that the alignment of principal extensional stiffness is different to the principal bending stiffness. By contrast, Grediac (2001) found approximate solutions with extensional isotropy and fully isotropic properties, for laminates with up to 11 plies, by solving the lamination parameter constraints using an optimisation strategy with free form ply angle orientations. The single, exact solution, found for an 8-ply fully isotropic laminate, with standard ply angle orientations, is reconfirmed in this thesis together with exact solutions for higher ply number groupings.

The number of solutions for Simple ($\mathbf{A}_S\mathbf{B}_0\mathbf{D}_S$) laminates is presented in Table 6.3 for each ply number grouping with up to 21 plies. These Simple laminates also contain sub-groups with quasi-homogeneous ($\mathbf{A}_S\mathbf{B}_0\mathbf{D}_S$) and fully isotropic ($\mathbf{A}_I\mathbf{B}_0\mathbf{D}_I$) properties, both satisfying Eq.(6.11), and extensionally isotropic ($\mathbf{A}_I\mathbf{B}_0\mathbf{D}_S$) properties, all of which are quantified in Table 6.3. Where single quasi-homogeneous solutions are reported for particular ply number groupings, the form of the stacking sequence is represented by $[\alpha]_{rT}$, where the number of repetitions, r, corresponds to the number of plies, *n*; all share the same non-dimensional properties as the single ply, shown in Fig. 6.7.

An abridged listing of stacking sequences for Simple ($\mathbf{A}_S\mathbf{B}_0\mathbf{D}_S$) laminates with up to 21 plies is presented in Table 6.4 since they amount to 52,983 individual stacking sequence; these are ordered by increasing compression buckling strength, corresponding to the infinitely long plate with simply supported edges, for which the closed form solution of Eq. (5.8) is applicable. The complete list of stacking sequences for fully isotropic laminates with up to 21 plies is presented in Table 6.5.

Table 6.3 – Summary on the number of Simple, uncoupled ($\mathbf{A_SB_0D_S}$) laminates for each ply number grouping, *n*, and the number that possess quasi-homogeneous ($\mathbf{A_SB_0D_S}$), fully isotropic ($\mathbf{A_IB_0D_I}$) or extensionally isotropic ($\mathbf{A_IB_0D_S}$) properties.

n	Simple $\mathbf{A_SB_0D_S}$	Quasi-homogeneous $\mathbf{A_SB_0D_S}$	Fully Isotropic $\mathbf{A_IB_0D_I}$	Extensionally Isotropic $\mathbf{A_IB_0D_S}$
2	1	1		
3	2	1		
4	2	1		1
5	4	1		
6	4	1		
7	10	2		
8	9	1	1	3
9	26	1		
10	24	1		
11	76	5		
12	69	1	1	28
13	236	12		
14	214	7		
15	760	12		
16	696	7	7	256
17	2522	53		
18	2326	22		
19	8556	122		
20	7942	67	24	2700
21	29504	99		

Table 6.4 – Abridged listing for Simple laminates ($A_S B_0 D_S$), corresponding to $\beta = 0$ and $\alpha = \beta + \pi/4$, for increasing buckling strength of the infinitely long plate with simply supported edges. Note that for ply number groupings $n = 4$ and above, the maximum buckling strength arises from stacking sequences of the form $[\alpha_n]_T$, corresponding to lamination parameter $\xi_2 = \xi_{10} = -1$ with $k_x = 5.06$ and corresponding buckling half-wavelength $\lambda = b$.

n	Stacking Sequences	ξ_2	ξ_{10}	k_x
2	$[\alpha/\alpha]_T$	–1.00	–1.00	5.06
3	$[\alpha/\beta/\alpha]_T$	–0.33	–0.93	4.98
3	$[\alpha_3]_T$	–1.00	–1.00	5.06
4	$[\alpha/\beta_2/\alpha]_T$	0.00	–0.75	4.80
:				
5	$[\alpha/\beta_3/\alpha]_T$	0.20	–0.57	4.60
:				
6	$[\alpha/\beta_4/\alpha]_T$	0.33	–0.41	4.43
:				
7	$[\alpha/\beta_3/\alpha_2/\beta]_T$	0.14	0.00	4.00
:				
8	$[\alpha/\beta_2/\alpha/\beta/\alpha_2/\beta]_T$	0.00	0.00	4.00
:				
9	$[\alpha/\beta_4/\alpha/\beta/\alpha/\beta]_T$	0.33	0.14	3.86
:				
10	$[\alpha/\beta_4/\alpha_3/\beta_2]_T$	0.20	0.30	3.69
:				
11	$[\alpha/\beta_6/\alpha_2/\beta_2]_T$	0.46	0.31	3.68
:				
12	$[\alpha/\beta_5/\alpha_2/\beta/\alpha/\beta_2]_T$	0.33	0.37	3.61
:				
13	$[\alpha/\beta_6/\alpha_3/\beta_3]_T$	0.39	0.45	3.52
:				
14	$[\alpha/\beta_6/\alpha/\beta/\alpha_2/\beta_3]_T$	0.43	0.46	3.51
:				
15	$[\alpha/\beta_7/\alpha_2/\beta/\alpha/\beta_3]_T$	0.47	0.50	3.47
:				
16	$[\alpha/\beta_8/\alpha_3/\beta_4]_T$	0.50	0.54	3.42
:				
17	$[\alpha/\beta_8/\alpha/\beta/\alpha_2/\beta_4]_T$	0.53	0.56	3.41
:				
18	$[\alpha/\beta_9/\alpha_2/\beta/\alpha/\beta_4]_T$	0.56	0.58	3.38
:				
19	$[\alpha/\beta_{10}/\alpha_3/\beta_5]_T$	0.58	0.61	3.35
:				
20	$[\alpha/\beta_{10}/\alpha/\beta/\alpha_2/\beta_5]_T$	0.60	0.62	3.34
:				
21	$[\alpha/\beta_{10}/\alpha_4/\beta_6]_T$	0.52	0.66	3.30

Table 6.5 – Fully isotropic ($A_I B_0 D_I$) laminates for each ply number groupings, *n*, with $\alpha = \beta + \pi/4$.

n	Stacking sequence
8	$[\alpha/\beta_2/\alpha/\beta/\alpha_2/\beta]_T$
12	$[\alpha/\beta/\alpha/\beta_3/\alpha_3/\beta/\alpha/\beta]_T$
16	$[\alpha/\beta_3/\alpha_4/\beta_2/\alpha/\beta_2/\alpha/\beta/\alpha]_T$ $[\alpha/\beta_2/\alpha/\beta/\alpha_2/\beta_2/\alpha_2/\beta/\alpha/\beta_2/\alpha]_T$ $[\alpha/\beta_2/\alpha/\beta/\alpha_2/\beta/\alpha/\beta_2/\alpha/\beta/\alpha_2/\beta]_T$ $[\alpha/\beta_2/\alpha_2/\beta_2/\alpha/\beta/\alpha_2/\beta_2/\alpha_2/\beta]_T$ $[\alpha/\beta/\alpha/\beta_2/\alpha/\beta_2/\alpha_4/\beta_3/\alpha]_T$ $[\alpha/\beta/\alpha/\beta_2/\alpha/\beta/\alpha/\beta/\alpha/\beta/\alpha_2/\beta/\alpha/\beta]_T$ $[\alpha_2/\beta_4/\alpha_2/\beta_2/\alpha_4/\beta_2]_T$
20	$[\alpha_2/\beta/\alpha/\beta_5/\alpha/\beta/\alpha_5/\beta/\alpha/\beta_2]_T$ $[\alpha_2/\beta_2/\alpha/\beta_3/\alpha/\beta/\alpha/\beta/\alpha_3/\beta/\alpha_2/\beta_2]_T$ $[\alpha_2/\beta_3/\alpha/\beta/\alpha/\beta_2/\alpha_2/\beta/\alpha/\beta/\alpha_3/\beta_2]_T$ $[\alpha/\beta_2/\alpha_2/\beta/\alpha/\beta/\alpha/\beta_3/\alpha/\beta/\alpha_4/\beta_2]_T$ $[\alpha/\beta/\alpha_2/\beta_4/\alpha/\beta/\alpha/\beta/\alpha_4/\beta_2/\alpha/\beta]_T$ $[\alpha/\beta/\alpha/\beta/\alpha/\beta/\alpha/\beta_4/\alpha_5/\beta_2/\alpha/\beta]_T$ $[\alpha/\beta/\alpha_2/\beta_5/\alpha_4/\beta/\alpha/\beta/\alpha/\beta/\alpha/\beta]_T$ $[\alpha/\beta/\alpha/\beta/\alpha/\beta_2/\alpha/\beta_2/\alpha_2/\beta/\alpha_2/\beta/\alpha/\beta/\alpha/\beta]_T$ $[\alpha/\beta/\alpha/\beta_2/\alpha_2/\beta_2/\alpha/\beta_2/\alpha_3/\beta/\alpha/\beta/\alpha/\beta]_T$ $[\alpha/\beta/\alpha/\beta/\alpha/\beta_3/\alpha_2/\beta/\alpha_2/\beta_2/\alpha_2/\beta/\alpha/\beta]_T$ $[\alpha/\beta/\alpha/\beta_2/\alpha_2/\beta_3/\alpha_3/\beta_2/\alpha_2/\beta/\alpha/\beta]_T$ $[\alpha/\beta/\alpha/\beta_3/\alpha_4/\beta_4/\alpha_3/\beta/\alpha/\beta]_T$ $[\alpha/\beta_2/\alpha/\beta/\alpha_2/\beta/\alpha/\beta/\alpha/\beta_3/\alpha_3/\beta/\alpha/\beta]_T$ $[\alpha_2/\beta_4/\alpha/\beta/\alpha_3/\beta/\alpha/\beta/\alpha/\beta_2/\alpha_2/\beta]_T$ $[\alpha/\beta_2/\alpha_2/\beta/\alpha/\beta_3/\alpha_3/\beta/\alpha/\beta_2/\alpha_2/\beta]_T$ $[\alpha/\beta/\alpha/\beta_3/\alpha_3/\beta/\alpha/\beta/\alpha/\beta_2/\alpha/\beta/\alpha_2/\beta]_T$ $[\alpha/\beta_2/\alpha/\beta/\alpha/\beta/\alpha_3/\beta_3/\alpha/\beta/\alpha/\beta/\alpha_2/\beta]_T$ $[\alpha/\beta_3/\alpha_3/\beta/\alpha_2/\beta_2/\alpha/\beta_3/\alpha_3/\beta]_T$ $[\alpha/\beta/\alpha/\beta/\alpha/\beta_3/\alpha/\beta/\alpha_4/\beta_2/\alpha/\beta_2/\alpha]_T$ $[\alpha/\beta/\alpha/\beta_3/\alpha_3/\beta/\alpha/\beta_2/\alpha_2/\beta/\alpha/\beta_2/\alpha]_T$ $[\alpha_2/\beta_5/\alpha_5/\beta/\alpha/\beta_3/\alpha/\beta/\alpha]_T$ $[\alpha/\beta_2/\alpha/\beta/\alpha_2/\beta_2/\alpha/\beta/\alpha_3/\beta_3/\alpha/\beta/\alpha]_T$ $[\alpha/\beta_2/\alpha/\beta_2/\alpha_4/\beta/\alpha/\beta_3/\alpha/\beta/\alpha/\beta/\alpha]_T$ $[\alpha/\beta/\alpha/\beta_3/\alpha/\beta/\alpha_5/\beta_5/\alpha_2]_T$

6.3 Coupled laminates with balanced plain weave

The coupled parent ($\mathbf{A}_S\mathbf{B}_S\mathbf{D}_S$) laminate class possesses Extension-Bending and Shearing-Twisting (*E-B*-*S-T*) coupling, which corresponds to the lamination parameter constraint:

$$\xi_6 \neq 0 \tag{6.12}$$

Additional coupling characteristics can be obtained from this parent laminate class by applying off-axis material alignment, β.

Note that the HTCS condition, present in a single layer of balanced plain weave material is retained for general off-axis material alignment, β. This extends to all plain weave laminates, irrespective of the number of plies in the laminate or the laminate stacking sequence. By contrast, fibre misalignment errors in the stacking sequences for HTCS laminates with unidirectional material, or unbalanced plain weave, will inevitably give rise to some degree of thermal warping. Additionally, HTCS laminates with unidirectional material are achievable only for certain ply number groupings when standard ply angle orientations are adopted (York, 2011), i.e., with 8, 12, 16 and 20 plies, etc. It has however recently been shown (York, 2013) that HTCS solutions can be achieved in all ply number groupings with 10 plies and above if non-standard ply orientations are adopted, i.e., $\theta = 0$, 90 and $\pm 60°$.

Seven classes of coupled laminate can be produced from balanced plain weave material. All are derived from the single parent ($\mathbf{A}_S\mathbf{B}_S\mathbf{D}_S$) laminate class, through the off-axis alignments detailed in Tables 6.1 and 6.2. The 6 derivatives are summarised in Table 6.6. In addition, a sub-group of these coupled laminates have been discovered with both extensional and bending stiffness isotropy; solutions which also possess compliance isotropy. Illustrations in Table 6.6 represent unconstrained thermal contraction responses

that would typically result at room temperature, following a standard high temperature curing process.

Table 6.6 – Classification of coupled laminates with balance plain weave, derived from the $A_SB_SD_S$ parent laminate with Bending-Extension and Twisting-Shearing (*B-E*-*T-S*) coupling, following off-axis material alignment, β. Illustrations highlight the coupling responses due to free thermal contraction in unbalanced plain weave. For stacking sequence definition, $\alpha = \beta + \pi/4$.

Uncoupled in Extension $[\mathbf{A}_S]$		**Extension-Shearing** $[\mathbf{A}_F]$	
Uncoupled in Bending $[\mathbf{D}_S]$	**Bending-Twisting** $[\mathbf{D}_F]$	**Bending-Twisting** $[\mathbf{D}_F]$	
$\mathbf{A_SB_tD_S}$ $[\alpha/\beta]_T$ 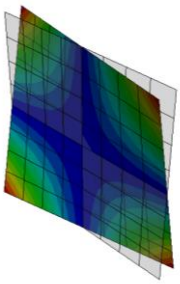 *B-S*-*T-E*	$\mathbf{A_SB_tD_F}$ $[\alpha/\beta/\alpha_2/\beta_2]_T$ 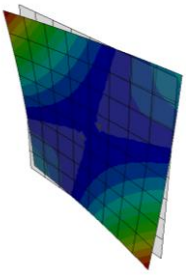 *B-S*-*T-E*;*B-T*	$\mathbf{A_FB_tD_F}$ $[\alpha/\beta_2]_T$ 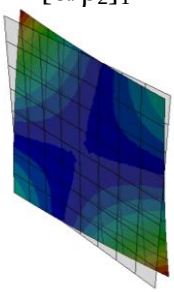 *E-S*;*B-S*-*T-E*;*B-T*	**$\beta = \pi/8 + m\pi/4$ ($m = 0, 1, 2, \ldots$) Bending-Shearing and Twisting-Extension [$\mathbf{B}_t$]**
$\mathbf{A_SB_FD_S}$ $[\alpha/\beta]_T$ 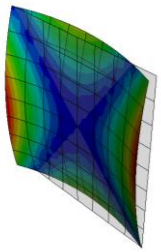 *B-E*-*B-S*-*T-E*-*T-S*	$\mathbf{A_SB_FD_F}$ $[\alpha/\beta/\alpha_2/\beta_2]_T$ 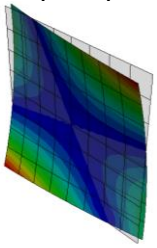 *B-E*-*B-S*-*T-E*-*T-S*;*B-T*	$\mathbf{A_FB_FD_F}$ $[\alpha/\beta_2]_T$ 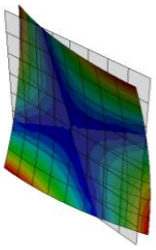 *E-S*;*B-E*-*B-S*-*T-E*-*T-S*;*B-T*	**$\beta \neq m\pi/4, \pi/8 + m\pi/4$ Bending-Extension, Bending-Shearing, Twisting-Extension and Twisting-shearing [$\mathbf{B}_F$]**

They provide classical laminate theory predictions of the warping behaviour that is avoided in balanced plain weave laminates, by virtue of their HTCS properties, for all 7 classes of mechanical coupling. Note that the stacking sequences given are representative samples

from the minimum ply number grouping for each class of coupled laminate; given as the parent laminate, with standard ply angle orientations, prior to off-axis material alignment, β, where $\alpha = \beta + \pi/4$.

The number of solutions in each of the 7 coupled laminate classes are listed in Table 6.7. The second column of the table represents the number of Extension-Bending and Shearing-Twisting (*E-B-S-T*) parent ($\mathbf{A_S B_S D_S}$) laminate solutions for each ply number grouping, *n*. Subsequent columns demonstrate the number of solutions in each coupled laminate derivative arising from a specific off-axis orientation, β.

Table 6.7 – Number of solutions for the *E-B-S-T* or *B-E-T-S* coupled parent ($\mathbf{A_S B_S D_S}$) laminate class for each ply number grouping, *n*, and number of solutions in each of the six other coupled laminate derivatives of Table 6.6, following off-axis alignment, β.

	Number of solutions						
	$\mathbf{A_S B_S D_S}$	$\mathbf{A_S B_t D_S}$	$\mathbf{A_S B_t D_F}$	$\mathbf{A_F B_t D_F}$	$\mathbf{A_S B_F D_S}$	$\mathbf{A_S B_F D_F}$	$\mathbf{A_F B_F D_F}$
n	$\beta = 0$	$\beta = \pi/8 + m\pi/4$ (m = 0, 1, 2, 3,...)			$\beta \neq m\pi/4, \pi/8 + m\pi/2$ (m = 0, 1, 2, 3,...)		
2	1	1			1		
3	2			2			2
4	6	2		4	2		4
5	12			12			12
6	28	4	6	18	4	6	18
7	54			54			54
8	119	7	24	88	7	24	88
9	230			230			230
10	488	16	110	362	16	110	362
11	948			948			948
12	1979	35	398	1546	35	398	1546
13	3860			3860			3860
14	7978	84	1632	6262	84	1632	6262
15	15624			15624			15624
16	32072	194	5978	25900	194	5978	25900
17	63014			63014			63014
18	128746	512	23798	104436	512	23798	104436
19	253588			253588			253588
20	516346	1352	88302	426692	1352	88302	426692
21	1019072			1019072			1019072

The results reveal that the two parent solutions for the 2-ply laminate (n = 2) give rise to either the $\mathbf{A}_S\mathbf{B}_t\mathbf{D}_S$ or the $\mathbf{A}_S\mathbf{B}_F\mathbf{D}_S$ coupled laminate classes following off-axis rotation. Both solutions are fully isotropic in Extension [**A**] and Bending [**D**] and therefore an off-axis rotation changes only the Coupling [**B**] matrix properties. For instance, off-axis material alignment, $\beta = \pi/8$, applied to the 2-ply $[\alpha/\beta]_T$ parent laminate (i.e., the configuration represented in the first column of Table 6.6,) gives rise to *E-T-S-B* coupling (or *B-S-T-E* since each *cause-effect* pairing is reversible), which corresponds to $\xi_6 = 0$ and the associated form of the coupling stiffness matrix in Table 6.2. Bending-Extension and Twisting-Shearing or *B-E-T-S* coupling exists for all other off-axis alignments.

The polar plots of Fig. 6.8 best illustrate the sinusoidal relationship of lamination parameters with off-axis material alignment. Extension-Twisting and Shearing-Bending or *E-T-S-B* coupled ($\mathbf{A}_S\mathbf{B}_t\mathbf{D}_S$) laminates are shown in Table 6.7 to exist only for even ply number groupings. An abridged listing of laminate stacking sequences is presented in Table 6.8, in order of increasing magnitude of the Extension-Twisting coupling magnitude, i.e., increasing ξ_8 or B_{16}. The polar plots demonstrate that the lamination parameters $\xi_2 = \xi_4 = 0$ and $\xi_{10} = \xi_{12} = 0$ for all axis alignments, signifying isotropic properties in extension and bending, respectively.

By contrast, Table 6.7 reveals that the parent solutions for the 3-ply laminates (n = 3) give rise to either the $\mathbf{A}_F\mathbf{B}_t\mathbf{D}_F$ or the $\mathbf{A}_F\mathbf{B}_F\mathbf{D}_F$ coupled laminate classes. The polar plots of Fig. 6.9 illustrate the variation in lamination parameters with off-axis alignment for the stacking sequence $[\alpha/\beta_2]_T$, which corresponds to the example stacking sequence in the third column of Table 6.6. Here, Extension-Shearing coupling is present ($\xi_4 \neq 0$) for all axis orientations, except those corresponding to orthogonal axes, i.e., $\beta = m\pi/4$ (m = 0, 1, 2, …), the Coupling [**B**] stiffness matrix properties are similar to the previous 2-ply example, but with

a reduced magnitude, and the bending stiffness properties approximate isotropic behaviour but are in fact numerically zero only for $\beta = m\pi/4$ ($m = 0, 1, 2, \ldots$).

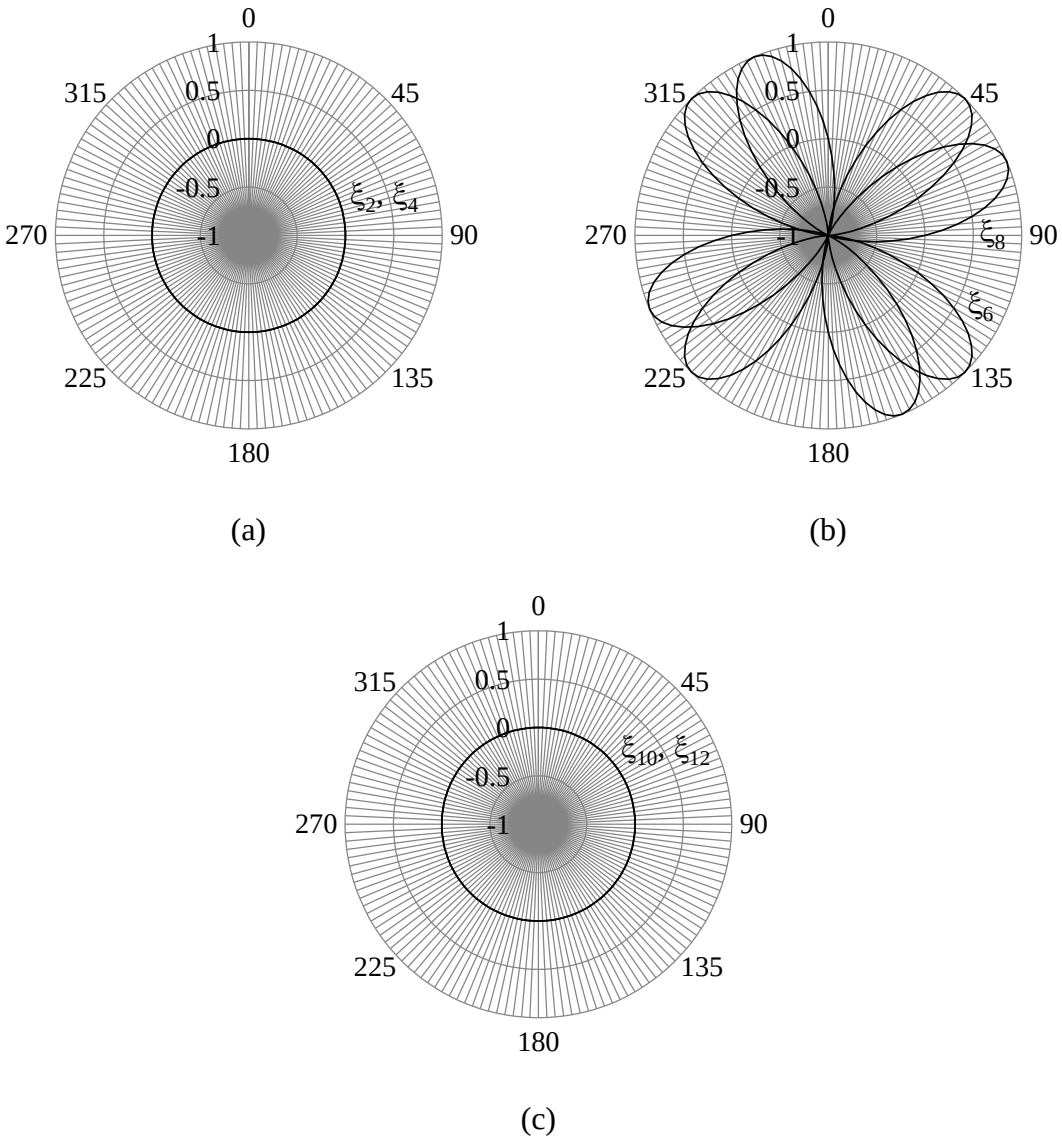

Figure 6.8 – Polar plots of the lamination parameters corresponding to: (a) A **(b)** B **and (c)** D **stiffness properties with off-axis material alignment, $0° \leq \beta \leq 360°$, for 2-ply $A_I B_S D_I$ balanced plain weave laminate stacking sequence $[\alpha/\beta]_T$, where $\alpha = \beta + \pi/4$.**

Table 6.8 – Abridged listing for Extension-Twisting and Shearing-Bending coupled laminates ($A_lB_tD_l$), corresponding to $\beta = \pi/8$ and $\alpha = \beta + \pi/4$, for increasing coupling magnitude, ξ_8, and corresponding buckling factor k_x for the infinitely long plate with simply supported edges calculated from Eq. 5.7. For ply number groupings above $n = 6$, the maximum coupling magnitude ($\xi_8 = 1$ and $k_x = 3.40$) arises from stacking sequences of the form $[\alpha_{n/2}/\beta_{n/2}]_T$, and are therefore omitted.

n	Stacking Sequences	ξ_8	k_x
2	$[\alpha/\beta]_T$	1.00	3.40
4	$[\alpha/\beta/\alpha/\beta]_T$	0.50	3.85
4	$[\alpha_2/\beta_2]_T$	1.00	3.40
6	$[\alpha/\beta_2/\alpha_2/\beta]_T$	0.11	3.99
:	:	:	
6	$[\alpha_3/\beta_3]_T$	1	3.40
8	$[\alpha/\beta_3/\alpha_3/\beta]_T$	-0.13	3.99
:	:	:	
10	$[\alpha/\beta_2/\alpha_2/\beta_2/\alpha_2/\beta]_T$	0.04	3.99
:	:	:	
12	$[\alpha/\beta_2/\alpha_2/\beta/\alpha/\beta_2/\alpha_2/\beta]_T$	0.06	3.99
:	:	:	
14	$[\alpha/\beta_2/\alpha/\beta/\alpha_2/\beta/\alpha/\beta/\alpha/\beta_2/\alpha]_T$	0.02	4.00
:	:	:	
16	$[\alpha/\beta_2/\alpha/\beta/\alpha_3/\beta_3/\alpha/\beta/\alpha_2/\beta]_T$	0.03	4.00
:	:	:	
18	$[\alpha/\beta_3/\alpha_4/\beta_2/\alpha/\beta/\alpha/\beta_2/\alpha/\beta/\alpha]_T$	0.01	4.00
:	:	:	
20	$[\alpha/\beta_3/\alpha_2/\beta/\alpha_4/\beta_3/\alpha/\beta_3/\alpha_2]_T$	0.02	4.00
:	:	:	:

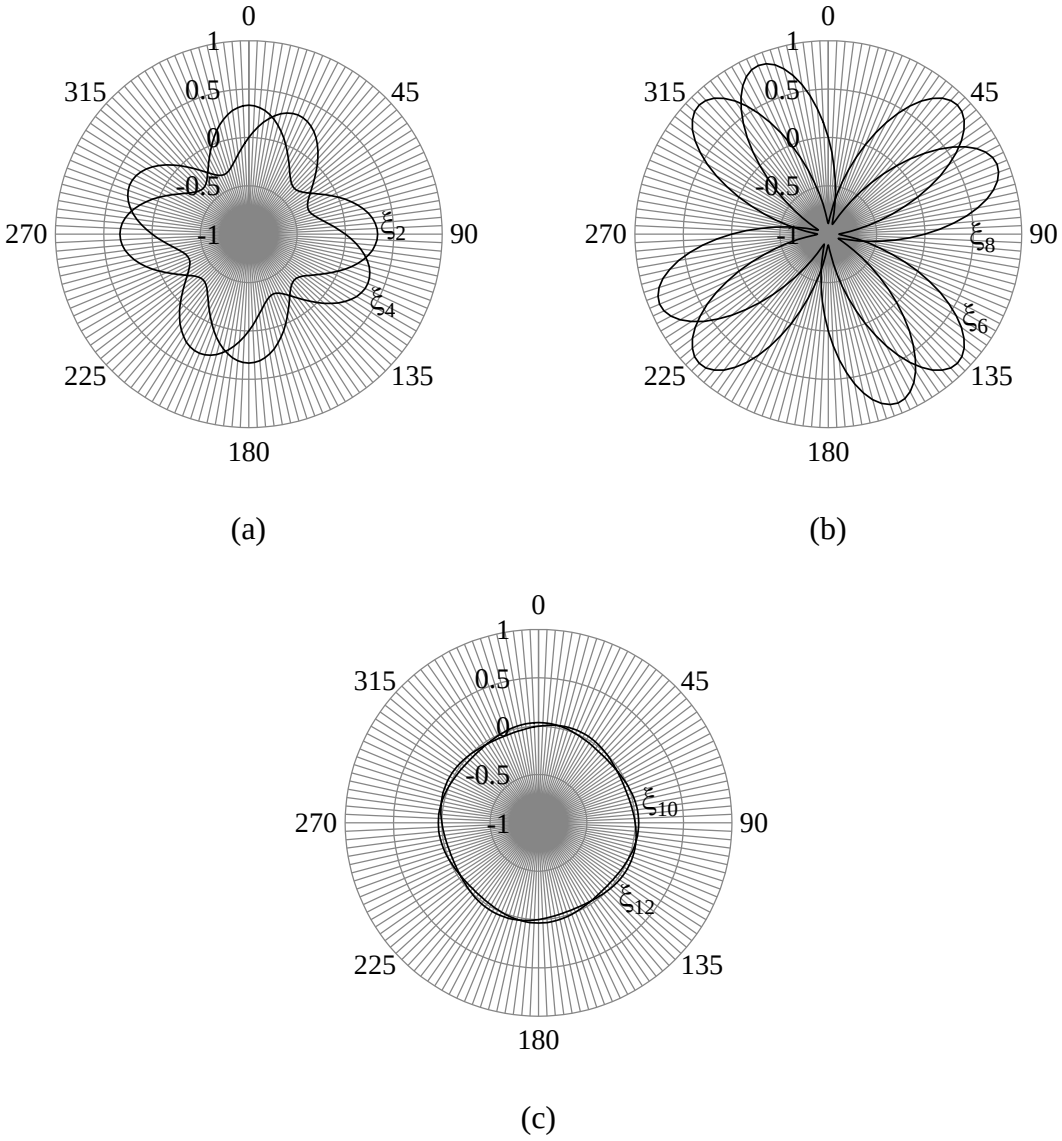

Figure 6.9 – Polar plots of the lamination parameters for: (a) A (b) B and (c) D matrices corresponding to off-axis material alignment, $0° \leq \beta \leq 360°$, for 3-ply $A_S B_S D_S$ laminate stacking sequence $[\alpha/\beta_2]_T$, where $\alpha = \beta + \pi/4$.

Finally, the 28 solutions for 6-ply laminates (n = 6), presented in Table 6.7 result in all six mechanically coupled classes as a result of off-axis orientation, β. Figure 6.10 illustrates the polar plots of lamination parameter relationships for the 6-ply stacking sequence $[\alpha/\beta/\alpha_2/\beta_2]_T$. In this case the lamination parameters $\xi_2 = \xi_4 = 0$ for all axis alignments, indicating that this laminate possesses isotropic extensional [**A**] stiffness properties. However, this is not a true isotropy condition since it is not reflected in the compliance relationship, where the isotropy is lost as a result of the influence of Bending-Twisting

coupling through the Coupling [**B**] matrix. Once again the Coupling [**B**] stiffness matrix properties are similar to the previous examples, albeit with different magnitude. Bending-Twisting coupling is present at all off-axis orientations, since $\xi_{12} = 0$ only for $\beta = m\pi/4$ ($m = 0, 1, 2, \ldots$). This example represents the $\mathbf{A_S B_t D_F}$ and $\mathbf{A_S B_F D_F}$ laminate classes in Table 6.6, depending on the specific off-axis orientation, β.

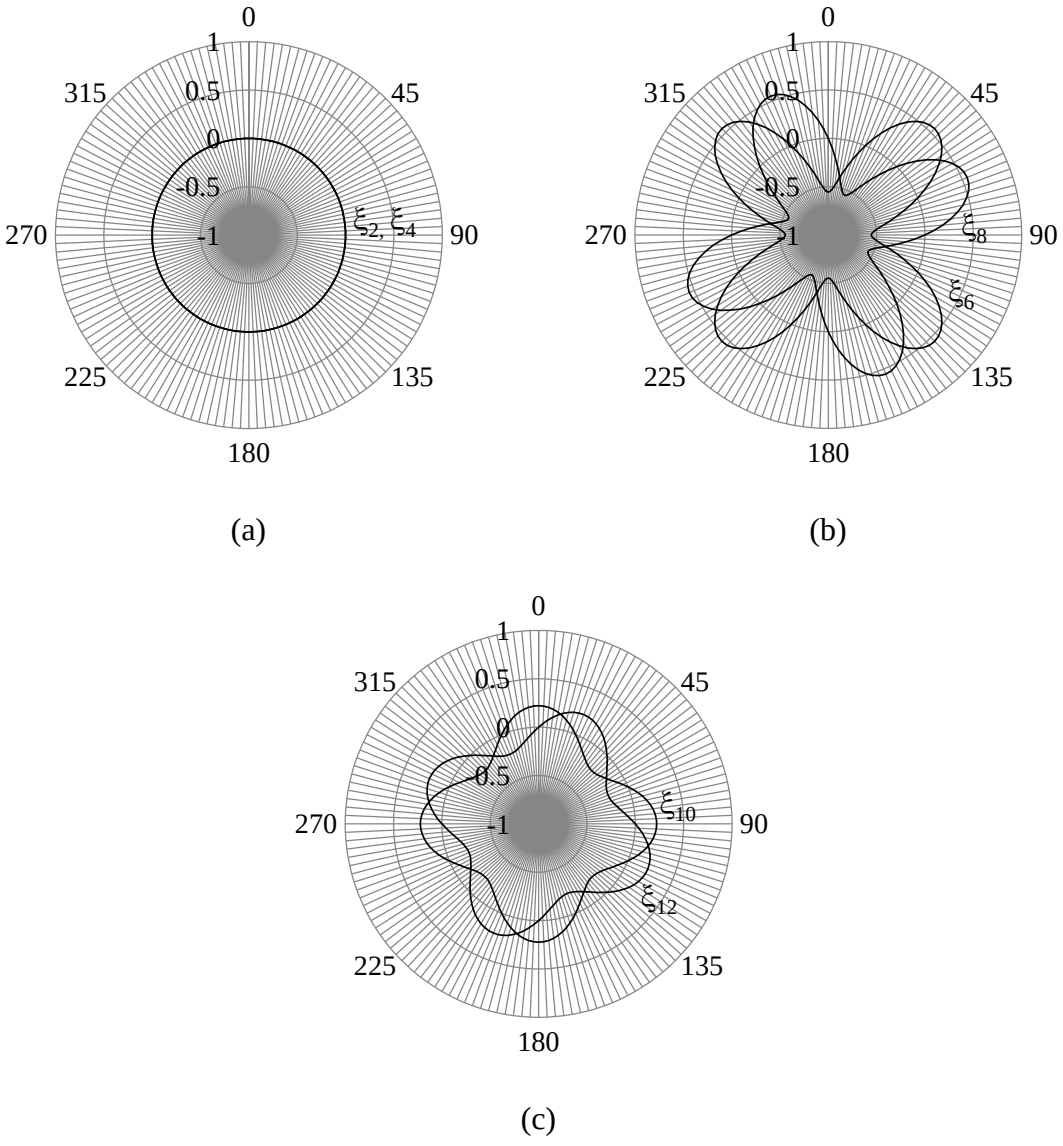

Figure 6.10 – Polar plots of the lamination parameters for: (a) A **(b)** B **and (c)** D **matrix corresponding to off-axis material alignment, $0° \leq \beta \leq 360°$, for 6-ply $A_I B_S D_S$ laminate stacking sequence $[\alpha/\beta/\alpha_2/\beta_2]_T$, where $\alpha = \beta + \pi/4$.**

6.4 Laminate design

This section presents two worked examples, the first of which is a comparison of unidirectional and balanced plain weave laminates for a rotor blade application in which maximum twist, through mechanical Extension-Twisting coupling, is required under a given centrifugal loading condition. The stacking sequences chosen have the highest coupling magnitude achievable using standard ply angle orientations, i.e. 0, 90 and ±45°. It should be noted however that whilst standard ply orientations were chosen to satisfy manufacturing constraints, the laminates are assumed to be loaded off-axis, in order to induce Extension-Twisting coupling. The stacking sequence chosen to represent the balanced plain weave laminate, $[\alpha_2/\beta_2]_T$, therefore corresponds to $[67.5_2/22.5_2]_T$ in accordance with the design rules of Table 6.2, i.e., an off-axis orientation, $\beta = \pi/8$. The competing unidirectional laminate of equal thickness, whose stacking sequence has been derived independently by others (Nixon, 1987, Weaver, 2005, York, 2011), corresponds to $[-22.5/67.5_2/-22.5/22.5/-67.5_2/22.5]_T$, following off-axis orientation.

The reduced stiffnesses are readily calculated from the material properties of Table 4.3 using Eq. (9.19), giving $Q_{11} = Q_{22} = 90{,}226$, $Q_{12} = 4{,}511$ and $Q_{66} = 5{,}000$ (N/mm^2) for balanced plain weave material. The laminate invariants $U_1 = 71{,}297$, $U_3 = 18{,}929$, $U_4 = 23{,}440$ and $U_5 = 23{,}929$ (N/mm^2) follow from Eq. (6.6) and the only non-zero lamination parameter, obtained from Eq. (6.7), is $\xi_8 = 1$. The elements of the **ABD** matrix then follow from Eqs. (6.2) - (6.4), giving:

$$\mathrm{A} = \begin{bmatrix} 104{,}379 & 34{,}316 & 0 \\ 34{,}316 & 104{,}379 & 0 \\ 0 & 0 & 35{,}031 \end{bmatrix} \quad \mathrm{B} = \begin{bmatrix} 0 & 0 & 10{,}142 \\ 0 & 0 & -10{,}142 \\ 10{,}142 & -10{,}142 & 0 \end{bmatrix}$$
$$\mathrm{D} = \begin{bmatrix} 18{,}643 & 6{,}129 & 0 \\ 6{,}129 & 18{,}643 & 0 \\ 0 & 0 & 6{,}257 \end{bmatrix} \tag{6.13}$$

For the unidirectional material comparator, the reduced stiffnesses also follow from Table 4.3, using Eq. (9.19), but now the laminate invariants follow from Eq. (2.15), the two non-zero lamination parameters, $\xi_8 = 1$ and $\xi_9 = 0.133$, follow from Eq. (2.16) and the elements of the **ABD** matrix follow from Eq. (2.17), giving:

$$\mathbf{A} = \begin{bmatrix} 102{,}765 & 32{,}342 & 0 \\ 32{,}342 & 102{,}765 & 0 \\ 0 & 0 & 35{,}212 \end{bmatrix} \quad \mathbf{B} = \begin{bmatrix} 0 & 0 & 10{,}530 \\ 0 & 0 & -10{,}530 \\ 10{,}530 & -10{,}530 & 0 \end{bmatrix}$$
$$\mathbf{D} = \begin{bmatrix} 21{,}156 & 5{,}776 & 0 \\ 5{,}776 & 21{,}156 & 0 \\ 0 & 0 & 6{,}289 \end{bmatrix} \tag{6.14}$$

The twisting magnitude of the two laminates is assessed using the geometrically non-linear finite element model which had been discussed in the previous chapter. Figure 6.11 shows the axial load vs. twist rate for the two laminate comparators, where the twisting magnitude of each laminate is assessed up to an axial load corresponding to the predicted first ply failure load of the Tsai-Wu failure criterion Eq. (5.6).

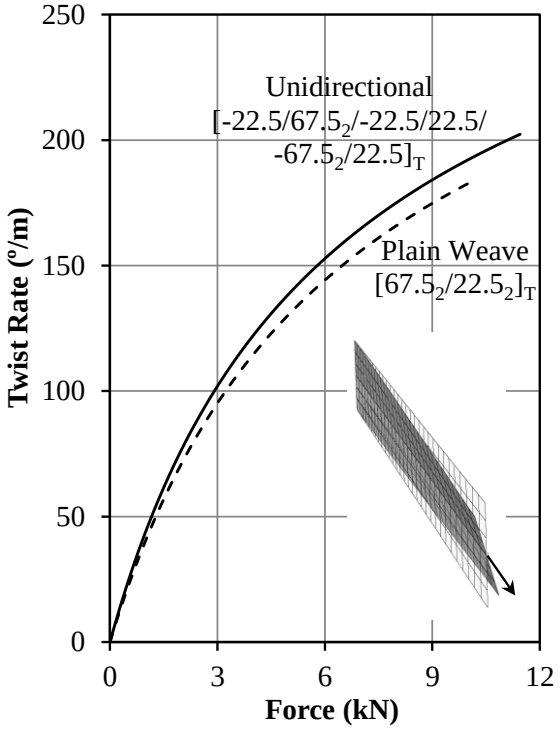

Figure 6.11 – Twist Rate vs Axial Force for the unidirectional and balanced plain weave laminate comparators with equal thickness.

The predicted failure loads under uniaxial tension, derived using the inverse of Eq. (2.1), see Table 6.9, are 10.72 kN and 9.42 kN for the unidirectional and balanced plain weave materials, respectively.

Table 6.9 – Comparisons of stiffness and compliance matrices for different *cause-effect* relationships. Note that $\alpha = \beta + \pi/4$ in stacking sequence definition.

	$\mathbf{A_S B_t D_S}$ laminate: $[\beta_3/\alpha_3]_T$ <u>*E-T-S-B*</u>	$\mathbf{A_S B_t D_F}$ laminate: $[\beta_2/\alpha_2/\beta/\alpha]_T$ <u>*E-T-S-B*</u>;<u>*B-T*</u>
Stiffness Matrix	$\begin{bmatrix} A_{11} & A_{12} & 0 & 0 & 0 & B_{16} \\ A_{12} & A_{11} & 0 & 0 & 0 & -B_{16} \\ 0 & 0 & A_{66} & B_{16} & -B_{16} & 0 \\ 0 & 0 & B_{16} & D_{11} & D_{12} & 0 \\ 0 & 0 & -B_{16} & D_{12} & D_{11} & 0 \\ B_{16} & -B_{16} & 0 & 0 & 0 & D_{66} \end{bmatrix}$	$\begin{bmatrix} A_{11} & A_{12} & 0 & 0 & 0 & B_{16} \\ A_{12} & A_{11} & 0 & 0 & 0 & -B_{16} \\ 0 & 0 & A_{66} & B_{16} & -B_{16} & 0 \\ 0 & 0 & B_{16} & D_{11} & D_{12} & D_{16} \\ 0 & 0 & -B_{16} & D_{12} & D_{11} & -D_{16} \\ B_{16} & -B_{16} & 0 & D_{16} & -D_{16} & D_{66} \end{bmatrix}$
Compliance Matrix	$\begin{bmatrix} a_{11} & -a_{12} & 0 & 0 & 0 & b_{16} \\ -a_{12} & a_{11} & 0 & 0 & 0 & -b_{16} \\ 0 & 0 & a_{66} & b_{16} & -b_{16} & 0 \\ 0 & 0 & b_{16} & d_{11} & -d_{12} & 0 \\ 0 & 0 & -b_{16} & -d_{12} & d_{11} & 0 \\ b_{16} & -b_{16} & 0 & 0 & 0 & d_{66} \end{bmatrix}$	$\begin{bmatrix} a_{11} & -a_{12} & a_{16} & b_{11} & -b_{11} & b_{16} \\ -a_{12} & a_{11} & -a_{16} & -b_{11} & b_{11} & -b_{16} \\ a_{16} & -a_{16} & a_{66} & b_{16} & -b_{16} & b_{66} \\ b_{11} & -b_{11} & b_{16} & d_{11} & -d_{12} & d_{16} \\ -b_{11} & b_{11} & -b_{16} & -d_{12} & d_{11} & -d_{16} \\ b_{16} & -b_{16} & b_{66} & d_{16} & -d_{16} & d_{66} \end{bmatrix}$

However, the finite element analyses predict failure loads of 11.45 kN and 10.10 kN due to the applied boundary conditions, which simulate the tension grips of a tension-torsion test machine. This example demonstrates that the unidirectional material possesses little significant advantage over balanced plain weave material.

A second example compares the compression buckling strength for unidirectional and balanced plain weave, using the same stacking sequences. Note that the elements of the **ABD** matrix in Eqs (6.13) and (6.14) must first be recalculated using the compressive moduli of Table 4.3. The Tsai-Wu failure criterion failure loads under uniaxial compression, derived using the inverse of Eq. (2.1), are now 12.83 kN and 8.76 kN, respectively.

Additionally the buckling strength of Extension-Twisting (and Shearing-Bending) coupled laminates can be calculated from a closed form solution of Eq. (5.8), where for the infinitely long case, m is a non-integer value, corresponding to the number of buckling half-waves along the plate length, *a*, or plate width, *b*, when $a = b$ is assumed. Following minimisation of N_X, with respect to m and n, the buckling load can be expressed in non-dimensional form, given by Eq. (5.7). This permits like-with-like comparison of laminates with any number of plies, *n*, and is the procedure adopted for generating k_x in Tables 6.4 and 6.8, since Eq. (5.8) degenerates to the closed form solution for orthotropic laminates when $\mathbf{B}_{ij} = 0$. Note that due to the square symmetric form of the **A**, **B** and **D** matrices in all balanced plain weave laminates, m = n = 1 in Eq. (5.8), which corresponds to a buckling half-wavelength $\lambda = b$, only for square plate.

Equation (5.8) is often associated with anti-symmetric angle –ply laminates (Whitney and Leissa, 1969, Jones, 1999), but the non-symmetric stacking sequences presented in Table 6.8 demonstrates that these conditions are not a requirement. Buckling factors, $k_x = 3.04$ and 3.40, are readily calculated for the comparator laminates with unidirectional and balanced plain weave materials, respectively. A lower k_x for the unidirectional laminate is expected, since it possesses the highest Extension-Twisting coupling magnitude of the two comparators; Extension-Twisting coupling has been shown in the previous chapter to be inversely proportional to the compression buckling strength. Table 6.8 demonstrates that for laminates with balanced plain weave the maximum coupling magnitude, $\xi_8 = 1$, gives a lower-bound buckling solution, $k_x = 3.40$, for stacking sequences of the form $[\alpha_{n/2}/\beta_{n/2}]_T$.

By contrast, the upper-bound buckling solution tends toward $k_x = 4.00$ as lamination parameter, ξ_8, approaches zero, i.e. the fully isotropic laminate. The stacking sequences in Table 6.8 possess lamination parameters $\xi_2 = \xi_4 = \xi_{10} = \xi_{12} = 0$ for all axis rotations, representing extensional and bending isotropy.

6.5 Tapered laminates

Mechanically coupled laminate designs are further complicated when thickness tapering is a design requirement. In fact this requirement will undoubtedly pose a major constraint for laminate designs that are tailored for maximum coupling through an optimisation routine, particularly when solutions converge on irregular free-form ply orientations, as shown in Eq. (5.3). Consequently ply terminations within such laminate designs will inevitably destroy both the mechanical coupling behaviour and the HTCS conditions.

Hence the challenge concerning coupled laminate design is to preserve both the HTCS conditions and the mechanical coupling attributes during the tapering process. York (2013) presented results for the unidirectional counterpart, with solutions given for standard and non-standard ply orientations. Restrictions however exist for these two cases; for standard angle-ply orientations where HTCS laminate solutions only exist under the 8-, 12-, 16- and 20-ply number groupings suggest that only 4-ply terminations are possible, for instance reducing the laminate thickness from 16-ply to 12-ply; although HTCS solutions exist for all ply number groupings with 10 plies and above for the non-standard angle ply case, however the distinct classes of mechanically coupled laminate are reduced to four classes to the previously nine identified in their standard ply angle orientation counterparts.

Given that all mechanically coupled laminates with balanced plain weave are HTCS, irrespective of the number of plies, terminating individual plies in order to taper the laminate thickness does not change this fact. Therefore the task is focused on identifying compatible designs within the tapering section, which preserve the coupled or uncoupled nature throughout. The listed solutions for both uncoupled and coupled laminates, presented in Table 6.3 and Table 6.7, respectively, suggest that there may be greater scope for ply termination strategy from balanced plain weave laminates, than from UD material (York, 2013).

The tapering strategy presented in this section will be confined to single and 2-ply terminations; equivalent to 2 and 4 UD layer thicknesses respectively. It consists of two parts: (a) filtering the solutions given in Table 6.3 and Table 6.7, by introducing ply terminations for each *n*-ply number grouping, with the first and last ply remaining throughout the tapered laminate to avoid surface delaminations: (b) and subsequently finding the matching stacking sequence within the *n*-1 ply number grouping.

Table 6.10 summarises the number of solutions with single ply tapering for the Simple, or $\mathbf{A_S B_0 D_S}$ laminate. The first column lists the ply number groupings, *n*. Column 2 list the stacking sequences under each ply number groupings.

Table 6.10 – Tapering solutions of the single ply termination for the fully uncoupled ($\mathbf{A_S B_0 D_S}$) laminates.

n	No. of Stacking sequences	Tapered Solutions (solutions *n* + 1)	No. of Stacking sequences with contiguity constraint = 1	Tapered Solutions (solutions *n* + 1)
21	29,504	15,884 (–)	1	1(–)
20	7,942	6,410 (↘7,942)	1	0 (↘ 1)
19	8,556	4,652 (↘8,556)	1	1 (↘ 0)
18	2,326	1,898 (↘2,326)	1	0 (↘ 1)
17	2,522	1,392 (↘2,522)	1	1 (↘ 0)
16	696	576 (↘696)	1	0 (↘ 1)
15	760	428 (↘760)	1	1 (↘ 0)
14	214	182 (↘214)	1	0 (↘ 1)
13	236	138 (↘236)	1	1 (↘ 0)
12	69	60 (↘69)	1	0 (↘ 1)
11	76	48 (↘76)	1	1 (↘ 0)
10	24	22 (↘24)	1	0 (↘ 1)
9	26	18 (↘26)	1	1 (↘ 0)
8	9	9 (↘9)	1	0 (↘ 1)
7	10	8 (↘10)	1	1 (↘ 0)
6	4	4 (↘4)	1	0 (↘ 1)
5	4	4 (↘4)	1	1 (↘ 0)
4	2	2 (↘2)	1	0 (↘ 1)
3	2	2 (↘2)	1	1 (↘ 0)
2	1	1 (↘1)	1	0 (↘ 1)

It is worth noting that the solutions shown under the second column is the number of solutions listed in Table 6.3 but are shown again here for comparison. The third column of Table 6.10 presents the numbers of solutions with single ply terminations for each ply number grouping. Numbers in parentheses represent solutions for the $n + 1$ ply number groupings, with the exception of the 21-ply number grouping. For example, 15,884 solutions exist for the 21-ply number grouping, which produce, after single ply termination, 7,942 solutions within the 20-ply number grouping. By contrast, introducing single ply terminations to the 7,942 stacking sequences with $n = 20$, results in 6,410 solutions with 20 plies, that are compatible with 8,556 solutions from the 19-ply number grouping.

Equation (6.15) illustrates the top-down single ply termination strategy performed on a 13-ply laminate, down to an 8-ply laminate. It is shown that the first termination from the 13- to 12-ply laminate corresponds to the middle ply i.e. '○'. However from the 12- to 11-ply laminate two solutions exist i.e. terminating either of the angle plies, corresponding to ply number 6 or 7.

$$\begin{array}{rc} \text{13-ply} & +/○/○/+/○/+/\underline{○}/+/○/+/○/○/+ \\ \text{12-ply} & +/○/○/+/○/\underline{+}/\underline{+}/○/+/○/○/+ \\ \text{11-ply} & +/○/○/+/○/\underline{+}/○/+/○/○/+ \\ \text{10-ply} & +/○/○/+/\underline{○}/\underline{○}/+/○/○/+ \\ \text{9-ply} & +/○/○/+/\underline{○}/+/○/○/+ \end{array} \qquad (6.15)$$

Alternatively this can be viewed as a laminate building process where a sequential pattern of adding two consecutive layers of '○' followed by two layers of '+', at the laminate mid-plane. This pattern can be applied continuously in order to build up a given laminate to any thickness required. Note that the laminate design in Eq. (6.15) possesses symmetry in both cross-ply and angle-ply. However, designs for uncoupled non-symmetric laminates also

exist, as shown in Eq. (6.16). Here the pattern of the central ply block, containing the ply terminations is identical to that of the symmetric laminate.

$$\begin{array}{ll} \text{15-ply} & +/\bigcirc/\bigcirc/+/\bigcirc/\underline{+}/\underline{\bigcirc}/\underline{+}/\underline{\bigcirc}/\underline{+}/\bigcirc/\bigcirc/+/+/\bigcirc \\ \text{14-ply} & +/\bigcirc/\bigcirc/+/\bigcirc/\underline{+}/\underline{\bigcirc}/\underline{\bigcirc}/\underline{+}/\bigcirc/\bigcirc/+/+/\bigcirc \\ \text{13-ply} & +/\bigcirc/\bigcirc/+/\bigcirc/\underline{+}/\underline{\bigcirc}/\underline{+}/\bigcirc/\bigcirc/+/+/\bigcirc \\ \text{12-ply} & +/\bigcirc/\bigcirc/+/\bigcirc/\underline{+}/\underline{+}/\bigcirc/\bigcirc/+/+/\bigcirc \\ \text{11-ply} & +/\bigcirc/\bigcirc/+/\bigcirc/\underline{+}/\bigcirc/\bigcirc/+/+/\bigcirc \end{array} \qquad (6.16)$$

Columns 4 and 5 of Table 6.10 list the stacking sequence solutions with contiguity constraint of 1 and the tapered solutions, respectively. Here the contiguity constraint implies the restriction imposed on equal angle repetition with respect to its adjacent layers in the laminate. It is clear that imposing contiguity constraints reduces the number of stacking sequence solutions, for example with contiguity factor of 1 result into a single solution. Here, only laminate with odd ply number groupings can be tapered, producing a single solution with $n - 1$ ply number groupings; by terminating the middle ply from the odd ply solution:

$$\begin{array}{ll} \text{15-ply} & +/\bigcirc/+/\bigcirc/+/\bigcirc/+/\underline{\bigcirc}/+/\bigcirc/+/\bigcirc/+/\bigcirc/+ \\ \text{14-ply} & +/\bigcirc/+/\bigcirc/+/\bigcirc/\underline{+}/\underline{+}/\bigcirc/+/\bigcirc/+/\bigcirc/+ \end{array} \qquad (6.17)$$

Note that the 14-ply laminate given in Eq. (6.17) will reduce to a 13-ply laminate with a contiguity factor of 1, if either of the middle plies, i.e. ply 7 or 8 is terminated, which possesses a solution under the 12-ply number grouping, see Table 6.10. Note that the laminate thickness in this example, can be reduced upto 2-ply number grouping, following similar tapering pattern:

$$\begin{array}{ll} \text{15-ply} & +/\bigcirc/+/\bigcirc/+/\bigcirc/+/\underline{\bigcirc}/+/\bigcirc/+/\bigcirc/+/\bigcirc/+ \\ \text{14-ply} & +/\bigcirc/+/\bigcirc/+/\bigcirc/\underline{+}/\underline{+}/\bigcirc/+/\bigcirc/+/\bigcirc/+ \\ \text{13-ply} & +/\bigcirc/+/\bigcirc/+/\bigcirc/\underline{+}/\bigcirc/+/\bigcirc/+/\bigcirc/+ \\ \text{12-ply} & +/\bigcirc/+/\bigcirc/+/\underline{\bigcirc}/\underline{\bigcirc}/+/\bigcirc/+/\bigcirc/+ \\ \vdots & \vdots \\ \text{5-ply} & +/\bigcirc/\underline{+}/\bigcirc/+ \end{array} \qquad (6.18)$$

4-ply	+/$\underline{\bigcirc}$/$\underline{\bigcirc}$/+
3-ply	+/$\underline{\bigcirc}$/+
2-ply	+/+

By contrast the coupled laminate solutions shown in Table 6.7, demonstrate that tapering of Extension-Twisting (and Shearing-Bending) $\mathbf{A_S B_t D_S}$ coupled laminates is permissible only for even ply number groupings. The numbers of tapered solutions for this laminate class is summarized in Table 6.11. A total of 146 stacking sequences are found for the 20-ply number grouping, which are compatible with 79 sequences from the 18-ply number grouping. The presentation of the results in Table 6.11 is the same format as Table 6.10.

Table 6.11 – Tapering solutions of the 2-ply terminations for the Extension-Twisting and shearing-bending ($A_S B_t D_S$) coupled laminate.

n	No. of Stacking sequences with contiguity constraint		Solutions (solutions with *n* + 1)
	>2	≤2	
20	1,352	146	146 (-)
18	512	79	77 (↘79)
16	194	39	37 (↘39)
14	84	23	21 (↘23)
12	35	13	13 (↘13)
10	16	8	8 (↘8)
8	7	4	4 (↘4)
6	4	3	3 (↘3)
4	2	2	1 (↘2)
2	1	1	(↘1)

An example of the tapering strategy for this class is given in Eq. (6.19).

$$
\begin{array}{c}
+/+/\bigcirc/+/+/\bigcirc/\underline{+/\bigcirc}/+/\bigcirc/\bigcirc/+/\bigcirc/\bigcirc \\
+/+/\bigcirc/+/+/\underline{\bigcirc/+}/\bigcirc/\bigcirc/+/\bigcirc/\bigcirc \\
+/+/\bigcirc/+/\underline{+/\bigcirc}/\bigcirc/+/\bigcirc/\bigcirc \\
+/+/\bigcirc/\underline{+/\bigcirc}/+/\bigcirc/\bigcirc \\
+/+/\bigcirc/+/\bigcirc/\bigcirc
\end{array}
\qquad (6.19)
$$

Here with terminations applied to 14-ply laminate; with terminated plies underlined. The tapered design attributes for this example are summarised in Table 6.12. Here the chosen laminates possesses maximum Extension-Twisting coupling within their respective ply number grouping, indicated by the magnitude of the lamination parameter $\xi_{8.}$ Column 3 of Table 6.12 indicates the number of possible tapering designs under the 2-ply termination scheme for each *n* ply number grouping, matching the *n*-2 laminate. Compatible tapering solutions corresponding to 7, 5, 4 and 6 for the *n*, 14-, 12-, 10- and 8-ply number grouping respectively, all involved the termination of an angle ply '+' and a cross ply '○' combination.

Table 6.12 – Summary of the 2-ply tapering strategy for the $\mathbf{A_S B_t D_S}$ laminates given in the example of Eq. (6.19) for 14-ply number grouping moving down to 6-ply number grouping.

n	ξ_8	Compatible tapering solutions with *n*-2
14	0.778	7
12	0.625	5
10	0.600	4
8	0.556	6
6	0.510	-

Laminate with Bending-Twisting coupling, in addition to Extension-Twisting and Shearing-Bending, result in a substantial increase in the number of tapered solutions. This is evident from Table 6.13, in which the solutions for the $\mathbf{A_S B_t D_F}$ class are summarised. Note that the tapering strategy for this $\mathbf{A_S B_t D_F}$ coupled class also result in only even ply number groupings. This is in contrast to the solutions for $\mathbf{A_F B_t D_F}$ coupled laminates, shown in Table 6.14, where the results span across all ply number groupings.

Table 6.13 – Tapering solutions of the 2-ply terminations for the Extension-Twisting, Shearing-Bending and Bending-Twisting ($A_S B_t D_F$) coupled laminate.

n	No. of Stacking sequences with contiguity constraint		Solutions (solutions with *n* + 1)
	>2	≤2	
20	88,302	3,742	3742 (-)
18	23,798	1,548	1548 (↘1548)
16	5,978	564	564 (↘564)
14	1,632	236	236 (↘236)
12	398	80	80 (↘80)
10	110	34	34 (↘34)
8	24	10	10 (↘10)
6	6	4	(↘4)

Table 6.14 – Tapering solutions of the single ply terminations for the Extension-Twisting, Shearing-Bending and Bending-Twisting ($A_F B_t D_F$) coupled laminate.

n	No. of Stacking sequences with contiguity constraint		Solutions (solutions with *n* + 1)
	>2	≤2	
21	1,019,072	17,265	17265 (-)
20	426,692	6,756	6756(↘6756)
19	253,588	6,382	6382 (↘6382)
18	104,436	2,420	2420 (↘2420)
17	63,014	2,418	2418 (↘2418)
16	25,900	934	934 (↘934)
15	15,624	914	914 (↘914)
14	6,262	322	322 (↘322)
13	3,860	344	344 (↘344)
12	1,546	126	126 (↘126)
11	948	128	127 (↘128)
10	362	40	40 (↘40)
9	230	48	48 (↘48)
8	88	16	16 (↘16)
7	54	18	14 (↘18)
6	18	4	4 (↘4)
5	12	6	4 (↘6)
4	4	2	1 (↘2)
3	2	2	(↘1)

6.6 Conclusion

A definitive list of laminate stacking sequences has been derived for balanced plain weave material with standard ply orientations used in industry.

Seven unique classes of coupled composite laminates have been demonstrated, and for completeness, uncoupled laminates have been included together with an important sub-group possessing fully isotropic properties. Isotropy in bending and/or extensional stiffness has been found in both coupled as well as uncoupled laminates.

The coupled classes arise from the judicious realignment of the principal material axis of a so-called parent laminate class, which possesses Extension-Bending and Shearing-Twisting: off-axis alignment, with respect to the structural or system axis, gives rise to other distinct forms of coupling interaction. All seven classes of coupled balanced plain weave laminate have immunity to thermal warping distortions, which generally arise as a result of the high temperature curing process. Laminate correspond to a buckling load factor, $k_x = 4$ (similar to fully isotropic laminates) is found for 6-ply number grouping and above for the $\mathbf{A}_I\mathbf{B}_t\mathbf{D}_I$ coupled laminate, which will be particularly useful as benchmark configurations to assess other laminates within their ply number grouping.

Tapering thickness solutions are also shown to exist within these coupled classes, with single and two ply terminations; where the latter applies to the $\mathbf{A}_S\mathbf{B}_t\mathbf{D}_S$, $\mathbf{A}_S\mathbf{B}_t\mathbf{D}_F$, $\mathbf{A}_S\mathbf{B}_F\mathbf{D}_S$ and $\mathbf{A}_S\mathbf{B}_F\mathbf{D}_F$ coupled classes, as solutions are only shown to exist for even ply number groupings. Meanwhile single ply tapering solutions exist across all ply number groupings from 21-ply to 2-ply $\mathbf{A}_F\mathbf{B}_t\mathbf{D}_F$ and $\mathbf{A}_F\mathbf{B}_F\mathbf{D}_F$ coupled laminates. This is also observed for uncoupled $\mathbf{A}_S\mathbf{B}_0\mathbf{D}_S$ laminates. Such laminates therefore provide a robust manufacturing solution for integrating complex mechanical coupling response, as an enabling technology, in future smart materials and structures.

CHAPTER 7

Thermal warping prediction for 5-harness Satin weave laminates

Satin weave architecture possess straighter load-carrying fibres in comparison to other biaxial fabric counterparts such as plain weave, 2 x 2 twill weave and etc., which give rise to improve mechanical performance. In addition Satin weave is also favoured for its good pliability characteristics, which are advantageous when manufacturing parts with intricate geometrical shapes. However the fundamental challenge when adopting Satin weave material, is in mitigating the warping distortions that are known to occur in a single layer as a consequence of the high temperature curing process. This is due to the inherent nature of the Satin weave architecture, with warp dominated fibres on one face of the material, and fill dominated fibres on the opposite face, see Fig. 7.1. The area of the fill fibres on the warp dominated side (and vice versa) has been shown by Ishikawa (1981) to be approximately the inverse of the number of 'repeats', *n*. In the case of the 5-harness Satin (5-HS) weave in Fig. 7.1 the value $n = 5$, assuming $n_{fill} = n_{warp} = n$, which results in an area ratio of 1:5 for the fill fibres on the warp fibre dominated side.

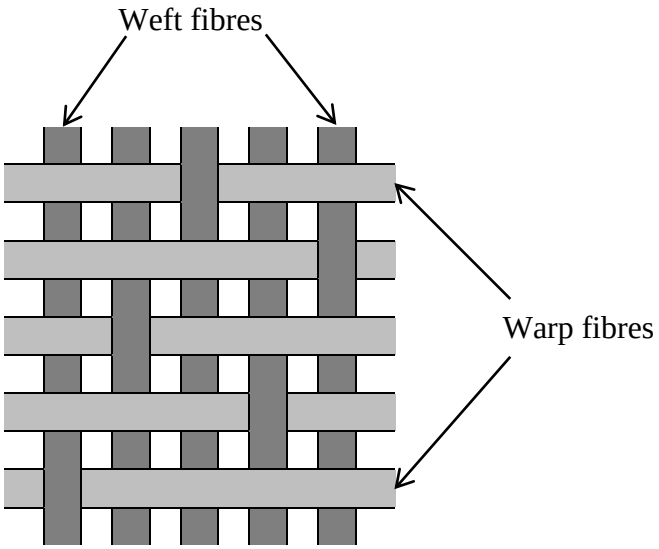

Figure 7.1 – The 5-harness satin weave architecture, with warp dominated fibres exists on one side of the material and weft-dominated fibres on the other side.

A single layer of the Satin weave material behaves similar to a cross-ply laminate i.e. $[0/90]_T$. This was the conclusion drawn from the work of Jacobsen *et al.* (2004), describing an experiment investigation for characterising the coupling properties of a 4-layered simply-stacked 5-HS weave laminates, from which the measured results of the compliance terms were found to be in close agreement with the prediction from classical laminate theory (CLT) for an equivalent cross-ply laminate of $[(0/90)_4]_T$.

By contrast Ishikawa (1981) proposed a lamination technique for mitigating the thermal instability from the Satin weave material, which involves flipping of the adjacent layers to produce what is known as a semi-symmetric configuration, see Fig. 7.2. Figure 7.2 (a) and (b) illustrate the 5-HS weave geometry under the non-flipped and flipped condition, respectively. Meanwhile Fig. 7.3 illustrate the condition for a two layered 5-HS weave laminate employing the semi-symmetric technique. Here the semi-symmetric condition is explained by observing the configuration of the warp and weft yarns about the laminate mid-plane, where the set of yarns highlighted by the box in Fig. 7.3 are shown to be symmetric about the laminate mid-plane, while the outer sets of yarns are not. Ishikawa *et al.* (1985) employed this technique in the fabrication of test specimens for performing

experimental investigation on the elastic properties of Satin weave composites. The test results were found to be in good agreement with earlier developed micro-mechanical modelling (Ishikawa, 1981), namely the Bridging model i.e. a combination of both the Mosaic and Crimp model, previously discussed on page 94 of Chapter 6. In addition, it was observed that the elastic modulus of Satin weave laminates remained unchanged with increasing numbers of plies, which is not the case for Plain weave laminates, where an increase in the elastic modulus was reported (Jekabsons and Bystrom, 2002, Naik and Shembekar, 1992b).

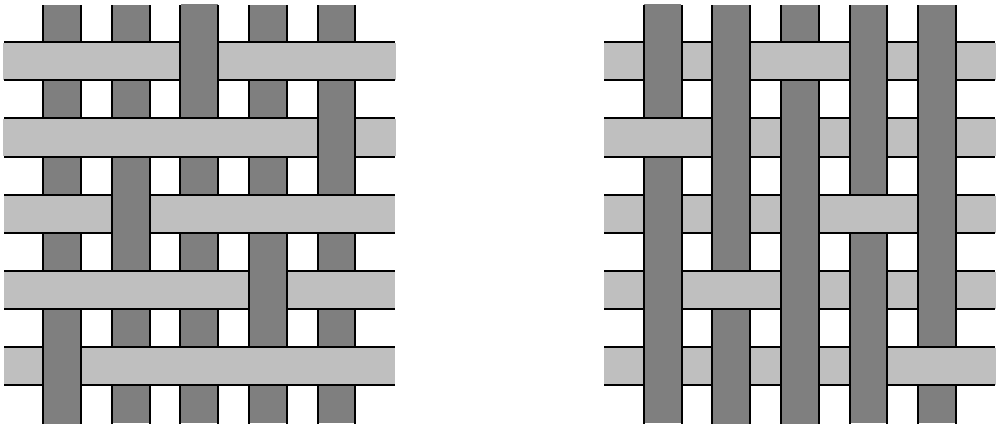

Figure 7.2 – Comparison view for the 5-harness satin weave architecture showing: (a) non-flipped geometry; (b) flipped geometry.

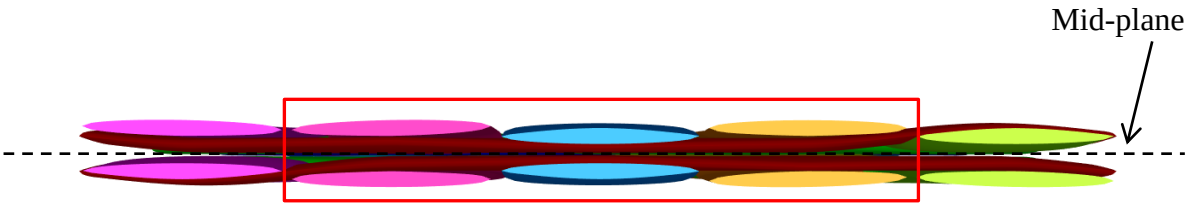

Figure 7.3 – Semi-symmetric laminate configuration proposed by Ishikawa (1981).

Abot *et al.* (2004) adopted a similar flipping lamination technique in their experimental investigation looking at the mechanical, viscoelastic and thermal properties of 4- and 8-plies of 5-HS weave laminates. Raju and Wang (1994) presented a similar analytical model based upon the Bridging model, aiming to characterise the (**ABD**) stiffness matrix for the 5- and 8-harness Satin weave. Here, the authors improved the existing Bridging model by taking into account the continuity of the fibres in the other coordinate direction i.e. a two-dimensional approach.

Bishop (1989) stated that the coupling or warping phenomenon in Satin weave arises due to the unbalanced crimp line angle in the laminates, see Fig. 7.4.

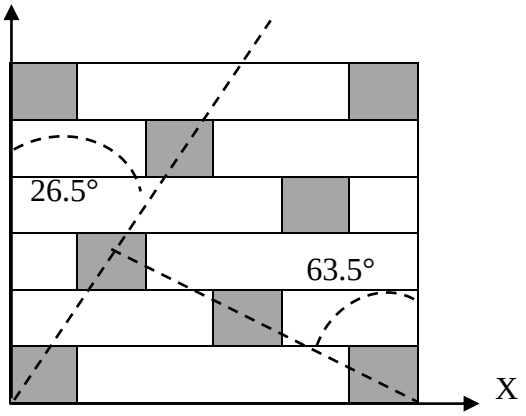

Figure 7.4 – Unbalanced crimp line angle of the 5-harness satin weave, (after Bishop, 1989), with respect to principal material axis system.

For this reason a similar layer manipulation technique was proposed to balance the crimp line angle, involving the rotation of layers (in addition to flipping). For example, the semi-symmetric laminate configuration, with a cross-ply laminate to represent a single layer of the Satin weave, can be described as:

	L	T	/	T	L
	0	90	/	90	0
Crimp line angle	–26.5º		/	26.5º	

(7.1)

The warp fibres aligned at 0º angle is given the letter L denoting longitudinal fibres and the weft fibres at 90 º angles with the letter T signifying transverse fibres, see Fig. 7.1. It is clear from Eq. (7.1) that the warp and weft fibres are symmetric about the laminate mid-plane, but the crimp line angles are not. By contrast, the simply-stacked (without layer manipulation) 2-ply laminate described by:

	L	T	/	L	T
	0	90	/	0	90
Crimp line angle	–26.5º		/	–26.5º	

(7.2)

has a symmetric crimp line angle about the laminate mid-plane but the fibres are not. Despite the unbalanced crimp line angle, a marked reduction in the thermal warping distortion was reported for the 2-ply laminate, by adopting the semi-symmetric method (Ishikawa, 1981). Furthermore, the influence of unbalanced crimp line angles was found to be less severe in the case of the 5-HS laminates when made from carbon fibre materials (Bishop, 1989); due to the high stiffness properties of carbon fibre composite material. However, the relationship between coupling behaviour and the number of plies, using either simply-stacked or semi-symmetric lamination techniques is less well understood.

This chapter will therefore investigate the coupling behaviour of Satin weave laminates, particularly 5-HS weave, from which the manifestation of such coupling behaviour will be assessed with respect to the thermal warping distortion following a high temperature curing during manufacturing. This will be studied for both simply-stacked and semi-symmetric lamination configurations for the 5-HS weave laminates. The laminate stiffness properties, which includes the coupling (**B**) stiffness, will be assessed using a finite element technique, which is fundamentally based upon a micro-mechanical modelling approach. However, unlike the approach adopted by others (Karkkainen and Sankar, 2006) the stiffness properties were obtained from the micro-mechanical modelling of a single layer in order to

calculate the laminate stiffness properties for multiple layers, the current work incorporates multiple layers within the geometrical model of the 5-HS weave in order to obtain their laminate stiffness properties.

An experimental investigation is also carried out to measure the warping curvatures that arise from the 5-HS weave laminates with 2, 4, 6 and 8 plies; each manufactured under the simply-stacked and semi-symmetric configurations. These laminates were manufactured using standard temperature and pressure curing cycles, where the resulting thermal warping from the laminates were later captured via scanning the plates using a 3D laser scanning machine. The scanned images were subsequently analysed in MATLAB (2014), using a curve fitting function, from which the principal curvatures of the plates are obtained, this provided a measure of the deviation from flatness in each plate sample.

7.1 Finite element modelling

The development of numerical models for Satin weave material has been based on successful models for Plain weave material and subsequently extended to the case of Satin weave material. For instance the work of Woo *et al*. (2002), which developed macro elements, was later applied to the study of the stress distribution within Satin weave laminates under the influence of phase shifts between individual layers in the laminates. Meanwhile, Rao *et al*. (2008) developed a detailed modelling approach for the geometry of Satin weave composite, by introducing a 'middle matrix layer' that was neglected from previously developed models in the literatures. However, this novel layer represents a marginally small volume from which could result in a considerably distorted mesh, and consequently in erroneous stress estimation for the region. More recent work by Khoun *et al*. (2012) presented results on the thermo-mechanical properties of 5-HS weave, in which the modelling of the Satin weave geometry was performed using an open source textile modelling software, TexGen (2007). The results were presented for different fibre volume fractions within the 5-HS weave material.

The geometric modelling of the 5-HS weave architecture in this current study will also use Texgen (2007), primarily due to the modelling features of the software, which permits a three dimensional geometrical model of any given woven architecture to be readily created. Another distinct feature is the option to generate a Voxel mesh, which is a volumetric rendering of the textile geometric architecture using polygons, for exporting to the commercial finite element code ABAQUS (2009b). Here the fibres and resin are discretised independently using 3D brick elements, which allow for material homogeneity within the geometrical model of the 5-HS weave.

7.1.1 Geometric modelling

The challenge when performing computer modelling of woven fabric composite relates to the level of geometric detail required to accurately describe the architecture. While crude modelling jeopardises the accuracy of the results, complex models which accurately capture the architecture lead to computationally expensive analyses, and often approach the current limits of computational capability.

A common approach taken by many in the literature (Ishikawa, 1981, Naik and Shembekar, 1992a, Raju and Wang, 1994, Woo *et al*., 2002, Rao *et al*., 2008, Khoun *et al*., 2012) have been perform to an analysis on an identifiable repeating unit cell (RUC) for a given woven fabric architecture. Analysis based on the RUC has shown accurate and reliable results for many fabric architecture. For instance, the prediction of the material properties of a single lamina (Ishikawa *et al*., 1985, Raju and Wang, 1994, Naik and Ganesh, 1992), as well as at laminate level (Ishikawa and Chou, 1982, Naik and Shembekar, 1992b, Shembekar and Naik, 1992, Whitcomb and Tang, 2001) have shown to be in good agreement with experimental results. By contrast, Woo (2005) emphasised that the use of RUC is valid only for axis aligned material, and not suitable for off-axis alignment.

The RUC for a 5-HS weave material is shown in Fig. 7.5. Using the geometrical dimensions given in Table 7.1, the RUC model of the 5-HS weave was created in Texgen, which is illustrated in Fig. 7.6. Here the dimension c denotes the width of the yarn, while the dimension d gives the centre line distance between two yarns. Two thicknesses are prescribed in Fig. 7.6: the yarn thickness, denoted by h_t and; the material thickness, denoted by t. The dimensions a and b give the length and width of the RUC in the x– and y–axis directions, respectively. It will be assumed that yarns in the warp and weft

directions have constant width, *c*, and consequently constant *d*. This also implies that the length of the RUC in the x– and y–axis directions are equal, i.e., $a = b$.

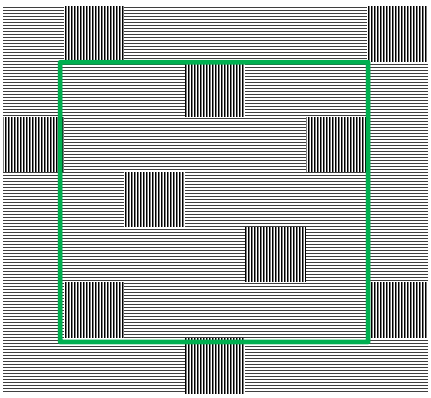

(a)

Figure 7.5 – Geometry of the repeating unit cell (RUC) for the 5-harness satin weave.

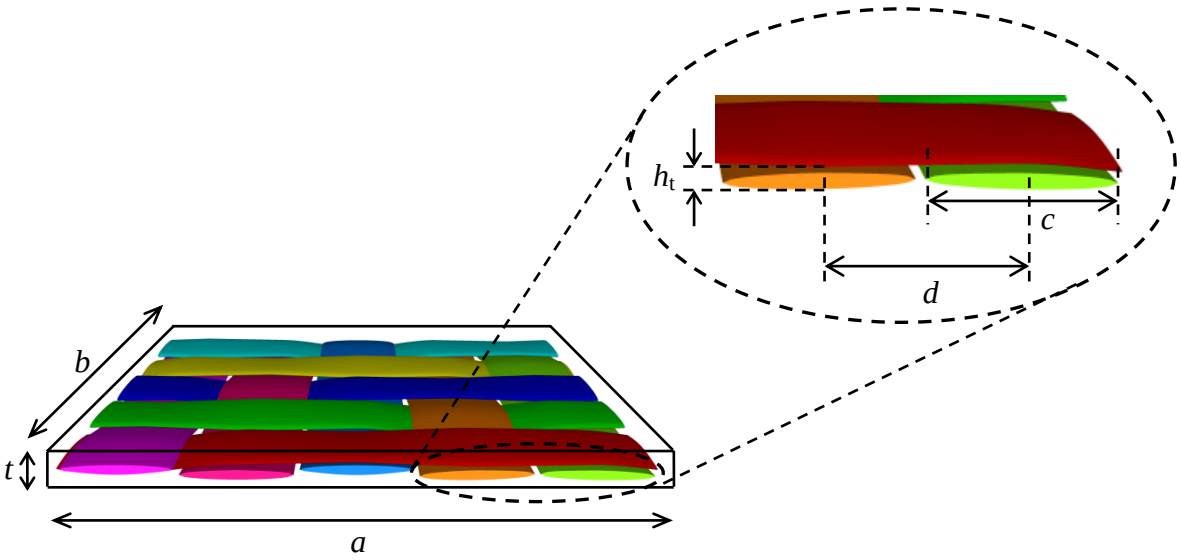

Figure 7.6 – Three dimensional geometry modelling of the 5-harness satin weave performed in Texgen, with values of the respective dimensions given in Table 7.1.

Table 7.1 – Geometry dimensions for the 5-harness weave architecture shown in Fig. 7.6.

Unit Cell dimensions (mm)				
c	d	*t*	*a*, *b*	h_t
2.1	2.2	0.37	11	0.1665

7.1.2 Periodic displacement boundary conditions

Woven fabric material is seen as a build-up periodic array of its RUC; hence when analysing a single RUC it is imperative to ensure the continuity in displacements at the boundaries of the RUC. This can be enforced through the use of periodic displacement boundary conditions, which enforce identical deformations on opposite faces of the RUC.

The voxel mesh from TexGen (2007) will result in equal mesh distribution on opposite faces of the 5-HS RUC model. In other words, the distribution of the nodes, i.e. the number of nodes and their relative position, on opposite boundaries of the RUC are identical, hence facilitating the use of periodic displacement boundary conditions. Through the pairing of nodes on opposite boundaries, the periodic boundary conditions are implemented using constraint equations, which in the case of 3D solid elements, with three degrees of freedom per node, the constraint equations can be applied to maintain periodicity in the three global directions. The periodic displacement boundary conditions adopted in the current work are similar to those developed from Karkkainen and Sankar (2006), given in Table 7.2. Under these periodic boundary conditions, only the lateral faces of the 5-HS weave RUC are subjected to constraint equations, i.e., faces A, B, C and D in Fig. 7.7. Meanwhile the top and bottom surfaces of the RUC are free from any constraint.

The periodic displacement boundary conditions are defined in Table 7.2 in terms of six unit strain or curvature conditions, shown in the first column. These unit strains and curvature act as uniformly applied loads on the RUC, which will be explained in detail later. For instance the first row of Table 7.2 where the RUC is subjected to a unit strains of $\varepsilon_x = 1$, the periodic displacement boundary conditions on the two lateral faces A and C, and faces B and D are described by the respective column in Table 7.2.

.

Table 7.2 – Periodic displacement boundary conditions imposed on lateral faces of the repetitive unit cell, after Karkkainen and Sankar (2006).

	Faces A and C			Faces B and D		
	u(*a*,y) – u(0,y)	v(*a*,y) – v(0,y)	w(*a*,y) – w(0,y)	u(x,*b*) – u(x,0)	v(x,*b*) – v(x,0)	w(x,*b*) – w(x,0)
$\varepsilon_x = 1$	*a*	0	0	0	0	0
$\varepsilon_y = 1$	0	0	0	*b*	0	0
$\gamma_{xy} = 1$	0	*a*/2	0	*b*/2	0	0
$\kappa_x = 1$	*a*z	0	$-a^2/2$	0	0	0
$\kappa_y = 1$	0	0	0	0	*b*z	$-b2/2$
$\kappa_{xy} = 1$	0	*a*z/2	–*a*y/2	*b*z/2	0	–*b*x/2

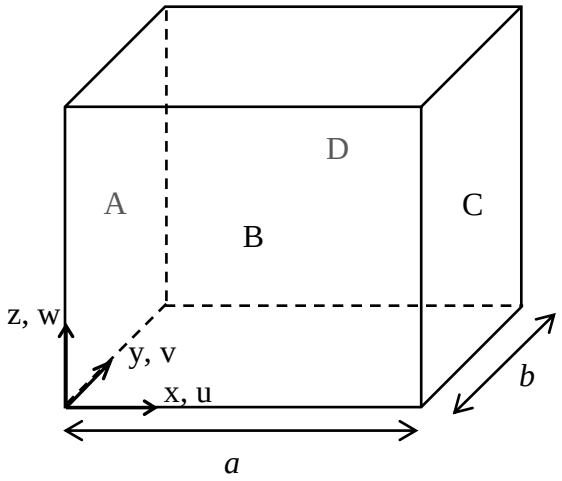

Figure 7.7 – Geometric model for displacement periodic boundary conditions, with the origin of the global coordinate system shown.

The periodic equations representing the constraint between the pairing of nodes on face A (0, y, z) and C (*a*, y, z) can be written by:

$$\begin{aligned} u^C - u^A &= \varepsilon_x a \\ v^C - v^A &= 0 \\ w^C - w^A &= 0 \end{aligned} \tag{7.3}$$

Similarly for the paired nodes of face B (x, 0, z) and D (x, *b*, z), the constraint periodic equation is given by:

$$\begin{aligned} u^D - u^B &= 0 \\ v^D - v^B &= 0 \\ w^D - w^B &= 0 \end{aligned} \tag{7.4}$$

The constraint equations of Eqs. (7.3) and (7.4), can be applied to the RUC 5-HS model in ABAQUS (2009a) using linking equations. The strain ε_x term, shown by the first of Eq. (7.3), can be applied through a dummy node, attached via rigid elements to all nodes on a given face of Fig. 7.7. An annotated ABAQUS input file for the RUC 5-HS model is given in Appendix C.

7.1.3 Loading conditions

The load applied to the RUC model is through displacement control, which is in the form of unit strain, given in Table 7.2. The six strains given in Table 7.2 are applied individually, in six different finite element analyses, where only the active strain component is non-zero. The element of the ABD stiffness matrix corresponding to the first column are calculated using the method from Marrey and Sankar (1997). Here the components of the force and moment resultant vector, are derived using the summation of the developing micro-stresses, σ_{ij}, within the elements of the model result from the applied unit strain, through Eqs. (7.6) and (7.7).

$$\begin{Bmatrix} N_x \\ N_y \\ N_{xy} \\ M_x \\ M_y \\ M_{xy} \end{Bmatrix} = \begin{bmatrix} A_{11} & A_{12} & A_{16} & B_{11} & B_{12} & B_{16} \\ A_{12} & A_{22} & A_{26} & B_{12} & B_{22} & B_{26} \\ A_{16} & A_{26} & A_{66} & B_{16} & B_{26} & B_{66} \\ B_{11} & B_{12} & B_{16} & D_{11} & D_{12} & D_{16} \\ B_{12} & B_{22} & B_{26} & D_{12} & D_{22} & D_{26} \\ B_{16} & B_{26} & B_{66} & D_{16} & D_{26} & D_{66} \end{bmatrix} \begin{Bmatrix} \varepsilon_x \\ \varepsilon_y \\ \gamma_{xy} \\ \kappa_x \\ \kappa_y \\ \kappa_{xy} \end{Bmatrix} \tag{7.5}$$

$$N_x, N_y, N_{xy} = \frac{1}{ab} \sum \sigma_{ij} \mathrm{V}^{\mathrm{e}} \tag{7.6}$$

$$M_x, M_y, M_{xy} = \frac{1}{ab} \sum \sigma_{ij} V^e z \tag{7.7}$$

where i, j = 1, 2.

Note that V^{e} is the element volume and *a*, *b* is the side length of the unit cell in the x- and y-direction, respectively. The *z* term in Eq. (7.7) represents the value for the z-coordinate (i.e, the through thickness distance from the laminate mid-plane) of the respective elements in the model. The remaining columns of the stiffness matrix of Eq. (7.5) are obtained by applying, separately, each of the other five strain cases. This procedure results in a complete characterisation of the laminate stiffness properties.

Prior to simulating the 5-HS weave model in Fig. 7.6, the laminate stiffness properties of a cross-ply model $[0/90]_T$, from which the physical behaviour of the 5-HS weave has previously been associated (Jacobsen *et al.*, 2004), is first analysed. The purposes of modelling the cross-ply laminate model are twofold: to serve as a means of comparison to the stiffness matrix of the 5-HS weave laminate; and also to validate the finite element model, from which the stiffness properties of the cross-ply laminate can be readily verified using the CLT method, discussed in section 2.1 of Chapter 2.

The modelling of the cross-ply laminate is also performed using TexGen (2007), with the modelling parameters is similar to those described in Table 7.1, however the value of the yarn thickness, h_t is set to equal half the of the laminate's thickness, t value. The geometry of the cross-ply model is illustrated in Fig. 7.8.

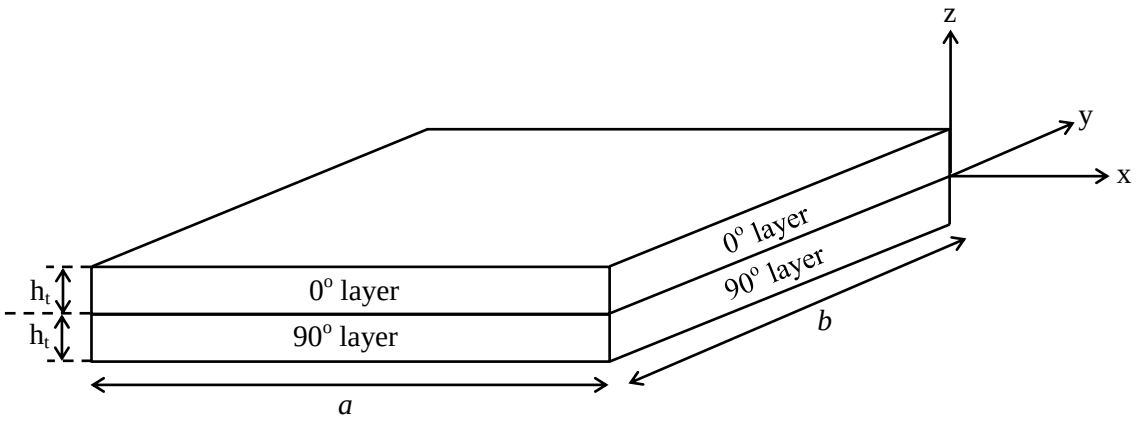

Figure 7.8 – Cross-ply laminate model performed in Texgen.

The ABAQUS (2009b) model is meshed using C3D8R elements with 55 elements across the length and across the width of the model, and 20 elements through the thickness, which result in a total of 60,500 elements. The homogeneous material properties of the carbon-fibre/epoxy listed in Table 4.3 are used for this investigation. Results on the predicted laminate stiffness matrix using the ABAQUS model are summarised in Table 7.3a, together with the laminate stiffness matrix for the cross-ply $[0/90]_T$ laminate calculated

from the classical laminate theory (CLT), demonstrating very good agreement between the two results.

Having verified the current FEM method, the attention is now turned to the 5-HS weave model in Fig. 7.6, where the geometry is meshed using similar 3D brick elements and with the same mesh density used for the cross-ply model. Now however, the fibres and resin are accounted in the 5-HS weave model, hence the carbon fibre and epoxy material properties listed in Table 7.4 and Table 7.5 respectively are used.

Table 7.3 – Stiffness properties for the extensional (A), coupling (B) and bending (D) stiffness of a single 5-harness Satin weave model, the cross-ply unit cell obtained under the finite element method and the analytical method from Raju and Wang (1994).

(a)

	Extensional (**A**)	Coupling (**B**)	Bending (**D**)
FEM $[0/90]_T$	$\begin{bmatrix} 33,244 & 902 & 0 \\ 902 & 33,244 & 0 \\ 0 & 0 & 1,628 \end{bmatrix}$	$\begin{bmatrix} 2,767 & 0 & 0 \\ 0 & -2,767 & 0 \\ 0 & 0 & 0 \end{bmatrix}$	$\begin{bmatrix} 379 & 10 & 0 \\ 10 & 379 & 0 \\ 0 & 0 & 19 \end{bmatrix}$
CLT $[0/90]_T$	$\begin{bmatrix} 33,243 & 903 & 0 \\ 903 & 33,243 & 0 \\ 0 & 0 & 1,628 \end{bmatrix}$	$\begin{bmatrix} 2,766 & 0 & 0 \\ 0 & -2,766 & 0 \\ 0 & 0 & 0 \end{bmatrix}$	$\begin{bmatrix} 379 & 10 & 0 \\ 10 & 379 & 0 \\ 0 & 0 & 19 \end{bmatrix}$

(b)

	Extensional (**A**)	Coupling (**B**)	Bending (**D**)
FEM 5-HS	$\begin{bmatrix} 25,071 & 3,227 & 0 \\ 3,227 & 25,071 & 0 \\ 0 & 0 & 1,668 \end{bmatrix}$	$\begin{bmatrix} 1,114 & 0 & 0 \\ 0 & -1,114 & 0 \\ 0 & 0 & 0 \end{bmatrix}$	$\begin{bmatrix} 183 & 31 & 0 \\ 31 & 183 & 0 \\ 0 & 0 & 13 \end{bmatrix}$
CLT Mosaic (Raju and Wang, 1994)	$\begin{bmatrix} 33,243 & 903 & 0 \\ 903 & 33,243 & 0 \\ 0 & 0 & 1628 \end{bmatrix}$	$\begin{bmatrix} 1,660 & 0 & 0 \\ 0 & -1,660 & 0 \\ 0 & 0 & 0 \end{bmatrix}$	$\begin{bmatrix} 379 & 10 & 0 \\ 10 & 379 & 0 \\ 0 & 0 & 19 \end{bmatrix}$

Table 7.4 – Intermediate AS4 Carbon fiber properties (Daniel and Ishai, 2006).

	AS4
Manufacturer	Hexcel
E_{11} (GPa)	235
$E_{22} = E_{33}$ (GPa)	15
G_{12} (GPa)	27
G_{13} (GPa)	7
ν_{12}	0.2
α_{11} (10^{-6}/°C)	–0.5
α_{22} (10^{-6}/°C)	15

Table 7.5 – Polymer matrix properties for 3501-6 epoxy (Daniel and Ishai, 2006).

	3501-6 epoxy
E (GPa)	4.3
G (GPa)	1.6
ν	0.35
α (10^{-6}/°C)	45

The fibre volume fraction for the 5-HS weave model in Fig. 7.6 is obtained from ABAQUS (2009b), calculated from the ratio of the volume of elements representing the yarns against the entire volume of the 5-HS weave RUC model. This result in a fibre volume fraction, V_f of 65%. In contrast the cross-ply model uses homogenous carbon-fibre/epoxy material properties, which were based upon a fibre volume fraction V_f = 65%. The result on the prediction of the laminate stiffness matrix for the 5-HS, obtained under the current FEM modelling is presented in Table 7.3b, together with the CLT Mosaic model, based on the analytical model developed for the 5-HS by Raju and Wang (1994). This model possesses the same geometrical configuration as the 5-HS geometry in Fig. 7.6 but without considering the undulation of the yarns, see Fig. 6.3.

It is evident from Table 7.3b, that the form of the ABD stiffness matrix for the 5-HS weave has the classification $\mathbf{A}_S\mathbf{B}_I\mathbf{D}_S$ using the subscript symbol notation from ESDU (1994),

representing an anti-symmetric cross-ply laminate. However, the magnitude of the elements of the 5-HS stiffness matrix, relative to the cross-ply model, reveals a reduction due to the waviness of the fibres presented in the 5-HS textile model; The higher magnitude of the elements of the coupling stiffness (**B**) matrix from the CLT Mosaic model is the result from the contributions from the $[0/90]_T$ and $[90/0]_T$ configurations that appear within the 5-HS weave RUC geometry, see Fig. 7.5, but not in the cross-ply model. The differences between the Mosaic and the 5-HS model represent the influence of the fibre undulation. By contrast, the continuity of the fibres in both the warp and weft directions of the 5-HS model, result in a higher value of $\mathbf{A}_{12}$ and $\mathbf{D}_{12}$, in comparison to the Mosaic model in Table 7.3b.

7.1.4 Stiffness properties of multiple layers of 5-HS laminate.

The strategy for investigating the laminate stiffness matrix for the 5-HS with multiple layers involves the same technique previously described for the single layer analysis. Once again the geometric modelling of 5-HS weave laminates is performed in TexGen (2007). Figure 7.9 illustrates the two-ply 5-HS RUC model, where Fig. 7.9(a) shows the geometry for the simply-stacked laminate configuration and Fig. 7.9(b) shows the geometry under the semi-symmetric laminate configuration. The element mesh distributions within the models are the same as for the single layer but with the number of elements through the thickness doubled to maintain the same fidelity in the two-ply laminate, i.e. 55 elements across the length and width and 40 elements through the thickness giving a total of 121,000 elements.

The results of the predicted laminate stiffness properties for the two lamination configurations, i.e. simply-stacked and semi-symmetric, are summarised in the second and third row of Table 7.6, respectively. Also presented in the table are the results of the stiffness matrices for $[0/90]_2$ and $[0/90]_S$ UD material, assuming CLT, where the former sequence serves as a means of comparison with the simply-stacked 5-HS, and the latter to the semi-symmetric 5-HS.

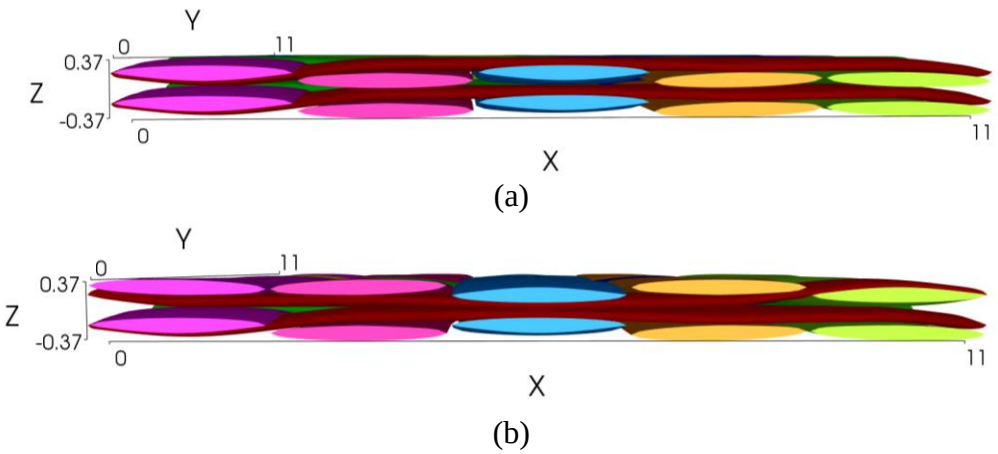

Figure 7.9 – Two-ply 5-HS weave laminates: (a) simply-stacked configuration and; (b) semi-symmetric configuration.

Table 7.6 – Laminate stiffness properties for the two-ply 5-HS under the simply-stacked and semi-symmetric lamination configuration.

	Extensional (**A**)	Coupling (**B**)	Bending (**D**)
FEM Simply-stacked	$\begin{bmatrix} 54,722 & 4,054 & 0 \\ 4,054 & 54,722 & 0 \\ 0 & 0 & 3354 \end{bmatrix}$	$\begin{bmatrix} 2,349 & 0 & 0 \\ 0 & -2,349 & 0 \\ 0 & 0 & 0 \end{bmatrix}$	$\begin{bmatrix} 2,233 & 214 & 0 \\ 214 & 2,233 & 0 \\ 0 & 0 & 140 \end{bmatrix}$
FEM Semi-symmetric	$\begin{bmatrix} 56,149 & 3,242 & 0 \\ 3,242 & 56,149 & 0 \\ 0 & 0 & 3,349 \end{bmatrix}$	$\begin{bmatrix} 0 & 0 & 3 \\ 0 & 0 & -3 \\ 3 & -3 & 0 \end{bmatrix}$	$\begin{bmatrix} 1,418 & 170 & 0 \\ 170 & 3218 & 0 \\ 0 & 0 & 141 \end{bmatrix}$
CLT $[0/90]_2$	$\begin{bmatrix} 66,487 & 1,805 & 0 \\ 1,805 & 66,487 & 0 \\ 0 & 0 & 3,256 \end{bmatrix}$	$\begin{bmatrix} 5,532 & 0 & 0 \\ 0 & -5,532 & 0 \\ 0 & 0 & 0 \end{bmatrix}$	$\begin{bmatrix} 3,034 & 82 & 0 \\ 82 & 3,034 & 0 \\ 0 & 0 & 149 \end{bmatrix}$
CLT $[0/90]_S$	$\begin{bmatrix} 66,487 & 1,805 & 0 \\ 1,805 & 66,487 & 0 \\ 0 & 0 & 3,256 \end{bmatrix}$	$\begin{bmatrix} 0 & 0 & 0 \\ 0 & 0 & 0 \\ 0 & 0 & 0 \end{bmatrix}$	$\begin{bmatrix} 987 & 82 & 0 \\ 82 & 5,081 & 0 \\ 0 & 0 & 149 \end{bmatrix}$

Karkkainen and Sankar (2006) used the value of the stiffness properties of a single layer, obtained under the same micro-mechanical modelling procedure, to calculate the stiffness properties for multiple layers using the following equations:

$$A_{ij} = \sum_{k=1}^{N} A_{ij}^{S} \;,\quad B_{ij} = \sum_{k=1}^{N} B_{ij}^{S} \;,\quad D_{ij} = \sum_{k=1}^{N} D_{ij}^{S} + t^2 A_{ij}^{S} \quad \text{with i = 1,2 and j = 1,2,6} \tag{7.8}$$

The superscript s in Eq. (7.8) denotes the value representing the single layer. Meanwhile the variable *t* that appears in the calculation for the bending stiffness (**D**) is the distance taken from the laminate mid-plane to the mid-point of the respective layer. For instance using the single layer stiffness properties for the 5-HS in Table 7.3 to calculate the two-ply simply-stacked laminate, yields the result shown in the first row of Table 7.7.

Table 7.7– The comparison between the stiffnesses of a two-layer simply-stacked 5-HS calculated using the value of a single layer stiffness properties from Table 7.3 and the FEM simply-stacked result in Table 7.6.

	Extensional (**A**)	Coupling (**B**)	Bending (**D**)
Calculated from a single layer properties	$\begin{bmatrix} 50{,}142 & 6{,}454 & 0 \\ 6{,}454 & 50{,}142 & 0 \\ 0 & 0 & 3{,}336 \end{bmatrix}$	$\begin{bmatrix} 2{,}228 & 0 & 0 \\ 0 & -2{,}228 & 0 \\ 0 & 0 & 0 \end{bmatrix}$	$\begin{bmatrix} 2{,}082 & 283 & 0 \\ 283 & 2{,}082 & 0 \\ 0 & 0 & 140 \end{bmatrix}$
FEM Simply-stacked	$\begin{bmatrix} 54{,}722 & 4{,}054 & 0 \\ 4{,}054 & 54{,}722 & 0 \\ 0 & 0 & 3354 \end{bmatrix}$	$\begin{bmatrix} 2{,}349 & 0 & 0 \\ 0 & -2{,}349 & 0 \\ 0 & 0 & 0 \end{bmatrix}$	$\begin{bmatrix} 2{,}233 & 214 & 0 \\ 214 & 2{,}233 & 0 \\ 0 & 0 & 140 \end{bmatrix}$

The most noticeable discrepancy between the two results shown in Table 7.7, is the extensional (**A**) stiffness values. This presents a problem when applying the laminate stiffness matrix to the prediction of the elastic material properties for a single layer of 5-HS material.

The FEM result for the semi-symmetric laminate configuration produces a stiffness matrix corresponding to an $\mathbf{A}_S\mathbf{B}_t\mathbf{D}_S$ coupled laminate, which is different to the expected CLT $[0/90]_S$ result, i.e., $\mathbf{A}_S\mathbf{B}_0\mathbf{D}_S$. Although the magnitude of the Extension-Twisting (and Shearing-Bending) coupling terms i.e. $\mathbf{B}_{16}$ and $\mathbf{B}_{26}$, are non-zero, they are insignificant, however the result serves to demonstrate the influence of the unbalanced crimp line angle in this two-layer semi-symmetric configuration; this form of coupling would be expected in anti-symmetric angle-ply laminates, which the crimp lines are producing as an artefact within the woven cloth architecture. Additionaly, the unbalanced crimp line angle appears as a discontinuous line rather than a continuous straight line in the RUC geometry, see Fig. 7.4, which perhaps explains the low magnitude of the coupling stiffness term.

Table 7.8 presents the results for the prediction of the stiffness properties studied under the 4-ply laminates. The second row of the table gives the result for the simply-stacked 4-layer laminates, followed by the result of the semi-symmetric laminate configuration in the third row of the table. The last row of the table gives the value for the stiffness matrix calculated by the method of Karkkainen and Sankar (2006). The form of the laminate stiffness matrices under this ply number grouping, for both simply-stacked and semi-symmetric laminate configurations remain identical to the two-ply results i.e. $\mathbf{A}_S\mathbf{B}_l\mathbf{D}_S$ and $\mathbf{A}_S\mathbf{B}_t\mathbf{D}_S$ coupled laminates, respectively; only the magnitude of the individual elements differ. Most significantly, the $\mathbf{D}_{11}$ and $\mathbf{D}_{22}$ values of the simply-stacked laminate increase relative to the increase in laminate thickness, whereas the coupling stiffness (**B**) values, diminish signifying that increasing the number of plies in the laminate suppresses the Extension-Bending coupling towards the warp-free condition. The magnitude of the Extension-Twisting coupling due to the crimp angle artefact remains relatively weak to the extent that it is effectively negligible.

Table 7.8 – Laminate stiffness properties for the 4-ply laminates obtained through the FEM modelling of simply-stacked and semi-symmetric configurations. Also presented is the result obtained by the method from Karkkainen and Sankar (2006).

	Extensional (**A**)	Coupling (**B**)	Bending (**D**)
Simply-stacked	$\begin{bmatrix} 111,303 & 7,050 & 0 \\ 7,050 & 111,303 & 0 \\ 0 & 0 & 6,727 \end{bmatrix}$	$\begin{bmatrix} 4,756 & 0 & 0 \\ 0 & -4,756 & 0 \\ 0 & 0 & 0 \end{bmatrix}$	$\begin{bmatrix} 19,763 & 1,372 & 0 \\ 1,372 & 19,763 & 0 \\ 0 & 0 & 1,199 \end{bmatrix}$
Semi-symmetric	$\begin{bmatrix} 113,239 & 5,913 & 0 \\ 5,913 & 113,239 & 0 \\ 0 & 0 & 6,707 \end{bmatrix}$	$\begin{bmatrix} 0 & 0 & 4 \\ 0 & 0 & -4 \\ 4 & -4 & 0 \end{bmatrix}$	$\begin{bmatrix} 18,358 & 1,148 & 0 \\ 1,148 & 21,938 & 0 \\ 0 & 0 & 1,199 \end{bmatrix}$
Karkkainen and Sankar	$\begin{bmatrix} 100,284 & 12,908 & 0 \\ 12,908 & 100,284 & 0 \\ 0 & 0 & 6,672 \end{bmatrix}$	$\begin{bmatrix} 4,456 & 0 & 0 \\ 0 & -4,456 & 0 \\ 0 & 0 & 0 \end{bmatrix}$	$\begin{bmatrix} 17,893 & 2,333 & 0 \\ 2,333 & 17,893 & 0 \\ 0 & 0 & 1,194 \end{bmatrix}$

By contrast, the magnitude for the extensional (**A**) and bending (**D**) stiffness matrix calculated from Eq. (7.8) (Karkkainen and Sankar, 2006) continue to show discrepancies, compared to the simply-stacked result of Table 7.8.

The results presented in Table 7.8 can be verified against experimental results available from the work of Abot *et al.* (2004), which investigated the elastic material properties of the 5-HS weave, using specimens fabricated from 4-ply laminates. It is worth noting that the 4-ply laminates in the work of Abot *et al.* (2004) were fabricated using the semi-symmetric laminate configuration. The 5-HS material used in the experimental work was the AGP-5H/3501-6 from Hexcel, 5-HS with AS4 carbon-fibre and 3501-6 epoxy matrix; equivalent to the ones used in the current FEM modelling.

The experimental results from Abot *et al.* (2004) were based upon a fibre volume fraction, V_f = 65% and is presented in the first row of Table 7.9. Meanwhile the results from the FEM modelling under the semi-symmetric and simply-stacked laminate configuration are presented in the second and third rows of Table 7.9, respectively. Note that the elastic material properties for these two cases were calculated from the inverse of their respective laminate stiffness matrices, which are presented in Table 7.8, using the following equations:

$$E_x = \frac{1}{a_{11}H} \ , \ E_y = \frac{1}{a_{22}H} \ , \ \nu_{xy} = -\frac{a_{12}}{a_{11}} \ , \ G_{xy} = \frac{1}{a_{66}H} \tag{7.9}$$

where the a_{ij} is the element of the extensional (**a**) compliance matrix obtained through the inverse of the whole 6 x 6 ABD stiffness matrix, and H is the total thickness of the laminate i.e. $H = nt$. With the exception the shear modulus, G_{xy}, for which the values are found to be slightly underestimated, the in-plane modulus, E_x and E_y and also the Poisson's ratio, ν_{xy}, are found to be in good agreement with the experimental results (Abot *et al.*,

2004) for the two laminate configurations. This demonstrates the high fidelity of the current FEM modelling for predicting the 5-HS weave laminate stiffness matrix with multiple layers.

Table 7.9 – Elastic material properties calculated from the laminate stiffness matrix of the 4-ply FEM results, from which the results are compared against the experimental results from Abot *et al.* (2004).

	E_x (GPa)	E_y (GPa)	G_{xy} (GPa)	ν_{xy}
Experiment from Abot *et al.* (2004)	77	75	6.5	0.07
FEM Semi-symmetric	76	76	4.5	0.05
FEM Simply-stacked	74	74	4.5	0.06
Karkkainen and Sankar (2006)	65	65	4.5	0.13

By contrast, the final row of Table 7.9, which presents the elastic material constant, calculated using the method by Karkkainen and Sankar (2006), shows discrepancy between the experimental results, i.e., in-plane modulus E_x and E_y are underestimated and the Poisson's ratio is overestimated. This demonstrates that FEM modelling cannot accurately predict the laminate stiffness matrix of a multiple layer laminate from a single layer properties, as has been suggested in the work of Karkkainen and Sankar (2006).

7.2 Experimental investigation of the thermal warping of 5-HS laminates.

This section presents the experimental work on the measurement of thermal warping of 5-HS weave laminates, under the two lamination configuration schemes, i.e. simply-stacked and semi-symmetric.

Two laminates with the dimension of 330 × 330 mm are fabricated with 2, 4, 6 and 8 plies and for each ply number grouping, are manufactured using the simply-stacked laminate configuration and the other using the semi-symmetric configuration. The 5-HS material used in this work is a proprietary carbon/epoxy prepreg material supplied by AIRBUS. The plates were manufactured under the temperature and pressure cycle shown in Fig 7.10. The thermal warping distortions in each plate, arising from the high temperature curing process, are captured by scanning the plates in a Roland 3D laser scanning machine as illustrated in Fig 7.11.

However due to limitations of the machine, the scan area was limited to a 254mm × 330mm aperture, with scanning resolution set to 2mm spacing. It is worth noting that prior to scanning, the plates were heated in an oven at 100 °C for 45 minutes, to remove the influence of any moisture ingress, which is known to significantly affect the plate curvatures. To avoid any reflection of the laser light during scanning, due to the glossy surface of the composite plate, the plate surface was sprayed with a white powder developer, a material commonly used for dye penetrant testing process. The scanned image of the plate was exported as a point cloud, i.e., in the form of –x, –y and –z coordinates, which is then post-processed in MATLAB (2014).

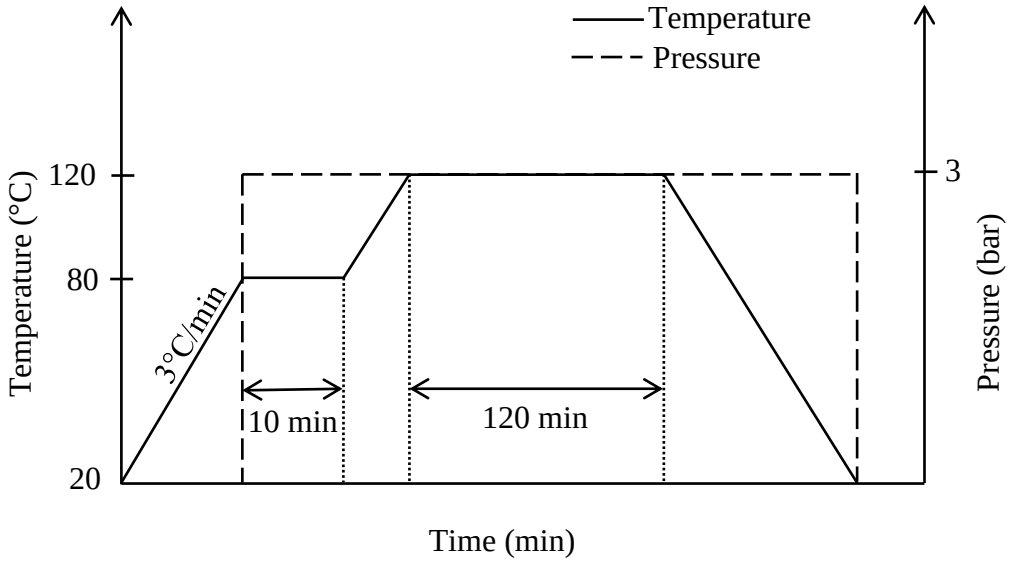

Figure 7.10 – Temperature and pressure cycle used for the manufacturing of the plates.

Figure 7.11 – Scanning of the plates surface curvature using Roland 3D laser scanning machine.

A surface function for the plate is derived using a second order geometry polynomial function:

$$f(x,y) = a + bx + cy + dx^2 + exy + fy^2 \tag{7.10}$$

with *a*, *b*, *c*, *d*, *e* and *f* being the unknown coefficients. The second order surface interpolation is generally not suitable for approximating cylindrical and spherical shapes. However the curve fitting function within MATLAB for obtaining the best fit shape to the scanned plate images, see Figs 7.12 to 7.15, since the majority of the laminates were paraboloid in shape and therefore readily represented by the second order surface function; the cylindrical nature of the plates were generally off-axis with respect to the principal material direction, which is aligned with the scanning direction.

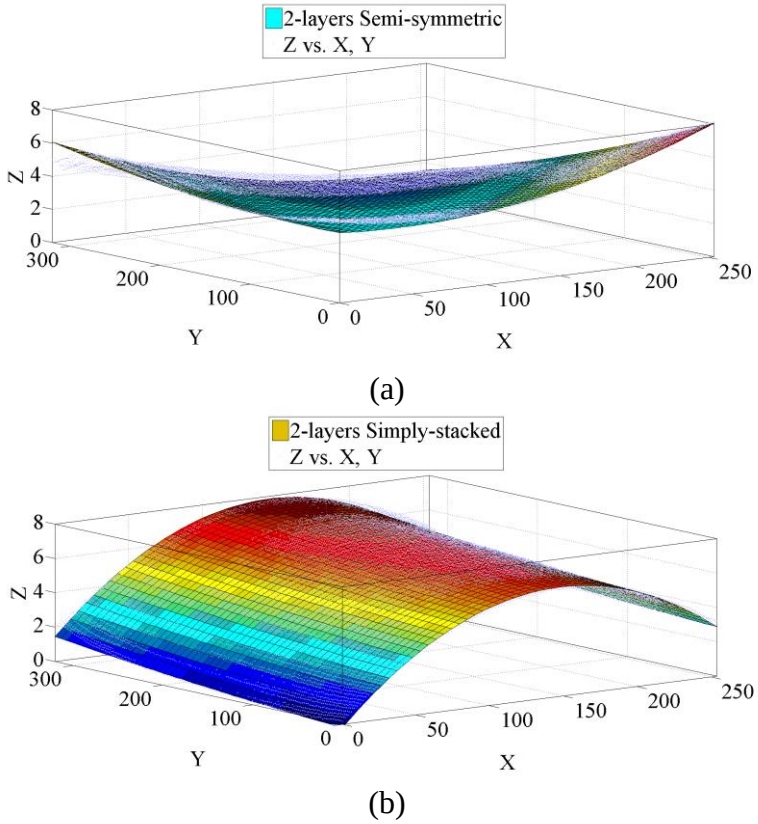

Figure 7.12 - Surface fitting of the scanned plate, performed in MATLAB for the: (a) 2-layer semi-symmetric; (b) 2-layer simply stacked.

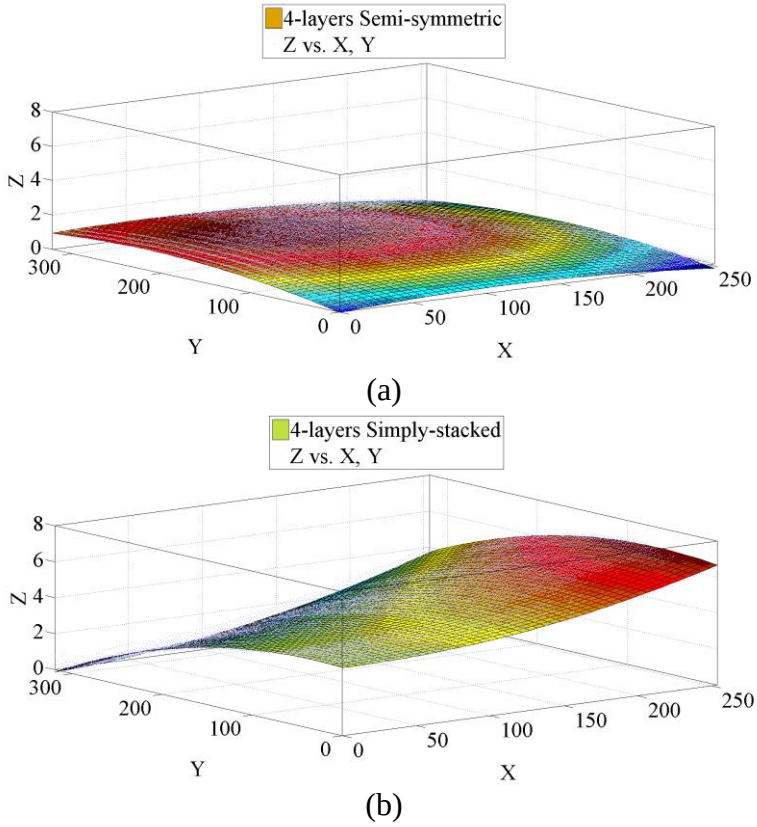

Figure 7.13 – Surface fitting of the scanned plate, performed in MATLAB for the: (a) 4-layer semi-symmetric; (b) 4-layer simply stacked.

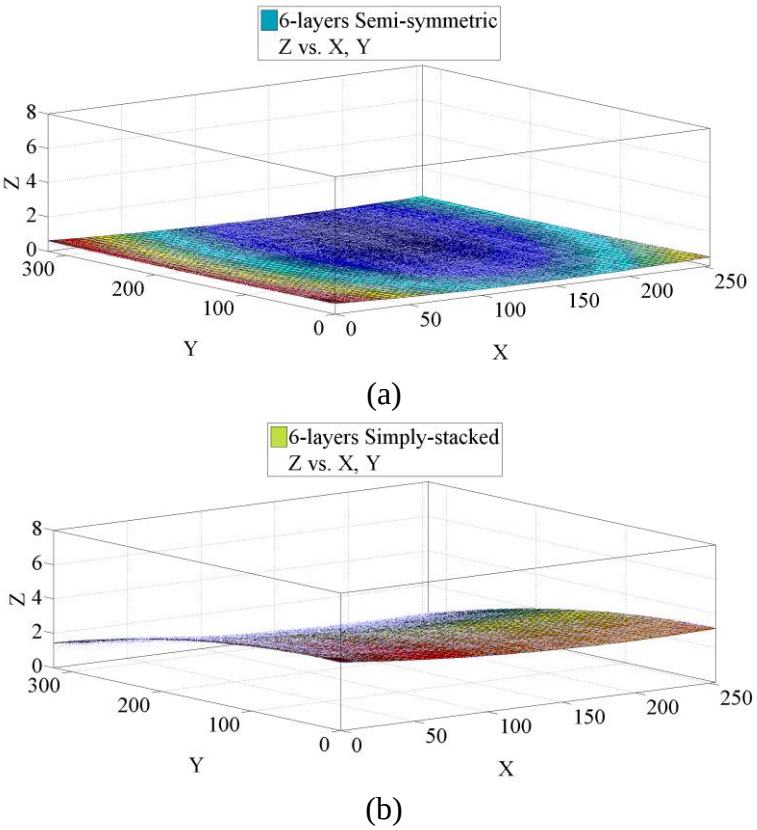

Figure 7.14 - Surface fitting of the scanned plate, performed in MATLAB for the: (a) 6-layer semi-symmetric; (b) 6-layer simply stacked.

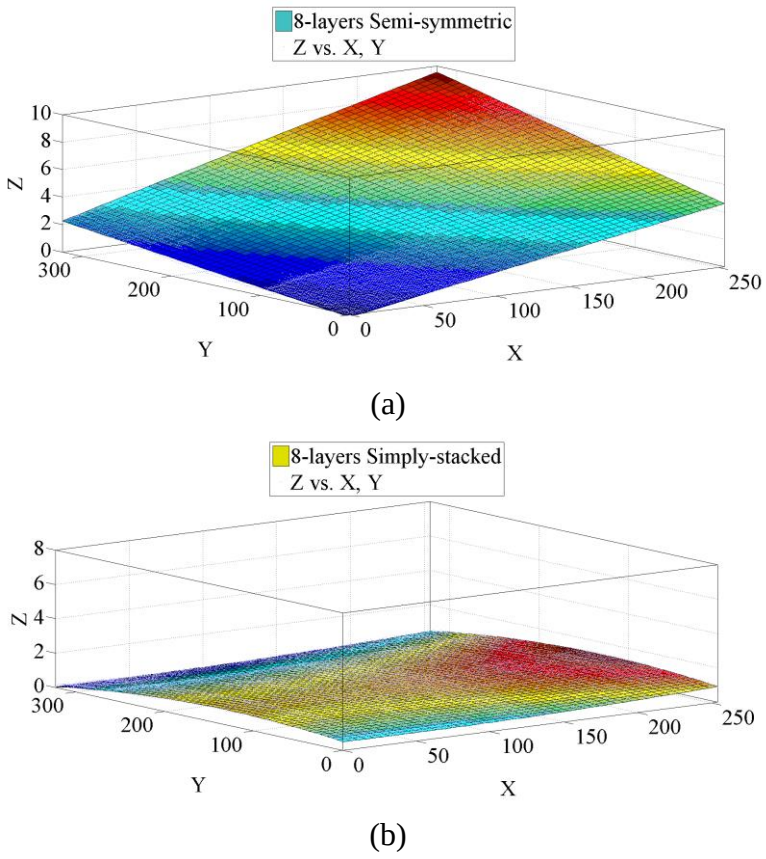

Figure 7.15 – Surface fitting of the scanned plate, performed in MATLAB for the: (a) 8-layer semi-symmetric; (b) 8-layer simply stacked.

The local curvatures for a given function with many variables can be obtained using the Hessian matrix, i.e., a square matrix consisting of the second-order partial derivatives of the function:

$$H(f)=\begin{bmatrix} \partial^2 f/\partial x_1^2 & \partial^2 f/\partial x_1\partial x_2 & \cdots & \partial^2 f/\partial x_1\partial x_n \\ \partial^2 f/\partial x_2\partial x_1 & \partial^2 f/\partial x_2^2 & \cdots & \partial^2 f/\partial x_2\partial x_n \\ \vdots & \vdots & \ddots & \vdots \\ \partial^2 f/\partial x_n\partial x_1 & \partial^2 f/\partial x_n\partial x_2 & \cdots & \partial^2 f/\partial x_n^2 \end{bmatrix} \tag{7.11}$$

Therefore the polynomial function of Eq. (7.10), which consist of two derivatives leads to the following reduced form of the Hessian matrix:

$$Hf(x,y) \equiv \begin{bmatrix} \dfrac{\partial^2 f}{\partial x^2} & \dfrac{\partial^2 f}{\partial x \partial y} \\ \dfrac{\partial^2 f}{\partial y \partial x} & \dfrac{\partial^2 f}{\partial y^2} \end{bmatrix} \tag{7.12}$$

Differentiating the function given in Eq. (7.10) with respect to the form given in Eq. (7.12) gives the following result:

$$Hf(x,y) \equiv \begin{bmatrix} 2d & e \\ e & 2f \end{bmatrix} \tag{7.13}$$

Through the Hessian matrix of Eq. (7.13), the principal curvatures can be obtained by solving the eigenvalues, express in the form of a diagonal matrix for the two principal curvatures:

$$H = \begin{bmatrix} \kappa_1 & 0 \\ 0 & \kappa_2 \end{bmatrix} \tag{7.14}$$

The curvatures from the scanned plates are shown in Table 7.10 and Table 7.11 for the case of simply-stacked laminates and semi-symmetric laminates, respectively, where the principle curvatures are given in the second and third rows of the tables. The fourth row gives the Gaussian curvature, which is the product of the two principle curvatures $(\kappa_x \times \kappa_y = \kappa_G)$. A negative Gaussian curvature, $0 < \kappa_G$ value suggest that the laminates possess a saddle shape curvature, which is observed to be the case for most of the laminates except for the 4- and 6-ply number groupings with semi-symmetric constructions, which have a positive value, indicating a dome shape curvature.

Table 7.10 – Curvature properties for the 2-, 4-, 6- and 8-ply number grouping, for laminates made under the simply- stacked lamination method.

Curvature properties	Number of plies			
	2	4	6	8
$\kappa_1\,(\mathrm{mm}^{-1})$	-6.07×10^{-4}	-9.79×10^{-5}	-5.18×10^{-5}	-4.53×10^{-5}
$\kappa_2\,(\mathrm{mm}^{-1})$	1.15×10^{-5}	9.63×10^{-5}	5.00×10^{-5}	1.85×10^{-5}
$\kappa_G\,(\mathrm{mm}^{-2})$	-7.00×10^{-9}	-9.44×10^{-9}	-2.59×10^{-9}	-8.38×10^{-10}

Table 7.11 – Curvature properties for the 2-, 4-, 6- and 8-ply number grouping, for laminates made under the semi-symmetric lamination method.

Curvature properties	Number of plies			
	2	4	6	8
$\kappa_1\,(\mathrm{mm}^{-1})$	2.28×10^{-4}	-6.17×10^{-5}	2.89×10^{-5}	-3.37×10^{-6}
$\kappa_2\,(\mathrm{mm}^{-1})$	-1.85×10^{-5}	-4.36×10^{-5}	5.22×10^{-6}	2.97×10^{-6}
$\kappa_G\ (\mathrm{mm}^{-2})$	-3.60×10^{-9}	2.69×10^{-9}	1.51×10^{-10}	-1.00×10^{-11}

From the principle curvatures under the semi-symmetric results in Table 7.11, the effectiveness of this lamination configuration for mitigating the thermal warping distortion can be measured by calculating the deviation from flatness of the laminates, which is the summation of the squared value of both principle curvatures $(\kappa_1^2+\kappa_2^2)$. Figure 7.16 illustrates the non-dimensionalised, deviation from flatness plotted against the laminate thickness for the different ply number groupings. By observation the 4-, 6- and 8-ply number groupings are relatively flat i.e. appearing as warp-free, which is in agreement to the earlier predictions made from the laminate stiffness matrices derived through FEM modelling.

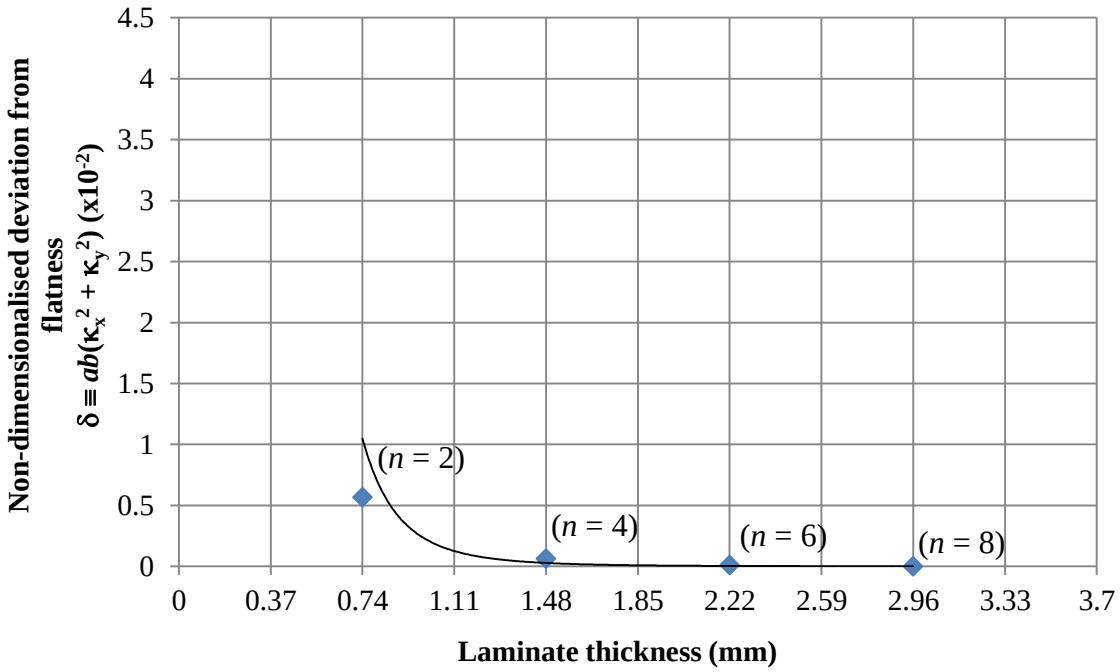

Figure 7.16 – Experimental results on the deviation from flatness for the 2-, 4-, 6- and 8-ply 5-harness satin laminates, for the semi-symmetric laminate condition.

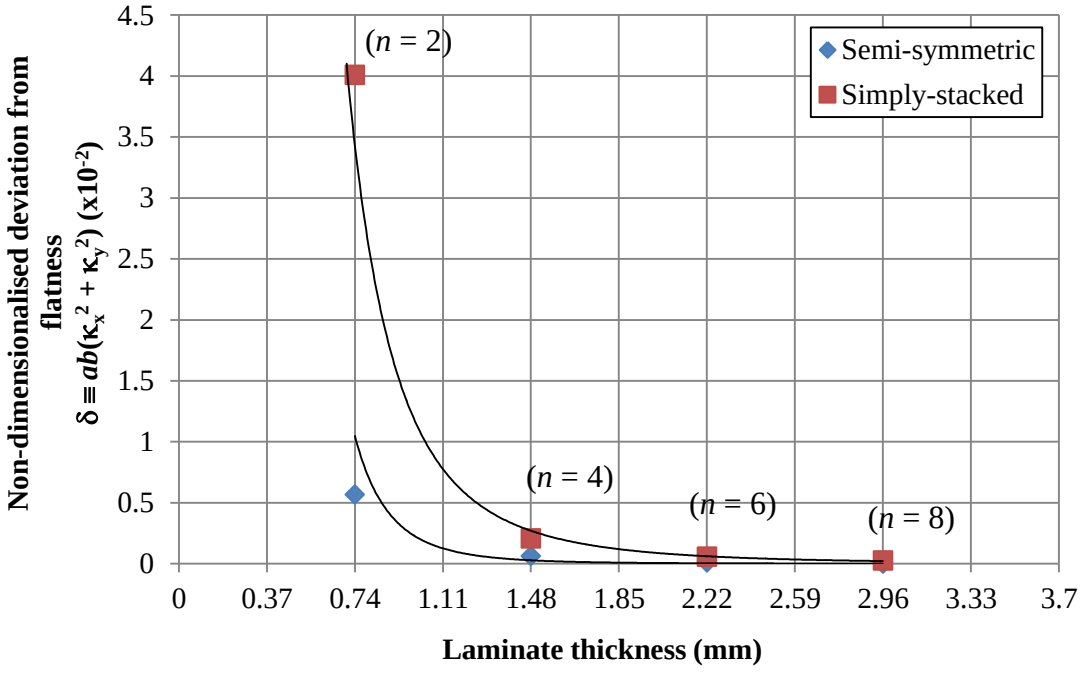

Figure 7.17 – Experimental results on the deviation from flatness for the 2-, 4-, 6- and 8-ply 5-harness satin laminates, for the simply-stacked laminate condition.

Nevertheless comparing the results for the deviation from flatness against the simply-stacked laminate configuration, see Fig. 7.17, it is evident that the 2-ply number grouping of the semi-symmetric laminate remains fairly effective in mitigating the thermal warping distortion. However very little difference is shown between the two results under the 4-ply number groupings. Above 4 plies the thermal warping due to the coupling for the simply-stacked laminate architecture converge rapidly towards warp-free behaviour, with the 6- and 8-ply laminates seemingly indistinguishable from fully uncoupled behaviour for semi-symmetric laminates. This suggests that for yet higher ply number groupings, the requirement for flipping of adjacent layers can be relaxed, allowing more flexibility for laminate tailoring. However, the effect of even small curvatures can be magnified in larger plates, hence it is important to assess the coupling behaviour within the laminate correctly, to avoid unquantified internal stresses that may ultimately lead to detrimental effects such as delamination or cracking.

The principal curvatures can be calculated from the laminate stiffness matrix obtained from FEM modelling of the woven cloth architecture, and subsequently used to measure the deviation from flatness for comparison with the experimental results in Fig. 7.17. This is accomplished from the inverse of the ABD stiffness matrix, as shown in Eq. (7.15). The thermal forces and moment vectors in Eq. (7.15) can be obtained through a similar FEM modelling procedure used for characterising the laminate stiffness matrix of the 5-HS weave by performing six individual analyses; one for each element of the respective thermal force and moment vector.

$$\begin{Bmatrix} \varepsilon_x \\ \varepsilon_y \\ \gamma_{xy} \\ \kappa_x \\ \kappa_y \\ \kappa_{xy} \end{Bmatrix} = \begin{bmatrix} a_{11} & a_{12} & a_{16} & b_{11} & b_{12} & b_{16} \\ a_{12} & a_{22} & a_{26} & b_{12} & b_{22} & b_{26} \\ a_{16} & a_{26} & a_{66} & b_{16} & b_{26} & b_{66} \\ b_{11} & b_{12} & b_{16} & d_{11} & d_{12} & d_{16} \\ b_{12} & b_{22} & b_{26} & d_{12} & d_{22} & d_{26} \\ b_{16} & b_{26} & b_{66} & d_{16} & d_{26} & d_{66} \end{bmatrix} \begin{Bmatrix} N_x^{th} \\ N_y^{th} \\ N_{xy}^{th} \\ M_x^{th} \\ M_y^{th} \\ M_{xy}^{th} \end{Bmatrix} \tag{7.15}$$

where:

$$N_x^{th}, N_y^{th}, N_{xy}^{th} = \left[\frac{1}{ab} \sum_{k=1}^{N} (\sigma_{11} V^e \alpha_{11} + \sigma_{22} V^e \alpha_{22} + \sigma_{12} V^e \alpha_{12}) \right] \Delta T$$
$$M_x^{th}, M_y^{th}, M_{xy}^{th} = \left[\frac{1}{ab} \sum_{k=1}^{N} (\sigma_{11} V^e \alpha_{11} + \sigma_{22} V^e \alpha_{22} + \sigma_{12} V^e \alpha_{12}) z \right] \Delta T \quad (7.16)$$

The description of the variables in Eq. (7.16) is similar to the ones presented from the previous section dealing with mechanical strains, but now with the addition of the coefficients of thermal expansion α_{11}, α_{22} and α_{12}, for the lamina; where the values are given in Table 7.4 and Table 7.5. The temperature difference, ΔT, during the curing, see Fig. 7.10, is, in this case, $\Delta T = -100^{o}$C.

Figure 7.18 illustrates the results on the deviation from flatness for the simply-stacked laminates the FEM model, for different ply number groupings. A good agreement is shown between the FEM predictions for the 4-, 6- and 8-ply number groupings compared with the experimental results. However for 2 ply laminates number groupings an 8% difference between the experimental results and numerical simulation is observed. This may be attributed to two reasons: (a) the carbon-fibre 5-HS material used in the experiment could possibly originate from a higher modulus family or; (b) the effect of phase shift between the layers within the laminate, which was assumed to be ideally stacked in the FE model, as shown in Fig. 7.9. During manufacturing, random phase often arises between the layers; it has been suggested that this may contribute to a higher elastic modulus value (Naik and Shembekar, 1992b). Figure 7.19 presents the results for the simply-stacked laminates calculated from the method of Karkkainen and Sankar (2006). It is clear that the result do not show good agreement with either the experimental or FEM results, since the curves show an average of 91% different for the deviation from flatness, especially at lower ply number groupings.

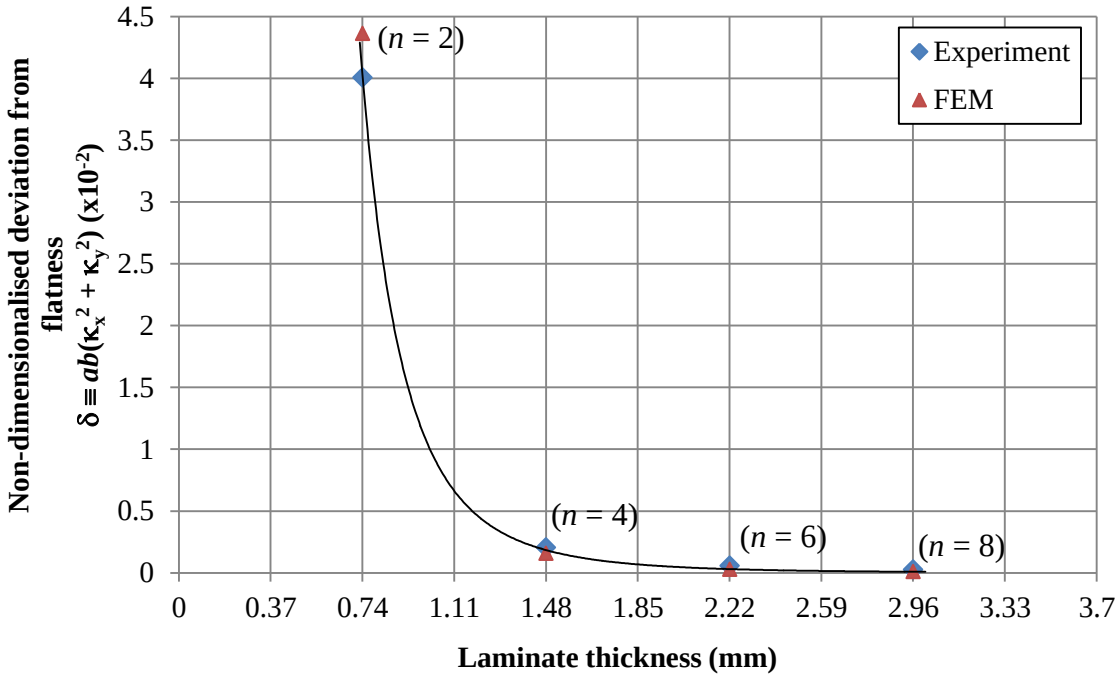

Figure 7.18 – Comparison of the results for the deviation from flatness obtained using the laminate stiffness properties from the FEM modelling against the experimental results, for the case of simply-stacked laminate configuration.

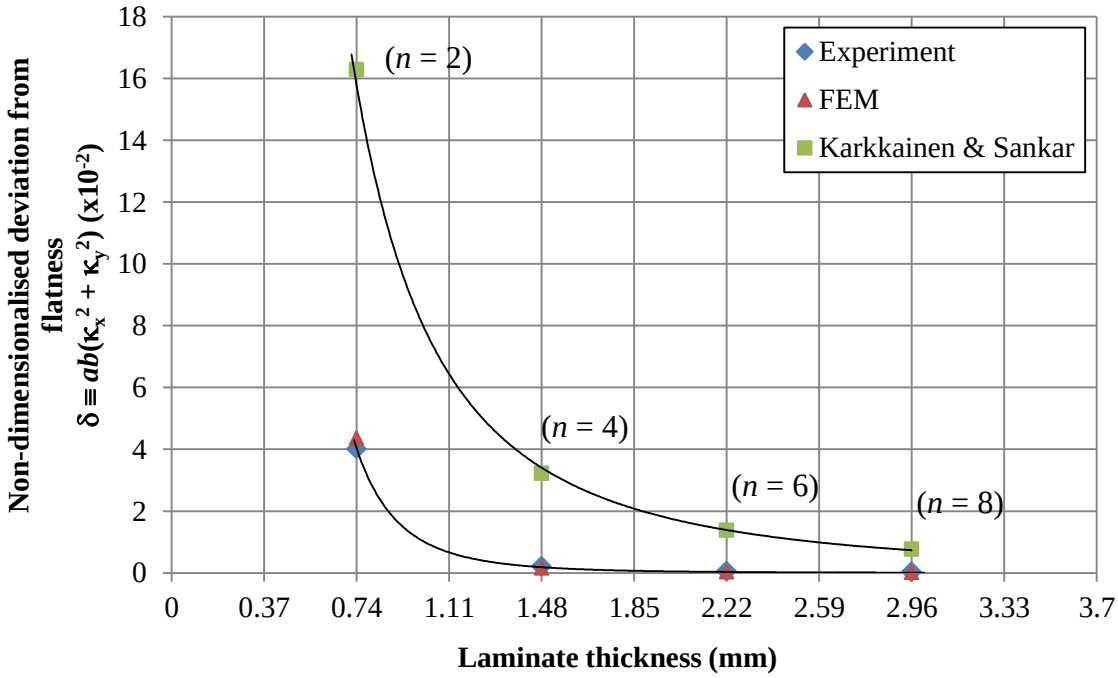

Figure 7.19 – Results showing the deviation from flatness for the simply-stacked laminates obtained from the laminate stiffness matrix derived using the properties a single layer of the 5-HS (Karkkainen and Sankar, 2006), showing discrepancy against the other two results.

7.3 Laminate design strategy for 5-HS weave

The semi-symmetric laminate configurations suggested by Ishikawa (1981) has been shown to be efficient for combating the thermal instability that exists within the 5-HS weave material. However for the carbon-fibre material investigated, experimental observations of the 2-ply semi-symmetric laminate suggest that it is not completely warp-free. However warp free conditions were observed in the semi-symmetric configuration for the 4-ply number groupings and above. Similarly, for the 4-ply number groupings the diminishing effect of Extension-Bending coupling for the simply-stacked laminate configurations was observed.

It is reasonable to suggest that if a cross-ply $[0/90]_T$ laminate is the unidirectional counterpart of a single layer of the 5-HS weave, then following a 45º off-axis orientation gives rise to an angle-ply $[45/-45]_T$ laminate, the coupled laminate solutions for which were presented in Chapter 4. Since those solutions were derived using standard angle orientations, the stacking sequences can be applied to laminate design with 5-HS weave wherever the layers within the stacking sequence are combinations of cross-ply and/or angle-ply semi-symmetric pairs. For example, the 8-ply laminate stacking sequences of Table 5.3, can be written in alternative form given as:

$$[(-/+)/(+/-)/(\bigcirc/\bullet)/(\bullet/\bigcirc)]_T \text{ and } [(-/+)/(+/-)/(\bullet/\bigcirc)/(\bigcirc/\bullet)]_T \qquad (7.17)$$

where the pairing of angle- and cross-ply layers are shown in brackets represent each layer of the 5-HS weave. In this example the laminate is composed of two different sub-laminates about the laminate mid-plane i.e. angle-ply and cross-ply sublaminates. These sub-laminates are also semi-symmetric i.e. contiguous layers of the 5-HS are flipped. By contrast other stacking sequences from Table 5.3, e.g.:

$$[(-/+)/(\bigcirc/\bullet)/(+/-)/(\bullet/\bigcirc)]_T \text{ and } [(-/+)/(\bullet/\bigcirc)/(+/-)/(\bigcirc/\bullet)]_T \quad (7.18)$$

possesses angle- and cross-ply pairs, but not semi-symmetric configurations. Note that the proposed strategy for deriving stacking sequence solutions for the 5-HS laminates with mechanical Extension-Twisting coupling behaviour from (an off-axis orientation of $\pi/8$ from the $\mathbf{A_S B_S D_S}$ parent laminate) unidirectional laminate solutions are also classified as HTCS; since the influence of the unbalanced crimp line angle in 5-HS laminate has been shown to be insignificant.

Applying this design strategy for higher ply number groupings, and limiting the scope of search to the HTCS $\mathbf{A_S B}_t\mathbf{D_S}$ solutions for 8, 12, 16 and 20 ply number groupings presented in Chapter 5, reveals that no solutions exist for the 12 and 20 ply number groupings. There are solutions for the 16-ply number groupings, which are equivalent to a repeating 8-ply 5-HS weave laminate, with the solutions presented in Table 7.12, where 4 solutions in Table 7.12 represent semi-symmetric configuration i.e. showing similar characteristics to those discussed for the laminates of Eq. (7.17), and 32 solutions are compatible with simply-stacked configuration.

Table 7.12 – 8-ply HTCS laminate solutions for 5-HS weave with $A_S B_t D_S$ coupling. Symbols in brackets represent paired single- and cross-ply sequences of the unidirectional material counterpart, which correspond to individual layers of 5-HS weave.

Semi-symmetric laminate configuration
(–/+)/(+/–)/(●/○)/(○/●)/(–/+)/(+/–)/(●/○)/(○/●)
(–/+)/(+/–)/(–/+)/(+/–)/(●/○)/(○/●)/(●/○)/(○/●)
(–/+)/(+/–)/(○/●)/(●/○)/(–/+)/(+/–)/(○/●)/(●/○)
(–/+)/(+/–)/(–/+)/ (+/–)/(○/●)/(●/○)/(○/●)/(●/○)
Simply-stacked laminate configuration
(–/+)/(+/–)/(–/+)/(○/●)/(+/–)/(●/○)/(○/●)/(●/○)
(–/+)/(+/–)/(●/○)/(+/–)/(○/●)/(–/+)/(○/●)/(●/○)
(–/+)/(○/●)/(+/–)/(–/+)/(●/○)/(○/●)/(+/–)/(●/○)
(–/+)/(○/●)/(+/–)/(●/○)/(–/+)/(○/●)/(+/–)/(●/○)
(–/+)/(○/●)/(○/●)/(●/○)/(–/+)/(+/–)/(+/–)/(●/○)
(–/+)/(○/●)/(–/+)/(+/–)/(○/●)/(●/○)/(+/–)/(●/○)
(–/+)/(○/●)/(–/+)/(○/●)/(+/–)/(●/○)/(+/–)/(●/○)
(–/+)/(○/●)/(●/○)/(○/●)/(+/–)/(–/+)/(+/–)/(●/○)
(–/+)/(–/+)/(+/–)/(+/–)/(○/●)/(○/●)/(●/○)/(●/○)
(–/+)/(–/+)/(+/–)/(○/●)/(+/–)/(○/●)/(●/○)/(●/○)
(–/+)/(–/+)/(○/●)/(+/–)/(○/●)/(+/–)/(●/○)/(●/○)
(–/+)/(–/+)/(○/●)/(○/●)/(+/–)/(+/–)/(●/○)/(●/○)
(–/+)/(●/○)/(+/–)/(+/–)/(○/●)/(○/●)/(–/+)/(●/○)
(–/+)/(●/○)/(○/●)/(○/●)/(+/–)/(+/–)/(–/+)/(●/○)
(–/+)/(–/+)/(●/○)/(●/○)/(+/–)/(+/–)/(○/●)/(○/●)
(–/+)/(–/+)/(●/○)/(+/–)/(●/○)/(+/–)/(○/●)/(○/●)
(–/+)/(–/+)/(+/–)/(●/○)/(+/–)/(●/○)/(○/●)/(○/●)
(–/+)/(–/+)/(+/–)/(+/–)/(●/○)/(●/○)/(○/●)/(○/●)
(–/+)/(●/○)/(–/+)/(●/○)/(+/–)/(○/●)/(+/–)/(○/●)
(–/+)/(●/○)/(–/+)/(+/–)/(●/○)/(○/●)/(+/–)/(○/●)
(–/+)/(●/○)/(●/○)/(○/●)/(–/+)/(+/–)/(+/–)/(○/●)
(–/+)/(●/○)/(+/–)/(–/+)/(○/●)/(●/○)/(+/–)/(○/●)
(–/+)/(●/○)/(+/–)/(○/●)/(–/+)/(●/○)/(+/–)/(○/●)
(–/+)/(●/○)/(○/●)/(●/○)/(+/–)/(–/+)/(+/–)/(○/●)
(–/+)/(+/–)/(–/+)/(●/○)/(+/–)/(○/●)/(●/○)/(○/●)
(–/+)/(+/–)/(+/–)/(●/○)/(–/+)/(○/●)/(○/●)/(●/○)
(–/+)/(+/–)/(●/○)/(–/+)/(○/●)/(+/–)/(●/○)/(○/●)
(–/+)/(+/–)/(○/●)/(–/+)/(●/○)/(+/–)/(○/●)/(●/○)
(–/+)/(+/–)/(+/–)/(○/●)/(–/+)/(●/○)/(●/○)/(○/●)
(–/+)/(+/–)/(○/●)/(+/–)/(●/○)/(–/+)/(●/○)/(○/●)
(–/+)/(○/●)/(●/○)/(●/○)/(+/–)/(+/–)/(–/+)/(○/●)
(–/+)/(○/●)/(+/–)/(+/–)/(●/○)/(●/○)/(–/+)/(○/●)

7.4 Conclusion

A finite element modelling method for deriving the laminate stiffness matrix of the 5-HS weave laminates has been presented. The approach is based upon the method proposed by Karkkainen and Sankar (2006), but extended to overcome the simplification made for multiple layer laminates; whereby the stiffness properties of a single layer of 5-HS material, leading to errors in overall laminate stiffness properties. By contrast, the extended FEM modelling includes multiple layers of 5-HS weave in the repeating unit cell (RUC) geometry definition, where the results from the laminate stiffness matrix predictions have been shown to produce good agreement against the experimental results from Abot *et al.* (2004) i.e. predicting the elastic material properties of the 5-HS material.

In addition good agreement was also observed for predicting the deviation from flatness for laminates with different ply number groupings. This demonstrates the higher fidelity of the extended FEM method to predict the laminate stiffness matrix with multiple layers of 5-HS weave laminates, compared to the previous method of using a single layer to predict the laminate stiffness matrix of multiple layer 5-HS laminates.

Two lamination methods for the 5-HS weave laminates were investigated i.e. the semi-symmetric and simply-stacked laminate configurations. For 2-ply laminates, the semi-symmetric configuration by Ishikawa (1981) was found to be effective for eliminating the thermal instability that exists within a single layer of 5-HS weave material; this was not found in the simply-stacked lamination method. However very little difference is shown between the two configurations under the 4-ply number groupings, and above 4 plies the thermal warping due to the coupling for the simply-stacked laminate architecture converge rapidly towards warp-free behaviour, with the 6- and 8-ply laminates seemingly indistinguishable from fully uncoupled behaviour for semi-symmetric laminates. The influence of the unbalanced crimp line angle in 5-HS laminate has been shown to be

insignificant, to the extent where the effect can be considered negligible with increasing number of plies.

A design strategy for achieving mechanically coupled HTCS laminates with 5-HS material has been demonstrated. This adopted standard angle stacking sequence solutions for unidirectional material counterpart containing contiguous angle-ply and/or cross-ply pairs laminates, which represent single layers of 5-HS weave. This design strategy demonstrated solutions within 8- and 16-ply number groupings, which are equivalent to the 4- and 8-ply laminates for 5-HS weave.

CHAPTER 8

Conclusions and Future work

The unique coupling interactions between in-plane and out-of-plane that can exist in composite laminates have been discussed in this thesis. The relatively unexplored potential of composite laminates, beyond the weight saving merit for which they have been long associated, can only be exploited if the current design constraint of balanced and symmetric rule is relaxed.

Thermal warping distortions, commonly associated with non-symmetric laminates is believed to be the contributing reason for the reluctance of many laminate designers to move away from balanced and symmetric laminate designs. Mechanically coupled laminates possessing hygro-thermally curvature-stable (HTCS), or warp-free properties are shown to be an attractive way to employ coupled laminate designs, without resulting in undesirable thermal warping distortions, which result from high temperature curing during manufacturing. However the number of classes from which these HTCS coupled laminates exist, are limited to only 9 from the 24 distinct classes of mechanically coupled laminates.

One particular class from the HTCS coupled laminate groups, which has gained increasing interest over the recent past, is the Extension-Twisting coupled laminates. Laminate solutions within this particular coupled family have been presented, where the solutions are derived using standard angle orientations. The ply number groupings were found to be limited to 8-, 12-, 16- and 20-ply for thin ply laminates. Extension-Twisting coupling performance for these ply number groupings has been assessed and compared against laminate solutions reported in the literature, which have been optimised for optimum twisting. The laminates have been assessed up to their maximum failure load, and results for the 8-ply number groupings show only a 5% difference in terms of the twisting performance of the laminate with respect to the highest twist from the optimised solution with free form ply angle. This shows a comparatively equal performance can be achieved using standard angle orientations, without having to compromise on the risks of having to employ free form angle laminates, which result from optimisation process. In contrast to the laminates manufactured from standard angle orientations, free form angle laminates are difficult in manufacturing due to the unique angle of each layers and practically impossible to apply ply terminations at the same time as maintaining the coupling behaviour and HTCS condition within the laminate.

The laminate with optimised twisting was also shown to represent the lower-bound buckling curve compared to the buckling curve results for standard angle laminate solutions. The buckling curves for the entire spectrum of Extension-Twisting coupled laminate solutions from standard angle orientations has been presented, for the 8-, 12-, 16- and 20-ply number groupings. This assessment of the buckling load presents an important design requirement, especially in the case of rotor blades under static load conditions. Extension-Twisting laminates with additional Extension-Shearing and/or Bending-Twisting coupling, i.e. $\mathbf{A}_S\mathbf{B}_t\mathbf{D}_F$ and $\mathbf{A}_F\mathbf{B}_t\mathbf{D}_F$ result in higher twisting magnitude, however

these laminates are shown to possess lower failure loads compared to $\mathbf{A_S B_t D_S}$ laminate with Extension-Twisting only.

The classification of mechanically coupled laminates from balanced Plain weave material has been presented. Due to the balanced nature of this material with equal fibre volume fraction in the longitudinal (0º) and transverse (90º) direction, an equal modulus ($E_1 = E_2$) assumption can be made. Adopting standard angle orientations with the equal modulus properties, reveals that seven classes of the coupled laminate can be attainable from balanced Plain weave. All seven classes were obtained through applying off-axis orientations to the parent class of $\mathbf{A_S B_S D_S}$ laminate. Fully uncoupled $\mathbf{A_S B_0 D_S}$ laminates have also been obtained, from which fully isotropic, extensionally isotropic and quasi-homogenous laminates have also been identified.

The benefit of employing Plain weave material has been highlighted, since a single layer of this material naturally inherits the HTCS property. Therefore laminates made from Plain weave material will continue to be warp-free, regardless of the stacking sequence and the number of plies within the laminate. This gives the opportunity to perform ply termination strategy with a much wider scope. By contrast to the unidirectional counterpart, where ply termination are only permissible with 4-ply terminations in order to maintain the HTCS condition within the laminate, the balanced plain weave design have fewer restrictions in terms of the number of terminated plies. Single ply terminations are possible in the uncoupled laminate class, across all ply number groupings. In the case of Extension-Twisting (and Shearing-Bending) coupled laminates, the tapering strategy exist only for the even ply number groupings, down to 2 plies. This is also observed for laminates with additional Bending-Twisting coupling i.e. $\mathbf{A_S B_t D_F}$. However for the $\mathbf{A_F B_t D_F}$ laminate with additional Extension-Shearing and Bending-Twisting coupling, a single ply termination can be achieved, down to 2 plies.

The benefit of the thermal stability that exists in the Plain weave material however is not present in 5-HS weave material, where a single layer of this material will generally warp due to the asymmetrical nature of its woven architecture. The assessment made on the laminate stiffness matrix for a single layer of 5-HS, which is performed using micro-mechanical modelling in ABAQUS, have shown that Extension-Bending coupling exist i.e. equivalent to an $\mathbf{A}_S\mathbf{B}_I\mathbf{D}_S$ laminate, mimicking a unidirectional cross-symmetric cross-ply laminate counterpart. Under a similar FEM modelling technique, an assessment of the laminate stiffness matrix for different ply number groupings was performed, for even ply number groupings, where two cases of lamination strategy was investigated for each of the ply number group involving a semi-symmetric technique where adjacent layers in the laminate were flipped and a simply-stacked technique, without manipulation of the layers.

The semi-symmetric configuration gives rise to Extension-Twisting (and Shearing-Bending) coupling, however the coupling was virtually zero, since the coupling arises from the influence of the unbalanced crimp line angle within the semi-symmetric laminate of the 5-HS weave. The coupling quickly dissipates for increasing ply number groupings, and good agreement is seen between the elastic material property predictions for the 5-HS and experimental results from the literature, demonstrating the fidelity of the extended FEM modelling used. This also highlight the lack of fidelity of using predictions of the laminate stiffness matrix on single layer properties of the 5-HS satin, as has been done previously in the literature, for which there is poor agreement with experimental results.

A strategy for acquiring the coupled laminate solutions for the 5-HS weave material has been presented, from which the proposed approach utilised the solutions obtained for the HTCS coupled laminate designs of the unidirectional material counterpart; where the solutions corresponded to stacking sequence designs with combinations of contiguous cross-ply (0/90) and/or angle-ply (45/−45) pairs within the laminate design. The HTCS

solutions from the unidirectional counterpart have a minimum ply number grouping of 8, which is equivalent to a 4-ply laminate with 5-HS weave material. The experimental results measuring the deviation from flatness for the 2-, 4-, 6-, and 8-ply number groupings for the 5-HS laminates, demonstrate that for the 4-ply laminate and above, very little difference was observed in terms of the results from the semi-symmetric and simply-stacked laminate configurations, both of which were flat. Solutions were found for both lamination techniques with 4-ply 5-HS (or 8-ply equivalent unidirectional counterpart).

The findings presented in this research work will benefit specialised laminate designers, who require solutions for composite laminates possessing special coupling attributes; free from warping distortions that arise as a resut of a standard high temperature curing system. Laminate designs have been presented for both material system i.e. unidirectional and woven cloth material, i.e., balanced plain weave and 5-HS weave. Solutions for both material systems have been developed using standard angle orientations; the benefits of which have been highlighted in the work. Balanced Plain weave material has been shown to be more versatile in terms of manipulation of the coupled properties, especially when ply terminations and thermal stability are a requirement. Coupled laminates from 5-HS weave material are more attractive if in-plane loading is the dominant design requirement, due to the straighter load-carrying fibres present in the 5-HS woven architecture compared to the highly undulated fibres in balanced Plain weave material.

8.1 Recommendation for future work

The majority of results presented in this thesis have been performed through a theoretical framework, in particular with the developments of the mechanically coupled laminates from woven cloth material. As an extension to this current research work, the author recommends future works focusing more towards establishing an experimental base for validating the results presented in this thesis.

The Extension-Twisting coupled laminate solutions from balanced Plain weave material alone are worthy of further exploration. The magnitude of the mechanical coupling in balanced Plain weave laminates predicted from this research work has been shown to be as equally attractive as that found in the unidirectional material counterpart. Therefore experimental work to further investigate the twisting magnitude from balanced Plain weave laminates is strongly recommended. The focus should however be towards the adopter of spread tow technology for balance Plain weave Textreme® material by Oxeon, since the characteristics of this newly developed material are improved by reduced crimp angle in the physical architecture, closly resembling the unidirectional material counterpart.

The experimental work should also be extended to investigate Extension-Twisting coupling performance in the tapered laminate solutions. Since balanced Plain weave laminates are not susceptible to thermal warping distortions, various aspects of the laminate tapering solutions can be investigated from an experimental perspective, including the twisting magnitude of Extension-Twisting (and Shearing-Bending) coupling and the effect on the twisting magnitude of secondary coupling i.e., Bending-Twisting and/or Extension-Shearing coupling.

These suggestions for the balanced Plain weave, can be equally applied to 5-HS weave material with due consideration given to the potential thermal instability i.e., that are present in Satin weave architecture.

Appendix A

In this appendix the discussion will begin by addressing the elastic stress-strain relationship in a single orthotropic layer of composite material. The attention is then directed to another important assumption made towards the study of composite material, which is the plane stress assumption. This follows on the discussion of Kirchhoff hypothesis for flat plate, and later will lead to the derivation of the well-known ABD stiffness matrix.

9.1 Stress-strain relationship

Composite materials consist of multiple orthotropic layers, which are aligned at different angle within the laminate. Due to this, the principle material coordinate system, as shown in Fig. A1 and denoted by the 1-2-3 coordinate, within the laminate differs from each layer. Note that 1-direction in the case of unidirectional material will always dictate the direction of the fibre. The principle material coordinate system is used to calculate the stress and strain behaviour within each respective layer. However, for laminate or

structural level analysis it is convenient to adopt the structural coordinate system or the x-y-z coordinate, since loading are applied at the laminate or structural level.

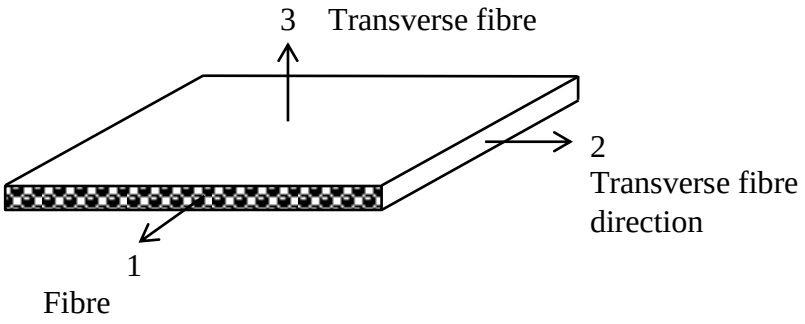

Figure A1 – Fibre-reinforced, resin-matrix composite materials. The fibres are aligned along the 1-direction, and the 2- and 3- directions are the direction transverse to the fibres.

This can then be used to calculate the stresses in each layer from using the tensor transformation relations. The two coordinate systems are also shown illustratively in Fig. A2. The constitutive stress-strain relationship for a single orthotropic layer in the principle material coordinate system can be described by:

$$\begin{Bmatrix} \varepsilon_1 \\ \varepsilon_2 \\ \varepsilon_3 \\ \gamma_{23} \\ \gamma_{13} \\ \gamma_{12} \end{Bmatrix} = \begin{bmatrix} S_{11} & S_{12} & S_{13} & 0 & 0 & 0 \\ S_{12} & S_{22} & S_{23} & 0 & 0 & 0 \\ S_{13} & S_{23} & S_{33} & 0 & 0 & 0 \\ 0 & 0 & 0 & S_{44} & 0 & 0 \\ 0 & 0 & 0 & 0 & S_{55} & 0 \\ 0 & 0 & 0 & 0 & 0 & S_{66} \end{bmatrix} \begin{Bmatrix} \sigma_1 \\ \sigma_2 \\ \sigma_3 \\ \tau_{23} \\ \tau_{13} \\ \tau_{12} \end{Bmatrix} \tag{9.1}$$

where S_{ij} is known as the compliance term, given by:

$$\begin{aligned} S_{11} &= \frac{1}{E_1} & S_{12} &= -\frac{\nu_{12}}{E_1} & S_{13} &= -\frac{\nu_{13}}{E_1} \\ S_{22} &= \frac{1}{E_2} & S_{23} &= -\frac{\nu_{23}}{E_2} & S_{33} &= \frac{1}{E_3} \\ S_{44} &= \frac{1}{G_{23}} & S_{55} &= \frac{1}{G_{13}} & S_{66} &= \frac{1}{G_{12}} \end{aligned} \tag{9.2}$$

There are 9 engineering properties or engineering constants involved in defining the compliance terms in Eq. (9.2), which are three elastic modulus E_1, E_2 and E_3, three Poisson ratio ν_{12}, ν_{13} and ν_{23}, and three shear modulus G_{12}, G_{13} and G_{23}. Meanwhile the inverse of the matrix in Eq. (9.1), will give the stiffness matrix as shown in Eq. (9.3). Equation (9.4) gives the component of the stiffness matrix in terms of the compliances.

$$\begin{Bmatrix} \sigma_1 \\ \sigma_2 \\ \sigma_3 \\ \tau_{23} \\ \tau_{13} \\ \tau_{12} \end{Bmatrix} = \begin{bmatrix} C_{11} & C_{12} & C_{13} & 0 & 0 & 0 \\ C_{12} & C_{22} & C_{23} & 0 & 0 & 0 \\ C_{13} & C_{23} & C_{33} & 0 & 0 & 0 \\ 0 & 0 & 0 & C_{44} & 0 & 0 \\ 0 & 0 & 0 & 0 & C_{55} & 0 \\ 0 & 0 & 0 & 0 & 0 & C_{66} \end{bmatrix} \begin{Bmatrix} \varepsilon_1 \\ \varepsilon_2 \\ \varepsilon_3 \\ \gamma_{23} \\ \gamma_{13} \\ \gamma_{12} \end{Bmatrix} \tag{9.3}$$

$$\begin{aligned} C_{11} &= \frac{S_{22}S_{33} - S_{23}S_{23}}{S} & C_{12} &= \frac{S_{13}S_{23} - S_{12}S_{33}}{S} & C_{13} &= \frac{S_{12}S_{23} - S_{13}S_{22}}{S} \\ C_{22} &= \frac{S_{33}S_{11} - S_{13}S_{13}}{S} & C_{23} &= \frac{S_{12}S_{13} - S_{23}S_{11}}{S} & C_{33} &= \frac{S_{11}S_{22} - S_{12}S_{12}}{S} \\ C_{44} &= \frac{1}{S_{44}} & C_{55} &= \frac{1}{S_{55}} & C_{66} &= \frac{1}{S_{66}} \end{aligned} \tag{9.4}$$

Since the compliance and the stiffness matrix relates the stress and strain in the principle material coordinate system, the transformation to the structural coordinate system or x-y-z coordinate is often required. Stress transformations from the 1-2-3 coordinate to the x-y-z coordinate system, as shown in Fig. A2, is given by Eq. (9.5).

$$\begin{aligned} \sigma_1 &= \cos^2\theta\sigma_x + \sin^2\theta\sigma_y + 2\sin\theta\cos\theta\tau_{xy} \\ \sigma_2 &= \sin^2\theta\sigma_x + \cos^2\theta\sigma_y - 2\sin\theta\cos\theta\tau_{xy} \\ \sigma_3 &= \sigma_z \\ \tau_{23} &= \cos\theta\tau_{yz} - \sin\theta\tau_{xz} \\ \tau_{13} &= \sin\theta\tau_{yz} + \cos\theta\tau_{xz} \\ \tau_{12} &= -\sin\theta\cos\theta\sigma_x + \sin\theta\cos\theta\sigma_y + (\cos^2\theta - \sin^2\theta)\tau_{xy} \end{aligned} \tag{9.5}$$

The relationship in Eq. (9.5) can be express in the form of matrix:

$$\begin{bmatrix}\sigma_1\\ \sigma_2\\ \sigma_3\\ \tau_{23}\\ \tau_{13}\\ \tau_{12}\end{bmatrix}=\begin{bmatrix}\cos^2\theta & \sin^2\theta & 0 & 0 & 0 & 2\sin\theta\cos\theta\\ \sin^2\theta & \cos^2\theta & 0 & 0 & 0 & -2\sin\theta\cos\theta\\ 0 & 0 & 1 & 0 & 0 & 0\\ 0 & 0 & 0 & \cos\theta & -\sin\theta & 0\\ 0 & 0 & 0 & \sin\theta & \cos\theta & 0\\ -\sin\theta\cos\theta & \sin\theta\cos\theta & 0 & 0 & 0 & (\cos^2\theta-\sin^2\theta)\end{bmatrix}\begin{bmatrix}\sigma_x\\ \sigma_y\\ \sigma_z\\ \tau_{yz}\\ \tau_{xz}\\ \tau_{xy}\end{bmatrix} \tag{9.6}$$

replacing $m = \cos\theta$ and $n = \sin\theta$

$$\begin{bmatrix}\sigma_1\\ \sigma_2\\ \sigma_3\\ \tau_{23}\\ \tau_{13}\\ \tau_{12}\end{bmatrix}=\begin{bmatrix}m^2 & n^2 & 0 & 0 & 0 & 2nm\\ n^2 & m^2 & 0 & 0 & 0 & -2nm\\ 0 & 0 & 1 & 0 & 0 & 0\\ 0 & 0 & 0 & m & -n & 0\\ 0 & 0 & 0 & n & m & 0\\ -nm & nm & 0 & 0 & 0 & m^2-n^2\end{bmatrix}\begin{bmatrix}\sigma_x\\ \sigma_y\\ \sigma_z\\ \tau_{yz}\\ \tau_{xz}\\ \tau_{xy}\end{bmatrix} \tag{9.7}$$

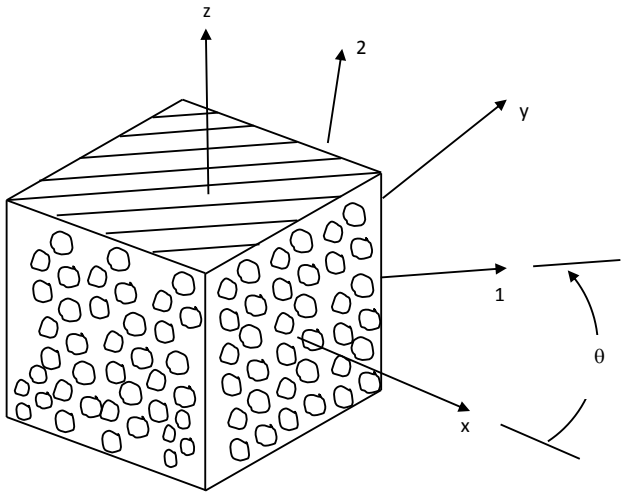

Figure A2 – Principle material coordinate system (1-2-3 coordinate) and structural coordinate system (x-y-z coordinate)

The relationship in Eq. (9.7) can be express in compact notation form, given by:

$$\{\sigma\}_{123}=[T_\sigma]\{\sigma\}_{xyz} \tag{9.8}$$

Similarly the strain transformation from 1-2-3 coordinate to the x-y-z coordinate can be done analogous to the stress transformation, which yield:

$$\begin{aligned}
\varepsilon_1 &= \cos^2\theta\varepsilon_x + \sin^2\theta\varepsilon_y + 2\sin\theta\cos\theta\frac{1}{2}\gamma_{xy} \\
\varepsilon_2 &= \sin^2\theta\varepsilon_x + \cos^2\theta\varepsilon_y - 2\sin\theta\cos\theta\frac{1}{2}\gamma_{xy} \\
\varepsilon_3 &= \varepsilon_z \\
\gamma_{23} &= \cos\theta\gamma_{yz} - \sin\theta\gamma_{xz} \\
\gamma_{13} &= \sin\theta\gamma_{yz} + \cos\theta\gamma_{xz} \\
\frac{1}{2}\gamma_{12} &= -\sin\theta\cos\theta\varepsilon_x + \sin\theta\cos\theta\varepsilon_y + (\cos^2\theta - \sin^2\theta)\frac{1}{2}\gamma_{xy}
\end{aligned} \tag{9.9}$$

and in matrix form, replacing the cosθ and sinθ with *m* and *n* respectively gives :

$$\begin{bmatrix} \varepsilon_1 \\ \varepsilon_2 \\ \varepsilon_3 \\ \gamma_{23} \\ \gamma_{13} \\ \frac{1}{2}\gamma_{12} \end{bmatrix} = \begin{bmatrix} m^2 & n^2 & 0 & 0 & 0 & 2nm \\ n^2 & m^2 & 0 & 0 & 0 & -2nm \\ 0 & 0 & 1 & 0 & 0 & 0 \\ 0 & 0 & 0 & m & -n & 0 \\ 0 & 0 & 0 & n & m & 0 \\ -nm & nm & 0 & 0 & 0 & m^2 - n^2 \end{bmatrix} \begin{bmatrix} \varepsilon_x \\ \varepsilon_y \\ \varepsilon_z \\ \gamma_{yz} \\ \gamma_{xz} \\ \frac{1}{2}\gamma_{xy} \end{bmatrix} \tag{9.10}$$

Similarly this can also be represented in the compact form as to Eq. (9.8), which gives:

$$\{\varepsilon\}_{123} = [T_\varepsilon]\{\varepsilon\}_{xyz} \tag{9.11}$$

Substituting the relationship given in Eqs. (9.8) and (9.11) into Eq. (9.3), from which using the same compact form Eq. (9.3) can be given in the form shown in Eq. (9.12), gives the result of the stress and strain in the structural coordinate system i.e. x-y-z coordinate system, shown in Eq. (9.13).

$$\{\sigma\}_{123} = [C]\{\varepsilon\}_{123} \tag{9.12}$$

$$\{\sigma\}_{xyz} = [T_\sigma]^{-1}[C][T_\varepsilon]\{\varepsilon\}_{xyz} \tag{9.13}$$

Expanding the relationship in Eq. (9.13) result in the following:

$$\begin{Bmatrix} \sigma_x \\ \sigma_y \\ \sigma_z \\ \tau_{yz} \\ \tau_{xz} \\ \tau_{xy} \end{Bmatrix} = \begin{bmatrix} \bar{C}_{11} & \bar{C}_{12} & \bar{C}_{13} & 0 & 0 & \bar{C}_{16} \\ \bar{C}_{12} & \bar{C}_{22} & \bar{C}_{23} & 0 & 0 & \bar{C}_{26} \\ \bar{C}_{13} & \bar{C}_{23} & \bar{C}_{33} & 0 & 0 & \bar{C}_{36} \\ 0 & 0 & 0 & \bar{C}_{44} & \bar{C}_{45} & 0 \\ 0 & 0 & 0 & \bar{C}_{45} & \bar{C}_{55} & 0 \\ \bar{C}_{16} & \bar{C}_{26} & \bar{C}_{36} & 0 & 0 & \bar{C}_{66} \end{bmatrix} \begin{Bmatrix} \varepsilon_x \\ \varepsilon_y \\ \varepsilon_z \\ \gamma_{yz} \\ \gamma_{xz} \\ \gamma_{xy} \end{Bmatrix} \tag{9.14}$$

with $\bar{C}_{ij}$ is known as the transformed stiffness matrix, where the individual elements are defined by:

$$\begin{aligned}
\bar{C}_{11} &= m^4 C_{11} + 2m^2 n^2 (C_{12} + 2C_{66}) + n^4 C_{22} \\
\bar{C}_{12} &= n^2 m^2 (C_{11} + C_{22} - 4C_{66}) + (n^4 + m^4) C_{12} \\
\bar{C}_{13} &= m^2 C_{13} + n^2 C_{23} \\
\bar{C}_{16} &= nm(m^2 (C_{11} - C_{12} - 2C_{66}) + n^2 (C_{12} - C_{22} + 2C_{66})) \\
\bar{C}_{22} &= n^4 C_{11} + 2m^2 n^2 (C_{12} + 2C_{66}) + m^4 C_{22} \\
\bar{C}_{23} &= n^2 C_{13} + m^2 C_{23} \\
\bar{C}_{26} &= nm(n^2 (C_{11} - C_{12} - 2C_{66}) + m^2 (C_{12} - C_{22} + 2C_{66})) \\
\bar{C}_{33} &= C_{33} \\
\bar{C}_{36} &= mn(C_{13} - C_{23}) \\
\bar{C}_{44} &= m^2 C_{44} + n^2 C_{55} \\
\bar{C}_{45} &= mn(C_{44} - C_{55}) \\
\bar{C}_{55} &= n^2 C_{44} + m^2 C_{55} \\
\bar{C}_{66} &= n^2 m^2 (C_{11} - 2C_{12} + C_{22}) + C_{66} (m^2 - n^2)^2
\end{aligned} \tag{9.15}$$

9.2 Plane stress assumptions

The plane stress assumptions set another important hypothesis towards the analysis of composite material. The plane stress assumptions simplify further the relationship of the stress strain given in Eq. (9.3). Because composite material are generally considered stronger in the direction of the fibre, wherein greater stress are found in plane to the fibres i.e. in the 1-2 plane of the material coordinate system, compared to the stresses perpendicular to the fibres. This leads to the plane stress assumptions, which assume that stresses perpendicular to the 1-2 plane, see Fig. A3, are small and may be considered zero. Therefore the σ_3, τ_{13} and τ_{23} stresses are set to zero.

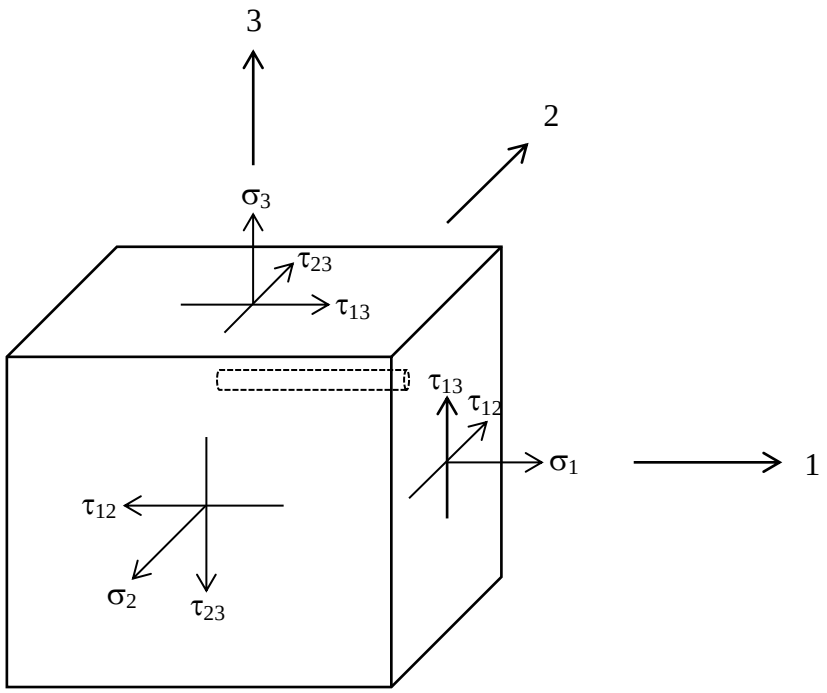

Figure A3– The six stresses acting on the surface of a small element of composite material.

This result in Eq. (9.3) to be

$$\begin{Bmatrix} \sigma_1 \\ \sigma_2 \\ 0 \\ 0 \\ 0 \\ \tau_{12} \end{Bmatrix} = \begin{bmatrix} C_{11} & C_{12} & C_{13} & 0 & 0 & 0 \\ C_{12} & C_{22} & C_{23} & 0 & 0 & 0 \\ C_{13} & C_{23} & C_{33} & 0 & 0 & 0 \\ 0 & 0 & 0 & C_{44} & 0 & 0 \\ 0 & 0 & 0 & 0 & C_{55} & 0 \\ 0 & 0 & 0 & 0 & 0 & C_{66} \end{bmatrix} \begin{Bmatrix} \varepsilon_1 \\ \varepsilon_2 \\ \varepsilon_3 \\ \gamma_{23} \\ \gamma_{13} \\ \gamma_{12} \end{Bmatrix} \tag{9.16}$$

with three of the stresses equates to zero, the matrix form in Eq. (9.16) can be simplify to

$$\begin{Bmatrix} \sigma_1 \\ \sigma_2 \\ \tau_{12} \end{Bmatrix} = \begin{bmatrix} Q_{11} & Q_{12} & 0 \\ Q_{12} & Q_{22} & 0 \\ 0 & 0 & Q_{66} \end{bmatrix} \begin{Bmatrix} \varepsilon_1 \\ \varepsilon_2 \\ \gamma_{12} \end{Bmatrix} \tag{9.17}$$

where Q_{ij} matrix is known as reduced stiffness matrix, with the individual element of the reduced stiffness is given by

$$\begin{aligned} Q_{11} &= C_{11} - \frac{C_{13}^2}{C_{33}} & Q_{12} &= C_{12} - \frac{C_{13}C_{23}}{C_{33}} \\ Q_{22} &= C_{22} - \frac{C_{23}^2}{C_{33}} & Q_{66} &= C_{66} \end{aligned} \tag{9.18}$$

The elements of the reduced stiffness in Eq. (9.18) can also be given in terms of engineering constant, which is shown in Eq. (9.19).

$$\begin{aligned} Q_{11} &= \frac{E_1}{1-\nu_{12}\nu_{21}} & Q_{12} &= \frac{\nu_{12}E_2}{1-\nu_{12}\nu_{21}} \\ Q_{22} &= \frac{E_2}{1-\nu_{12}\nu_{21}} & Q_{66} &= G_{12} \end{aligned} \tag{9.19}$$

It is important to note, under the plain stress assumptions to assume that the strain $\varepsilon_3 = 0$ due to $\sigma_3 = 0$ will be completely misleading, because it is evident from Eq. (9.16) that ε_3 can exist as a result of the stresses in the 1- and 2- direction i.e.

$$\varepsilon_3 = -\frac{C_{13}}{C_{33}}\varepsilon_1 - \frac{C_{23}}{C_{33}}\varepsilon_2 \tag{9.20}$$

The reduced stiffness matrix in Eq. (9.17) can be transformed to the structural coordinate system i.e. x-y-z coordinate following similar transformation equation shown in Eq. (9.13), from which gives:

$$\begin{Bmatrix} \sigma_x \\ \sigma_y \\ \tau_{xy} \end{Bmatrix} = \begin{bmatrix} \bar{Q}_{11} & \bar{Q}_{12} & \bar{Q}_{16} \\ \bar{Q}_{12} & \bar{Q}_{22} & \bar{Q}_{26} \\ \bar{Q}_{16} & \bar{Q}_{26} & \bar{Q}_{66} \end{bmatrix} \begin{Bmatrix} \varepsilon_x \\ \varepsilon_y \\ \gamma_{xy} \end{Bmatrix} \tag{9.21}$$

with now the $\bar{Q}_{ij}$ is known as the transformed reduced stiffness, where they are defined by

$$\begin{aligned}
\bar{Q}_{11} &= Q_{11}m^4 + 2(Q_{12} + 2Q_{66})n^2m^2 + Q_{22}n^4 \\
\bar{Q}_{12} &= (Q_{11} + Q_{22} - 4Q_{66})n^2m^2 + Q_{12}(n^4 + m^4) \\
\bar{Q}_{16} &= (Q_{11} - Q_{12} - 2Q_{66})nm^3 + (Q_{12} - Q_{22} + 2Q_{66})n^3m \\
\bar{Q}_{22} &= Q_{11}n^4 + 2(Q_{12} + 2Q_{66})n^2m^2 + Q_{22}m^4 \\
\bar{Q}_{26} &= (Q_{11} - Q_{12} - 2Q_{66})n^3m + (Q_{12} - Q_{22} + 2Q_{66})nm^3 \\
\bar{Q}_{66} &= (Q_{11} + Q_{22} - 2Q_{12} - 2Q_{66})n^2m^2 + Q_{66}(n^4 + m^4)
\end{aligned} \tag{9.22}$$

9.3 Kirchhoff Hypothesis for flat thin plate

The prediction on the response of thin composite plates has been closely related to the assumption from Kirchhoff hypothesis (Love, 1944). Condition for thin plate is defined as the ratio of the plate's thickness, *h* to a characteristic dimension *a* of the mean surface to be less than 1/20 (Decolon, 2002). To understand the influence of the Kirchhoff hypothesis, an example describing the concept from Hyer (2009) will be used and discuss in this section. Consider the laminated plate in Fig. A4, which is shown subjected to a variety of loading conditions: that are distributed load (q), point load (p), moment (M) and in-plane load (N).

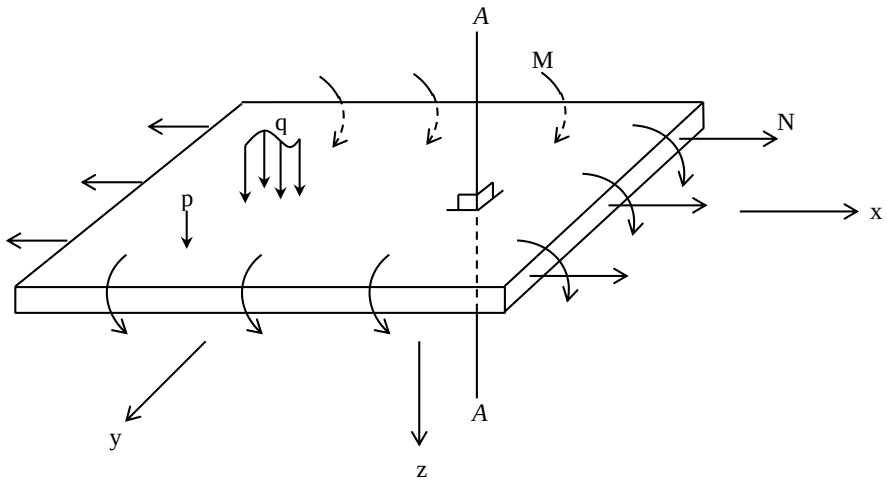

Figure A4 – Different possible loading conditions on a laminated composite plate.

Line *AA'* is shown to be normal to the laminate and parallel with the z- axis before the laminate is deformed. This line is shown in Fig. A5 to be normal with every layer within the laminate and with the geometrical laminate mid-plane. Layers within the laminate are assumed to be perfectly bonded and no slippage occurring between them. Kirchhoff hypothesis than state that despite the deformations caused by any of the loadings shown in Fig. A4, line *AA*' remains straight and normal to the geometric mid-plane of the plate and does not change in length, as illustrated in Fig. A6. The line is said to simply translate or rotate, as shown by Fig. A7.

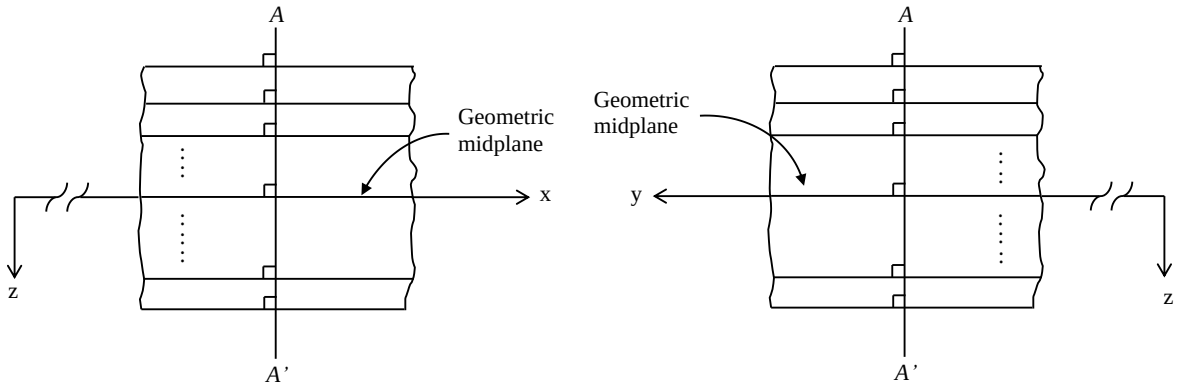

(a) (b)

Figure A5 – Laminate cross-section showing the line AA' to be normal with the geometric midplane and with every layer within the laminate. Figure (a) shows the cross-section made with respect to the x-z plane, while (b) shows the cross-section with respect to the y-z plane.

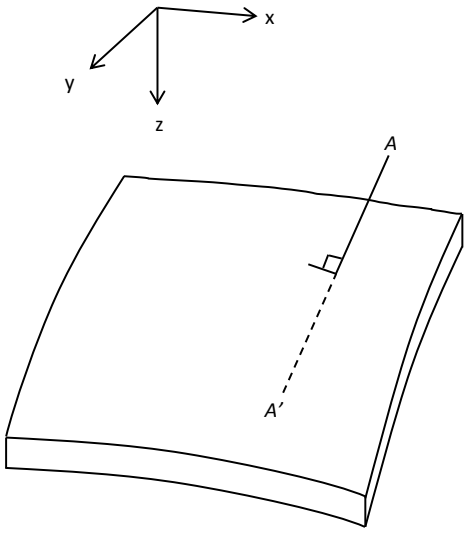

Figure A6 – Showing a deformed composite plate, however the line AA' is shown to remain normal with the surface; where line AA' simply translating and rotating.

Note that the distance between the point *t* and *t'* from line *AA'* in the figure remain to be at the same length before and after deformation. This implies that there is no through thickness strain, ε_z occurring along line *AA'*, which obviously contradict to the plane stress assumption mentioned earlier, see Eq. (9.20). Nevertheless it will be shown later that the assumption of the line *AA'* remain to be at same length, does not play into the actual use of the hypothesis.

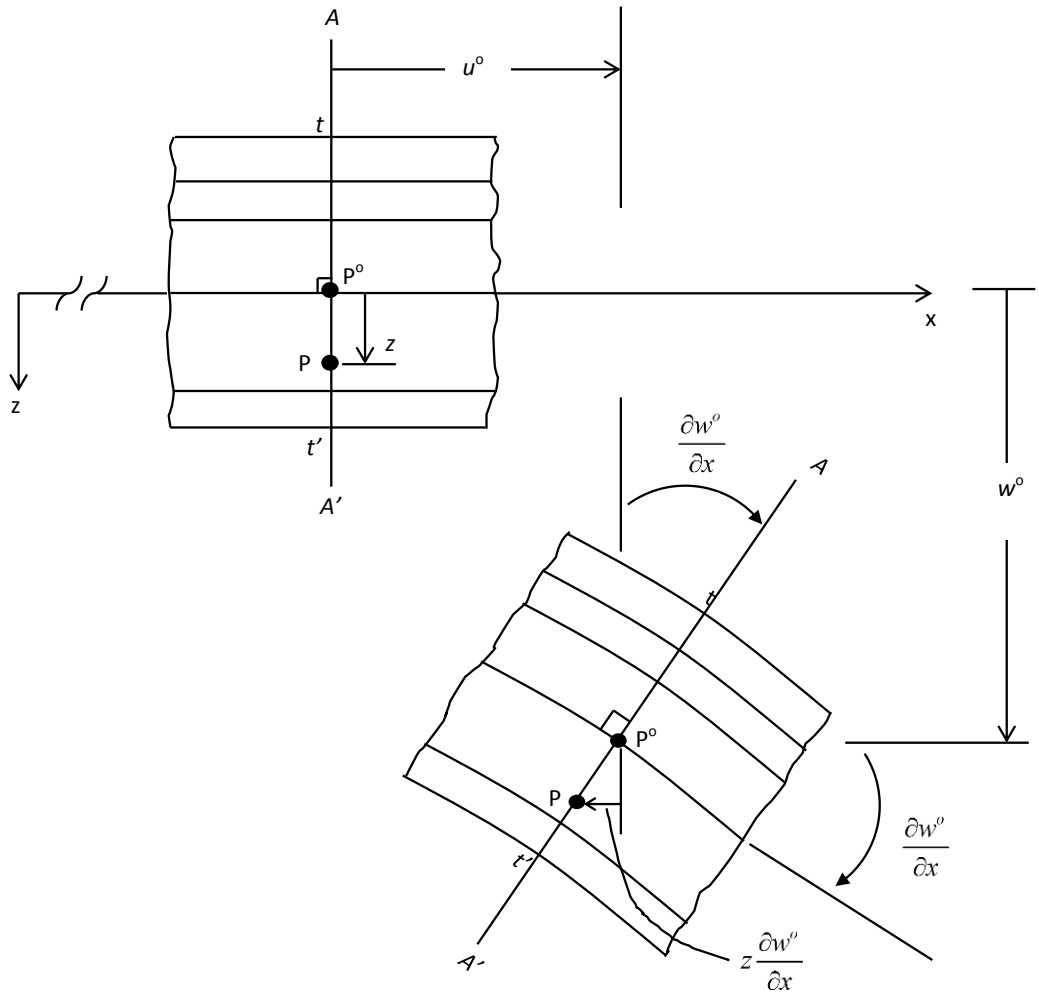

Figure A7– Kinematics of deformation as viewed from the x-z plane.

In fact attention is focused on point P, shown in Fig. A7, from which after deformation this point P is observed to rotate in the negative –x axis. Because line AA' is seen only to translate and rotate, therefore the translation of point P after deformation in the –x direction or denoted as u(x, y, z) is given by

$$u(x, y, z) = u^o(x, y) - z \tan \frac{\partial w^o(x, y)}{\partial x} \tag{9.23}$$

and since the rotation angle is considered too small, hence the tangents value will be replace with only the value of the angle rotation, which gives

$$u(x,y,z) = u^o(x,y) - z\frac{\partial w^o(x,y)}{\partial x} \tag{9.24}$$

Displacement of point P in the y-direction, which can view from the y-z plane is given by:

$$v(x,y,z) = v^o(x,y) - z\frac{\partial w^o(x,y)}{\partial y} \tag{9.25}$$

and the displacement in the z-direction:

$$w(x,y,z) = w^o(x,y) \tag{9.26}$$

Equation (9.26) indicates that the vertical displacement of point P is independent of *z*. In other words all the points on line *AA'* will have equal vertical displacement occurring.

The displacement equations of Eqs. (9.24), (9.25) and (9.26) is an important contribution of the Kirchhoff hypothesis, especially towards the strain-displacement relationship. For instance the strain-displacement equation for extensional strain in the x-direction given by:

$$\varepsilon_x = \frac{\partial u}{\partial x} \tag{9.27}$$

using Eq. (9.24) into Eq. (9.27) result in the following relationship for the extensional strain:

$$\varepsilon_x(x,y,z) = \frac{\partial u(x,y,z)}{\partial x} = \frac{\partial u^o(x,y)}{\partial x} - z\frac{\partial^2 w^o(x,y)}{\partial x^2} \tag{9.28}$$

The first term in the equation i.e. $\frac{\partial u^o(x,y)}{\partial x}$ indicates the extensional strain of the reference surface in the x-direction, where it is often substitute with the notation $\varepsilon^o(x,y)$. Meanwhile

the second term, $-\frac{\partial^2 w^o(x,y)}{\partial x^2}$, signify the curvature of the reference surface in the x-direction, and often substitute with the notation $\kappa_x^o(x,y)$. Therefore Eq. (9.28) can also be written as:

$$\varepsilon_x(x,y,z) = \varepsilon_x^o(x,y) + z\kappa_x^o(x,y) \tag{9.29}$$

This can be similarly performed for the remaining strain-displacement equations as shown in Eq. (9.30),

$$\begin{aligned}
\varepsilon_y(x,y,z) &\equiv \frac{\partial v^o(x,y,z)}{\partial y} = \varepsilon_y^o(x,y) + z\kappa_y^o(x,y) \\
\varepsilon_z(x,y,z) &\equiv \frac{\partial w(x,y)}{\partial z} = \frac{\partial w^o(x,y)}{\partial z} = 0 \\
\gamma_{yz}(x,y,z) &\equiv \frac{\partial w(x,y,z)}{\partial y} + \frac{\partial v(x,y,z)}{\partial z} = \frac{\partial w^o(x,y)}{\partial y} - \frac{\partial w^o(x,y)}{\partial y} = 0 \\
\gamma_{xz}(x,y,z) &\equiv \frac{\partial w(x,y,z)}{\partial x} + \frac{\partial u(x,y,z)}{\partial z} = \frac{\partial w^o(x,y)}{\partial x} - \frac{\partial w^o(x,y)}{\partial x} = 0 \\
\gamma_{xy}(x,y,z) &\equiv \frac{\partial v(x,y,z)}{\partial x} + \frac{\partial u(x,y,z)}{\partial y} = \gamma_{xy}^o - z\kappa_{xy}^o
\end{aligned} \tag{9.30}$$

where,

$$\begin{aligned}
\varepsilon_y^o(x,y) &= \frac{\partial v^o(x,y)}{\partial y} & \kappa_y^o(x,y) &= -\frac{\partial^2 w^o(x,y)}{\partial y^2} \\
\gamma_{xy}^o(x,y) &= \frac{\partial v^o(x,y)}{\partial x} + \frac{\partial u^o(x,y)}{\partial y} & \kappa_{xy}^o(x,y) &= -2\frac{\partial^2 w^o(x,y)}{\partial x \partial y}
\end{aligned} \tag{9.31}$$

Equation (9.29) and the first and last equation of Eq. (9.30) is the result of the Kirchhoff hypothesis and play a very important part in the classical lamination theory. These three equations are summarized below:

$$\begin{aligned}\varepsilon_x(x,y,z) &= \varepsilon_x^o(x,y) + z\kappa_x^o(x,y)\\ \varepsilon_y(x,y,z) &= \varepsilon_y^o(x,y) + z\kappa_y^o(x,y)\\ \gamma_{xy}(x,y,z) &= \gamma_{xy}^o(x,y) + z\kappa_{xy}^o(x,y)\end{aligned} \tag{9.32}$$

The strain relationship given in Eq. (9.32) can be replaced in Eq. (9.21), which yield a new stress-strain relationship given by:

$$\begin{Bmatrix}\sigma_x\\ \sigma_y\\ \tau_{xy}\end{Bmatrix} = \begin{bmatrix}\bar{Q}_{11} & \bar{Q}_{12} & \bar{Q}_{16}\\ \bar{Q}_{12} & \bar{Q}_{22} & \bar{Q}_{26}\\ \bar{Q}_{16} & \bar{Q}_{26} & \bar{Q}_{66}\end{bmatrix} \begin{Bmatrix}\varepsilon_x^o(x,y) + z\kappa_x^o(x,y)\\ \varepsilon_y^o(x,y) + z\kappa_y^o(x,y)\\ \gamma_{xy}^o(x,y) + z\kappa_{xy}^o(x,y)\end{Bmatrix} \tag{9.33}$$

The stress-strain relationship of Eq. (9.33) plays an important role towards the derivation of the laminate stiffness matrix or the *ABD* matrix, which will be discussed the following section.

9.4 The *ABD* stiffness matrix

In the analysis of composite material structure, loadings i.e. forces and moments are often applied or act on the laminate, in which the engineers would assess the stresses and deformations as the direct consequence from the applied loadings. Therefore it would be viewed as convenient to have a relationship between the applied forces and/or moments relating to the prediction of the laminate's behaviour.

In fact the forces and moments acting on a laminate are actually the integrals through the laminate thickness of the stresses, which are known as stress resultants (Hyer, 2009). Figures A8 and A9 shows the behaviour of the force and moment resultant respectively, acting on a laminate. Meanwhile Eqs. (9.34) and (9.35) gives the mathematical definition of the force and moment resultant respectively.

$$N_x \equiv \int_{-\frac{H}{2}}^{\frac{H}{2}} \sigma_x dz \qquad N_y \equiv \int_{-\frac{H}{2}}^{\frac{H}{2}} \sigma_y dz \qquad N_{xy} \equiv \int_{-\frac{H}{2}}^{\frac{H}{2}} \tau_{xy} dz \tag{9.34}$$

$$M_x \equiv \int_{-\frac{H}{2}}^{\frac{H}{2}} \sigma_x z dz \qquad M_y \equiv \int_{-\frac{H}{2}}^{\frac{H}{2}} \sigma_y z dz \qquad M_{xy} \equiv \int_{-\frac{H}{2}}^{\frac{H}{2}} \tau_{xy} z dz \tag{9.35}$$

The stress-strain relationship given in Eq. (9.33) can be substituted into Eq. (9.34) and (9.35), which derives the ABD stiffness matrix. Performing this for the force resultant, N_x and the moment resultant M_x in Eq. (9.34) and (9.35) respectively yield the followings:

$$N_x = \int_{-H/2}^{H/2} \left\{ \bar{Q}_{11}(\varepsilon_x^o + z\kappa_x^o) + \bar{Q}_{12}(\varepsilon_y^o + z\kappa_y^o) + \bar{Q}_{16}(\gamma_{xy}^o + z\kappa_{xy}^o) \right\} dz \tag{9.36}$$

$$M_x = \int_{-H/2}^{H/2} \left\{ \bar{Q}_{11}(\varepsilon_x^o + z\kappa_x^o) + \bar{Q}_{12}(\varepsilon_y^o + z\kappa_y^o) + \bar{Q}_{16}(\gamma_{xy}^o + z\kappa_{xy}^o) \right\} z dz \tag{9.37}$$

Expanding these relationship and rearranging them leads to respective equations given in Eq. (9.38) and (9.39).

$$N_x = \left\{\int_{-H/2}^{H/2} \bar{Q}_{11} dz\right\}\varepsilon_x^o + \left\{\int_{-H/2}^{H/2} \bar{Q}_{12} dz\right\}\varepsilon_y^o + \left\{\int_{-H/2}^{H/2} \bar{Q}_{16} dz\right\}\gamma_{xy}^o + \left\{\int_{-H/2}^{H/2} \bar{Q}_{11} z dz\right\}\kappa_x^o + \left\{\int_{-H/2}^{H/2} \bar{Q}_{12} z dz\right\}\kappa_y^o + \left\{\int_{-H/2}^{H/2} \bar{Q}_{16} z dz\right\}\kappa_{xy}^o \tag{9.38}$$

$$M_x = \left\{\int_{-H/2}^{H/2} \bar{Q}_{11} z dz\right\}\varepsilon_x^o + \left\{\int_{-H/2}^{H/2} \bar{Q}_{12} z dz\right\}\varepsilon_y^o + \left\{\int_{-H/2}^{H/2} \bar{Q}_{16} z dz\right\}\gamma_{xy}^o + \left\{\int_{-H/2}^{H/2} \bar{Q}_{11} z^2 dz\right\}\kappa_x^o + \left\{\int_{-H/2}^{H/2} \bar{Q}_{12} z^2 dz\right\}\kappa_y^o + \left\{\int_{-H/2}^{H/2} \bar{Q}_{16} z^2 dz\right\}\kappa_{xy}^o \tag{9.39}$$

The first three integrals relating to the in-plane strain in Eq. (9.38) can be solved fairly straight forwards since the transformed reduced stiffness $\bar{Q}_{ij}$ are constant value and only dependent on the material properties.

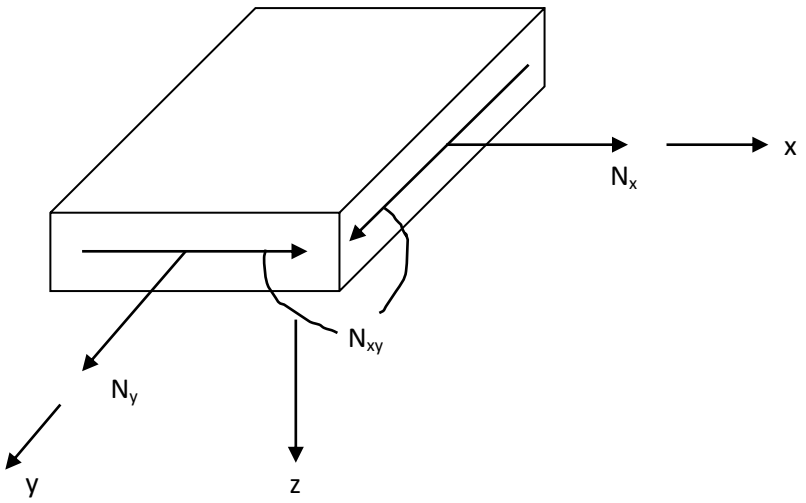

Figure A8 – Definition of the force resultant, N_x, N_y and N_{xy}.

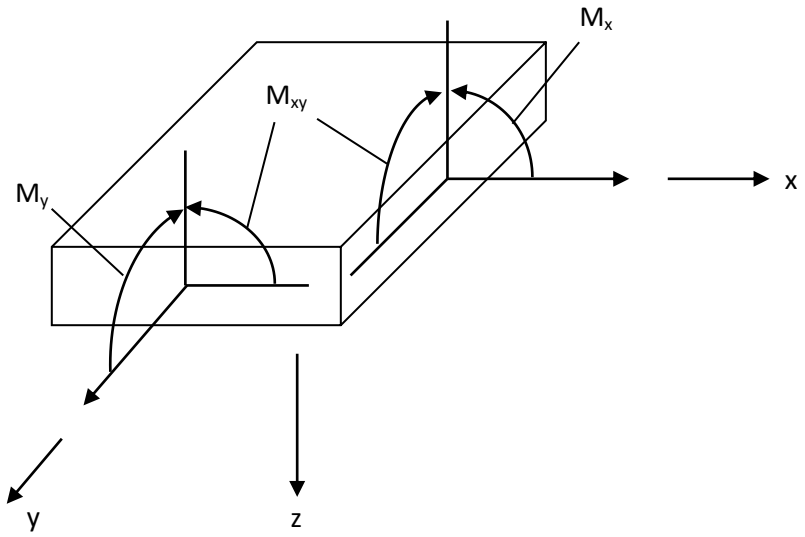

Figure A9 – Definition of moment resultants, M_x, M_y and M_{xy}.

Therefore the $\bar{Q}_{ij}$ can be taken out from the integration, leaving only the element of the thickness of every respective layer within the laminate. Hence can be summarize in the following form:

$$\int_{-H/2}^{H/2} \bar{Q}_{ij} dz = \bar{Q}_{11_1} \int_{z_0}^{z_1} dz + \bar{Q}_{11_2} \int_{z_1}^{z_2} dz + \ldots + \bar{Q}_{11_k} \int_{z_{k-1}}^{z_k} dz + \bar{Q}_{11_N} \int_{z_{N-1}}^{z_N} dz = \sum_{k=1}^{N} \bar{Q}_{ij_k} (z_k - z_{k-1}) \tag{9.40}$$

$$A_{ij} = \int_{-H/2}^{H/2} \bar{Q}_{ij} dz = \sum_{k=1}^{N} \bar{Q}_{ij_k} (z_k - z_{k-1}) \tag{9.41}$$

Meanwhile the last three integrals relating the reference surface to the curvature deformation can be solved similarly to Eq. (9.40) and result to the following form:

$$B_{ij} = \int_{-H/2}^{H/2} \bar{Q}_{ij} z dz = \frac{1}{2} \sum_{k=1}^{N} \bar{Q}_{ij_k} (z_k^2 - z_{k-1}^2) \tag{9.42}$$

As for the moment resultant given in Eq. (9.39), the first three integrals is shown to have similar form with the last three integrals of the force resultant in Eq. (9.38), hence the

outcome will be similar to the one given in Eq. (9.42). Solving the last three integrals of Eq. (9.39) analogous to Eq. (9.40) yield the following result:

$$D_{ij} = \int_{-H/2}^{H/2} \bar{Q}_{ij} z^2 dz = \frac{1}{3}\sum_{k=1}^{N} \bar{Q}_{ij_k} (z_k^3 - z_{k-1}^3) \tag{9.43}$$

Therefore substituting the appropriate notation for the A_{ij}, B_{ij} and D_{ij} into Eq. (9.38) and (9.39) gives the following relationship:

$$N_x = A_{11}\varepsilon_x^o + A_{12}\varepsilon_y^o + A_{16}\gamma_{xy}^o + B_{11}\kappa_x^o + B_{12}\kappa_y^o + B_{16}\kappa_{xy}^o \tag{9.44}$$

$$M_x = B_{11}\varepsilon_x^o + B_{12}\varepsilon_y^o + B_{16}\gamma_{xy}^o + D_{11}\kappa_x^o + D_{12}\kappa_y^o + D_{16}\kappa_{xy}^o \tag{9.45}$$

Similarly the expression above can be obtained for the remaining of the force and moment resultant in Eq. (9.38) and (9.39) respectively, from which the result is expressed in matrix form given as:

$$\begin{Bmatrix} N_x \\ N_y \\ N_{xy} \end{Bmatrix} = \begin{bmatrix} A_{11} & A_{12} & A_{16} \\ A_{22} & A_{22} & A_{26} \\ A_{16} & A_{26} & A_{66} \end{bmatrix} \begin{Bmatrix} \varepsilon_x^o \\ \varepsilon_y^o \\ \gamma_{xy}^o \end{Bmatrix} + \begin{bmatrix} B_{11} & B_{12} & B_{16} \\ B_{12} & B_{22} & B_{26} \\ B_{16} & B_{26} & B_{66} \end{bmatrix} \begin{Bmatrix} \kappa_x^o \\ \kappa_y^o \\ \kappa_{xy}^o \end{Bmatrix}$$
$$\begin{Bmatrix} M_x \\ M_y \\ M_{xy} \end{Bmatrix} = \begin{bmatrix} B_{11} & B_{12} & B_{16} \\ B_{12} & B_{22} & B_{26} \\ B_{16} & B_{26} & B_{66} \end{bmatrix} \begin{Bmatrix} \varepsilon_x^o \\ \varepsilon_y^o \\ \gamma_{xy}^o \end{Bmatrix} + \begin{bmatrix} D_{11} & D_{12} & D_{16} \\ D_{12} & D_{22} & D_{26} \\ D_{16} & D_{26} & D_{66} \end{bmatrix} \begin{Bmatrix} \kappa_x^o \\ \kappa_y^o \\ \kappa_{xy}^o \end{Bmatrix} \tag{9.46}$$

The matrix containing the elements of the A_{ij}, B_{ij} and D_{ij} is known as the stiffness matrix, or more commonly known as the *ABD* matrix. Here the A_{ij} are referred to as the extensional matrix and the D_{ij} are referred to as the bending matrix. Meanwhile the B_{ij} are known as the coupling matrix, which indicates the coupling between the in-plane and out-of-plane deformation, a behaviour that do not exist for metallic structures.

Appendix B

Table B1 – Abridged listing for Extension-Twisting (and Shearing-Bending), $A_S B_t D_S$ laminates, derived through off-axis alignment of parent class laminate of $A_I B_S D_F$ for the 16-ply number groupings.

n	No.	Stacking sequences		ξ_8
		$\beta = \pi/8 + m\pi/4$	$\beta = -\pi/8 + m\pi/4$	
16	1	$[-++--++-\bigcirc\bullet\bullet\bigcirc\bigcirc\bullet\bullet\bigcirc]_T$	$[--++++--\bullet\bullet\bigcirc\bigcirc\bigcirc\bigcirc\bullet\bullet]_T$	±1.00
	:	:	:	:
	3	$[--++++--\bigcirc\bigcirc\bullet\bullet\bullet\bullet\bigcirc\bigcirc]_T$	$[-++--++-\bullet\bigcirc\bigcirc\bullet\bullet\bigcirc\bigcirc\bullet]_T$	±1.00
	4	$[-++-+-\bullet\bigcirc-+\bigcirc\bullet\bigcirc\bullet\bullet\bigcirc]_T$	$[-+-++-\bullet\bigcirc+-\bullet\bigcirc\bigcirc\bullet\bigcirc\bullet]_T$	±0.88
	:	:	:	:
	6	$[-+-++-\bigcirc\bullet+-\bigcirc\bullet\bullet\bigcirc\bullet\bigcirc]_T$	$[-++-+-\bigcirc\bullet-+\bullet\bigcirc\bullet\bigcirc\bigcirc\bullet]_T$	±0.88
	7	$[-++-+\bullet-\bigcirc-\bigcirc+\bullet\bigcirc\bullet\bullet\bigcirc]_T$	$[--+++\bullet-\bigcirc+\bullet-\bigcirc\bigcirc\bigcirc\bullet\bullet]_T$	±0.81
	:	:	:	:
	9	$[--+++\bigcirc-\bullet+\bigcirc-\bullet\bullet\bullet\bigcirc\bigcirc]_T$	$[-++-+\bigcirc-\bullet-\bullet+\bigcirc\bullet\bigcirc\bigcirc\bullet]_T$	±0.81
	10	$[-+-++\bullet\bigcirc-\bigcirc-+\bullet\bullet\bigcirc\bullet\bigcirc]_T$	$[--++\bullet+-\bigcirc+\bullet\bigcirc-\bigcirc\bigcirc\bullet\bullet]_T$	±0.75
	:	:	:	:
	13	$[--++\bigcirc+-\bullet+\bigcirc\bullet-\bullet\bullet\bigcirc\bigcirc]_T$	$[-+-++\bigcirc\bullet-\bullet-+\bigcirc\bigcirc\bullet\bigcirc\bullet]_T$	±0.75
	14	$[-++-\bigcirc-\bullet+\bullet+\bigcirc-\bigcirc\bullet\bullet\bigcirc]_T$	$[--+\bullet++-\bigcirc+\bullet\bigcirc\bigcirc-\bigcirc\bullet\bullet]_T$	±0.69
	:	:	:	:
	19	$[--+\bigcirc++-\bullet+\bigcirc\bullet\bullet-\bullet\bigcirc\bigcirc]_T$	$[-++\bigcirc+--\bullet-\bullet\bullet\bigcirc+\bigcirc\bigcirc\bullet]_T$	±0.69
	20	$[-++-\bigcirc\bullet-+\bullet\bigcirc+-\bigcirc\bullet\bullet\bigcirc]_T$	$[--\bullet+++-\bigcirc+\bullet\bigcirc\bigcirc\bigcirc-\bullet\bullet]_T$	±0.63
	:	:	:	:
	26	$[--\bigcirc+++-\bullet+\bigcirc\bullet\bullet\bullet-\bigcirc\bigcirc]_T$	$[-++\bigcirc-+\bullet-\bullet-\bigcirc\bullet+\bigcirc\bigcirc\bullet]_T$	±0.63
	27	$[-++\bullet-\bigcirc+-\bigcirc\bullet-\bigcirc+\bullet\bullet\bigcirc]_T$	$[--\bullet+++\bigcirc-\bullet+\bigcirc\bigcirc\bigcirc-\bullet\bullet]_T$	±0.56
	:	:	:	:
	33	$[--\bigcirc+++\bullet-\bigcirc+\bullet\bullet\bullet-\bigcirc\bigcirc]_T$	$[-+\bigcirc++-\bullet-\bullet-\bullet\bigcirc\bigcirc+\bigcirc\bullet]_T$	±0.56

	34	$[-++-\bigcirc\bullet\bullet\bigcirc-++-\bigcirc\bullet\bullet\bigcirc]_T$	$[--++\bullet\bullet\bigcirc\bigcirc++--\bigcirc\bigcirc\bullet\bullet]_T$	± 0.50
	:	:	:	:
	39	$[--++\bigcirc\bigcirc\bullet\bullet++--\bullet\bullet\bigcirc\bigcirc]_T$	$[-++\bigcirc\bullet--+\bigcirc\bullet\bullet-+\bigcirc\bigcirc\bullet]_T$	± 0.50
	40	$[-\bigcirc\bigcirc\bullet\bigcirc\bullet\bullet+\bullet++-+--\bigcirc]_T$	$[-\bullet\bullet\bigcirc\bullet\bigcirc\bigcirc+\bigcirc++-+--\bullet]_T$	∓ 0.50
	41	$[-++\bullet-\bigcirc\bigcirc\bullet+--\bigcirc+\bullet\bullet\bigcirc]_T$	$[--+\bullet+\bullet\bigcirc\bigcirc++-\bigcirc-\bigcirc\bullet\bullet]_T$	± 0.44
	:	:	:	:
	48	$[-\bullet+++\bigcirc--\bigcirc\bigcirc-\bullet\bullet\bullet+\bigcirc]_T$	$[-\bigcirc+++\bullet--\bullet\bullet-\bigcirc\bigcirc\bigcirc+\bullet]_T$	± 0.44
	49	$[-\bigcirc\bigcirc\bullet\bullet\bigcirc+\bullet+\bullet-++--\bigcirc]_T$	$[-\bullet\bullet\bigcirc\bigcirc\bullet+\bigcirc+\bigcirc-++--\bullet]_T$	∓ 0.44
	50	$[-\bigcirc\bullet\bigcirc\bigcirc\bullet+\bullet+\bullet+--+-\bigcirc]_T$	$[-\bullet\bigcirc\bullet\bullet\bigcirc+\bigcirc+\bigcirc+--+-\bullet]_T$	∓ 0.44
	51	$[-++\bullet\bigcirc-\bullet\bigcirc-+\bigcirc-+\bullet\bullet\bigcirc]_T$	$[--\bullet++\bullet\bigcirc\bigcirc++-\bigcirc\bigcirc-\bullet\bullet]_T$	± 0.38
	:	:	:	:
	59	$[-\bullet++\bigcirc+--\bigcirc\bigcirc\bullet-\bullet\bullet+\bigcirc]_T$	$[-\bigcirc++\bullet+--\bullet\bullet\bigcirc-\bigcirc\bigcirc+\bullet]_T$	± 0.38
	60	$[-\bigcirc\bigcirc\bullet\bullet+\bigcirc\bullet+-\bullet++--\bigcirc]_T$	$[-\bullet\bullet\bigcirc\bigcirc+\bullet\bigcirc+-\bigcirc++--\bullet]_T$	∓ 0.38
	61	$[-\bullet\bigcirc\bigcirc\bigcirc+\bullet\bullet++\bullet---+\bigcirc]_T$	$[-\bigcirc\bullet\bullet\bullet+\bigcirc\bigcirc++\bigcirc---+\bullet]_T$	∓ 0.38
	62	$[-++\bullet\bigcirc\bullet-\bigcirc-\bigcirc+-+\bullet\bullet\bigcirc]_T$	$[--\bullet+\bullet+\bigcirc\bigcirc++\bigcirc-\bigcirc-\bullet\bullet]_T$	± 0.31
	:	:	:	:
	71	$[-\bullet+\bigcirc++--\bigcirc\bigcirc\bullet\bullet-\bullet+\bigcirc]_T$	$[-\bigcirc+\bullet++--\bullet\bullet\bigcirc\bigcirc-\bigcirc+\bullet]_T$	± 0.31
	72	$[-\bigcirc\bigcirc\bullet+\bullet\bullet\bigcirc-++\bullet+--\bigcirc]_T$	$[-\bullet\bullet\bigcirc+\bigcirc\bigcirc\bullet-++\bigcirc+--\bullet]_T$	∓ 0.31
	:	:	:	:
	73	$[-\bullet\bigcirc\bigcirc+\bigcirc\bullet\bullet++-\bullet--+\bigcirc]_T$	$[-\bigcirc\bullet\bullet+\bullet\bigcirc\bigcirc++-\bigcirc--+\bullet]_T$	∓ 0.31
	74	$[-++\bullet\bullet\bigcirc\bigcirc-\bigcirc--++\bullet\bullet\bigcirc]_T$	$[--\bullet\bullet++\bigcirc\bigcirc++\bigcirc\bigcirc--\bullet\bullet]_T$	± 0.25
	:	:	:	:
	81	$[-\bullet\bigcirc+++--\bigcirc\bigcirc\bullet\bullet\bullet-+\bigcirc]_T$	$[-\bigcirc\bullet+++--\bullet\bullet\bigcirc\bigcirc\bigcirc-+\bullet]_T$	± 0.25
	82	$[-\bigcirc\bigcirc\bullet\bullet++-\bigcirc\bullet\bullet++--\bigcirc]_T$	$[-\bullet\bullet\bigcirc\bigcirc++-\bullet\bigcirc\bigcirc++--\bullet]_T$	∓ 0.25
	:	:	:	:
	84	$[-\bullet\bigcirc+\bigcirc\bigcirc\bullet\bullet++--\bullet-+\bigcirc]_T$	$[-\bigcirc\bullet+\bullet\bullet\bigcirc\bigcirc++--\bigcirc-+\bullet]_T$	∓ 0.25
16	85	$[-+\bigcirc-\bigcirc\bullet\bullet+\bullet++-\bigcirc-\bullet\bigcirc]_T$	$[-\bullet-+\bullet\bigcirc+\bigcirc+\bigcirc+-\bigcirc\bullet-\bullet]_T$	± 0.19
	:	:	:	:
	93	$[-\bullet++\bigcirc\bigcirc-\bullet+\bigcirc--\bullet\bullet+\bigcirc]_T$	$[-\bigcirc++\bullet\bullet-\bigcirc+\bullet--\bigcirc\bigcirc+\bullet]_T$	± 0.19
	94	$[-\bigcirc+\bullet\bigcirc\bullet\bullet\bigcirc-++-+\bullet-\bigcirc]_T$	$[-\bullet\bullet\bigcirc+\bigcirc-+\bigcirc\bullet+\bigcirc+--\bullet]_T$	∓ 0.19
	:	:	:	:
	98	$[-\bullet+\bigcirc\bigcirc\bigcirc\bullet\bullet++---\bullet+\bigcirc]_T$	$[-\bigcirc+\bullet\bullet\bullet\bigcirc\bigcirc++---\bigcirc+\bullet]_T$	∓ 0.19
	99	$[-+\bullet\bigcirc+\bullet\bigcirc-\bigcirc-+\bullet-+\bullet\bigcirc]_T$	$[-\bullet\bigcirc++\bigcirc+-\bullet-\bullet\bigcirc-\bullet\bigcirc+]_T$	± 0.13
	:	:	:	:
	107	$[-\bigcirc\bullet++\bullet+-\bigcirc-\bigcirc\bullet-\bigcirc\bullet+]_T$	$[-\bigcirc++\bullet\bullet\bigcirc-\bullet+--\bigcirc\bigcirc+\bullet]_T$	± 0.13
	108	$[-+\bigcirc\bullet\bigcirc\bullet\bullet\bigcirc-++-+-\bullet\bigcirc]_T$	$[-\bullet\bigcirc+\bullet\bigcirc+\bigcirc+-\bullet--\bullet\bigcirc+]_T$	∓ 0.13
	:	:	:	:
	115	$[-\bigcirc\bullet+\bigcirc\bullet+\bullet+-\bigcirc--\bigcirc\bullet+]_T$	$[-\bigcirc\bullet\bullet++\bigcirc-\bullet+\bigcirc\bigcirc--+\bullet]_T$	∓ 0.13
	116	$[-+\bigcirc\bullet\bigcirc-\bullet+\bullet+\bigcirc-+-\bullet\bigcirc]_T$	$[-+\bullet\bigcirc\bullet-\bigcirc+\bigcirc+\bullet-+-\bigcirc\bullet]_T$	± 0.06
	:	:	:	:
	120	$[-\bullet\bigcirc++\bigcirc-\bullet+\bigcirc-\bullet\bullet-+\bigcirc]_T$	$[-\bigcirc+\bullet+\bullet\bigcirc-\bullet+-\bigcirc-\bigcirc+\bullet]_T$	± 0.06
	121	$[-\bigcirc+\bullet\bigcirc\bullet-+\bullet\bigcirc+-+\bullet-\bigcirc]_T$	$[-\bullet\bullet\bigcirc-++\bigcirc+\bigcirc\bigcirc\bullet+--\bullet]_T$	∓ 0.06
	:	:	:	:
	126	$[-\bullet\bigcirc\bigcirc++-\bullet+\bigcirc\bullet\bullet--+\bigcirc]_T$	$[-\bigcirc\bullet+\bullet+\bigcirc-\bullet+\bigcirc-\bigcirc-+\bullet]_T$	∓ 0.06

Table B2 - Abridged listing for Extension-Twisting (and Shearing-Bending), $A_S B_t D_S$ laminates, derived through off-axis alignment of parent class laminate of $A_I B_S D_F$ for the 20-ply number groupings.

n	No.	Stacking sequences		ξ_8
		$\beta = \pi/8 + m\pi/4$	$\beta = -\pi/8 + m\pi/4$	
20	1	[−+++−−+−●+○●○○○●●●○]	[−−++−+++−●−●○○○●○○●●]	±0.98
	:	:	:	:
	9	[−−++−+++−○−○●●●○●●○○]	[−+++−−+−○+●○●●●○○○●]	±0.98
	10	[−+++−−−+●−○+●○○○●●●○]	[−−+−++++●−●−○○○○●○●●]	±0.94
	:	:	:	:
	17	[−−+−++++○−○−●●●●○●○○]	[−+++−−−+○−●+○●●●○○○●]	±0.94
	18	[−++−+−+●−−○○+●○●○●●○]	[−−+−+++●+−●○−○○○●○●●]	±0.90
	:	:	:	:
	24	[−−+−+++○+−○●−●●●○●○○]	[−++−+−+○−−●●+○●○●○○●]	±0.90
	25	[−+++−−●+−−○○●+○○●●●○]	[−−+−++●++−●○○−○○●○●●]	±0.86
	:	:	:	:
	31	[−−+−++○++−○●●−●●○●○○]	[−+++−−○+−−●●○+●●○○○●]	±0.86
	32	[−+++−−−○●●++−○○○●●●○]	[−−+−+●+++−●○○○−○●○●●]	±0.82
	:	:	:	:
	44	[−−+−+○+++−○●●●−●○●○○]	[−+++−○−+−−●●○●+●○○○●]	±0.82
	45	[−+++●−−+−−○○●○○+●●●○]	[−−+−●++++−●○○○○−●○●●]	±0.78
	:	:	:	:
	55	[−−+−○++++−○●●●●−○●○○]	[−+++○−−+−−●●○●●+○○○●]	±0.78
	56	[−+++−−●○−●+○−+○○●●●○]	[−−+++●+−○○−−●○+●●○●○]	±0.74
	:	:	:	:
	75	[−−+++○+−●●−−○●+○○●○●]	[−++○+−+−−−●●●○●○+○○●]	±0.74
	76	[−+++−−●○●−○+−+○○●●●○]	[−−++●++−○−○○●−+●●○●○]	±0.70
	:	:	:	:
	103	[−−++○++−●−●●○−+○○●○●]	[−+○+++−−−−●●●●○○○+○●]	±0.70
	104	[−+++−●−○●−○+−○+○●●●○]	[−−+−●++●+○+○−○○−●○●●]	±0.66
	:	:	:	:
	129	[−−+−○++○+●+●−●●−○●○○]	[−++○−+−+●●−−○●○●+○○●]	±0.66
	130	[−+++●−−○●−○+−○○+●●●○]	[−−+●+++−○○○−●−●+●○●○]	±0.62
	:	:	:	:
	161	[−−+○+++−●●●−○−○+○●○●]	[−+○++−−+●●−−○●●○○+○●]	±0.62
	162	[−○○○●●●○●●++−+++−−−○]	[−●●●○○○●○○++−+++−−−●]	∓0.62
	:	:	:	:
	164	[−○●○○○●●●●++++−−−+−○]	[−●○●●●○○○○++++−−−+−●]	∓0.62
	165	[−+++−●●○−−○○−++○●●●○]	[−−●−+++●+○+○−○○○●−●●]	±0.58
	:	:	:	:
	203	[−●+++−+−○○−−○●○●●●+○]	[−○+++−+−●●−−●○●○○○+●]	±0.58
	204	[−+++●−●○−−○○−+○+●●●○]	[−−●−++●++○+○○−○○●−●●]	±0.54
	:	:	:	:
	238	[−●++−++○−○−○−●●○●●+○]	[−○++−++●−●−●−○○●○○+●]	±0.54
	239	[−○○●●○●○++●●−+−++−−○]	[−●●○○●○●++○○−+−++−−●]	∓0.54
	:	:	:	:
	242	[−●○○○●○●++●●+−+−−−+○]	[−○●●●○●○++○○+−+−−−+●]	∓0.54
	243	[−+++●●−○−−○○−○++●●●○]	[−●−+−+++○●○○○−+●−●●○]	±0.50

	:	:	:	:
	301	[–++●+○●–––+–○○○●○●+●]	[–○+++–●–+●–○●–●○○○+●]	±0.50
	302	[–○○○●●●+●–○+●+++–––○]	[–●●●○○○+○–●+○+++–––●]	∓0.50
	:	:	:	:
	306	[–●○○●○○+●+●+●––+––+○]	[–○●●○●●+○+○+○––+––+●]	∓0.50
	307	[–++○●––+●–○+●○○+–●●○]	[––●–●++++○+○○○○–●–●●]	±0.46
	:	:	:	:
	351	[–●+–++○+○–○–●–●●○●+○]	[–○+++–●–●+○–●–●○○○+●]	±0.46
	352	[–○○○●●●+–●+○●+++–––○]	[–●●●○○○+–○+●○+++–––●]	∓0.46
	:	:	:	:
	360	[–●○●○○○++●+●●–––+–+○]	[–○●○●●●++○+○○–––+–+●]	∓0.46
	361	[–++○––●○●●++–+○○–●●○]	[––+●●–+○++○○+○●––○●●]	±0.42
	:	:	:	:
	409	[–●+–+○++○–○–●●–●○●+○]	[–○++●–+–+●–○●○●–○○+●]	±0.42
	410	[–○○●○●+●–●+○+●+–+––○]	[–●●○●○+○–○+●+○+–+––●]	∓0.42
	:	:	:	:
	418	[–●○●○○+○+●+●–●––+–+○]	[–○●○●●+●+○+○–○––+–+●]	∓0.42
	419	[–++○–●–○●●++–○+○–●●○]	[–●–+++○–○●○+●–○+–●●○]	±0.38
	:	:	:	:
	485	[–++●○–●+○–+–●–○○○●+●]	[–○++●–+–●+○–●○●–○○+●]	±0.38
	486	[–○○○●●–+●●++●○++–––○]	[–●○●●○○+++○––●+○–●–+]	∓0.38
	:	:	:	:
	500	[–○●○○●●+++●––○+●–○–+]	[–○●○●+●●+○+○––○–+–+●]	∓0.38
20	501	[–○+●+––○+–+●●●○+○●○–]	[–●–+++○○–●○●+–○+–●●○]	±0.34
	:	:	:	:
	579	[–+●+○+●––○–○+●–○●○+●]	[–●+○+––●+–+○○○●+●○●–]	±0.34
	580	[–○●○+○●●●+–+○––+●+○–]	[–●●○○●○+++––○+○●●––+]	∓0.34
	:	:	:	:
	598	[–○○●●○●+++––●+●○○––+]	[–●○●+●○○○+–+●––+○+●–]	∓0.34
	599	[–○–+○+–●●+●++–●○●○○–]	[––●+●++○○–○○+–+●●–●○]	±0.30
	:	:	:	:
	665	[––○+○++●●–●●+–+○○–○●]	[–●–+○●++–+○–○○●+○●●–]	±0.30
	666	[–○○●+○●●–●+–++○●+–○–]	[–●○●○●++○–+○–+●○–●–+]	∓0.30
	:	:	:	:
	702	[–○●○●○++●–+●–+○●–○–+]	[–●●○+●○○–○+–++●○+–●–]	∓0.30
	703	[–○+–+○●●–●+–++○●○●○–]	[–+○●–++●–●○○○–++–●●○]	±0.26
	:	:	:	:
	771	[–●+++○○–●●––○–+○○●+●]	[–●+–+●○○–○+–++●○●○●–]	±0.26
	772	[–○●○○+–●●+●++–●○–+○–]	[–○●●○++●○+–●○––+○–●+]	∓0.26
	:	:	:	:
	799	[–●○○●++○●+–○●––+●–○+]	[–●○●○●++–+○–○○●+–+●–]	∓0.26
	800	[–○●+–○++–+●–●●○○●+○–]	[––●●+++○○○○–+–●+●–●○]	±0.22
	:	:	:	:
	870	[–●+○+○+––●–●+●○○○–+●]	[–●○+–●++–+○–○○●●○+●–]	±0.22
	871	[–○+●○○●●–●+–++○–+●○–]	[–○●○+●+●+○●–○–––+○●+]	∓0.22

:	:	:	:
902	[–●○●+○+○+●○–●–––+●○+]	[–●+○●●○○–○+–++●–+○●–]	∓0.22
903	[–○+●○––++●+●●–○○+●○–]	[–●–●++○+○○–○–++●●●○–]	±0.18
:	:	:	:
973	[–○–○++●+●●–●–++○○○●–]	[–●+○●––++○+○○–●●+○●–]	±0.18
974	[–●○○○++–●–●●+●++○–○–]	[–●●–○●○+++○○○+–+●––●]	∓0.18
:	:	:	:
1000	[–●○●○+++○–○–●●●–+–+○]	[–●○+●●–○○+○++––●○+●–]	∓0.18
1001	[–○+●+○–●–●+–+○○●+●○–]	[–+●○+–○●●–+○○–++●–●○]	±0.14
:	:	:	:
1072	[–+○●○–●++–+●●–○○○–+●]	[–●+○+●–○–○+–+●●○+○●–]	±0.14
1073	[–○○●++●●––○●+○+–+●○–]	[–●○++●○○–●○●+––+–+●○]	∓0.14
:	:	:	:
1132	[–●○++○○●●●––+–+○○–+●]	[–●○+○●●+–+○–○–●+○+●–]	∓0.14
1133	[–○○–++●●–●+●+○+–○●○–]	[–●○+●+–+–○○○–●+●+●○–]	±0.10
:	:	:	:
1237	[–○●+○+–+●–●–●+○○○+●–]	[–●○+●+––○+○+●–○●○+●–]	±0.10
1238	[–○+●○●–○+●+●––+○+●○–]	[–+○●●●○+–○○––+++●●○–]	∓0.10
:	:	:	:
1291	[–+●○○○●+–●●––+++○○●–]	[–●○●++○○–+–●●–○+○+●–]	∓0.10
1292	[–○●+–+○○●+●––●++●○○–]	[–●○++●○+––○–○●●+●+–○]	±0.06
:	:	:	:
1348	[–●○+○++–●–●●○–+○○–+●]	[–●○+●+–○–+○●+–○●○+●–]	±0.06
1349	[–○○●++●––●+●○○+–+●○–]	[–●○+○●–●+++–○○–○●●–+]	∓0.06
:	:	:	:
1404	[–○●+●○–○+++–●●–●○○–+]	[–●●○++○––○+○●●+–+○●–]	∓0.06
1405	[–●+○+○○–●●––+●++○●○–]	[–●○●++–+○○–○–●+●●+○–]	±0.02
:	:	:	:
1478	[–○●○++–+●●–●–○+○○+●–]	[–●+○+●○○––●–++●○+○●–]	±0.02
1479	[–●+○○+○–●–●●+–++○●○–]	[–●○●++○+––○○–●●+●+○–]	∓0.02
:	:	:	:
1538	[–○●○++●+––●●–○○+○+●–]	[–●○+○●++–●––○○●+○+●–]	∓0.02

20

Appendix C

An example on the ABAQUS command function for this first constraint equations of Eq. (7.3) is given in Eq. (10.1).

Constraint equation	ABAQUS command	
$u^C - u^A - \varepsilon_x a = 0$	*Equation 3 FaceC, 1, 1, FaceA, 1, −1, Constraint1, 1, $-a$	(10.1)

Note that the steps begin by bringing all the terms in the constraint equations to the left hand side. The second line, after the command *Equation, gives the number 3 that indicates three sets of terms exist within the constraint equation. Each set consist of three variables defined by node, degree-of-freedom, and coefficient, which are listed in the third line. The third line begins first by defining the three variables for node u^C; with FaceC is the node name, followed by the number 1 indicating the first degree-of-freedom, and subsequently with the number 1 representing the coefficient of the term u^C in the constraint

equation shown in Eq. (10.1). The second set of term defines for the second node i.e. u^A, where the description on the three variables shown follows the same rationale to the one before. Meanwhile the third term is presented by a dummy node, in this case named as Constraint1 that represent the strain ε_x, and followed by the number 1 that designates the first component of the dummy node. The coefficient is designated by the term $-a$ i.e. the length of the RUC in the –x direction.

References

ABAQUS (2009a) (Abaqus Documentation 6.9-1.) Dassault Systemes, Providence, Rhode Island, United States.

ABAQUS (2009b) (Abaqus release 6.9.) Dassault Systemes, Providence, Rhode Island, United States.

Abot, J. L., Yasmin, A., Jacobsen, A. J. & Daniel, I. M. (2004) In-plane mechanical, thermal and viscoelastic properties of a satin fabric carbon/epoxy composite. *Composites Science and Technology* **64(2)**:263-268.

Armanios, E. A., Makeev, A. & Hooke, D. (1996) Finite-displacement analysis of laminated composite strips with extension-twist coupling. *Journal of Aerospace Engineering* **9(3)**:80-91.

Bartholomew, P. (1977) Ply stacking sequences for laminated plates having in-plane and bending orthotropy. *Fibre Science and Technology* **10(4)**:239-253.

Betts, D. N., Salo, A. I. T., Bowen, C. R. & Kim, H. A. (2010) Characterisation and modelling of the cured shapes of arbitrary layup bistable composite laminates. *Composite Structures* **92(7)**:1694-1700.

Bishop, S. M. (1989) Chapter 6 - Strength and failure of woven carbon-fibre reinforced plastics for high performance applications. In *Composite Materials Series*. (Chou, T. W., andKo, F. K. (eds)) Elsevier, vol. 3, pp. 173-207.

Caprino, G. & Visconti, I. C. (1982) A Note on Specially Orthotropic Laminates. *Journal of Composite Materials* **16(5)**:395-399.

Chen, H. P. (2003) Study of hygrothermal isotropic layup and hygrothermal curvature-stable coupling composite laminates. In *44th AIAA/ASME/ASCE/AHS/ASC Structures, Structural Dynamics, and Materials Conference*, Norfolk, United States.

Cross, R. J., Haynes, R. A. & Armanios, E. A. (2008) Families of Hygrothermally Stable Asymmetric Laminated Composites. *Journal of Composite Materials* **42(7)**:697-716.

Dancila, D. S., Kim, I. B. & Armanios, E. A. (1998) Star-shape cross-section extension-twist-coupled composite beams for rotorcraft applications. In *54th American Helicopter Society International Annual Forum*, Washington, USA.

Daniel, I. M. & Ishai, O. (2006) *Engineering Mechanics of Composite Materials.* 2nd edn. New York, United States Oxford University Press.

Dano, M. L. & Hyer, M. W. (2002) Snap-through of unsymmetric fiber-reinforced composite laminates. *International Journal of Solids and Structures* **39(1)**:175-198.

Decolon, C. (2002) Chapter 5 - Multi-layer kirchhoff-love thin plates. In *Analysis of Composite Structures*. (Decolon, C. (ed)) Kogan Page Science, London, pp. 73-104.

Diaconu, C. G. & Sekine, H. (2003) Flexural characteristics and layup optimization of laminated composite plates under hygrothermal conditions using lamination parameters. *Journal of Thermal Stresses* **26(9)**:905-922.

Diaconu, C. G. & Sekine, H. (2004) Erratum on Flexural Characteristics and Layup Optimization of Laminated Composite Plates Under Hygrothermal Conditions using Lamination Parameters. *Journal of Thermal Stresses* **27(12)**:1213-1216.

Dobyns, A., Rousseau, C. Q. & Minguet, P. (2000) 6.12 - Helicopter Applications and Design. In *Comprehensive Composite Materials*. (Kelly, A., andZweben, C. (eds)) Pergamon, Oxford, pp. 223-242.

ESDU (1982) Laminate stacking sequences for special orthotropy. *Engineering Sciences Data Unit* **Item No. 82013**:1-40.

ESDU (1994) Stiffnesses of laminated flat plates *Engineering Science Data Unit* **Item No. 94003**:1-28.

Foye, R. L. (1993) *Approximating the stress field within the unit cell of a fabric reinforced composite using replacement elements*. Hampton, VA.

Freissinet, S. (2011) "Worries about new composite made airplane". Retrieved 21 June 2014, from http://www.1001crash.com/index-page-composite-lg-2.html.

Fukunaga, H. (1990) On Isotropic Laminate Configurations. *Journal of Composite Materials* **24(5)**:519-535.

Fukunaga, H. & Sekine, H. (1994) A Laminate Design for Elastic Properties of Symmetrical Laminates with Extension-Shear or Bending-Twisting Coupling. *Journal of Composite Materials* **28(8)**:708-731.

Fukunaga, H. & Vanderplaats, G. N. (1991) Stiffness Optimization of Orthotropic Laminated Composites Using Lamination Parameters. *AIAA Journal* **29(4)**:641-646.

Grediac, M. (2001) On the stiffness design of thin woven composites. *Composite Structures* **51(3)**:245-255.

Greenhalgh, E. S., Pastore, C. M. & Garfinkle, M. (1993a) A continuous-fiber composite wing box-beam exhibiting twist-bend coupling. *Composites Engineering* **3(7–8)**:691-697.

Greenhalgh, S., Pastore, C. & Garfinkle, M. (1993b) Aeroelastic airfoil smart spar. *Composites Manufacturing* **4(4)**:195-198.

Haynes, R. & Armanios, E. (2011) Hygrothermally stable extension-twist and bend-twist coupled laminates. In *67th American Helicopter Society International Annual Forum*, Virginia Beach, United states.

Haynes, R. A. & Armanios, E. A. (2010) New Families of Hygrothermally Stable Composite Laminates with Optimal Extension-Twist Coupling. *AIAA Journal* **48(12)**:2954-2961.

Hearmon, R. F. S. (1943) The significance of coupling between shear and extension in the elastic behaviour of wood and plywood. *Proceedings of the Physical Society* **55(1)**:67.

Hodges, R. V., Nixon, M. W. & Rehfield, L. W. (1987) *Comparison of composite rotor blade models: A coupled-beam analysis and an MSC/NASTRAN finite-element model.*, Report 04999320.

Hyer, M. W. (1981a) Calculations of the Room-Temperature Shapes of Unsymmetric Laminates. *Journal of Composite Materials* **15(Jul)**:296-310.

Hyer, M. W. (1981b) Some Observations on the Cured Shape of Thin Unsymmetric Laminates. *Journal of Composite Materials* **15(2)**:175-194.

Hyer, M. W. (1982) The Room-Temperature Shapes of Four-Layer Unsymmetric Cross-Ply Laminates. *Journal of Composite Materials* **16(4)**:318-340.

Hyer, M. W. (2009) *Stress Analysis of Fiber-Reinforced Composite Materials: Updated Edition.* Updated Edition edn. Pennsylvania U.S.A, DEStech Publications, Inc.

Ilcewicz, L. B., Hoffman, D. J. & Fawcett, A. J. (2000) 6.07 - Composite Applications in Commercial Airframe Structures. In *Comprehensive Composite Materials*. (Kelly, A., andZweben, C. (eds)) Pergamon, Oxford, pp. 87-119.

Ishikawa, T. (1981) Anti-symmetric elastic properties of composite plates of satin weave cloth. *Fibre Science and Technology* **15(2)**:127-145.

Ishikawa, T. & Chou, T. W. (1982) Stiffness and strength behaviour of woven fabric composites. *Journal of Materials Science* **17(11)**:3211-3220.

Ishikawa, T., Matsushima, M., Hayashi, Y. & Chou, T. W. (1985) Experimental Confirmation of the Theory of Elastic Moduli of Fabric Composites. *Journal of Composite Materials* **19(5)**:443-458.

Jacobsen, A. J., Luo, J. J. & Daniel, I. M. (2004) Characterization of Constitutive Behavior of Satin-Weave Fabric Composite. *Journal of Composite Materials* **38(7)**:555-565.

Jekabsons, N. & Bystrom, J. (2002) On the effect of stacked fabric layers on the stiffness of a woven composite. *Composites Part B: Engineering* **33(8)**:619-629.

Jones, R. M. (1975) *Mechanics of composite materials.* New York ; London, McGraw-Hill.

Jones, R. M. (1999) *Mechanics of Composite Materials.* 2nd Edition edn. Blacksburg, Virginia, Taylor & Francis, Inc.

Jun, W. J. & Hong, C. S. (1990) Effect of residual shear strain on the cured shape of unsymmetric cross-ply thin laminates. *Composites Science and Technology* **38(1)**:55-67.

Jun, W. J. & Hong, C. S. (1992) Cured shape of unsymmetric laminates with arbitrary lay-up angles. *Journal of Reinforced Plastics and Composites* **11(12)**:1352-1366.

Kandil, N. & Verchery, G. (1988) New methods of design for stacking sequences of laminates. In *Computer Aided Design in Composite Materials Conference*. (Brebbia, C. A., De Wilde, W. P., andBlain, W. R. (eds)), vol. Computation Mechanics, pp. 243-257.

Karkkainen, R. L. & Sankar, B. V. (2006) A direct micromechanics method for analysis of failure initiation of plain weave textile composites. *Composites Science and Technology* **66(1)**:137-150.

Khoun, L., Challagulla, K. & Hubert, P. (2012) Thermo-Mechanical Properties of 5-Harness Satin Fabric Composites. *Journal of Composite Materials*.

Lagace, P. A., Jensen, D. W. & Finch, D. C. (1986) Buckling of unsymmetric composite laminates. *Composite Structures* **5(2)**:101-123.

Lake, R. C., Nixon, M. W., Wilbur, M. L., Singleton, J. D. & Mirick, P. H. (1992) A Demonstration of Passive Blade Twist Control Using Extension-Twist Coupling. In *AIAA/ASME/ASCE/AHS/ASC Structures, Structural Dynamics and Materials Conference*, Dallas, United States.

Lake, R. C., Nixon, M. W., Wilbur, M. L., Singleton, J. D. & Mirick, P. H. (1994) Demonstration of an elastically coupled twist control concept for tilt rotor blade application. *AIAA Journal* **32(7)**:1549-1551.

Love, A. E. H. (1944) *A Treatise on the Mathematical Theory of Elasticity.* New York, Dover Publications.

Marrey, R. V. & Sankar, B. V. (1993) Stress Gradient Effects on Stiffness and Strength of Textile Composites. In *Composite Materials and Structures*. (Bert, C. W., Birman, V., andHui, D. (eds)) AMD edn. American Society of Mechanical Engineers, New York, vol. 179, pp. 133-148.

Marrey, R. V. & Sankar, B. V. (1997) A Micromechanical Model for Textile Composite Plates. *Journal of Composite Materials* **31(12)**:1187-1213.

Martin, D. M., Demo, J. G. & Daniel, C. D. (2000) *The History of the XV-15 Tilt Rotor Research Aircraft: From Concept to Flight.* Washington, D. C., Office of Policy and Plans, NASA History Division, National Aeronautics and Space Administration.

MATLAB (2014) (Matlab release 2014a.) The MathWorks Inc., Natick, Massachusetts, United States.

Naik, N. K. & Ganesh, V. K. (1992) Prediction of on-Axes Elastic Properties of Plain Weave Fabric Composites. *Composites Science and Technology* **45(2)**:135-152.

Naik, N. K. & Shembekar, P. S. (1992a) Elastic Behavior of Woven Fabric Composites: I--Lamina Analysis. *Journal of Composite Materials* **26(15)**:2196-2225.

Naik, N. K. & Shembekar, P. S. (1992b) Elastic Behavior of Woven Fabric Composites: III -- Laminate Design. *Journal of Composite Materials* **26(17)**:2522-2541.

Niu, M. C. (1999) *Airframe Structural Design: Practical design information and data on aircraft structures, 2nd Edition.* Hong Kong, Conmilit Press.

Nixon, M. W. (1987) Extension-twist coupling of composite circular tubes with application to tilt rotor blade design. In *28th AIAA/ASME/ASCE/AHS/ASC Structures, Structural Dynamics, and Materials Conference*, Monterey, United States.

Nixon, M. W. (1988) *Improvements to Tilt Rotor Performance through Passive Blade Twist Control*. Report TM-100583.

Raju, I. S. & Wang, J. T. (1994) Classical Laminate Theory Models for Woven Fabric Composites. *Journal of Composites Technology & Research* **16(4)**:289-303.

Rao, M. P., Pantiuk, M. & Charalambides, P. G. (2008) Modeling the Geometry of Satin Weave Fabric Composites. *Journal of Composite Materials* **43(1)**:19-56.

Rousseau, J., Verchery, G. & York, C. B. (2011) Experimental validation of laminated composites with thermal and/or mechanical coupling response: a search for hygro-thermally curvature-stable designs. In *Deformation and Fracture of Composites and 5th Structural Integrity and Multi-scale Modelling*, Cambridge, England.

Schlecht, M. & Schulte, K. (1999) Advanced calculation of the room-temperature shapes of unsymmetric laminates. *Journal of Composite Materials* **33(16)**:1472-1490.

Schlecht, M., Schulte, K. & Hyer, M. W. (1995) Advanced calculation of the room-temperature shapes of thin unsymmetric composite laminates. *Composite Structures* **32(1-4)**:627-633.

Shamsudin, M. H., Chen, J. & York, C. B. (2013a) Bounds on the compression buckling strength of hygro-thermally curvature-stable laminate with extension-twisting coupling. *International Journal of Structural Integrity* **4(4)**:477-486.

Shamsudin, M. H., Rousseau, J., Verchery, G. & York, C. B. (2011) Experimental Validation of the Mechanical Coupling Response for Hygro-Thermally Curvature-

Stable Laminated Composite Materials. In *6th International Conference on Supply on the Wings*, Frankfurt, Germany.

Shamsudin, M. H., Rousseau, J. & York, C. B. (2013b) Warping Curvature Predictions for Non-Symmetric Woven Cloth Laminates. In *12th Deformation and Fracture of Composites and 6th Structural Integrity and Multi-scale Modelling* ,Cambridge, England.

Shembekar, P. S. & Naik, N. K. (1992) Elastic Behavior of Woven Fabric Composites: II--Laminate Analysis. *Journal of Composite Materials* **26(15)**:2226-2246.

Soykasap, O. (2011) Analaysis of Plain Weave Composites. *Mechanics of Composite Materials* **47(2)**:161-176.

TexGen (2007), See http://texgen.sourceforge.net/index.php/Main_Page (accessed July 2012).

Thuwis, G. a. A., Breuker, R., Abdalla, M. M. & Gürdal, Z. (2009) Aeroelastic tailoring using lamination parameters. *Structural and Multidisciplinary Optimization* **41(4)**:637-646.

Tsai, S. W. & Hahn, H. T. (1980) *Introduction To Composite Materials.* Technomic Publishing Co. Inc., Lancaster.

Vannucci, P. & Verchery, G. (2002) A new method for generating fully isotropic laminates. *Composite Structures* **58(1)**:75-82.

Verchery, G. (1979) Les invariants d'ordre 4 du type de l'elasticité In *Proceedings of Euromech Colloquium 115*, pp. 93–104.

Verchery, G. (2011) Design Rules for the Laminate Stiffness. *Mechanics of Composite Materials* **47(1)**:47-58.

Vincenti, A., Verchery, G. & Vannucci, P. (2001) Anisotropy and symmetry for elastic properties of laminates reinforced by balanced fabrics. *Composites Part A: Applied Science and Manufacturing* **32(10)**:1525-1532.

Weaver, P. M. (2005) Anisotropic laminates that resist warping during manufacture. In *15th International Conference on Composite Materials*, Durban, South Africa.

Werren, F. & Norris, C. B. (1953) *Mechanical properties of a laminate designed to be isotropic*. Madison, Wisconsin, Report 1841.

Whitcomb, J. & Tang, X. (2001) Effective moduli of woven composites. *Journal of Composite Materials* **35(23)**:2127-2144.

Whitcomb, J. D. (1989) *Three-dimensional stress analysis of plain weave composites*. Hampton, VA, Report NASA TM-101672.

Whitcomb, J. D., Woo, K. & Sitaram, G. (1994) Macro finite element for analysis of textile composites. *Journal of Composite Materials* **28(7)**:607-618.

Whitney, J. M. (1969) Bending-Extensional Coupling in Laminated Plates Under Transverse Loading. *Journal of Composite Materials* **3(1)**:20-28.

Whitney, J. M. & Leissa, A. W. (1969) Analysis of Heterogenous Anisotropic Plates. *Journal of Applied Mechanics* **36**:261.

Whitney, J. M. & Leissa, A. W. (1970) Analaysis of simply supported laminated anisotropic rectangular plate. *AIAA Journal* **1(8)**:pp. 28 - 33.

Winckler, S. J. (1985) Hygrothermally Curvature Stable Laminates with Tension-Torsion Coupling. *Journal of the American Helicopter Society* **30(3)**:56-58.

Woo, K. (2005) Effect of Phase Shift on Engineering Properties of [±θ] Plain Weave Laminates. *Journal of Composite Materials* **39(6)**:479-495.

Woo, K., Suh, Y. W. & Whitcomb, J. D. (2002) Phase Shift Effect on the Stress Distribution for Satin Weave Composites. *Journal of Composite Materials* **vol. 36(3)**:pp. 271-286.

Woo, K. & Whitcomb, J. D. (1997) Effects of fiber tow misalignment on the engineering properties of plain weave textile composites. *Composite Structures* **37(3-4)**:343-355.

Wu, K. M. & Avery, B. L. (1992) Fully Isotropic Laminates and Quasi-Homogeneous Anisotropic Laminates. *Journal of Composite Materials* **26(14)**:2107-2117.

York, C. B. (2008) On composite laminates with extensional-anisotropy. In *49th AIAA/ASME/ASCE/AHS/ASC Structures, Structural Dynamics, and Materials*, Schaumburg, United States.

York, C. B. (2009) Characterization of Nonsymmetric Forms of Fully Orthotropic Laminates. *Journal of Aircraft* **46(4)**:1114-1125.

York, C. B. (2010) Unified Approach to the Characterization of Coupled Composite Laminates: Benchmark Configurations and Special Cases. *Journal of Aerospace Engineering* **23(4)**:219-242.

York, C. B. & Weaver, P. M. (2010) Balanced and symmetric laminates - New perspectives on an old design rule. In *51st AIAA/ASME/ASCE/AHS/ASC Structures, Structural Dynamics, and Materials*, Orlando, United States.

York, C. B. (2011) Unified approach to the characterization of coupled composite laminates Hygro-thermally curvature-stable configurations. *International Journal of Structural Integrity* **2(4)**:406-436.

York, C. B. (2012) Extension-Twist coupled laminates for aero-elastic compliant blade design. In *53rd AIAA/ASME/ASCE/AHS/ASC Structures, Structural Dynamics and Materials Conference*, Honolulu, United states.

York, C. B. (2013) Tapered hygro-thermally curvature-stable laminates with non-standard ply orientations. *Composites Part a-Applied Science and Manufacturing* **44**:140-148.

York, C. B. (2015) On Extension–Shearing coupled laminates. *Composite Structures* **120(0)**:472-482.